

# PROBING THE STELLAR INITIAL-FINAL MASS RELATION

By

Richard Bruce Baxter

A THESIS SUBMITTED TO MACQUARIE UNIVERSITY  
FOR THE DEGREE OF  
MASTER OF PHILOSOPHY  
DEPARTMENT OF PHYSICS  
JULY 2011



MACQUARIE  
UNIVERSITY  
FACULTY OF SCIENCE



Except where acknowledged in the customary manner, the material presented in this thesis is, to the best of my knowledge, original and has not been submitted in whole or part for a degree in any university.

---

Richard Bruce Baxter





# Acknowledgements

I would like to thank my supervisors Dr Paul Dobbie and Professor Quentin Parker for their careful guidance and constant support.

This thesis is dedicated in memory of my grandmother Mrs Betty Baxter who died in 2010.

- Richard



# Abstract

I have tested our current understanding of the form of the stellar initial-final mass relation (IFMR) by performing a preliminary study of twelve (12) wide double-degenerate binaries. I identified these systems by applying colour and magnitude selection criteria, in software, to identify blue object close pairs in the imaging data of the Sloan Digital Sky Survey (SDSS). A selection of these were then targeted for spectroscopic follow-up while performing astrometric analysis to determine if the components in each had significant, common proper motions. Subsequently, I used existing grids of white dwarf synthetic spectra and evolutionary models to interpret the spectroscopic data. The white dwarf parameters of mass,  $M_f$ , and cooling time,  $t_{\text{cool}}$ , were then used to probe the form of the IFMR. Using the white dwarfs in my sample whose derived parameters confirmed they were coeval and physically associated, I have also constructed a preliminary mass distribution for the components of these binary systems.



# Contents

<b>Acknowledgements</b>	<b>v</b>
<b>Abstract</b>	<b>vii</b>
<b>List of Figures</b>	<b>xiii</b>
<b>List of Tables</b>	<b>xix</b>
<b>1 Introduction</b>	<b>1</b>
1.1 Overview . . . . .	1
1.2 White Dwarf and their fundamental Physics . . . . .	2
1.2.1 White Dwarf Cooling . . . . .	3
1.2.2 White Dwarf Spectral Classification . . . . .	4
1.3 Stellar Evolution . . . . .	4
1.3.1 Main sequence (MS) . . . . .	4
1.3.2 Red Giant Branch (RGB) . . . . .	5
1.3.3 Horizontal Branch . . . . .	6
1.3.4 Asymptotic Giant Branch (AGB) . . . . .	7
1.3.5 White Dwarf Cooling Sequence . . . . .	7
1.3.6 White Dwarf Survey Statistics . . . . .	8
1.4 The stellar initial-final mass relation (IFMR) . . . . .	11
1.4.1 A light introduction to the stellar IFMR . . . . .	11
1.4.2 Using open clusters to map the IFMR . . . . .	13
1.4.3 IFMR Calculations To Date . . . . .	14
1.4.4 Sources of Uncertainty . . . . .	19
1.5 Thesis Outline . . . . .	21
<b>2 Data</b>	<b>23</b>
2.1 The identification of candidate wide double-degenerate systems . . . . .	23
2.1.1 Summary . . . . .	23
2.1.2 The SDSS Data Release 7 . . . . .	23
2.1.3 Initial Identification of candidate wide DD systems . . . . .	25
2.1.4 Simulations . . . . .	28
2.2 Follow-up spectroscopic observations . . . . .	38
2.2.1 Prioritisation of candidate wide DD systems for follow-up . . . . .	38

2.2.2	The spectroscopic follow-up observations . . . . .	45
2.3	Data Reduction . . . . .	49
2.3.1	Spectroscopic Data Reduction . . . . .	49
2.4	Data modelling . . . . .	57
2.4.1	Atmospheric modelling . . . . .	57
2.4.2	Evolutionary modelling . . . . .	61
2.4.3	Proper motion verification of physical association . . . . .	67
<b>3</b>	<b>Results</b>	<b>75</b>
3.1	Properties of the components of the wide double-degenerate systems. .	75
3.1.1	Hot DA + hot DA systems . . . . .	75
3.1.2	Cool DA + hot DA systems . . . . .	76
3.1.3	Cool DA + cool DA systems . . . . .	76
3.1.4	HFMWD (DAH) + hot DA systems . . . . .	76
3.1.5	HFMWD (DAH) + cool DA systems . . . . .	77
3.1.6	Estimation of the uncertainties in derived parameters . . . . .	77
3.2	The double-degenerate systems on a case-by-case basis . . . . .	77
3.2.1	DD-01 . . . . .	78
3.2.2	DD-02 . . . . .	79
3.2.3	DD-03 . . . . .	80
3.2.4	DD-04 . . . . .	81
3.2.5	DD-05 . . . . .	81
3.2.6	DD-06 . . . . .	82
3.2.7	DD-07 . . . . .	83
3.2.8	DD-08 . . . . .	84
3.2.9	DD-09 . . . . .	85
3.2.10	DD-10 . . . . .	86
3.2.11	DD-11 . . . . .	87
3.2.12	DD-12 . . . . .	88
3.2.13	My systems overall and understanding of the IFMR . . . . .	88
3.3	IFMR probing . . . . .	94
3.4	A preliminary investigation of the double degenerate mass distribution	105
3.4.1	Comparing the DD mass distribution to the field WD mass distribution . . . . .	110
3.4.2	Why might the DD mass distribution be skewed to higher mass?	114
3.5	A preliminary investigation of the double degenerate magnetic WD distribution . . . . .	114
<b>4</b>	<b>Moving forward</b>	<b>115</b>
4.1	Further optical spectroscopy . . . . .	115
4.1.1	Non-magnetic systems . . . . .	115
4.1.2	Systems containing HFMWDs . . . . .	116
4.2	Preliminary investigation of IFMR form derivation . . . . .	119
4.3	Conclusion . . . . .	121

<b>A</b>	<b>Appendix</b>	<b>131</b>
A.1	Overview . . . . .	131
A.1.1	Standard Libraries . . . . .	131
A.2	Target Selection Code and Data . . . . .	131
A.2.1	SDSS SQL Scripts for blue object list generation . . . . .	131
A.2.2	Count Close Pairs within a BO List Code . . . . .	132
A.2.3	Count Close Pairs within a Random Distribution Code . . . . .	133
A.2.4	Plot Clustering Code . . . . .	133
A.2.5	Create Blue Object Close Pair List (BOCPL) . . . . .	134
A.2.6	Create BOCPL Subset using Is Quasar Data . . . . .	134
A.2.7	create BOCPL Subset using Visual Check Bad List . . . . .	134
A.2.8	create BO Subset Using Generic Ra and Dec Data . . . . .	134
A.2.9	create BOCP Subset Using Generic Ra and Dec Data . . . . .	135
A.2.10	create BOCPL Subset Using Bergeron Theoretical Data . . . . .	135
A.2.11	Calculate probability of chance alignment using distance limited volume method . . . . .	137
A.3	Proper Motions Code and Data (Target Selection Part II) . . . . .	137
A.3.1	Proper Motion Calculation Procedure . . . . .	137
A.3.2	Proper Motion Calculations in Pixels . . . . .	139
A.3.3	Proper Motion Calculations in RA/Dec (Calibration of pixel val- ues) . . . . .	140
A.3.4	Calculation Probability of Chance Proper Motion Alignment - PDD Method . . . . .	140
A.3.5	Calculation Probability of Chance Proper Motion Alignment - RBB Method . . . . .	141
A.4	Observations Code and Data . . . . .	141
A.4.1	calculate the angle between WD components in double degener- ate system (for aligning slit) . . . . .	141
A.4.2	Flux Calibrated WD Data . . . . .	141
A.4.3	WHT Data Reduction . . . . .	143
A.4.4	Gemini South/North Data Reduction . . . . .	147
A.4.5	VLT Data Reduction . . . . .	150
A.4.6	Flux Calibration . . . . .	150
A.4.7	Signal to Noise Calculations . . . . .	150
A.5	Stellar Modelling Scripts . . . . .	151
A.5.1	Balmer Line Extraction . . . . .	151
A.5.2	White Dwarf Parameter Extraction . . . . .	151
A.5.3	Thusty And Koester ASCII Model Grid Comparison Using GDL . . . . .	152
A.5.4	Interpolate ASCII Spectroscopic Model Grid and create ASCII model using Best Fit Temperature and Surface Gravity values . . . . .	153
A.5.5	White Dwarf Parameter Extraction - including gravitational red- shift values - NOT USED . . . . .	153
A.5.6	Flux Recalibration using Best Fit ASCII Spectroscopic Model . . . . .	154

A.5.7	Interpolate ASCII Main Sequence Stellar evolutionary model grid using theoretical main sequence mass or age values to calculate a best fit main sequence age or mass . . . . .	154
A.5.8	ASCII Model Grid Creation Software - performed by PDD and Koester . . . . .	155
A.5.9	XSpec Software . . . . .	155
A.5.10	PDD IDL ASCII Model Interpolation Software Pre-requisites - NOT USED . . . . .	156
A.5.11	Model Grids . . . . .	156
A.5.12	Xspec Model Files . . . . .	157
A.5.13	Operational Manuals . . . . .	158
A.6	Data Analysis . . . . .	161
A.6.1	Calculate Main Sequence Ages . . . . .	161
A.6.2	compare DD System Age Difference Distribution Across Published IFMRs . . . . .	162
A.6.3	Distance Moduli Comparison of DD components . . . . .	163
A.6.4	DD Mass Distribution Comparison with Field WD Survey . . . . .	164
A.7	List of Documentation . . . . .	164
A.7.1	Object Table . . . . .	164
A.7.2	Target Selection Confirmations . . . . .	165
A.7.3	Private Projects . . . . .	165
A.7.4	WHT Observing Proposals . . . . .	166
A.7.5	WHT 2008A Proposal . . . . .	166
A.7.6	Gemini Observing Proposals . . . . .	173
A.7.7	VLT Observing Proposals . . . . .	191
A.8	original analytical method for determining the properties of the components of the wide double-degenerate systems . . . . .	200
A.8.1	Uncertainty Calculations . . . . .	200
A.9	example IDL routine . . . . .	202
<b>List of Symbols</b>		<b>207</b>
<b>References</b>		<b>209</b>



# List of Figures

1.1	Diagram of Stellar Evolution from Herwig (2005). This diagram shows the evolution of a low-intermediate mass star, from the Main-sequence, to the Red Giant Branch (RGB), Horizontal Branch (ZAHB), Asymptotic Giant Branch (AGB), and finally the post-AGB phase with the formation of a central star of a planetary nebula (CSPN) afterwards becoming a WD. . . . .	6
1.2	HST Spectrum of the heliux nebula (NGC7293) planetary nebula central star, compared with three models with different effective temperatures (Traulsen et al. 2005). . . . .	8
1.3	The SDSS WD mass distribution as determined by Kepler et al. (2007). Histogram for the 1859 DA stars brighter than $g = 19$ and hotter than $T_{\text{eff}} = 12000K$ , compared to the PG survey published by Liebert et al. (2005a) and the SDSS DR1 sample published by Madej et al. (2004). Gaussian fits are also shown. The bins are $0.025M_{\odot}$ wide. . . . .	10
1.4	The IFMR (Casewell et al. 2009). A state-of-the-art representation of the known form of the IFMR, showing the revised locations of the Praesepe white dwarfs in initial mass-final mass space (filled circles). The locations of the degenerate members of the NGC 6633 (square star), NGC 7789 (cross), NGC 6819 (asterisk), Hyades (open triangles), Sirius binary system (open circle), the Pleiades (open stars), NGC 2168 (open diamonds), NGC 1039 (open squares), NGC 6791 (filled triangles) and NGC 2516 (open '+' signs) are also shown. The relation of Weidemann (2000) (dotted line) and a revised linear fit to 41 white dwarfs (dashed line) are overplotted. The radial velocity variable, WD0837+185 is labelled. . . . .	12

- 1.5 The IFMR (Dobbie et al. 2009). Another state-of-the-art representation of the known form of the IFMR, showing that the bulk of stars appear to follow fairly closely a monotonic relation. The locations of the white dwarf members of NGC 3532 and NGC 2287 in initial mass-final mass space. Data points from a number of other populations with metallicities close to the solar value are also shown. The theoretical IFMR of Marigo and Girardi (2007) (dot - dashed heavy line), the semi-empirical IFMR of Weidemann (2000) (heavy dotted line) and the initial mass-core mass at first thermal pulse relation from Karakas et al. (2002) (medium solid line) are overplotted. The peak in the field white dwarf mass distribution ( $\pm 1\sigma$ ) is represented by the band of grey shading. . . . . 16
- 1.6 Ferrario et al. (2005) volume corrected mass distribution of field WDs in the Palomar-Green survey (Liebert et al. 2005a) (shaded histogram) for stars hotter than  $13000K$  with the best linear IFMR fit model (top panel) and the IFMR with curvature (bottom panel). WDs with masses less than  $0.5M_{\odot}$  are believed to be helium WDs resulting from close binary evolution and are not modelled in this paper . . . . . 17
- 1.7 The Liebert et al. (2005a) comparison of their  $T_{eff}$  and  $\log g$  determinations of PG stars in common with the data sets of Finley and Koester (1997), Vennes et al. (1997), Marsh et al. (1997), Homeier et al. (1998), and Koester et al. (2001). In each panel they plot the differences between these investigations and their results (PG) as a function of their determinations of  $T_{eff}$  or  $\log g$ . Effective temperatures are in units of  $10^3K$ . . . . . 20
- 2.1 A graph of the passbands of the SDSS filters ( $u, g, r, i, z$ ) with a WD spectrum overlaid . . . . . 24
- 2.2 WD photometry selection criteria diagram, from Harris et al. (2003). Colour-colour diagrams ( $u - g$  vs.  $g - r$ ) showing the WDs and hot subdwarfs. Different types are shown with different symbols. Small dots show all objects with stellar image profiles with  $15 < g < 20$  in a region of  $25deg^2$ . The curves show the colours of WD model atmospheres Bergeron et al. (1995b) of pure H (solid curves) and pure He (dashed curves) with  $\log g = 7, 8$ , and  $9$ , where the  $\log g = 7$  curve is toward the lower right and the  $\log g = 9$  curve is toward the upper left. The dotted lines with labels connect models with the same effective temperature. . . . . 26
- 2.3 All WD Candidates (Blue Objects from SDSS DR7 Survey) shown with Aitoff projection of galactic coordinates . . . . . 27
- 2.4 Plot showing the number of BOCPs found in my simulated random distribution of single objects as a function of separation in arc-seconds (lower line) overlaid with the analytical estimate of Struve 1852. The number of BOCPs measured in the SDSS DR7 to a given maximum separation is also shown (upper line). The difference between these two curves provides a handle on the frequency of physically associated BOCPs found in the SDSS within a given maximum separation. . . . . 30

2.5	Same as Figure 2.4 but shown out to a much larger angular separation ( $\sim 6'$ ) . . . . .	30
2.6	The likelihood (expressed as a percentage) that a BOCP is a physically associated system within a given maximum separation (solid curve). The probability that a BOCP is physically associated at a given separation is also overplotted (dashed curve). . . . .	31
2.7	Examples of “bad” objects within my initial sample. These were rejected by my visual inspection of all pairs selected initially. . . . .	31
2.8	Finder charts (part 1/3) for the candidate wide double-degenerate systems found in SDSS DR7 ( $< 30''$ ). Note that these are arc $30'' \times 30''$ , with North at top end and East at the left. . . . .	33
2.9	Finder charts (part 2/3) for the candidate wide double-degenerate systems found in SDSS DR7 ( $< 30''$ ). Note that these are arc $30'' \times 30''$ , with North at top end and East at the left. . . . .	34
2.10	Finder charts (part 3/3) for the candidate wide double-degenerate systems found in SDSS DR7 ( $< 30''$ ). Note that these are arc $30'' \times 30''$ , with North at top end and East at the left. . . . .	35
2.11	SDSS Double-Degenerate Survey - Target Selection ( $1 \times 1'$ ). Systems which have been followed up spectroscopically. . . . .	39
2.12	Relative response of the WHT ISIS blue arm . . . . .	43
2.13	VLT FORS2 red and blue CCD quantum efficiency curves . . . . .	43
2.14	GMOS North (top) and South (bottom) CCD quantum efficiency curves . . . . .	44
2.15	Flux Calibrated Spectrum - DD01 to DD02 . . . . .	51
2.16	Flux Calibrated Spectrum - DD03 to DD04 . . . . .	52
2.17	Flux Calibrated Spectrum - DD05 to DD06 . . . . .	53
2.18	Flux Calibrated Spectrum - DD07 to DD08 . . . . .	54
2.19	Flux Calibrated Spectrum - DD09 to DD10 . . . . .	55
2.20	Flux Calibrated Spectrum - DD11 to DD12 . . . . .	56
2.21	Bergeron Theoretical WD Cooling Tracts - Temperature versus Age for a given mass. The cooling tracts for both a low mass ( $0.5M_{\odot}$ ) and a high mass ( $1.0M_{\odot}$ ) WD are shown. . . . .	62
2.22	“Christmas Tree” graphs of my spectra with models overlayed (DD-01 to DD-03). Note DD-02B and DD-08A are missing (as they have been modeled externally using magnetic models). . . . .	63
2.23	“Christmas Tree” graphs of my spectra with models overlayed (DD-04 to DD-06). . . . .	64
2.24	“Christmas Tree” graphs of my spectra with models overlayed (DD-07 to DD-09). Note DD-02B and DD-08A are missing (as they have been modeled externally using magnetic models). . . . .	65
2.25	“Christmas Tree” graphs of my spectra with models overlayed (DD-10 to DD-12). . . . .	66
2.26	Proper motion diagrams for the 12 blue object close pairs for which I observed spectroscopic follow-up data (DD01 to DD06). The DD system components are marked as stars. . . . .	70

2.27	Proper motion diagrams for the 12 blue object close pairs for which I observed spectroscopic follow-up data (DD07 to DD12). The DD system components are marked as stars. . . . .	71
2.28	Colour-Colour for my 12 DD candidates (u-g vs g-r). Bergeron cooling tracts are shown with specific ages ( $t_{cool} = 1 \times 10^4 yrs - t_{cool} = 1 \times 10^9 yrs$ ) and temperatures ( $T_{eff} = 30000K - T_{eff} = 5000K$ ) marked. . .	73
3.1	A plot in which my effective spectroscopic mass offsets (to align cool component distances with their hot components) are compared to that of Tremblay et al. (2011) across temperature. The blue curve is that of Tremblay et al. (2011), while the red data points are calculated from my Double Degenerate survey. The error in my derived mass offset is displayed with error bars, while my derived mass offset itself is displayed as a dashed red line about $dM = -0.17 \pm 0.04 M_{\odot}$ . . . . .	86
3.2	Distance Modulii (m - M) for all DD systems (u, g, r), with cool component mass corrections / distance matching . . . . .	90
3.3	Distance Modulii (m - M) for DD systems with at least one cool component (u, g, r), without cool component mass corrections / distance matching . . . . .	90
3.4	Distance Modulii (m - M) for DD systems with at least one cool component (u, g, r), with cool component mass corrections / distance matching	91
3.5	Distance Modulii (m - M) for DD systems with two cool components or a HFMWD system (u, g, r), without cool component mass corrections / distance matching . . . . .	91
3.6	Distance Modulii (m - M) for DD systems with two cool components or a HFMWD system (u, g, r), with cool component mass corrections / distance matching . . . . .	92
3.7	Distance Modulii (m - M) for DD systems with hot components (u, g, r)	92
3.8	Plots of all published IFMRs used in this analysis; solid (Dobbie et al. 2006), dotted (Kalirai et al. 2008), dashed (Williams et al. 2009). . . .	96
3.9	Calculated System Age for SDSS DD systems, using known IFMR from Dobbie et al. (2006). . . . .	96
3.10	Calculated System Age for SDSS DD systems, using known IFMR from Kalirai et al. (2008). . . . .	97
3.11	Calculated System Age for SDSS DD systems, using known IFMR from Williams et al. (2009). . . . .	97
3.12	Plots of the system age difference distribution for DD-01 to DD-06, based upon a generated monte carlo distribution of 25000 hypothetical WDs with parameters selected within their error limits. For each plot a number of published IFMR forms are assumed; solid (Dobbie et al. 2006), dotted (Kalirai et al. 2008), dashed (Williams et al. 2009). . . .	98

3.13	Plots of the system age difference distribution for DD-07 to DD-12, based upon a generated monte carlo distribution of 25000 hypothetical WDs with parameters selected within their error limits. For each plot a number of published IFMR forms are assumed; solid (Dobbie et al. 2006), dotted (Kalirai et al. 2008), dashed (Williams et al. 2009). . . . .	99
3.14	Plots of the system age difference distribution for external WDs PG0922+162 (DD-13) and HS2240+125A (DD-14) respectively, based upon a generated monte carlo distribution of 25000 hypothetical WDs with parameters selected within their error limits. For each plot a number of published IFMR forms are assumed; solid (Dobbie et al. 2006), dotted (Kalirai et al. 2008), dashed (Williams et al. 2009). . . . .	100
3.15	Plots of the system age difference distributions for all DD systems, based upon a generated monte carlo distribution of 25000 hypothetical WDs with parameters selected within their error limits. For this plot the following published IFMR form has been assumed; Dobbie et al. (2006).	100
3.16	Plots of the system age difference distributions for all DD systems, based upon a generated monte carlo distribution of 25000 hypothetical WDs with parameters selected within their error limits. For this plot the following published IFMR form has been assumed; Kalirai et al. (2008).	101
3.17	Plots of the system age difference distributions for all DD systems, based upon a generated monte carlo distribution of 25000 hypothetical WDs with parameters selected within their error limits. For this plot the following published IFMR form has been assumed; Williams et al. (2009).	101
3.18	Plots of the initial-final mass for each component WD (of DD-01 through to DD-06) according to the (Dobbie et al. 2006) IFMR (A/B). . . . .	103
3.19	Plots of the initial-final mass for each component WD (of DD-07 through to DD-12) according to the (Dobbie et al. 2006) IFMR (A/B). . . . .	104
3.20	Kepler SDSS $V_{max}$ Corrected Mass Distribution (Kepler et al. 2007) . .	106
3.21	Liebert PG Survey $V_{max}$ Corrected Mass Distribution (Liebert et al. 2005a)	107
3.22	DD mass distribution (Solid) versus the PG Survey Vmax corrected mass distribution (Dotted), the Kepler SDSS DR4 WD mass distribution (Kepler et al. 2007) (Dashed), and the Kepler SDSS DR4 WD Vmax corrected mass distribution (Kepler et al. 2007) (Dash Dot) . . . . .	108
3.23	Kepler SDSS Survey Mass Distribution Modelled With Gaussians . . .	111
3.24	PG Survey $V_{max}$ Corrected Mass Distribution Modelled With Gaussians	111
3.25	KS Test Method 2 - Comparison of DD masses with masses derived from Kepler theoretical SDSS WD mass distribution modelled with Gaussians	112
3.26	KS Test Method 6 - Comparison of DD masses with masses derived from Kepler theoretical $V_{max}$ corrected SDSS WD mass distribution modelled with Gaussians . . . . .	112
3.27	KS Test Method 5 - Comparison of DD masses with masses derived from Liebert theoretical PG Survey $V_{max}$ corrected mass distribution modelled with Gaussians . . . . .	113

4.1	SDSS $z$ band image of two candidate spatially resolved magnetic/non-magnetic double-degenerate systems, CBS 229 (Gianninas et al. 2009) and SDSS J074853.07+302543.5. Images are approximately $1' \times 1'$ with N at the top and E to the left. . . . .	116
4.2	DR8 Only DD Candidates . . . . .	118
4.3	A plot of the derivation of the form of the IFMR for each DD system individually, by selecting a linear IFMR form ( $m$ and $c$ parameters) resulting in a common system age. A statistical derivation of the form of the IFMR is shown by averaging these parameters (with error bars showing min/max mass/cooling age assumption extremes). This graph also shows the Dobbie et al. (2006) linear IFMR form for comparison (with cited errors). . . . .	120
4.4	A second plot of the derivation of the form of the IFMR as in Figure 4.3 - excluding systems with an uncommon distance between components (DD-04 and DD-09). . . . .	120
4.5	La Palma - Cloud Valley . . . . .	122
4.6	La Palma - Volcano . . . . .	122
4.7	La Palma - INT . . . . .	123
4.8	La Palma - From Top . . . . .	123
4.9	La Palma - Sunset . . . . .	124
4.10	La Palma - Forest Mountain . . . . .	124
4.11	Cerro Paranal in Chile - Accomodation Paronama . . . . .	125
4.12	Cerro Paranal in Chile - From Top . . . . .	125
4.13	VLT Unit Telescope view 1 . . . . .	126
4.14	VLT Unit Telescope view 2 . . . . .	126
4.15	VLT Unit Telescope view 3 . . . . .	126
4.16	VLT Unit Telescope view 4 . . . . .	127
4.17	VLT Unit Telescope view 5 . . . . .	127
4.18	VLT Platform 1 . . . . .	128
4.19	VLT Platform 2 . . . . .	128
4.20	VLT Platform 3 . . . . .	129
4.21	Cerro Paranal in Chile - Sunset . . . . .	130

# List of Tables

1.1	A summary of the current white dwarf spectral classification scheme. (The P, H, Z, or X designator gets added after the main classification). Percentage representation is also displayed from Eisenstein et al. (2006).	5
2.1	Blue Object List (BOL) and Blue Object Close Pair List (BOCPL) Statistics - this table identifies the percentage contamination of my sample of blue objects due to quasars. “Bad” objects have not been removed from this sample. Note the ‘ideal’ case column assumes that the photometric target selection of quasars for spectroscopic follow-up within the SDSS program has been perfect (i.e. every quasar within the sample of blue objects has been targeted for spectroscopic follow-up based on its photometric properties and has been subsequently identified). The ‘Worst’ case column assumes that the spectroscopic follow-up of quasars within the SDSS program has not been biased based upon photometric data (any more than the effective biasing/probability of spectroscopic follow-up for my sample of blue objects). This table also includes an indication of the expected percentage of WDs within my sample based upon known WDs from Eisenstein et al. (2006), and assumes that the spectroscopic follow-up of objects within the SDSS program has not been biased in any way based upon photometric data towards the selection of WDs (i.e. constraints were purely chosen based upon expected quasar photometric signatures).	32
2.2	Blue Object Close Pair Data - SDSS	36
2.3	Blue Object Close Pair Data - SDSS (continued)	37
2.4	Double-Degenerate Data - SDSS	40
2.5	Telescope Instrument Properties	42
2.6	Double-Degenerate Data - Observations and Signal to Noise	48
2.7	Standard WD Stars	50
2.8	Double-Degenerate Data - Proper Motions	72
2.9	Double-Degenerate Data - Probability of Chance Alignment	73
3.1	Double Degenerate Data - Results	93

3.2	Published forms of the IFMR (linear gradient $m$ and $y$ intersection $c$ parameters). It displays statistics calculated from a monte carlo generated distribution of 25000 hypothetical WDs with parameters selected within their error limits. Firstly it displays the number of DD systems determined to have components with a common system age; [1] using an independent system age comparison, and [2] using the interdependent/-covariant system age difference derivation - from Figures 3.9, 3.10, and 3.11. Secondly, it displays the median system age difference, averaged across all systems, and the number of DD systems best satisfied by the published IFMR (i.e. having the lowest system age difference with the given published IFMR). . . . .	95
3.3	Additional (third party) Double Degenerate systems added to my mass distribution . . . . .	109
4.1	A table of my preliminary IFMR linear parameter derivations, [1] for all systems, and [2] excluding systems with an uncommon distance between components (DD-04 and DD-09) . . . . .	119



*"He had achieved harmony simply by accepting it."*

from Frank Herbert's *Children of Dune*

# 1

## Introduction

### 1.1 Overview

The stellar initial-final mass relation (IFMR) describes a theoretical correlation between small to intermediate mass stars on the main sequence and their final mass in the white dwarf (WD) state at the end of their evolution. It defines how much mass is lost during the lifetime of a star in this mass range, i.e. through the difference between the initial mass and the final mass.

The aim of this project is to probe our current estimate of the stellar IFMR using new observations of wide double-degenerate (white dwarf binary) systems uncovered in the Sloan Digital Sky Survey (SDSS) imaging. Current constraints in the form of the IFMR are almost exclusively derived from white dwarf members of open star clusters. These new data will provide an independent verification of the results obtained from open clusters.

The primary tasks in this research project involved, firstly, identifying double-degenerate candidates in imaging data from a pre-existing sky survey through the application of judiciously chosen colour, magnitude and angular separation selection criteria. Secondly, confirmatory follow-up spectroscopy of a selection of the brightest systems was obtained and these data processed using common reduction utilities. Thirdly, white dwarf effective temperatures, surface gravities, masses and cooling times were obtained from these data by comparing them to grids of synthetic white dwarf spectra and evolutionary models. Finally, these data were interpreted in the context of our current understanding of the form of the IFMR.

## 1.2 White Dwarf and their fundamental Physics

White dwarfs (WDs) are the end product of approximately 98% (Wood 1992) of main sequence (MS) stars. WDs do not generate energy by nuclear fusion, but instead dissipate their stored energy through thermal radiation released over a long period of time (Kippenhahn and Weigert 1990). WDs are extremely dense with  $\rho_{centre} \approx 10^7 gcm^{-3}$ . They are supported from further gravitational collapse by electron degeneracy pressure. Electron degeneracy pressure is a consequence of Pauli's exclusion principle. Pauli's exclusion principle states that particles of half integer spin (e.g. electrons) cannot occupy the same space (quantum cell), whose dimensions are constrained by Heisenberg's uncertainty relation to be  $\approx h^3$ , where  $h$  is Planck's constant. During the evolution of a star, when the core's primary fuel in the core has been spent, and it does not have a high enough central temperature to generate further energy from nuclear reactions, the core contracts to a higher density. When the particle density in the centre of the star is so great that free electrons (free from their nuclei, ionised under extreme pressure) fill all of the lowest energy quantum cells (limited by the exclusion principle), the remaining electrons are forced into higher momentum states, which results in a degeneracy pressure which halts further collapse.

It has been calculated that the pressure provided by the non-degenerate ions is negligible compared to that of the electrons (Fowler 1926). As degenerate electron velocities do not exhibit significant temperature dependency, the pressure countering gravitational collapse arises primarily due to the degenerate nature of the electrons and not the temperature of the WD (Chandrasekhar 1931). It was also calculated, counter-intuitively, that in WDs, stellar radius is inversely proportional to mass ( $R \propto M^{-1/3}$ ); this contrasts to stellar radius being positively correlated with mass, as is the case for MS stars.

The electron velocities increase in WDs with greater mass, to the level where they become relativistic. The star's hydrostatic balance ultimately becomes independent of radius. In cores of mass greater than the Chandrasekhar limit ( $> M_{Ch} \approx 1.459M_{\odot}$ ), the electron degeneracy pressure is unable to support against further collapse. The Chandrasekhar limit is defined by Equation 1.1 (Chandrasekhar 1939) below, where  $\mu_e$  is the average molecular weight per electron,  $\approx 2$ .

$$M_{Ch} = (2/\mu_e)^2 \times 1.459M_{\odot} \quad (1.1)$$

Chandrasekhar made the simplifying assumption that WDs were zero temperature objects ( $T = 0K$ ). More recent zero temperature structural calculations involving a more accurate treatment of the way in which gas particles interact (Salpeter 1961) indicate that for lower densities ( $\rho \approx 10^5 gcm^{-3}$ ) corresponding to lower mass WDs, the Coulomb electrostatic interactions between ions and electrons become significant resulting in less of a reduction in radius as proposed by Chandrasekhar's theory (Hamada and Salpeter 1961). Moreover, for higher densities ( $\rho \approx 10^9 gcm^{-3}$ ) corresponding to higher mass WDs, inverse beta decays occur, where electrons and protons merge to form neutrons, reducing the number of supporting electrons, and therefore lowering the limiting WD mass (Hamada and Salpeter 1961).

### 1.2.1 White Dwarf Cooling

WDs contain a degenerate interior with a non-degenerate ionised surface for the majority of their observable evolution ( $t_{\text{cool}} \approx 8\text{Gyr}$ ), during which time their effective temperatures fall from  $100000K$  to  $5000K$ . The interior of most WDs in the Galaxy, whose MS progenitors have had high enough mass to have already evolved into WDs and are not the byproducts of interacting binaries, and many WDs to be formed in the future (MS mass  $\gtrsim 0.5M_{\odot}$ ), are composed of carbon and oxygen. However, the visible exteriors of the majority of WDs are either predominately hydrogen or helium.

The interior of a WD is isothermal, due to the high heat conductivity of the degenerate electron gas. Gravitational contraction or the thermal motions of the degenerate electrons are not the source of WD radiation. Thermal energy cannot be extracted from degenerate electrons to produce the observed radiation, since they already occupy the lowest quantum states limited by the exclusion principle. The energy emitted by a WD comes from the non-degenerate nuclei in the core.

The cooling rate of a WD is dependent upon its radius and its chemical composition, including the thickness of the atmosphere. The size of the WD determines the surface area across which radiation may escape into space. Since higher mass WDs have smaller radii, they take longer to cool (decreased luminosity). However, WDs also lose energy through neutrino emission early in their life times (O'Brien and Kawaler 1996), when their temperatures are still very high,  $T_{\text{eff}} \approx 100000K$ .

For high mass WDs, the amount of energy lost through neutrino emission can exceed the thermal radiative luminosity by a factor of 5 – 10, so these cool more rapidly in their initial stages than lower mass objects. For example, a  $1M_{\odot}$  WD reaches  $\log[L_*/L_{\odot}] \approx -0.5$  or  $T_{\text{eff}} \approx 40000K$  after  $3 \times 10^6\text{yr}$  where as a  $0.4M_{\odot}$  WD will take  $1.5 \times 10^7\text{yr}$  to reach  $\log[L_*/L_{\odot}] \approx -0.5$  or  $T_{\text{eff}} \approx 40000K$  (Wood 1990).

Once the white dwarf has cooled significantly ( $T_{\text{eff}} \lesssim 5000K$ ), the ions in the central regions of the WD begin to crystallise (Lamb and van Horn 1975). Both the latent energy and the gravitational energy released during crystallisation (due to changes in the distribution of carbon and oxygen atoms as the oxygen crystallises at higher temperatures and shifts towards the centre of the star) reduces the cooling rate temporarily. For example, theoretically a  $0.6M_{\odot}$  CO WD takes  $\approx 20\%$  longer to cool to  $\log[L_*/L_{\odot}] = -4.5$ ,  $T_{\text{eff}} \approx 3800K$  (Isern et al. 1997) if crystallisation is taken into account. After crystallisation, the cooling rate is greater for higher mass WDs, where the heat capacity of the non-degenerate ions is proportional to  $T^x$  where  $x > 1$ .

As the degeneracy pressure support of the electrons is relatively weakly dependent on temperature, WDs cool at approximately constant radii. However, a  $0.6M_{\odot}$ ,  $T = 80000K$  WD with a (non-degenerate) helium surface layer of  $0.02M_{\odot}$  has a radius 36% larger than a pure C degenerate model (Hamada and Salpeter 1961). This effect is even greater with a surface envelope composed of hydrogen.

It has proved difficult to confirm the theoretical WD mass-radius relationship (e.g. Schmidt 1996; Provencal et al. 1997). This is because it is challenging to measure the mass and the radius independently with current instrumentation and the WD mass distribution is sharply peaked at around  $0.6M_{\odot}$  (Gennaro et al. 2008). The Hipparcos satellite has been used to establish very accurate distances to some of the closest WDs

in binaries, including Sirius B, 40 Eri, and Procyon B. This has allowed mass and radius to be reliably determined for these objects. The radius/mass values calculated are in reasonable support of theoretical mass-radius relations (Provencal et al. 1998).

### 1.2.2 White Dwarf Spectral Classification

WDs are primarily classified according to their optical spectra. The current classification scheme uses the prefix character ‘D’ to specify the degenerate nature of the object, which takes into account all WDs with  $\log g \gtrsim 7.0$  (McCook and Sion 1999, Wesemael et al. 1993). The next characters specify the composition of the atmosphere, from the most dominant element observable to the least dominant element observable. The character ‘A’ is used to designate hydrogen exhibited by strong Balmer lines, observed with temperatures  $5000K \lesssim T \lesssim 80000K$ . The character ‘O’ is used to designate helium where the HeII line at  $4686\text{\AA}$  is dominant with possible weak HeI lines at  $4471\text{\AA}$  and  $4921\text{\AA}$  including weak H, observed with temperatures  $T \gtrsim 50000K$ . The character ‘B’ is used to designate helium where only HeI lines are present, observed with temperatures  $12000K \lesssim T \lesssim 30000K$  (Sion et al. 1983). The character ‘C’ is used to specify atmospheres lacking in distinct hydrogen and helium features, observed with temperatures  $5000K \lesssim T \lesssim 12000K$ . It is presumed many of these are low temperature helium atmosphere WDs. In this scheme, for example, a hydrogen rich WD is classified as a DA, and a table giving the full classification scheme here is shown in Table 1.1.

A number ranging from 1 to 10, immediately after the atmospheric composition identification character, may be used to specify the temperature, where it approximates to  $50400/T_{eff}$ .  $T_{eff}$  here is generally calculated based upon the colour of the star (Wesemael et al. 1993). For example, DA4 would indicate a 12600K DA WD. Additional letters are used to specify secondary spectral characteristics, indicating the presence of additional but less abundant elements, and/or the presence of an observed magnetic field. The character Z is generally used to designate weak metal features. P or H are used to designate a polarised and unpolarised magnetic field respectively (Sion et al. 1983). The character Q is used to designate the presence of carbon.

For example, a DAO object exhibits strong H Balmer lines with a weak HeII absorption line at  $4686\text{\AA}$ . For example also, a hydrogen rich WD with a magnetic field is classified as a DAH. Objects with strange or unidentifiable spectra are given the classification X.

## 1.3 Stellar Evolution

### 1.3.1 Main sequence (MS)

Stars fuse hydrogen into helium in their cores for approximately 90% of their lives, where an equilibrium is maintained between the gravity of the star pulling its mass inwards, and the energy and pressure generated in the core by the nuclear fusion effectively pushing its mass outward. This phase is known as the Main Sequence

Classification	Observed spectral lines	Percentage Representation
DA	H Balmer only	85.9%
DB	HeI only (4471Å and 4921Å)	7.7%
DO	Strong HeII (4686Å), possible weak HeI (4471Å and 4921Å) and H Balmer	0.3%
DC	No features exhibited stronger than 5% of continuum flux level	3%
DQ	Carbon features present	3.1%
DZ	Metallic features	1.4%
DH	Magnetic, no observable polarisation	0.1%
DAB	Strong H Balmer with HeI (4471Å and 4921Å)	-
DAO	Strong H Balmer with HeII (4686Å)	-
P	Magnetic, observable polarisation	
H	Magnetic, no observable polarisation	
X	Peculiar or unidentifiable	
Z	Metallic features	

TABLE 1.1: A summary of the current white dwarf spectral classification scheme. (The P, H, Z, or X designator gets added after the main classification). Percentage representation is also displayed from Eisenstein et al. (2006).

(MS) on the Hertzsprung-Russell (HR) diagram (see Figure 1.1). The mass of a star determines its hydrogen burning MS, including stellar temperature, luminosity, and age. The nuclear reaction rates, being temperature dependent, are higher in the cores of more massive stars which have hotter and denser cores. For example,  $1.0M_{\odot}$  stars like our Sun have MS lifetimes of  $1.0 \times 10^{10}\text{yr}$ , while  $4.0M_{\odot}$  stars have MS lifetimes of only  $1.5 \times 10^8\text{yr}$  (Girardi et al. 2000). As a consequence of this and the finite age of the Galaxy, stars less than  $\approx 0.8M_{\odot}$  cannot yet have completed their main sequence lives and should not yet have evolved into WDs.

### 1.3.2 Red Giant Branch (RGB)

After most of the hydrogen has been transformed into helium in the core, nuclear energy release ceases, the radiative pressure decreases, and the core starts to resume gravitational contraction. The gravitational potential energy released in turn raises the temperature such that hydrogen fusion continues in a thin shell around the inert helium core. The stellar envelope expands as a result of the shell burning. The theoretical basis for this expansion of the star is still to be fully established, e.g. see Iben and Livio (1993). As the core of the star continues to contract, the shell luminosity increases and the envelope of the star expands. As the star's radius increases, its surface temperature decreases, and the star becomes a Red Giant on the Red Giant Branch (RGB) of the HR diagram (see Figure 1.1).

The outer layers of the star are cooled by the expansion of the envelope, which results in a change in its transparency to radiation. The envelope becomes convective under the buoyancy of its gas (Loore and Doom 1992, Stothers and Chin 1995). The cooling of the stellar layers reduces the number density of free electrons in the envelope gas, where they recombine with the hydrogen and helium nuclei. The number of  $H^{-}$  ions therefore decreases rapidly, and the stellar luminosity increases linearly with respect to  $T_{eff}$  due to the convection and its opacity lowers. Consequently, as the red giant star evolves it moves upwards in the HR diagram (Iben 1965). During this phase of evolution, a star may lose a significant amount of mass through a stellar wind, e.g.  $10^{-6}M_{\odot}\text{yr}^{-1}$  (Dupree 1986).

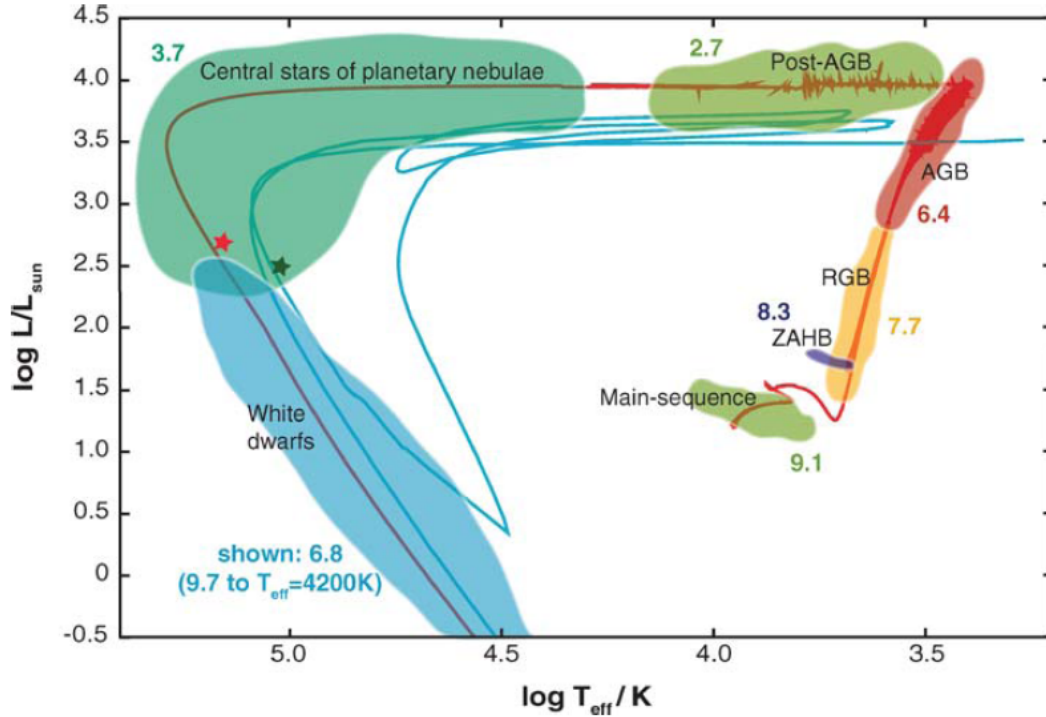


FIGURE 1.1: Diagram of Stellar Evolution from Herwig (2005). This diagram shows the evolution of a low-intermediate mass star, from the Main-sequence, to the Red Giant Branch (RGB), Horizontal Branch (ZAHB), Asymptotic Giant Branch (AGB), and finally the post-AGB phase with the formation of a central star of a planetary nebula (CSPN) afterwards becoming a WD.

The method of ignition of helium in the core is dependent upon the mass of the star, where if the initial mass is less than approximately  $2.0M_{\odot}$  the helium becomes electron degenerate by the time the star reaches the tip of the RGB. In these stars when the mass of the core eventually exceeds  $\approx 10\%$  of the total stellar mass, which is known as the Schonberg-Chandrasekar limit, the helium is ignited explosively (the helium flash) to form carbon and oxygen. In stars  $\gtrsim 2.0M_{\odot}$ , the core continues increasing in mass and temperature but avoids degeneracy. When it attains  $T \gtrsim 100$  million K, the helium ignites and begins burning to carbon. At this point, the star moves onto the core helium burning sequence.

### 1.3.3 Horizontal Branch

In both the lower mass and higher mass cases, stars then settle on either the horizontal branch (low metallicity population II) or the red clump (high metallicity population I) regions of the HR diagram, depending upon their primordial metallicity. The helium core burning phase of the star is the second longest after the hydrogen core burning phase of the star, lasting approximately one tenth of the hydrogen burning phase (Loore and Doom 1992). The majority of a star's luminosity on the horizontal branch

is provided by the hydrogen burning shell which remains active in this phase.

### 1.3.4 Asymptotic Giant Branch (AGB)

When the helium in the core is exhausted, the core contracts, and the rise in temperature due to release of gravitational potential energy increases the temperature of the surrounding helium. This ignites helium in a shell around an inert CO core. For stars  $\leq 8M_{\odot}$  carbon does not ignite, and the CO core contracts and becomes increasingly electron degenerate. The envelope then increases in radius, and decreases in temperature as a consequence. The star reaches the early-Asymptotic Giant Branch (AGB), where the outer hydrogen burning shell is initially dormant. During this phase, the helium shell dominates the nuclear energy release, burning outwards until it approaches the hydrogen/helium discontinuity. However, beyond this point the hydrogen shell re-ignites and becomes the dominant source of the stars luminosity (e.g.  $\approx 90\%$  Schoenberner 1983). During the thermally pulsing (TP)-AGB phase the burning of the hydrogen shell adds fuel to the now dormant helium shell. However, periodically, the star is interrupted by a thermonuclear runaway helium shell flash event. It is theorised that a significant number of these TPs occur during the late stages in the evolution of low and intermediate mass stars. During a TP the star is temporarily ( $\approx 500\text{yr}$ ) taken out of thermal equilibrium and the hydrogen burning shell is extinguished. When the star regains thermal equilibrium ( $\approx 20000\text{yr}$ ), the hydrogen shell starts to burn again. The peak flash luminosity increases with every cycle (Bloeker 1993).

During the evolution up the AGB, the envelope mass loss rate increases significantly. This ultimately results in an overall radius decrease and temperature increase, without a significant change in luminosity. As the remaining star is observed to have  $T_{\text{eff}} \gtrsim 30000\text{K}$  during the final envelope ejection and formation of a planetary nebula (PN) ( $\approx 50000\text{yr}$ ), it must lose envelope mass at an extremely high rate (e.g.  $10^{-3} - 10^{-4}M_{\odot}\text{yr}^{-1}$ ). Superwinds lasting  $\approx 1000\text{yr}$  have been proposed as providing these high rates of mass loss (Renzini and Voli 1981, Schoenberner 1983), where shock waves driven by stellar pulsation instabilities may explain their origin (Bowen 1988, Wachter et al. 2002). Indeed, CO line emission from circumstellar clouds support theoretical mass loss rates of  $10^{-4}M_{\odot}\text{yr}^{-1}$  at the end of the AGB (Knapp 1986).

### 1.3.5 White Dwarf Cooling Sequence

After the final envelope ejection, the remaining stellar cores exhibit high levels of elemental purity where the atmospheres are observed to be either hydrogen rich or helium rich. Strong gravitational fields are expected to cause elements heavier than hydrogen and helium to sink inwards in a relatively short period of time - as compared to the cooling time of the WD (Schatzman 1958). The ratio of the number of hot DAs to DOs observed ( $T_{\text{eff}} \gtrsim 40000\text{K}$ ) is 7 : 1, which may be compared with the number of hydrogen abundant to non-hydrogen abundant planetary nebula central stars (CSPN),  $\approx 2 : 1$ . Considering stars resulting in hydrogen rich WDs evolve approximately 3 times faster than the stars resulting in non-hydrogen rich WDs, these ratios are well matched. Figure 1.2 displays the spectrum of a CSPN for reference.



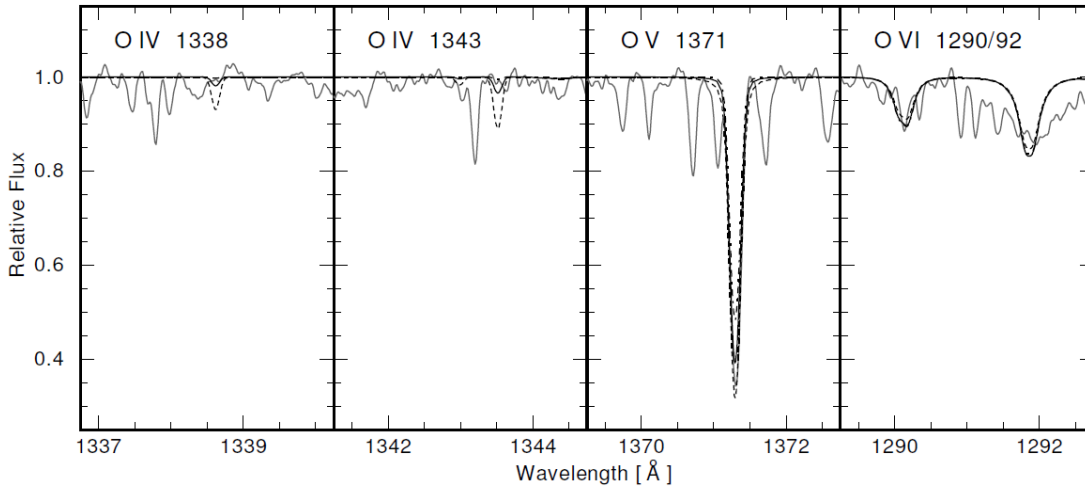


FIGURE 1.2: HST Spectrum of the helix nebula (NGC7293) planetary nebula central star, compared with three models with different effective temperatures (Traulsen et al. 2005).

Under a primordial evolution model, these two classes of WDs may be explained by two different AGB termination scenarios. If the star undergoes high mass loss rates on the AGB while burning hydrogen in its shell, as it is theorised it should do 80% of the time (Schoenberner 1983), then it will most likely evolve to become a hydrogen rich planetary nebula central star (CSPN), with a thick hydrogen layer ( $10^{-4}M_{\odot}$ ).

Alternatively, if the star undergoes high mass loss rates on the AGB during or immediately after thermal pulse before thermal equilibrium has been reestablished (without an active hydrogen shell), then the majority of the stellar hydrogen may be dispersed in the stellar wind. The resultant object is classified as a PG1159 star based upon the prototype PG1159 - a helium rich pre-degenerate star (in transition between being a CSPN and a hot WD). PG1159 type stars are extremely hot and have spectra showing helium as well as carbon and oxygen absorption lines. Upon cooling, gravitational settling is expected to remove remaining C and O in the atmosphere, resulting in first a DO star ( $45000 - 100000K$ ) - hydrogen deficient with strong HeII absorption lines, a DB star ( $12000 - 30000K$ ) - hydrogen deficient with strong HeI absorption lines, and then a DC ( $\lesssim 12000K$ ) - hydrogen deficient without helium absorption lines. In support of this theory, DOs are observed to have C and O abundances less than 0.1% of that of helium (Dreizler and Werner 1996).

### 1.3.6 White Dwarf Survey Statistics

#### WD Luminosity Function

The WD Luminosity function (LF) or number of WDs per unit interval in absolute magnitude for a given volume of space can be used to constrain the age and the star formation history of the Galactic disk (Winget et al. 1987, Wood 1990). The WD luminosity function and space density has been measured numerous times. One of the most widely referenced efforts involved the Palomar-Green (PG) survey of 1986



and yielded a space density of  $0.00049 \pm 0.00005 pc^{-3}$  (Fleming et al. 1986). Another, which was a by-product of the AAT faint QSO survey, yielded a DA space density of  $0.00060 \pm 0.00009 pc^{-3}$  and a scale height of  $275 \pm 50 pc$  (Boyle 1989). More recently, the WD space density has been estimated as  $0.0034 pc^{-3}$  (Leggett et al. 1998),  $0.0050 pc^{-3}$  (Holberg et al. 2002) and  $0.0046 \pm 0.0005 pc^{-3}$  (Harris et al. 2006). A latest estimate provided by Holberg et al. (2008) gives a WD space density of  $0.0048 \pm 0.0005 pc^{-3}$  and is directly measured from a volume-limited sample of local WDs, as opposed to other determinations of the local density

The estimated WD space density is a function of both the birth rate and the theoretical cooling time for a WD to fade below the limiting magnitude/colour of the sample. The DA birth rate in the local disk has previously been calculated as  $\chi_{WD} = 0.39 - 0.61 \times 10^{-12} yr^{-1} pc^{-3}$  (Fleming et al. 1986), with a total WD birth rate including helium WDs as  $\chi_{WD} = 0.49 - 0.75 \times 10^{-12} yr^{-1} pc^{-3}$ . More recent determinations are  $\chi_{WD} = 0.75 \pm 0.25 \times 10^{-12} pc^{-3} yr^{-1}$  (Liebert et al. 2005a) using the PG survey, and  $\chi_{WD} = 0.75 \pm 0.25 \times 10^{-12} pc^{-3} yr^{-1}$  (Vennes et al. 2002).

Early estimates of the formation rates of PNe were substantially higher than this. For example Pottasch (1996) calculated  $\chi_{WD} = 3 \times 10^{-12} pc^{-3} yr^{-1}$ . Frew (2008) however summarises the historical evolution of both planetary nebula formation rates and WD formation rates, while providing his latest estimates of the former,  $0.8 \pm 0.3 \times 10^{-12} pc^{-3} yr^{-1}$ . He finds that his value is in very good agreement with the WD birthrates determined by both Vennes et al. (2002) and Liebert et al. (2005a). Taking into account the assumption that WD production also involves other post-RGB processes which do not involve creation of a PNe, the WD birth rate is expected to be slightly higher than the PNe birth rate but within the errors of these PNe/WD birth rate estimates. These channels include AGB-manqué evolution, where H-deficient stars do not pass through the AGB phase and are characterised by a lack of thermal pulses, and ‘lazy PNe’, with central stars that evolve too slowly to ionise the ejected nebula shell.

It is known that the space density of WDs drops off steeply below  $M_v \approx 16.0$ . This is attributed to the finite age of the Galactic disk, where WDs have not had sufficient time to yet cool below these luminosities (Liebert et al. 1988). Using WD cooling models and the observed WD LF, it has been calculated that star formation began in the Galactic disk  $8 \pm 1.5 \times 10^9$  years ago (Leggett et al. 1998), or  $10_{-1}^{+3} \times 10^9$  years ago (Knox et al. 1999) with a broader estimate of  $7 - 10$  Gyr Liebert et al. (1988).

### WD Mass Function

Latest determinations of the field white dwarf mass distribution (for single stars), or number of objects per unit interval in mass, have been obtained using SDSS data (Kepler et al. 2007) and confirm earlier results that it peaks sharply at  $0.6 M_{\odot}$ . See Figure 1.3, where it can be noted also that a low mass peak is present, and is product of He-cores arising from close binary evolution. The shape of the WD mass function is believed to be due to the form of both the stellar initial mass function and the stellar initial-final mass relation (IFMR). The initial mass function favours the production of lower mass stars, while the IFMR links these to the formation of less massive WDs.

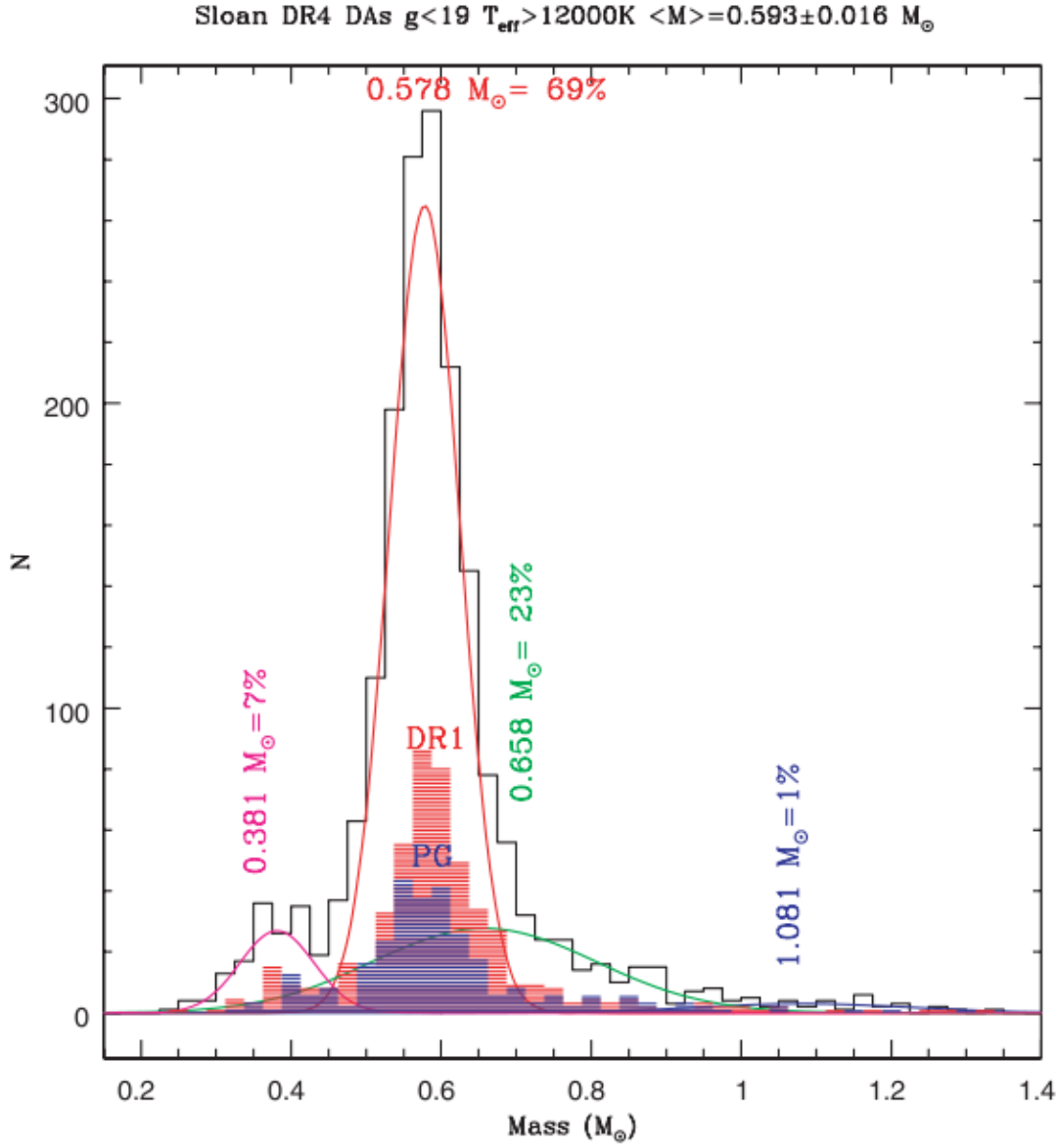


FIGURE 1.3: The SDSS WD mass distribution as determined by Kepler et al. (2007). Histogram for the 1859 DA stars brighter than  $g = 19$  and hotter than  $T_{\text{eff}} = 12000\text{K}$ , compared to the PG survey published by Liebert et al. (2005a) and the SDSS DR1 sample published by Madej et al. (2004). Gaussian fits are also shown. The bins are  $0.025 M_{\odot}$  wide.

## 1.4 The stellar initial-final mass relation (IFMR)

### 1.4.1 A light introduction to the stellar IFMR

The benefits of a solid understanding of the form of the stellar initial-final mass relation (IFMR) have been well documented in the literature. The nature of the relationship between the initial mass  $M_{\text{init}}$  of a star and the final mass  $M_{\text{final}}$  of the star has been of interest for many decades (Weidemann 1981). The hypothesis that stars with MS mass much greater than the Chandrasekhar limit  $M_{\text{init}} \gg 1.4M_{\odot}$  can still lead to the formation of WDs was confirmed by Weidemann (1977). Koester and Reimers (1981) conducted a search for WDs in young open clusters where only stars with  $M_{\text{init}} > 4 - 5M_{\odot}$  had yet evolved beyond the main sequence. Inferring that WDs produced within the cluster NGC 2516 would generally have to have come from stars at least as massive as the current highest mass (most luminous) stars within this population, they concluded that they had discovered a number of WDs whose progenitors were approximately  $M_{\text{init}} \approx 6 - 8M_{\odot}$  (Reimers and Koester 1982).

As discussed previously, the majority of a star's envelope is lost after the main sequence phase, primarily during the ascent of the asymptotic giant branch (AGB) (Herwig 2005, Iben and Renzini 1983). As these late stages in a star's evolution remain extremely challenging to model (Marigo and Girardi 2007) empirical data are required to tease out the details of this mass loss process. Observations of circumstellar shells and planetary nebulae around pre-WD stars provide some handles on the rate of AGB mass loss (Weidemann 2000). The mapping of the masses of WDs to their progenitor masses through the IFMR is the method of choice for assessing quantitatively, at least, the total stellar mass loss and can also be useful for gaining some insight into the mechanisms behind this mass loss.

The total amount of mass lost by stars has a strong bearing on our understanding of the minimum mass of a Type II (core collapse) supernova (SNe) progenitor (Williams et al. 2009) and thus the frequency of these events. Moreover, the vast quantity of envelope gas expelled by stars during their final evolutionary phases contains the products of nucleosynthesis (e.g. C, N, O and s-process elements) so a sound understanding of the form of the IFMR is very important for refining models of stellar and Galactic chemical evolution. The form of the top end of the IFMR also has some relevance to cosmology through type Ia SNe which are generally considered to involve the thermonuclear detonations of high mass CO white dwarfs (Howell et al. 2006).

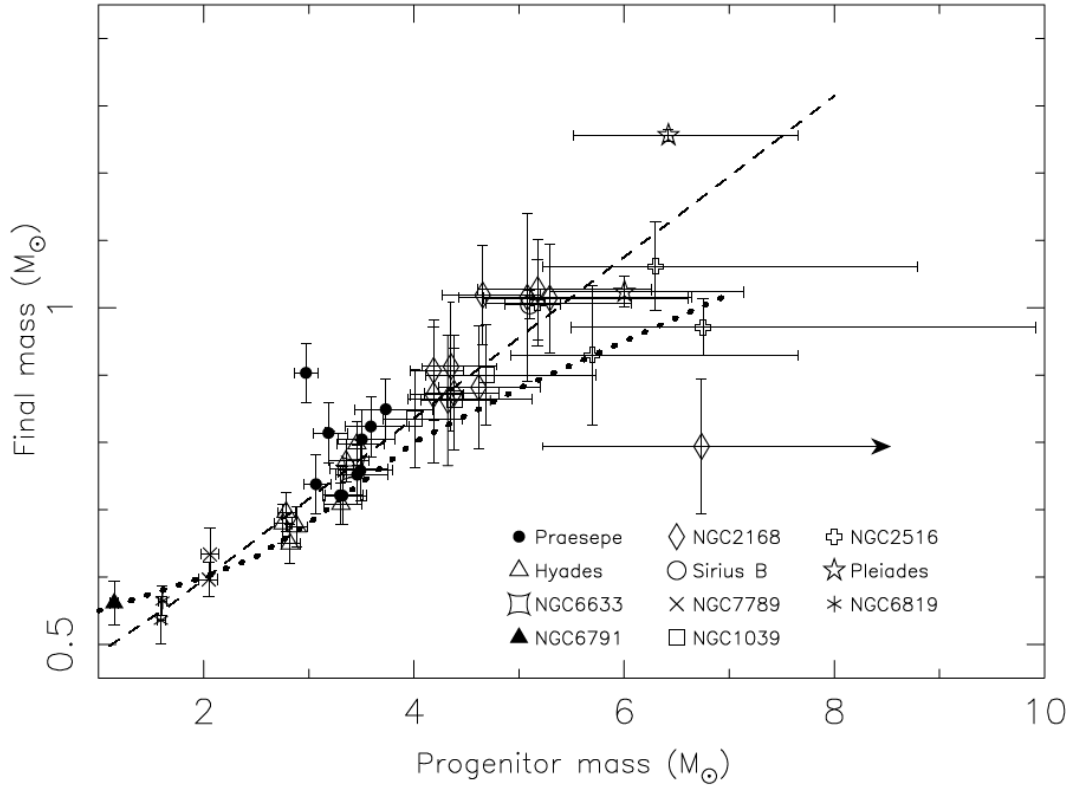


FIGURE 1.4: The IFMR (Casewell et al. 2009). A state-of-the-art representation of the known form of the IFMR, showing the revised locations of the Praesepe white dwarfs in initial mass-final mass space (filled circles). The locations of the degenerate members of the NGC 6633 (square star), NGC 7789 (cross), NGC 6819 (asterisk), Hyades (open triangles), Sirius binary system (open circle), the Pleiades (open stars), NGC 2168 (open diamonds), NGC 1039 (open squares), NGC 6791 (filled triangles) and NGC 2516 (open ‘+’ signs) are also shown. The relation of Weidemann (2000) (dotted line) and a revised linear fit to 41 white dwarfs (dashed line) are overplotted. The radial velocity variable, WD0837+185 is labelled.

### Stars on the tip of the AGB

The relationship between the AGB core mass and the AGB tip luminosity, which is predicted by standard stellar evolutionary models, has been used in the past to place constraints on the form of the IFMR (Weidemann 1987). In this approach, the brightnesses of stars towards the tip of the AGB in very rich clusters are measured and their absolute magnitudes and luminosities then derived. Subsequently, assuming strict adherence to a core - mass luminosity relation, the masses of their cores is calculated. A WD final mass of  $M_{\text{final}} = 0.8M_{\odot}$  was estimated for a progenitor of  $M_{\text{init}} = 4.5M_{\odot}$  in the NGC 1866 cluster of the LMC using this method (Weidemann 1987). However, the assumption of a classical core - mass luminosity relation is stretched somewhat by the levels of overshoot adopted in modern theoretical AGB models (Weidemann 2000). Other methods have since taken precedence in the determination of the IFMR, such as the open cluster method described below.

#### 1.4.2 Using open clusters to map the IFMR

Arguably the best current way to map the form of the IFMR is through studying WDs in open cluster systems. Here, all stars have a common age, and both this and the distance to these stars can be determined from the brighter members of the population. Deriving the initial progenitor mass,  $M_{\text{init}}$ , of a cluster WD first involves obtaining optical spectroscopy so that the relative shape of its broad Balmer lines (due to the atmospheric distortion under gravity of the absorption of light through its hydrogen atmosphere) can be assessed. Generally, the lines  $\beta$  through to 8 are chosen for this purpose (i.e.  $\beta$ ,  $\gamma$ ,  $\delta$ ,  $\epsilon$ , and 8). These observed Balmer lines are compared to synthetic profiles (Bergeron et al. 1992) to extract estimates of the surface gravity,  $\log g$ , and effective temperature,  $T_{\text{eff}}$ . WD evolutionary mass-radius models are then used to determine the mass  $M_{\text{final}}$  and cooling age  $t_{\text{cool}}$  of the WD.  $M_{\text{final}}$  is strongly dependent upon  $\log g$  while  $t_{\text{cool}}$  is more dependent upon  $T_{\text{eff}}$ . Finally, the cooling age is subtracted from the cluster age to obtain an estimate of the progenitor lifetime, and theoretical stellar evolutionary models are then used to determine the initial mass  $M_{\text{init}}$  of the star (Weidemann 2000).

There are a number of potential sources of error in this method of mapping the IFMR, ranging from uncertainties in the open cluster ages to the limitations in the physical realism of the WD atmosphere and evolution models. It is known that there are still significant systematic discrepancies in the atmospheric models in certain effective temperature ranges e.g. spectroscopic surface gravity measurements at  $T_{\text{eff}} \lesssim 12000K$  (Kepler et al. 2007). Open clusters also must be chosen judiciously as they vary in their usefulness for constraining the form of specific areas of the IFMR. Younger populations are most useful for constraining the high mass end of the IFMR, as their high mass white dwarfs are still relatively hot and therefore bright ( $M_{\text{WD}} \gtrsim 4M_{\odot}$ ). Older open clusters,  $\gtrsim 1$  Gyr, are better suited for constraining the intermediate and lower mass end of the IFMR, as they contain WDs which have had relatively large main sequence life times, and are therefore of relatively low mass ( $M_{\text{WD}} \lesssim 2M_{\odot}$ ).

The age of a cluster, which is usually known a priori, is defined assuming that

the vast majority of stars within the system have evolved from a single burst of star-formation in a molecular cloud of near uniform composition (Bate et al. 1995). It is generally calculated using photometric data, taking into account the distance and the reddening due to foreground interstellar dust and gas, where observed colours and magnitudes (e.g.  $B-V, V$ ) at which stars move off the main sequence are matched to the predictions of stellar evolutionary models. Similarly, the distance can be derived from the offsets between the apparent magnitudes of stars as predicted by the model and their observed magnitudes (e.g.  $V$  magnitude), allowing for any foreground reddening.

### 1.4.3 IFMR Calculations To Date

Empirical based determinations of the form of the IFMR have not always sat well with expectations based on stellar evolutionary models. For example, estimates based on stars at the tip of the AGB, discussed in section 1.4.1, failed to lead to mass loss measurements in agreement with theoretical predictions. Furthermore, empirical determinations based on different approaches produced mixed results e.g. mass loss estimated from planetary nebula (PNe) formation led to final masses that were inconsistent with those obtained from open clusters (Weidemann 1981). In the early 1990s WD evolutionary models saw substantial improvements in their physical accuracy (Wood 1992) which allowed for more robust determinations of their ages/cooling times and masses from spectroscopic effective temperature and surface gravity measurements. The revised models were widely adopted in the study of WDs within open cluster systems. Volker Weidemann published a summary of the state of empirical based knowledge of the IFMR to 2000 (Weidemann 2000). By this time the WD populations of several open clusters had been included in attempts to map the relation. First, the Hyades WDs had been the subject of multiple studies and successfully harvested for data within the range  $2.9M_{\odot} \leq M_{\text{init}} \leq 3.5M_{\odot}$ . Second, the WDs of the NGC 3532 cluster had been targeted and provided data for the progenitor range  $3.5M_{\odot} \leq M_{\text{init}} \leq 5M_{\odot}$ . Third, the WD members of the Pleiades and NGC 2516 had been studied and found to have progenitor masses in the range  $6M_{\odot} \leq M_{\text{init}} \leq 7M_{\odot}$ . Fourth, studies of the 4Gyr old cluster M67 had resulted in a single additional data point at  $M_{\text{init}} \approx 1.35M_{\odot}$ .

However, since Weidemann's 2000 summary on the IFMR, there has been a substantial increase in the number of known cluster WDs, which are suitable for further advancing our understanding of the relation's form. In particular, new datapoints have been added to the following mass ranges: 1)  $3_{\odot} \leq M_{\text{init}} \leq 4_{\odot}$  using Praesepe cluster WDs (Casewell et al. 2009, Claver et al. 2001, Dobbie et al. 2004; 2006, Williams et al. 2004), 2)  $3.6_{\odot} \leq M_{\text{init}} \leq 4.6_{\odot}$  and  $4.4_{\odot} \leq M_{\text{init}} \leq 4.6_{\odot}$  using NGC 3532 and NGC 2287 cluster WDs respectively (Dobbie et al. 2009), 3)  $3.5_{\odot} \leq M_{\text{init}} \leq 4.75_{\odot}$  using NGC1039 WDs (Rubin et al. 2008), and 4)  $M_{\text{init}}$  between  $2.8_{\odot}$  and  $3.4_{\odot}$  using 18 NGC 2099 (M37) WDs (Kalirai et al. 2005a). Williams and Bolte (2007) have also spectroscopically studied WD candidates of the NGC 6633 and NGC 7063 clusters providing a single additional point to the IFMR at  $M_{\text{init}} \approx 3.5M_{\odot}$ .

There has also been a substantial number of new data points added towards the upper end of the IFMR, which is particularly pertinent to clarifying the supernova progenitor lower mass limit. Williams et al. (2009) have identified and spectroscopically

investigated twelve WDs in the young, rich cluster NGC 2168. Assuming a simple linear form to the IFMR, they extrapolated to  $M_{\text{final}} \simeq 1.4M_{\odot}$  to infer an upper initial mass limit for the production of a WD of  $6M_{\odot} \leq M_{\text{up}} \leq 9M_{\odot}$  taking into account all available open cluster IFMR data. Dobbie et al. (2006) had previously established an upper mass limit of  $6.8M_{\odot} \leq M_{\text{up}} \leq 8.6M_{\odot}$ . At the low mass end of the IFMR ( $M_{\text{init}} < 2.5M_{\odot}$ ,  $M_{\text{final}} < 0.6M_{\odot}$ ), Kalirai et al. (2007) and Kalirai et al. (2008) have added a small number of important new data points based on observations of WDs in NGC 6791, NGC 7789 and NGC 6819 e.g.  $M_{\text{init}} \approx 1.16M_{\odot}$  –,  $M_{\text{final}} \approx 0.53M_{\odot}$  and  $M_{\text{init}} \approx 1.6M_{\odot}$  –  $M_{\text{final}} \approx 0.54M_{\odot}$ .

### Limitations on IFMR calculations to date

This solid recent progress in mapping the form of the IFMR is due to greater access to mosaic imagers and 8/10m telescopes with blue sensitive spectrographs. This has allowed a larger number of clusters to be investigated to very faint magnitude limits (Kalirai et al. 2007). Recent work by Dobbie et al. (2009), using data from approximately 50 WDs in 11 open clusters, suggests that the bulk of stars follow closely a monotonic relation (see Figure 1.5). Tentative evidence has also been found suggesting that the IFMR is somewhat steeper in the range  $3M_{\odot} < M_{\text{init}} < 4M_{\odot}$  than elsewhere. This is consistent with theoretical expectations and the sharp drop seen in the number density of objects on the high mass side of the main peak in the field WD mass distribution (Ferrario et al. 2005). However, it has been questioned as to whether such an inference can be drawn from the data subject to its current uncertainties (Salaris et al. 2009).

Despite clear headway, the IFMR remains sparsely sampled in several important initial mass regimes. For example, there are only two secure data points at  $M_{\text{init}} \gtrsim 5.5 - 6M_{\odot}$ . Thus, the form of the upper IFMR remains somewhat uncertain. Furthermore, there are still only a handful of objects at  $M_{\text{init}} \lesssim 2.5 - 3M_{\odot}$  yet understanding the fate of the numerous stars with masses more closely resembling that of our Sun is of significant interest.

In the open cluster approach, mapping the higher initial mass regime of the IFMR requires targeting young ( $\approx 100 - 300$  Myr) populations that are sufficiently rich to have harboured a substantial number of stars with  $M_{\text{init}} \gtrsim 5 - 6M_{\odot}$  and where the progeny of these stars are still relatively young, hot and luminous. Investigation of the lower initial mass regime requires targeting old ( $> 1 - 2$  Gyr) open clusters, where populations are sufficiently mature such that stars with  $M_{\text{init}} \lesssim 2.5 - 3M_{\odot}$  have evolved beyond the main sequence. Such clusters are comparatively rare so to identify good examples it is necessary to probe large volumes of space. Consequently, while high signal-to-noise optical spectroscopy is critical to determining WD masses and cooling times, the great distances involved make it extremely challenging to obtain the necessary data even with today's large telescopes.

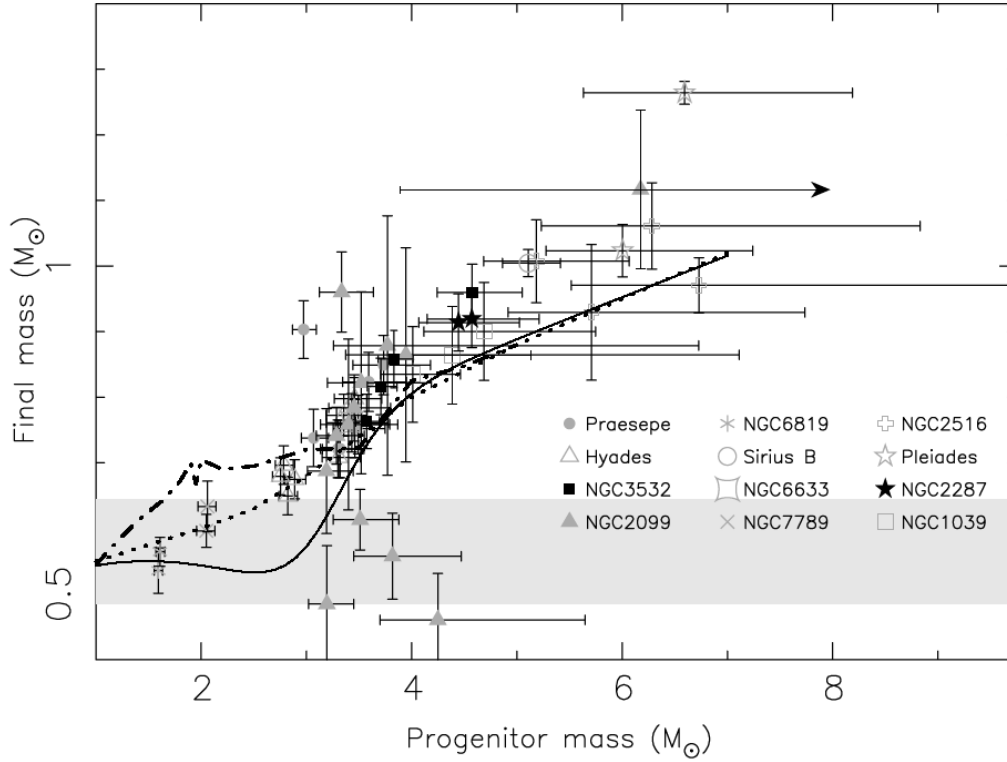


FIGURE 1.5: The IFMR (Dobbie et al. 2009). Another state-of-the-art representation of the known form of the IFMR, showing that the bulk of stars appear to follow fairly closely a monotonic relation. The locations of the white dwarf members of NGC 3532 and NGC 2287 in initial mass-final mass space. Data points from a number of other populations with metallicities close to the solar value are also shown. The theoretical IFMR of Marigo and Girardi (2007) (dot - dashed heavy line), the semi-empirical IFMR of Weidemann (2000) (heavy dotted line) and the initial mass-core mass at first thermal pulse relation from Karakas et al. (2002) (medium solid line) are overplotted. The peak in the field white dwarf mass distribution ( $\pm 1\sigma$ ) is represented by the band of grey shading.



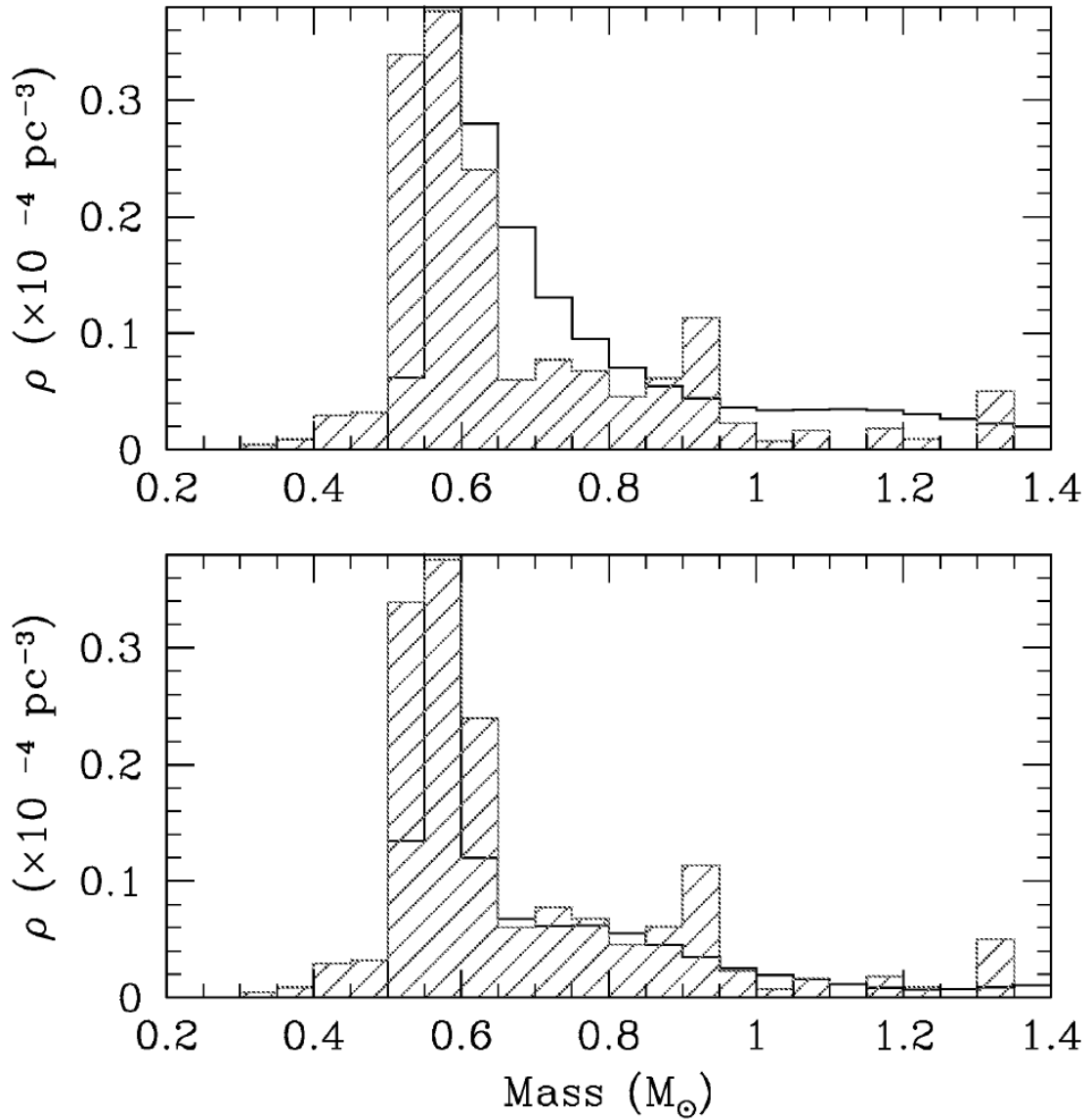


FIGURE 1.6: Ferrario et al. (2005) volume corrected mass distribution of field WDs in the Palomar-Green survey (Liebert et al. 2005a) (shaded histogram) for stars hotter than 13000K with the best linear IFMR fit model (top panel) and the IFMR with curvature (bottom panel). WDs with masses less than  $0.5M_{\text{odot}}$  are believed to be helium WDs resulting from close binary evolution and are not modelled in this paper

## Using Double-Degenerate systems to probe the IFMR

Multiple stellar systems have the potential to improve our understanding of the evolution of stars, including testing our knowledge of the form of the IFMR (Greenstein et al. 1983). Like open cluster systems, their components share a common system age and this factor can, in suitable cases, be exploited for similar purposes. They also have the capacity to provide constraints on the birth and dynamical evolution of stellar binaries and the mechanisms behind the production of magnetic WDs (Girven et al. 2010).

Greenstein et al. (1983) attempted to use a wide WD+WD binary system to constrain the IFMR but both the quality of their data and models at this time led to results with very large uncertainties. A small number of additional hot double-degenerate (DD) systems have been discovered since but generally the component masses and their ratios have not been particularly suitable for placing meaningful constraints on the system age (Jordan et al. 1998b). Alternatively, the systems have not been wide enough to be confident that the components have evolved essentially as separate entities (Holberg et al. 1995). The radii of AGB stars can extend up to 4-5AU so in binary systems with primordial separations of  $a \lesssim 10\text{AU}$  the components could potentially experience Roche Lobe overflow and exchange significant quantities of mass. Nevertheless, Finley and Koester (1997) were able to demonstrate the potential of wide DD systems for probing the form of the IFMR by obtaining a firm data point in the central region of the IFMR with  $3.6M_{\odot} \leq M_{\text{init}} \leq 4M_{\odot}$  and  $0.76M_{\odot} \leq M_{\text{final}} \leq 0.82M_{\odot}$ , through their study of PG 0922+16.

The identification of additional wide WD+WD pairs which exhibit common proper motions, such that they are highly likely to be physically associated and thus co-eval, is highly desirable so that this method can be more fully exploited. Noting that mass loss, primarily during the AGB phase (and being more pertinent for higher mass WDs, subject to the form of the IFMR), could lead to the expansion of the orbit by up to a factor 5-10, so to be confident that two WDs are unlikely to have exchanged mass in the past, I seek systems with a minimum projected separation of  $a \approx 100\text{AU}$ . This is satisfied by visual binary pairs with an angular separation  $> 1''$  and which lie at  $d \gtrsim 100\text{pc}$ .

The most interesting systems for investigating the form of the IFMR are those in which the ratio of the masses of the component WDs is relatively low, for example, a high ( $M_{\text{final}} > 0.9M_{\odot}$ ) and low ( $M_{\text{final}} < 0.7M_{\odot}$ ) mass pairing. However, the details of this approach depend upon the masses of the components. In all cases, the mass  $M_{\text{final}}$  and cooling age  $t_{\text{cool}}$  for both components are first derived using theoretical WD atmospheric and cooling models, where the effective temperature and surface gravity are measured from the line profiles of their spectroscopic observation. If one of the component WDs is found to have a mass corresponding to a part of the IFMR which is currently well delineated by data, its initial mass, main sequence lifetime and the total system age can be estimated. Subsequently, the main sequence life time and hence initial mass of the second component is calculated by subtracting its cooling time from the system age. Alternatively, if one of the component WDs is found to be of particularly high mass (ie.  $M_{\text{final}} > 1M_{\odot}$ ), the DD system age is largely constrained

by the cooling age  $t_{\text{cool}}$  of the higher mass WD component, since the main sequence life time is significantly shorter than that of the lower mass component, in some cases almost negligible (e.g. Finley and Koester 1997). The main sequence lifetime of the younger component is approximately the difference between the cooling ages of the two WDs ( $t_{\text{MS}} = T_{\text{cool1}} - t_{\text{cool2}}$ ). Finally, the main sequence (initial) mass  $M_{\text{init}}$  of the younger component is inferred from its estimated main sequence life time  $t_{\text{MS}}$  using main sequence stellar evolution models.

#### 1.4.4 Sources of Uncertainty

##### Theoretical models of stars and WDs

Current techniques for determining the form of the IFMR rely upon theoretical stellar evolutionary models to determine the mass of a star for a given lifetime. Poorly understood processes occurring within stars, especially the level of convective overshooting, affect the precision to which we can derive the form of the IFMR. This limits our ability to study in detail the dependencies of the form of the IFMR on parameters such as metallicity (Salaris et al. 2009). It is suggested that systematic uncertainties of this nature impact our ability to make secure assertions that the IFMR departs from a non-linear form. The main source of uncertainty highlighted by Salaris et al. (2009) is that related to the cluster age estimates.

A number of investigations have also examined the level of uncertainty which stems from the choice of synthetic line profile grid used in determining the effective temperatures and surface gravities of WDs. These have looked at magnitudes of the systematic offsets in  $\log g$  and  $T_{\text{eff}}$  estimates for samples of WDs that are common to multiple studies. For example, Liebert et al. (2005a) undertook a comparison between their effective temperature and surface gravities measurements for WDs in the PG survey and those derived independently by Finley and Koester (1997), Vennes et al. (1997), Marsh et al. (1997), Homeier et al. (1998), and Koester et al. (2001). Figure 1.7 shows the results of this procedure, in which they found systematic departures in  $\log g / T_{\text{eff}}$  from their estimates of 0.06 dex / 1.7%, 0.03 dex / 0.6%, 0.1 dex / 3.3%, 0.08 dex / 0.3%, and 0.08 dex / 0.6%, respectively.

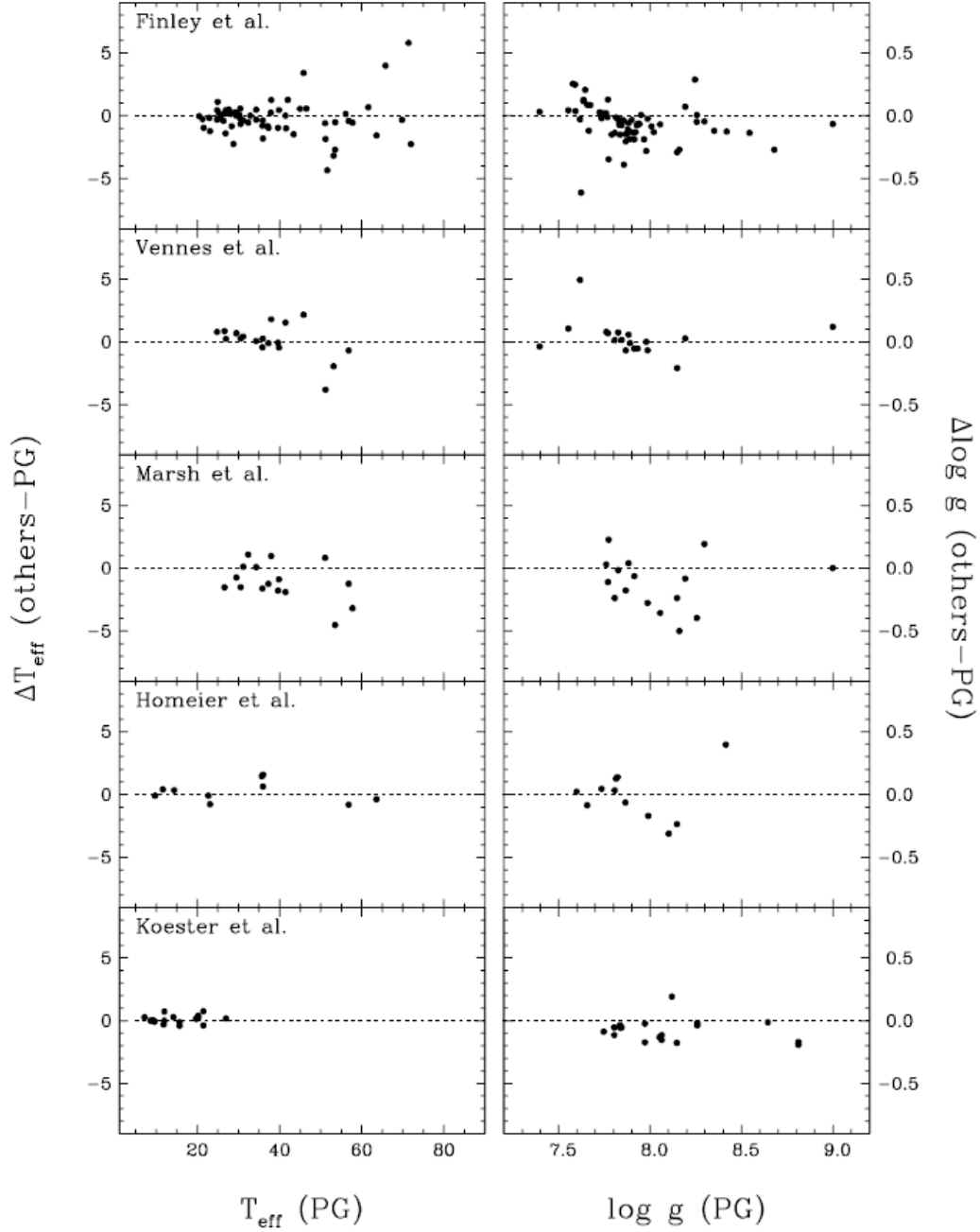


FIGURE 1.7: The Liebert et al. (2005a) comparison of their  $T_{\text{eff}}$  and  $\log g$  determinations of PG stars in common with the data sets of Finley and Koester (1997), Vennes et al. (1997), Marsh et al. (1997), Homeier et al. (1998), and Koester et al. (2001). In each panel they plot the differences between these investigations and their results (PG) as a function of their determinations of  $T_{\text{eff}}$  or  $\log g$ . Effective temperatures are in units of  $10^3 K$ .

### Open Cluster age and distance calculations

Robust open cluster age and distance estimates are integral to our understanding of the IFMR as the majority of IFMR points are derived using these populations. Distance calculations must be adjusted for estimated interstellar reddening, which can add significantly to their uncertainties. With the increasing availability of more powerful ground based telescopes however, refinement of some cluster age estimations using the lithium depletion boundary technique (Stauffer et al. 1998) will be possible, where the depletion results from the slow nuclear burning of this element deep within cores of the lowest mass stellar and largest mass substellar members.

### Metallicity and Magnetism effects on IFMR

Theoretical models of stellar evolution predict some dependence of the form of the IFMR on stellar metallicity (ratio of hydrogen versus heavier elements) based upon subtle differences in the processes that occur during the AGB phase (e.g. third dredge-up, mass loss). Exploring observationally the relationship between the IFMR and the system metallicity is therefore a goal of astronomers working on understanding the IFMR. It is quite likely that the uncertainties in our current understanding of the form of the IFMR exceed the effects which arise as a result of differing metallicities. It has been argued that there is no evidence yet for a metallicity dependence of the IFMR to within the current observational errors, at least for  $M_{\text{init}} \approx 3$  (Williams 2007).

Magnetism of WDs has also been proposed as a potential contributor to variations in the IFMR. Wickramasinghe and Ferrario (2005) surmise that the presence of a magnetic field may affect the convective dredge-up process which retards the growth of the CO core during the AGB phase of evolution. This could lead to larger white dwarfs than expected from an IFMR which is delineated largely by non-magnetic stars. Indeed, the apparently single high field magnetic WD EG 59 ( $B \sim 3\text{MG}$ ), which is a member of Praesepe, appears to be somewhat too massive, relative to similarly aged WDs in the cluster (e.g. Claver et al. 2001).

## 1.5 Thesis Outline

This project involves the identification of candidate wide DD systems within the Sloan Digital Sky Survey imaging data. For a selection of bright candidates I have obtained follow-up optical spectroscopy, which has been reduced using common utilities, and interpreted with the help of pre-existing WD atmospheric and cooling models.

The low resolution follow-up spectra are necessarily of high signal to noise and span the range  $3700\text{\AA}$  to  $5200\text{\AA}$  (which encapsulates the  $\beta - 9$  Balmer lines of a DA WD). Subsequently, I have used the SDSS DR7 imaging, Palomar Sky Survey photographic data and frames obtained with the Wide Field Camera (WFC) on the Isaac Newton Telescope to assess the proper motions of the components of each double-degenerate system. In addition to using some of these binaries to probe the IFMR, I have also constructed a preliminary DD mass function for the components of the systems.

In the next chapter, I outline my target selection process, my observations, data reduction, and data modelling processes. In Chapter 3 I analyse each system in turn, discussing my results in the context of the IFMR and stellar evolution. In the final Chapter I summarise my main results, and outline future work to extend my initial findings.

*"All proofs inevitably lead to propositions which have no proof! All things are known because we want to believe in them!"*

The Lady Jessica, to Bene Gesserit delegation, from Frank Herbert's Children of Dune

# 2

## Data

## 2.1 The identification of candidate wide double-degenerate systems

### 2.1.1 Summary

A list of candidate wide double-degenerate systems has been extracted from the SDSS DR7 sky survey database using an SQL query. This was filtered by comparing it to a list of known quasars within the SDSS database and by undertaking a visual inspection to remove spurious pairings. Subsequently, high signal-to-noise, low resolution optical spectroscopy was obtained for these systems which ultimately allowed me to both probe the IFMR and to construct a preliminary mass distribution for WDs in wide double-degenerate systems. The spectroscopic follow-up was prioritised, by constraints on time of year, the location of the object in the sky, weather, seeing, and the brightness/exposure times. As a result, brighter, more widely separated systems were favoured. A total of 12 pairs were observed. Each were confirmed to contain WDs and are likely to be physically associated double-degenerate binaries.

### 2.1.2 The SDSS Data Release 7

The SDSS is a large scale imaging survey with fiber spectroscopic follow-up (Abazajian et al. 2009). The 7th public data release of the data (DR7) includes imaging for a total of 11663 sq. deg. of sky and has photometry in five bands,  $u$  (3551Å),  $g$  (4686Å),  $r$  (6165Å),  $i$  (7481Å), and  $z$  (8931Å), for 357 million unique cataloged objects. Figure 2.1 displays the passbands of the SDSS filter set. The SDSS data extends to  $5\sigma$  limits at  $u$ ,  $g$ , and  $r$  of 22.0, 22.2, and 22.2 respectively. However, my faint magnitude selection criteria was much brighter than these limits. The imaging pixel size is 0.396'' and the

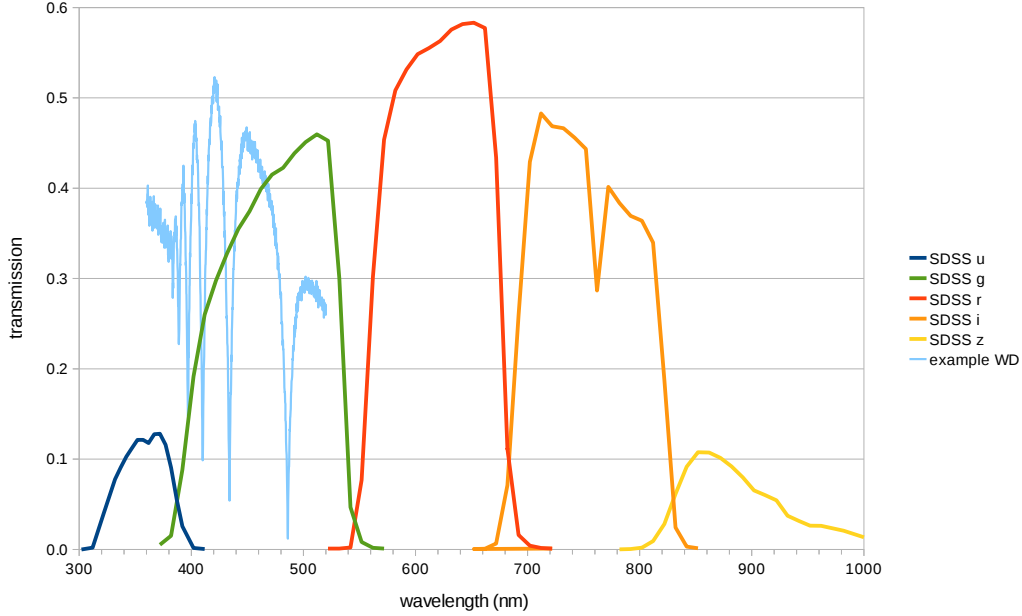


FIGURE 2.1: A graph of the passbands of the SDSS filters ( $u$ ,  $g$ ,  $r$ ,  $i$ ,  $z$ ) with a WD spectrum overlayed

typical width of the point spread function (PSF) is  $\sim 1.4''$ . The SDSS DR7 also includes spectroscopic data for 1.6 million objects. This data was used only to confirm (when available) that my blue candidates were WDs.

The SDSS DR7 mainly covers the northern Galactic cap region of the sky which is not heavily affected by the interstellar dust of the Milky Way. This is greatly beneficial for galaxy studies which was one of the SDSS's primary science missions. As the SDSS also was designed for quasar detection its wavelength coverage extends to the blue end of the visible spectrum, making it well suited to the photometric identification of WDs with  $T_{\text{eff}} > 8000\text{K}$ . The SDSS data can be accessed in a number of different ways, all of which operate through a dedicated SQL query server (SDSS Sky Server). This included the SDSS DR7 Image List Tool (<http://cas.sdss.org/dr7/en/tools/chart/list.asp>) - for generating coloured images of target lists, the SDSS DR7 Finding Chart Tool (<http://cas.sdss.org/dr7/en/tools/chart/chart.asp>) - for providing database lookup on individual SDSS objects, and their science front end (CAS). The various SQL queries I used in the extraction of SDSS photometry are outlined in the Appendix Section A.2.1 and one of which is shown below in Section 2.1.3.



### 2.1.3 Initial Identification of candidate wide DD systems

#### The selection of Blue Objects (BO)

The SDSS has unearthed a vast number of spectroscopically confirmed WDs and several studies have been conducted to determine their masses and temperatures (Harris et al. 2003, Kepler et al. 2007). Figure 2.2 from Harris et al. (2003) shows the location of WDs in a  $u - g$ ,  $g - r$  colour-colour diagram and highlights how well separated those with  $T_{\text{eff}} > 8000 - 9000K$  are from the bulk of main sequence stars. I confine my investigation here to objects with  $T_{\text{eff}} > 8000 - 9000K$  since, in addition to being more readily identified using the SDSS photometry, at lower temperatures, the atmospheres are considerably more difficult to model reliably due to the emergence of more physically complex sources of opacity (Kepler et al. 2007). I also imposed moderately bright constraints upon the minimum observed brightnesses of the candidates so that these could be observed spectroscopically on an 8m class in a reasonable time (e.g. 15 minutes in photometric conditions, or 2 hours in bad weather conditions).

An SQL query (see below) was executed on the SDSS DR7 sky server to search for close pairs of blue objects (BOCP) with clean photometry and a maximum angular separation of  $d \leq 60''$  while passing the following criteria:  $u - g \geq -0.7$ ,  $u - g \leq 0.5$ ,  $g - r \geq -0.7$ ,  $g - r \leq 0.0$ ,  $r - i < 0.0$ ,  $r \leq 20$ , and  $g \geq 15.3$ .

```
SELECT P.ObjID as SDSSID, P.ra as RIGHT_ASCENSION, P.dec as DECLINATION, P.b as GALATIC_LATITUDE, P.
l as GALATIC_LONGITUDE, P.psfmag-u as u, P.psfmag-g as g, P.psfmag-r as r, P.clean as pok
FROM Star P
WHERE
    P.clean > 0
    and (P.psfmag-u-P.psfmag-g)<=0.5
    and (P.psfmag-u-P.psfmag-g)>=-0.7
    and (P.psfmag-g-P.psfmag-r)<=0.0
    and (P.psfmag-g-P.psfmag-r)>=-0.7
    and (P.psfmag-r-P.psfmag-i)<0.0
    and P.psfmag-r<=20
    and P.psfmag-g>=15.3
```

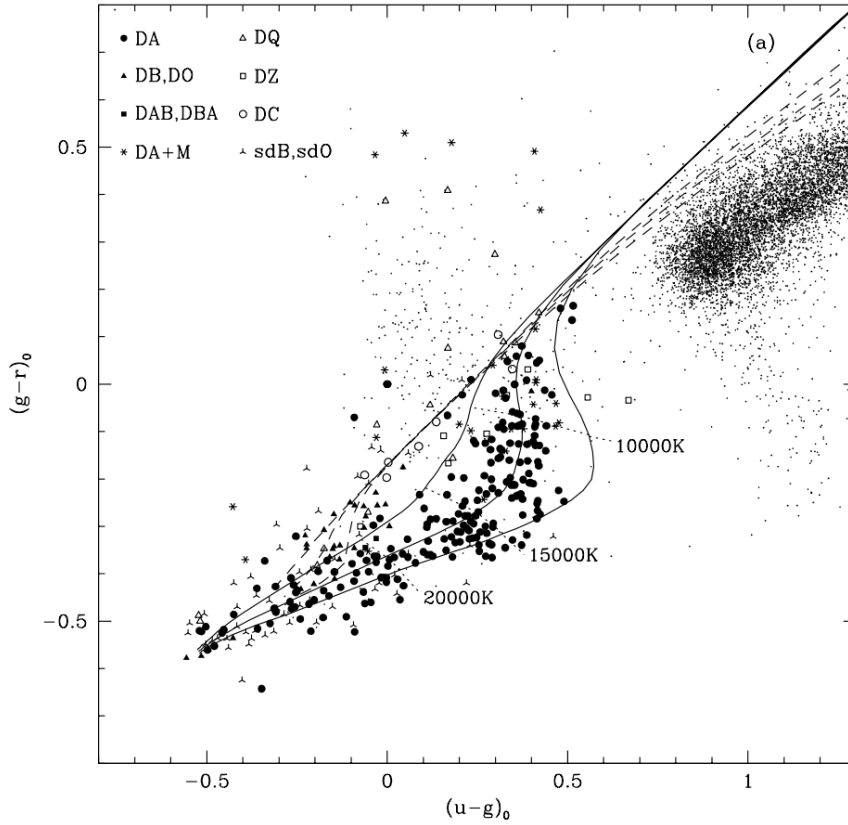


FIGURE 2.2: WD photometry selection criteria diagram, from Harris et al. (2003). Colour-colour diagrams ( $u - g$  vs.  $g - r$ ) showing the WDs and hot subdwarfs. Different types are shown with different symbols. Small dots show all objects with stellar image profiles with  $15 < g < 20$  in a region of  $25 \text{ deg}^2$ . The curves show the colours of WD model atmospheres Bergeron et al. (1995b) of pure H (solid curves) and pure He (dashed curves) with  $\log g = 7, 8$ , and  $9$ , where the  $\log g = 7$  curve is toward the lower right and the  $\log g = 9$  curve is toward the upper left. The dotted lines with labels connect models with the same effective temperature.

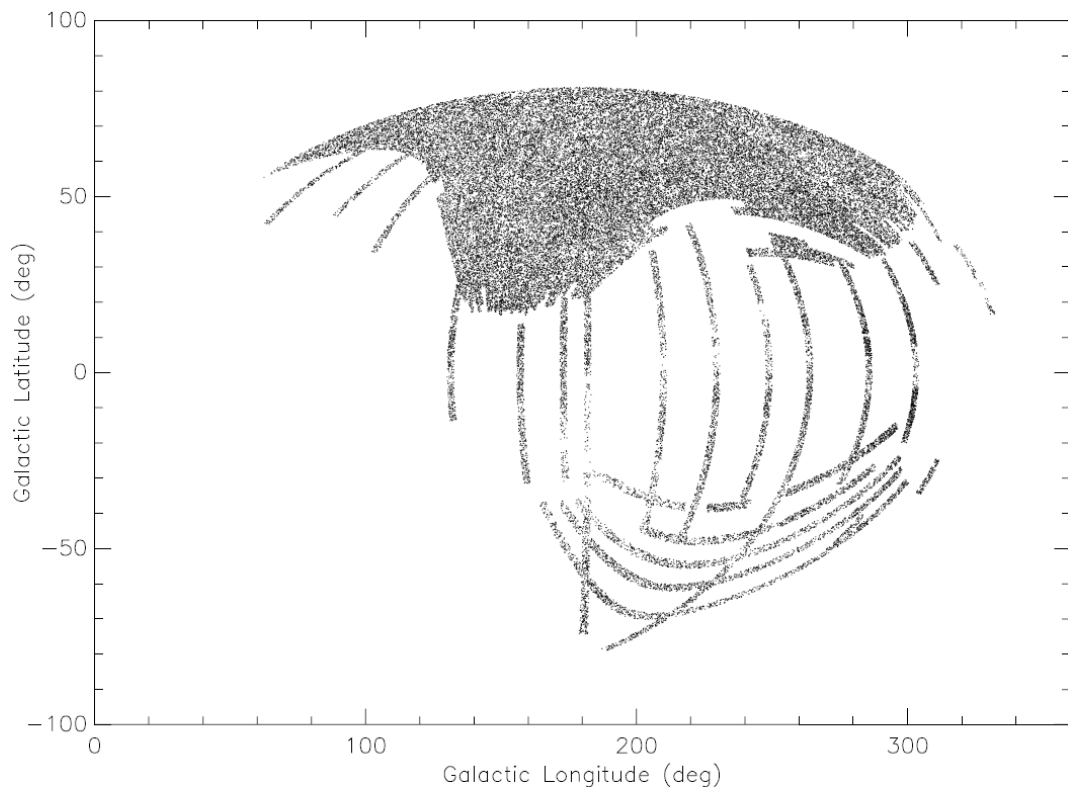


FIGURE 2.3: All WD Candidates (Blue Objects from SDSS DR7 Survey) shown with Aitoff projection of galactic coordinates

## Blue Object Close Pair (BOCP) selection

I initially drew together a list of candidate double-degenerate systems based on all pairs with separations  $d \leq 30''$ . Routines written in Interactive Data Language (IDL) were used to analyse the SDSS data after performing the query to further refine the selection of WD candidates. For example, sources that were spectroscopically confirmed to be quasars were eliminated from this sample using a list based upon SDSS DR7 (Schneider et al. 2010). In addition, obviously “bad” systems, such as spurious pairings in nearby galaxies, were eliminated using a visual check. Figure 2.7 below gives examples of these “bad” objects. The codes used to generate the list of close pairs, to eliminate quasars and to eliminate “bad” objects are listed in Appendix Sections A.2.5, A.2.6 and A.2.7. I also excluded all BOCPs with angular separations  $< 1''$ , since given the typical spatial resolution of the SDSS imaging these were deemed most likely to be spurious.

Figures 2.8, 2.9, and 2.10 below display all wide DD candidates selected using this method. Tables 2.2 and 2.3 display their SDSS coordinates and photometry. Table 2.1 provides my estimates of the percentage quasar contamination of my BO and BOCP lists respectively. Generic BO list and BOCP list filtering code (for known “bad” objects, spectroscopically confirmed quasars, spectroscopically confirmed white dwarfs etc) was developed for the purposes of refining and confirming my simulations for this thesis.

## 2.1.4 Simulations

### Monte-Carlo like simulations

Before applying for and conducting new spectroscopic follow-up of my candidate wide DD systems, I performed a basic statistical analysis on the spatial distribution of blue objects in the SDSS DR7 data to estimate the probability that a pairing was an actual physical system and not merely a chance alignment (ie. a visual binary). This was made with regards to the number of blue object pairs expected to be found in the SDSS sample where no physical association existed between objects (field WDs or quasars). A comparison was then made between this simulated random distribution and that observed.

In my Monte-Carlo like analysis, firstly I randomly distributed a specified number of simulated blue objects within an area of a particular size, such that the mean projected spatial density of these sources was consistent with that observed in the SDSS frames. For every object within this random field, the angular distance to its nearest neighbour was then calculated, and a frequency distribution was generated for each object within the random field having a nearest neighbour up to a chosen maximum separation. This distribution was found to be exponential in shape. The code used to generate this distribution and calculate the probability of close pairs is referenced in Appendix Section A.2.3. The distribution from my simulations was verified to be equivalent to that predicted using the analytical equation of Struve 1852 (Halbwachs 1988), shown in Equation 2.1.

$$n(\rho_{max}) = N(N - 1)\pi\rho_{max}^2/(2A). \quad (2.1)$$

Next, for every blue object within the SDSS DR7 data, the angular separation to its nearest neighbour was calculated, and a second frequency distribution, based on the observed data, was generated. The code used to calculate the probability of close pairs within a BO list is referenced in Appendix Section A.2.2.

When performing these latter calculations, I used a cleaned list of observed sources (ie. excluding spurious, misclassified, pairings such as blue point-like sources within the same nearby galaxies and known quasars). By comparing these two frequency distributions, I was able to estimate the number of real (physically associated) BOCP in the DR7 data. The results of these comparisons are displayed in Figures 2.4 and 2.6. It was found that there was a clear excess of blue object pairings in the observed over the simulated (random) samples at smaller separations ( $\sim 50''$  at separations less than  $30''$ ). Indeed, from the simulations I estimated that within  $30''$ , there is a  $\approx 80\%$  probability that a blue object close pair is physically associated (ie. not merely a chance alignment), and similarly within  $10''$ , a  $\approx 95\%$  probability of a physical association. A slight discrepancy is apparent between the shape of the observed distribution and the theoretical distribution at large angular separations ( $\gtrsim 100''$ , see Figure 2.5). This is likely due to the breakdown of the assumption in my simulations of a uniform density of blue objects across the SDSS footprint. However, giving the limited time frame for this project and my desire that a high proportion of genuine systems are followed-up spectroscopically, I concentrated on pairings that had separations  $< 30''$  (the vast majority actually have  $\lesssim 10''$ ).

The probability of finding a chance alignment is one minus the probability of physical association of a single system to the power of the number of BOCPs in the sample. So in the case of 10 BOCPs (DD candidates), each with an angular separation of  $10''$ , given the probability of physical association of a single system (using the monte-carlo statistics alone) is  $\approx 90\%$ , the probability of at least one of these systems being a chance alignment (not associated) is  $65\%$  ( $1 - \frac{9}{10}^{10}$ ) as per Equation 2.2, where  $x$  is the probability of any one of a number of DD candidates being a chance alignment,  $y$  is the probability of a system being a chance alignment, and  $z$  is the number of DD candidates.

$$x = 1 - (1 - y)^z \quad (2.2)$$

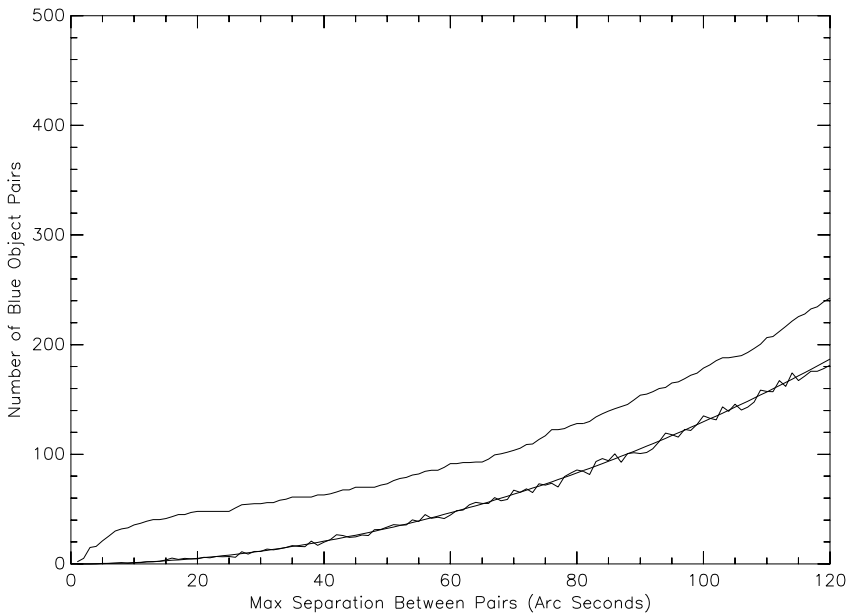


FIGURE 2.4: Plot showing the number of BOCPs found in my simulated random distribution of single objects as a function of separation in arc-seconds (lower line) overlaid with the analytical estimate of Struve 1852. The number of BOCPs measured in the SDSS DR7 to a given maximum separation is also shown (upper line). The difference between these two curves provides a handle on the frequency of physically associated BOCPs found in the SDSS within a given maximum separation.

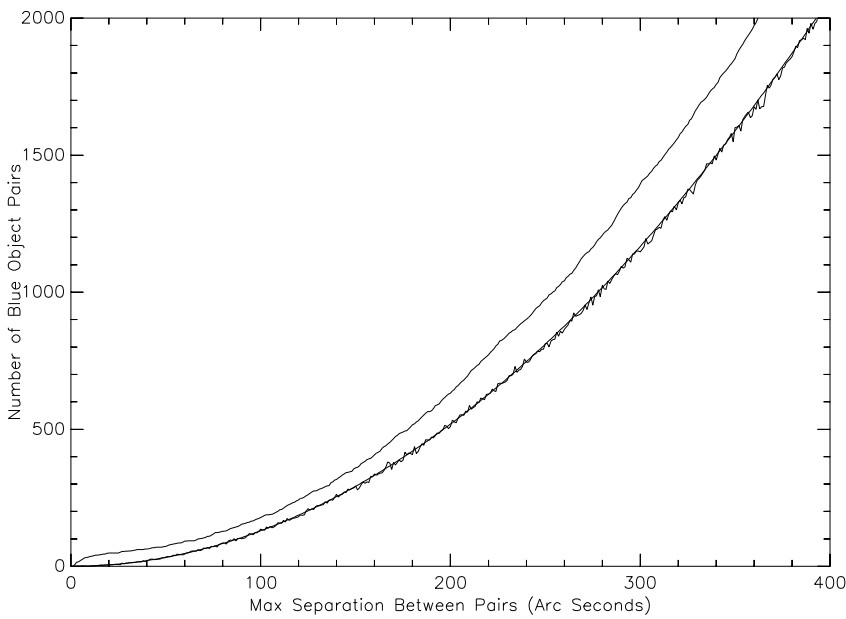


FIGURE 2.5: Same as Figure 2.4 but shown out to a much larger angular separation ( $\sim 6'$ )

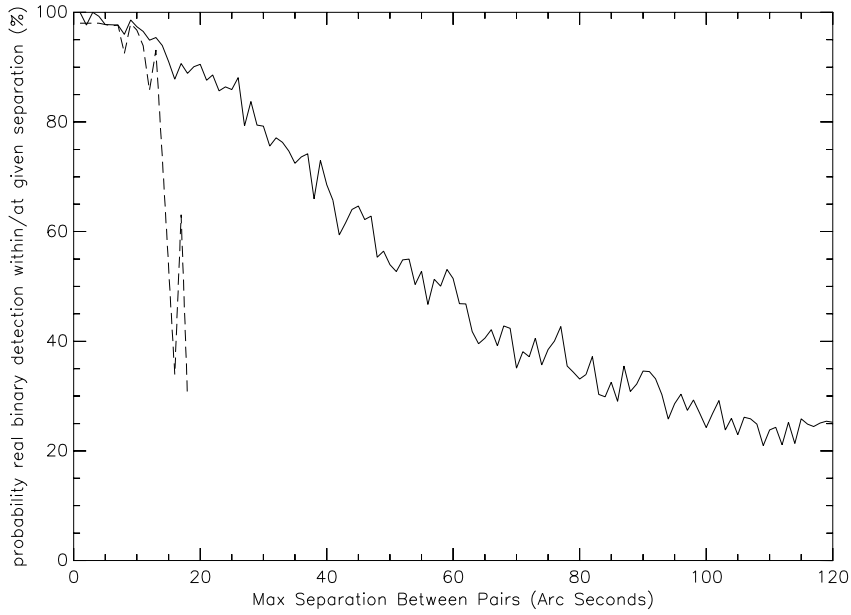


FIGURE 2.6: The likelihood (expressed as a percentage) that a BOCP is a physically associated system within a given maximum separation (solid curve). The probability that a BOCP is physically associated at a given separation is also overplotted (dashed curve).



FIGURE 2.7: Examples of “bad” objects within my initial sample. These were rejected by my visual inspection of all pairs selected initially.

Sample	number	DR	DR coverage (sq deg)	DR total num objects (million)	% representation (in sample)	% (DR corrected)	% (DR & have spectra corr. - worst case)	% (DR & have spectra corr. - ideal)
BOL Blue Objects	36681	DR7	11663	357	100	100	NA	NA
BOL SDSS Spectra available	9788	DR7	11663	357	26.7	26.7	NA	NA
BOL known Quasars	1291	DR7	11663	357	3.5	3.5	13.2	3.5
BOL known WDs	5350	DR4	6670	180	14.6	25.5	95.6	95.6
BOCPL Blue Object Close Pairs	53	DR7	11663	357	100	100	NA	NA
BOCPL BOCPs with SDSS Spec. for a component	13	DR7	11663	357	24.5	24.5	NA	NA
BOCPL BOCPs with a known Quasar component	0	DR7	11663	357	0	0	0	0
BOCPL BOCPs with a known WD component	12	DR4	6670	180	22.6	39.6	161.4	161.4

TABLE 2.1: Blue Object List (BOL) and Blue Object Close Pair List (BOCPL) Statistics - this table identifies the percentage contamination of my sample of blue objects due to quasars. “Bad” objects have not been removed from this sample. Note the ‘ideal’ case column assumes that the photometric target selection of quasars for spectroscopic follow-up within the SDSS program has been perfect (i.e. every quasar within the sample of blue objects has been targeted for spectroscopic follow-up based on its photometric properties and has been subsequently identified). The ‘Worst’ case column assumes that the spectroscopic follow-up of quasars within the SDSS program has not been biased based upon photometric data (any more than the effective biasing/probability of spectroscopic follow-up for my sample of blue objects). This table also includes an indication of the expected percentage of WDs within my sample based upon known WDs from Eisenstein et al. (2006), and assumes that the spectroscopic follow-up of objects within the SDSS program has not been biased in any way based upon photometric data towards the selection of WDs (i.e. constraints were purely chosen based upon expected quasar photometric signatures).



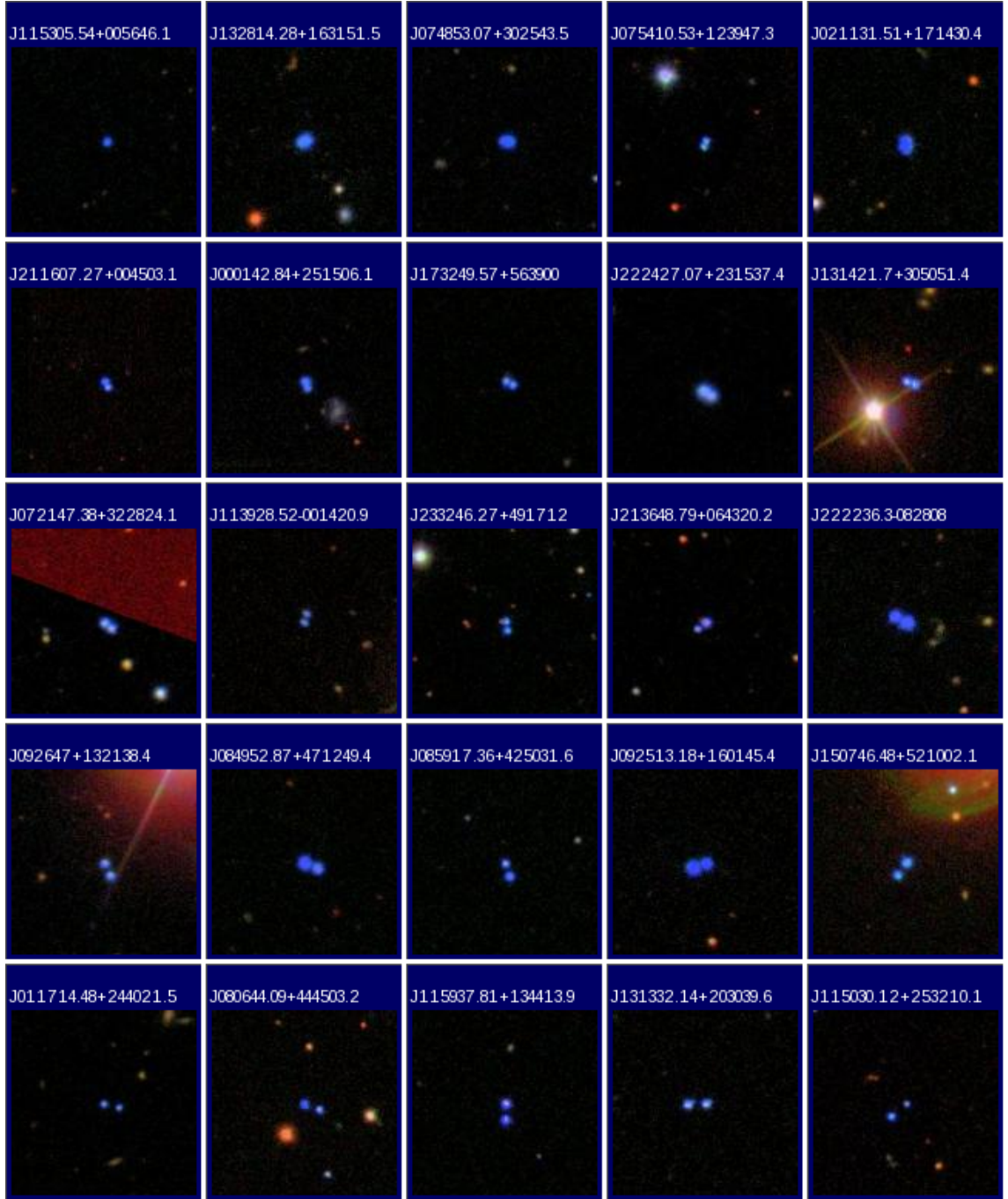


FIGURE 2.8: Finder charts (part 1/3) for the candidate wide double-degenerate systems found in SDSS DR7 ( $< 30''$ ). Note that these are arc  $30'' \times 30''$ , with North at top end and East at the left.

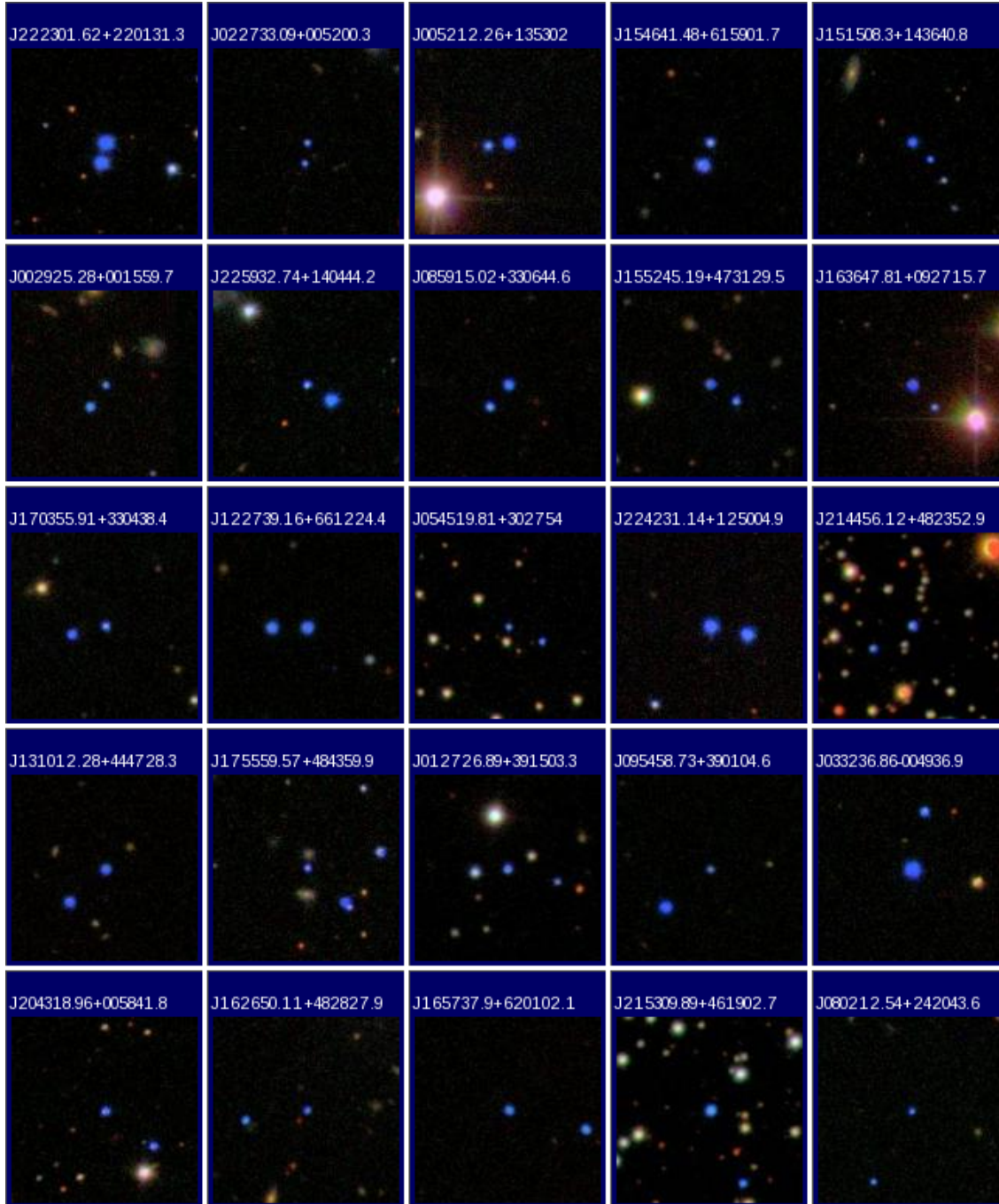


FIGURE 2.9: Finder charts (part 2/3) for the candidate wide double-degenerate systems found in SDSS DR7 ( $< 30''$ ). Note that these are arc  $30'' \times 30''$ , with North at top end and East at the left.



FIGURE 2.10: Finder charts (part 3/3) for the candidate wide double-degenerate systems found in SDSS DR7 ( $< 30''$ ). Note that these are arc  $30'' \times 30''$ , with North at top end and East at the left.

TABLE 2.2: Blue Object Close Pair Data - SDSS

BOCP ID	DD ID	RA Dec (A) (J2000)	u (A) (psf)	g (A) (psf)	r (A) (psf)	$\delta u$ (A) (psf)	$\delta g$ (A) (psf)	$\delta r$ (A) (psf)	RA Dec (B) (J2000)	u (B) (psf)	g (B) (psf)	r (B) (psf)	$\delta u$ (B) (psf)	$\delta g$ (B) (psf)	$\delta r$ (B) (psf)	Sep. ( $''$ )
BOCP1	DD-11	J115305.54+005646.1	18.42	18.89	19.38	0.02	0.02	0.02	J115305.47+005645.8	18.5	18.91	19.34	0.02	0.02	0.02	1.22
BOCP2		J132814.28+163151.5	16.34	16.27	16.63	0.02	0.02	0.02	J132814.36+163150.9	17.75	17.65	17.74	0.27	0.23	0.19	1.32
BOCP3		J074853.07+302543.5	17.41	17.59	17.88	0.07	0.05	0.05	J074852.95+302543.4	17.57	17.59	17.96	0.05	0.04	0.04	1.5
BOCP4	DD-06	J075410.53+123947.3	19.23	18.76	18.96	0.06	0.06	0.08	J075410.58+123945.5	19.22	18.84	19.04	0.06	0.07	0.09	2
BOCP5		J021131.51+171430.4	17.36	17.26	17.65	0.12	0.09	0.07	J021131.52+171428.3	16.69	16.76	17.19	0.03	0.03	0.03	2.04
BOCP6		J211607.27+004503.1	18.61	18.7	18.91	0.03	0.04	0.04	J211607.2+004501.3	19.43	18.96	19.05	0.1	0.07	0.09	2.06
BOCP7		J000142.84+251506.1	17.82	17.81	18.18	0.02	0.02	0.02	J000142.79+251504	19.16	18.7	19.01	0.19	0.16	0.16	2.16
BOCP8		J173249.57+563900	19.55	19.07	19.22	0.07	0.05	0.05	J173249.32+563858.8	18.99	19.12	19.27	0.04	0.05	0.06	2.36
BOCP9		J222427.07+231537.4	17.6	17.2	17.43	0.03	0.03	0.03	J222426.91+231536	18.22	17.77	17.92	0.08	0.07	0.07	2.64
BOCP10		J131421.7+305051.4	18.59	18.2	18.22	0.1	0.08	0.09	J131421.5+305050.5	18.23	17.86	17.88	0.04	0.04	0.05	2.76
BOCP11		J072147.38+322824.1	18.24	18.1	18.22	0.03	0.04	0.03	J072147.2+322822.4	18.73	18.28	18.32	0.08	0.04	0.05	2.77
BOCP12		J113928.52-001420.9	19.92	19.45	19.61	0.06	0.04	0.04	J113928.47-001418	20.13	19.8	19.85	0.07	0.06	0.06	2.95
BOCP13	DD-12	J233246.27+491712	18.8	18.67	18.94	0.05	0.05	0.04	J233246.23+491709.1	19.02	18.76	19.04	0.06	0.04	0.04	2.96
BOCP14		J213648.79+064320.2	18.07	17.94	18.24	0.02	0.02	0.01	J213648.98+064318.2	19.72	19.35	19.39	0.04	0.02	0.03	3.44
BOCP15		J222236.3-082808	16.68	16.41	16.67	0.02	0.02	0.03	J222236.56-082806	17.56	17.11	17.3	0.03	0.07	0.07	4.29
BOCP16	DD-08	J092647+132138.4	18.74	18.4	18.46	0.03	0.03	0.05	J092646.88+132134.5	18.46	18.34	18.39	0.02	0.02	0.02	4.35
BOCP17		J084952.87+471249.4	16.64	16.77	17.08	0.02	0.02	0.02	J084952.47+471247.7	18.14	17.77	17.79	0.14	0.08	0.06	4.37
BOCP18		J085917.36+425031.6	19.37	18.94	19.01	0.03	0.05	0.02	J085917.23+425027.4	18.83	18.38	18.53	0.02	0.04	0.02	4.39
BOCP19	DD-02	J092513.18+160145.4	17.05	17.13	17.51	0.08	0.07	0.1	J092513.48+160144.1	16.05	16.13	16.55	0.02	0.02	0.02	4.51
BOCP20		J150746.48+521002.1	17.14	16.91	17.29	0.02	0.03	0.01	J150746.8+520958	17.98	17.76	18.06	0.02	0.03	0.01	5.05
BOCP21		J011714.48+244021.5	19.94	19.63	19.77	0.03	0.02	0.02	J011714.12+244020.3	20.29	19.83	19.96	0.04	0.02	0.02	5.05
BOCP22	DD-09	J080644.09+444503.2	18.54	18.14	18.32	0.02	0.02	0.01	J080643.64+444501.4	19.18	18.74	18.82	0.02	0.02	0.01	5.09
BOCP23		J115937.81+134413.9	18.45	18.07	18.12	0.03	0.02	0.02	J115937.82+134408.7	18.42	18.28	18.52	0.03	0.02	0.02	5.18
BOCP24		J131332.14+203039.6	18.13	17.8	17.98	0.02	0.02	0.01	J131332.56+203039.3	17.86	17.48	17.69	0.02	0.02	0.01	5.93
BOCP25	DD-05	J115030.12+253210.1	20.43	19.95	19.97	0.05	0.02	0.02	J115030.48+253206	19.28	18.86	19.09	0.03	0.02	0.02	6.38
BOCP26		J222301.62+220131.3	15.66	15.6	15.91	0.01	0.02	0.01	J222301.72+220124.9	16.37	16.01	16.2	0.01	0.03	0.03	6.56
BOCP27		J022733.09+005200.3	20.02	19.62	19.69	0.05	0.02	0.02	J022733.15+005153.6	20.3	19.86	19.91	0.06	0.02	0.02	6.72

TABLE 2.3: Blue Object Close Pair Data - SDSS (continued)

BOCP ID	DD ID	RA Dec (A) (J2000)	u (A) (psf)	g (A) (psf)	r (A) (psf)	$\delta u$ (A) (psf)	$\delta g$ (A) (psf)	$\delta r$ (A) (psf)	RA Dec (B) (J2000)	u (B) (psf)	g (B) (psf)	r (B) (psf)	$\delta u$ (B) (psf)	$\delta g$ (B) (psf)	$\delta r$ (B) (psf)	Sep (")
BOCP28	DD-01	J005212.26+135302	17.79	17.71	17.98	0.02	0.03	0.02	J005212.73+135301.1	19.35	18.89	18.92	0.03	0.03	0.02	6.78
BOCP29		J154641.48+615901.7	19.07	18.63	18.75	0.03	0.02	0.02	J154641.79+615854.3	17.16	16.89	17.16	0.02	0.02	0.02	7.64
BOCP30		J151508.3+143640.8	18.38	18	18.2	0.02	0.02	0.01	J151507.9+143635.4	19.76	19.63	19.88	0.03	0.02	0.02	7.9
BOCP31		J002925.28+001559.7	20.02	19.59	19.59	0.05	0.02	0.02	J002925.62+001552.7	18.91	18.48	18.53	0.03	0.01	0.02	8.64
BOCP32	DD-04	J225932.74+140444.2	19.02	18.57	18.68	0.03	0.02	0.01	J225932.21+140439.2	16.16	16.36	16.78	0.02	0.01	0.01	9.14
BOCP33		J085915.02+330644.6	18.27	18.01	18.34	0.02	0.02	0.02	J085915.5+330637.6	19.07	18.7	18.87	0.03	0.02	0.02	9.29
BOCP34		J155245.19+473129.5	18.79	18.71	19.05	0.02	0.02	0.02	J155244.41+473124	19.21	18.99	19.3	0.04	0.03	0.02	9.65
BOCP35		J163647.81+092715.7	18.13	17.72	17.93	0.02	0.01	0.01	J163647.33+092708.4	19.98	19.54	19.54	0.04	0.02	0.02	10.12
BOCP36	DD-03	J170355.91+330438.4	19.16	18.81	18.86	0.02	0.01	0.01	J170356.77+330435.7	18.48	18.16	18.27	0.02	0.01	0.01	11.16
BOCP37		J122739.16+661224.4	17.72	17.86	18.13	0.02	0.02	0.02	J122741.05+661224.3	18.23	17.99	18.21	0.02	0.02	0.02	11.43
BOCP38		J054519.81+302754	20.19	19.82	19.96	0.05	0.02	0.02	J054518.98+302749.3	20.05	19.64	19.8	0.05	0.02	0.02	11.72
BOCP39		J224231.14+125004.9	16.48	16.23	16.5	0.01	0.02	0.01	J224230.33+125002.3	16.83	16.5	16.75	0.01	0.02	0.01	12.13
BOCP40		J214456.12+482352.9	19.19	18.74	18.83	0.03	0.01	0.02	J214457.39+482345.5	19.81	19.49	19.49	0.05	0.02	0.02	14.67
BOCP41		J131012.28+444728.3	17.88	17.84	18.02	0.01	0.02	0.01	J131013.38+444717.8	17.95	17.59	17.85	0.01	0.02	0.01	15.71
BOCP42		J175559.57+484359.9	19.04	19.21	19.39	0.03	0.02	0.02	J175558.35+484348.8	18.03	17.69	17.91	0.02	0.02	0.02	16.41
BOCP43		J012726.89+391503.3	19.16	18.7	18.83	0.03	0.02	0.02	J012725.51+391459.2	20.35	19.99	19.99	0.06	0.02	0.02	16.55
BOCP44		J095458.73+390104.6	20.31	19.86	19.95	0.05	0.02	0.03	J095459.97+390052.4	17.96	17.69	18.02	0.02	0.02	0.02	18.87
BOCP45	DD-07	J033236.86-004936.9	15.32	15.64	16.09	0.01	0.02	0.02	J033236.6-004918.4	18.64	18.2	18.3	0.03	0.02	0.02	18.91
BOCP46		J204318.96+005841.8	18.51	18.24	18.42	0.03	0.02	0.01	J204317.93+005830.5	18.96	18.59	18.75	0.03	0.02	0.01	19.13
BOCP47		J162650.11+482827.9	19.72	19.62	19.94	0.03	0.02	0.03	J162652.12+482824.7	19.14	18.98	19.3	0.02	0.01	0.02	20.22
BOCP48		J165737.9+620102.1	18.72	18.65	18.98	0.02	0.01	0.03	J165734.39+620055.9	18.88	18.53	18.76	0.02	0.01	0.02	25.47
BOCP49		J215309.89+461902.7	18.15	17.72	17.9	0.02	0.01	0.01	J215308.9+461839.1	18.88	19.08	19.36	0.03	0.01	0.02	25.68
BOCP50		J080212.54+242043.6	19.87	19.54	19.78	0.04	0.02	0.02	J080213.44+242020.9	20.24	19.85	19.97	0.05	0.02	0.02	25.85
BOCP51		J135713.14-065913.7	18.94	19.25	19.76	0.04	0.02	0.02	J135714.5-065856.9	18.58	18.16	18.35	0.04	0.02	0.02	26.29
BOCP52		J100245.86+360653.3	19.42	19.04	19.09	0.03	0.02	0.02	J100244.88+360629.6	19.32	18.92	19.01	0.03	0.02	0.02	26.53
BOCP53		J105306.13+025052.5	19.57	19.14	19.28	0.04	0.02	0.02	J105306.82+025027.9	19.37	18.98	19.18	0.03	0.02	0.02	26.6

## 2.2 Follow-up spectroscopic observations

To confirm my sources as WDs and to better determine their parameters (i.e. their surface gravities and effective temperatures) it was necessary to obtain high signal-to-noise low resolution optical spectroscopy in the range of  $\lambda \approx 3800 - 5200\text{\AA}$ . Therefore a series of observing proposals were written and submitted to a number of different telescopes to secure these follow-up datasets.

### 2.2.1 Prioritisation of candidate wide DD systems for follow-up

I initially considered prioritising the spectroscopic follow-up of systems suspected on the grounds of their magnitudes and colours as having the most suitable mass ratios for probing the IFMR (Appendix Section [A.2.10](#)). Ultimately, due to observing constraints, I was forced not to implement this. However as a result, I can provide a first estimate of the mass distribution of WDs in wide binary systems. Targets were instead selected based upon brightness and separation. Figure [2.11](#) below gives a list of my candidates selected for spectroscopic follow-up, and Table [2.4](#) displays their SDSS coordinates and photometry.

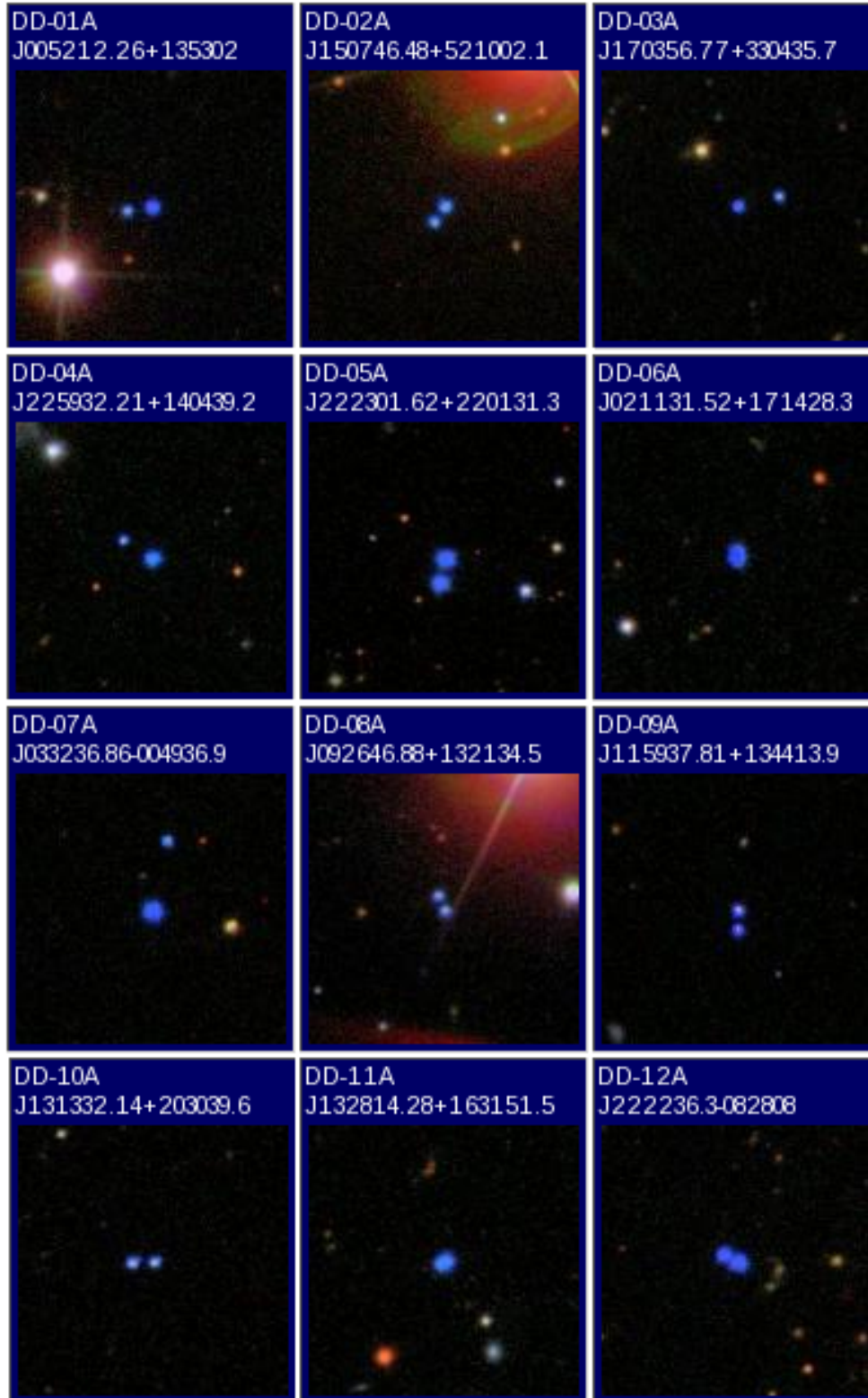


FIGURE 2.11: SDSS Double-Degenerate Survey - Target Selection ( $1 \times 1'$ ). Systems which have been followed up spectroscopically.

TABLE 2.4: Double-Degenerate Data - SDSS

WD	SDSS ID	RA Dec ( <i>J2000</i> )	Ra ( <i>J2000</i> )	Dec ( <i>J2000</i> )	psf u	psf g	psf r	psf u error	psf g error	psf r error	Separation (arc sec)
DD-01A	587724231565246516	005212.73+135301.1	13.05304438	13.88365572	19.35	18.89	18.92	0.029	0.033	0.019	6.78
DD-01B	587724231565246515	005212.26+135302.0	13.05112233	13.88390554	17.79	17.71	17.98	0.019	0.033	0.017	6.78
DD-02A	587733604259332157	150746.48+521002.1	226.9436913	52.16725612	17.14	16.91	17.29	0.023	0.028	0.013	5.05
DD-02B	587733604259332160	150746.80+520958.0	226.94503382	52.16612142	17.98	17.76	18.06	0.025	0.028	0.014	5.05
DD-03A	587729752747475228	170355.91+330438.4	255.98296977	33.07733943	19.16	18.81	18.86	0.023	0.013	0.012	11.16
DD-03B	587729752747475236	170356.77+330435.7	255.98656627	33.07660731	18.48	18.16	18.27	0.017	0.012	0.011	11.16
DD-04A	587727221943959713	225932.74+140444.2	344.88642274	14.07895147	19.02	18.57	18.68	0.025	0.015	0.015	9.14
DD-04B	587727221943959712	225932.21+140439.2	344.88422825	14.07756995	16.16	16.36	16.78	0.015	0.014	0.013	9.14
DD-05A	587740712426537180	222301.62+220131.3	335.75675515	22.02537688	15.66	15.6	15.91	0.012	0.016	0.009	6.56
DD-05B	587740712426537181	222301.72+220124.9	335.75717854	22.02359622	16.37	16.01	16.2	0.012	0.033	0.03	6.56
DD-06A	758881524261781580	021131.52+171428.3	32.88134033	17.24121308	16.69	16.76	17.19	0.026	0.029	0.028	2.04
DD-06B	758881524261781581	021131.51+171430.4	32.88133036	17.24177863	17.36	17.26	17.65	0.115	0.093	0.071	2.04
DD-07A	588015508218904600	033236.86-004936.9	53.1535948	-0.82692479	15.32	15.64	16.09	0.011	0.021	0.023	18.91
DD-07B	588015508218904597	033236.60-004918.4	53.15251716	-0.82178397	18.64	18.2	18.3	0.025	0.022	0.023	18.91
DD-08A	587745403612430400	092646.88+132134.5	141.69533369	13.35958843	18.46	18.34	18.39	0.02	0.022	0.017	4.35
DD-08B	587745403612430401	092647.00+132138.4	141.69584285	13.36069038	18.74	18.4	18.46	0.033	0.032	0.047	4.35
DD-09A	587735346962432035	115937.81+134413.9	179.90758042	13.73720478	18.45	18.07	18.12	0.03	0.025	0.018	5.18
DD-09B	587735346962432036	115937.82+134408.7	179.90760447	13.73576715	18.42	18.28	18.52	0.026	0.019	0.019	5.18
DD-10A	587742578058395699	131332.14+203039.6	198.38394049	20.5110005	18.13	17.8	17.98	0.02	0.021	0.015	5.93
DD-10B	587742578058395698	131332.56+203039.3	198.38569698	20.51094081	17.86	17.48	17.69	0.018	0.021	0.014	5.93
DD-11A	587742774031024218	132814.28+163151.5	202.05953933	16.53098677	16.34	16.27	16.63	0.017	0.024	0.018	1.32
DD-11B	587742774031024219	132814.36+163150.9	202.05987454	16.5308083	17.75	17.65	17.74	0.269	0.234	0.186	1.32
DD-12A	587726878883381389	222236.30-082808.0	335.65128196	-8.46888943	16.68	16.41	16.67	0.015	0.021	0.026	4.29
DD-12B	587726878883381390	222236.56-082806.0	335.65235447	-8.46834597	17.56	17.11	17.3	0.031	0.07	0.067	4.29



### Gemini Observing Proposals

Four applications were submitted to the Australian Time Allocation Committee (ATAC) to obtain service mode observations for the components of a number of my pairings with the Gemini telescopes during periods of poorer weather in the 2009B and 2010A semesters. The following objects were included in the target lists of these proposals:

GDD-01A/B (00:29:25.62 00:15:52.74), GDD-02A/B (03:32:36.6 -00:49:18.42) and GDD-07A/B (22:22:36.31 -8:28:8.0), were submitted for Gemini South 2009B. GDD-03A/B (08:49:52.87 47:12:49.47), GDD-04A/B (09:25:13.48 16:01:44.15), GDD-05A/B (09:26:46.88 13:21:34.52), GDD-06A/B (10:02:44.88 36:06:29.68), GDD-08A/B (22:23:1.62 22:01:31.36), GDD-20A/B (02:11:31.52+17:14:28.3), were submitted for Gemini North 2009B. GDD-01A/B (00:29:25.62 00:15:52.74), GDD-07A/B (22:22:36.31 -8:28:8.0), were submitted for Gemini South 2010A. GDD-101 (07:48:53.07 30:25:43.56), GDD-102 (08:49:52.9 47:12:49.5), GDD-104 (12:27:39.17 66:12:24.46), GDD-105 (13:13:32.57 20:30:39.39), and GDD-106 (22:24:27.08 23:15:37.49), were submitted for Gemini North 2010A.

Two of these proposals were successful with 5.5 and 4.0 hours being awarded on Gemini-N (2009B) and Gemini-S (2010A) respectively. The two successful Gemini observing proposals are included in the Appendix Section [A.7.6](#).

### WHT Observing Proposal

A proposal was also submitted to the UK Panel for the Allocation of Telescope Time (PATT) prior to the commencement of this thesis for the purposes of obtaining 3 nights of time on the William Herschel Telescope (WHT) during the 2008A semester. This proposal was approved and observations were carried out by Paul Dobbie on 24-25 July 2008. The observations were originally proposed to test both our understanding of spectroscopic mass determinations at  $T_{\text{eff}} < 12000\text{K}$  (e.g. Kepler et al. 2007) and to probe the IFMR across a broad mass range, by constraining their age using calculations from the higher mass components. This proposal successfully secured 2 nights of observing time and has been added to the Appendix Section [A.7.4](#).

### VLT Observing Proposal

An application for observing time on the European Southern Observatory's Very Large Telescope for another project on the IFMR was granted 2 nights in February 2010. The aims of the proposal were the targeting of 10 faint, suspected high mass ( $M_i \geq 5-6M_{\odot}$ ) WDs with high probability of membership of the young open cluster systems, NGC2287 and NGC3532. A selection of double-degenerate systems were included as backup targets, in case observing conditions were not favourable for observing the extremely faint primary targets. The VLT observing proposal has been added to the Appendix Section [A.7.7](#).

TABLE 2.5: Telescope Instrument Properties

Telescope	Instrument	Grating	Central $\lambda$ ( $\text{\AA}$ )	$\lambda$ range ( $\text{\AA}$ )	disp ( $\text{\AA}/\text{mm}$ )	disp ( $\text{\AA}/\text{pixel}$ )	$\delta\lambda$ (FWHM in $\text{\AA}$ ) (with binning)	$\delta\lambda$ (FWHM in ch) (with binning)	pixel width ( $\mu\text{m}/\text{pixel}$ )	R ( $\lambda/\delta\lambda$ )	binning (1/2/4x)	Slit ( $''$ )
VLT	FORS2	600B	4650	3300 - 6210	50	0.75	3.9	5.2	15	600	2	1.3
Gemini	GMOS-N/S	B600	4100	2760	37	0.5	2.7	5.5	13.5	422	4	2
WHT	IRIS blue	R300B	4503	3539	64	0.86	3.4	4	13.5	1309	1	1

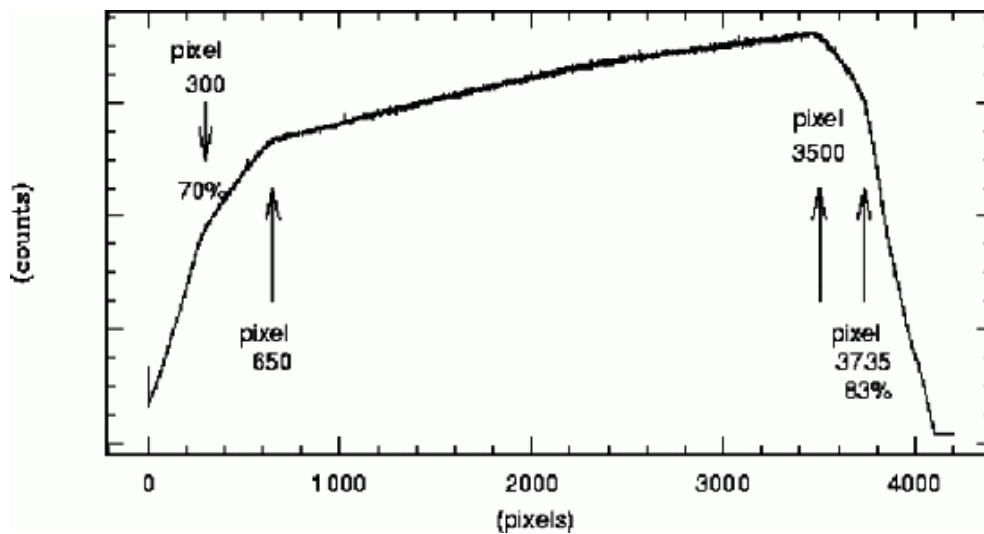


FIGURE 2.12: Relative response of the WHT ISIS blue arm

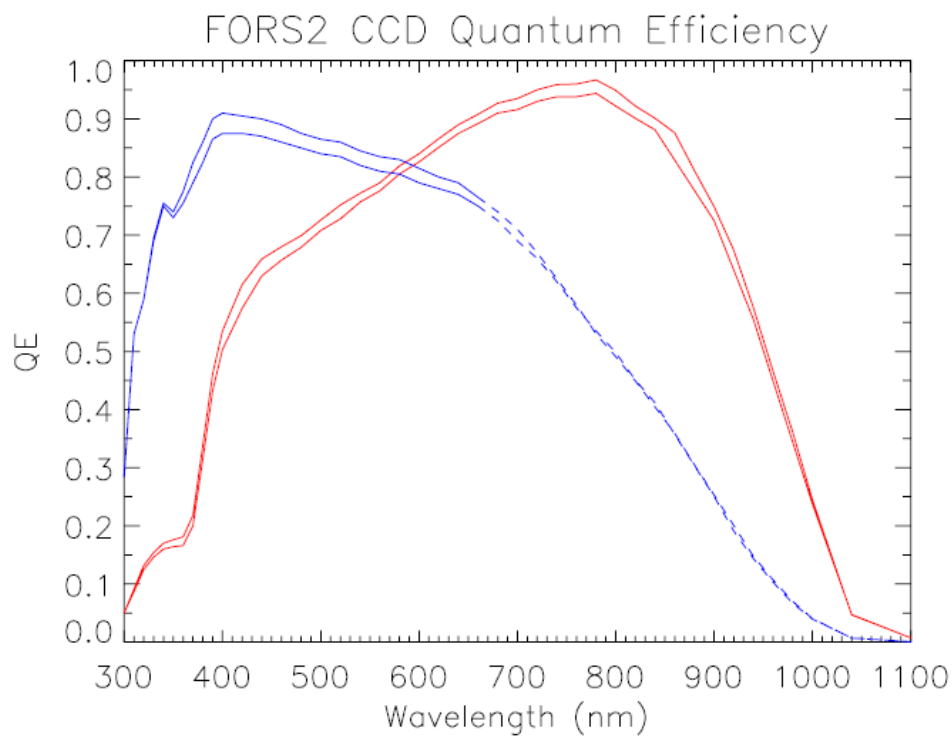


FIGURE 2.13: VLT FORS2 red and blue CCD quantum efficiency curves

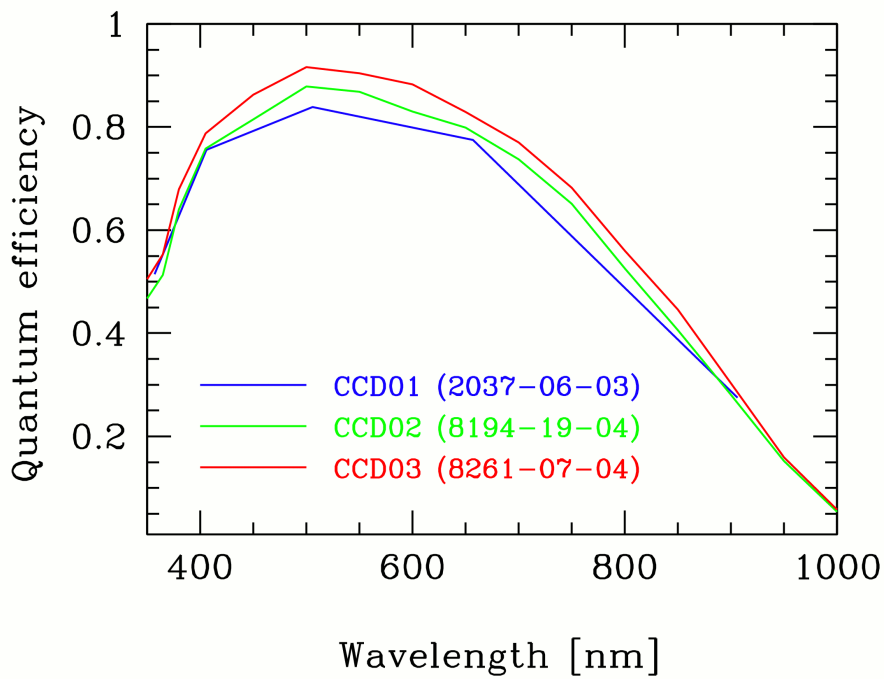
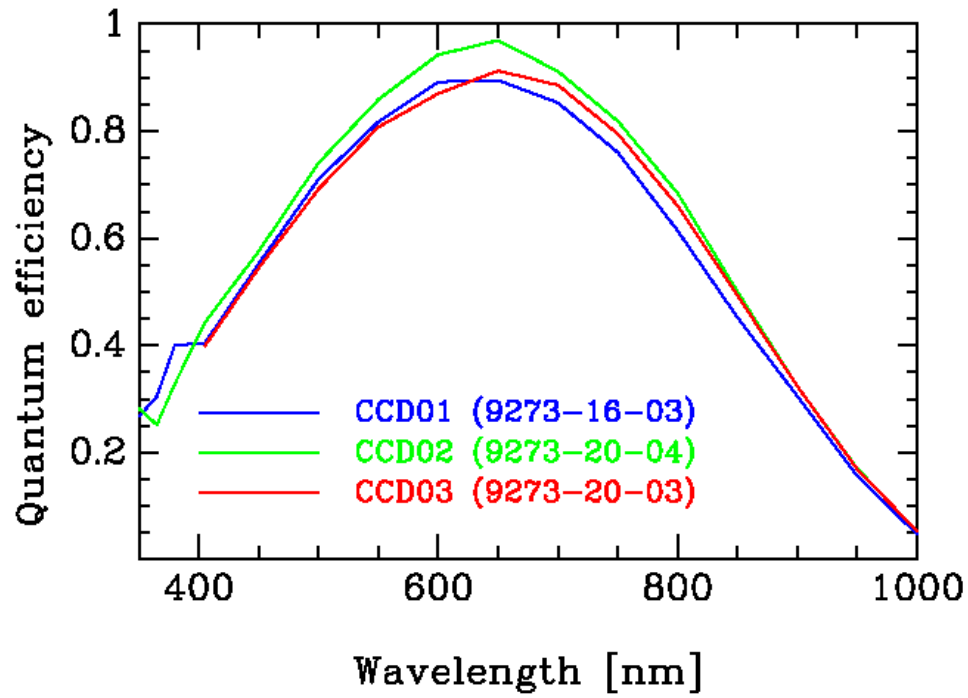


FIGURE 2.14: GMOS North (top) and South (bottom) CCD quantum efficiency curves

### 2.2.2 The spectroscopic follow-up observations

In the period July 2008 to May 2010 optical spectroscopy was obtained with various telescope and instrument combinations for the components of 12 blue object close pairs. The details of these telescopes and instruments are summarised in Table 2.5. All spectroscopically observed sources were confirmed as WD stars.

I adopted a common scheme for the reduction of the data from each observing run. A DC (virtually spectrally featureless) WD of known effective temperature was observed to remove instrument signature and to provide a first order flux calibration. Multiple exposures were taken (typically 3) of each system such that I could remove cosmic rays using either a  $\approx 4$  sigma-clipped mean or Laplacian “edge-detection” filtering of the data, which ever appeared to be more efficient. In general, the individual exposures were between 10 and 30 minutes long. This insured that the total counts in each CCD pixel from my brightest candidates remained well within the linear regime of the detectors and were also never close to their saturation levels.

#### WHT Observations

My first batch of follow-up observations were performed with the 4.2m William Herschel Telescope (WHT) and the Intermediate dispersion Spectrograph and Imaging System (ISIS) instrument prior to me starting this project. The 4.2 metre diameter WHT is located on the island of La Palma, Canary Islands, and is part of the Isaac Newton Group of Telescopes (ING). The ISIS spectrograph is mounted at the Cassegrain focus of the WHT and is of double-arm design, with the two channels being separately optimised for the blue and red spectral regions. Only the data from the blue arm is considered in this work. The relative response curve for the blue arm of ISIS is shown below in Figure 2.12.

Four double-degenerate (DD) systems were observed on 24-25 July 2008 with the WHT. The program ID for this observing run was WHT/08A/24. For the purposes of this thesis, these systems are labelled as DD-01A+B, DD-02A+B, DD-03A+B, and DD-04A+B. The slit was aligned to capture the light of component stars simultaneously. All observations were made in visitor mode, in good weather, with  $\approx 0.6 - 0.9''$  seeing. They were made using the R300B grating, a  $1.0''$  slit width, and with 5x2400s, 3x1800s, 4x1800s+3x1800s, and 4x1800s+1x1800s+1x1700s+1x1200s exposures respectively. Additionally, 3x540s exposures of the DC WD1917+386 (herein called 1918+38 based upon its current/J2000 coordinates) were also taken using a  $1.0''$  slit for the purposes of removing instrument response.

#### Gemini Observations

My second batch of spectroscopic follow-up observations was obtained with the two 8.1m Gemini telescopes and their respective Gemini Multi-Object Spectrograph (GMOS) instruments (GMOS South and GMOS North). The Gemini South telescope resides on the summit of Cerro Pachón in Chile, and the Frederick C. Gillett Gemini North telescope resides on the summit of Mauna Kea in Hawaii. Like ISIS on the WHT, the

GMOS instruments are mounted at the Cassegrain foci of each telescope. GMOS provides long-slit and multi-slit spectroscopy over the range  $0.36 - 1.10\mu m$ . At the time of my observations, the GMOS-North CCDs favoured somewhat (in terms of response) the red end of the optical regime, whereas the response of those in GMOS-South was more suitable for observing the blue end. This can be seen clearly in Figure 2.14 below.

Two candidate DD systems were observed in service mode on 20 July 2009 and 25 July 2009 using GMOS-North in longslit mode. For the purposes of this thesis these pairings are referred to as DD-05A+B and DD-06A+B. The program ID for this observing run was GN-2009B-Q-80. The slit was aligned along the binary to capture the light of both component stars simultaneously. All observations were made using the B600/410.0 grating/disperser, a  $2.0''$  slit/mask width, using 3x1800s exposures for DD-05A+B and 3x2000s exposures for DD-06A+B. 3x750s exposures of the DC WD1918+38 were taken for the purposes of removing instrument response.

A further candidate DD system, DD-12A+B, was observed in service mode on 11 May 2010 using GMOS-South in long-slit mode. The program ID for this observing run was GS-2010A-Q-70. As before, the slit was aligned to capture the light of component stars simultaneously. All observations were made using the B600/410.0 grating/disperser, a  $2.0''$  slit/mask width, with 3x1800s exposures. Two 1560s exposures of the DC WD0000+345 were also acquired.

## VLT Observations

My final new spectra were acquired with the European Southern Observatory's 8.2m Very Large Telescope UT1 (Antu) and the FOcal Reducer and low dispersion Spectrograph (FORS2). The Very Large Telescope (VLT) is located at the ESO Paranal Observatory, Chile. FORS2 is mounted at the Cassegrain focus of VLT Antu. FORS2 was designed for the wavelength range from 330 nm to 1100 nm and provides an image scale of  $0.0025/\text{pixel}$  (and  $0.00125/\text{pixel}$ ) with the standard resolution collimator (and the high resolution collimator, respectively), in the default binned ( $2 \times 2$ ) read-out mode of its mosaic of two CCD chips. FORS2 supports two CCD chip generations in visitor mode, the current generation (FORS2) MIT CCDs and the previous generation (FORS1) E2V CCDs. Each configuration consists of two  $2k \times 4k$  chips with pixel size of  $15 \times 15\mu m$ . The E2V CCDs are particularly sensitive to the blue end of the spectrum. The response curves of the E2V blue optimised CCDs are shown below in Figure 2.13, as compared with the red optimised MIT CCDs.

I observed five candidate DD systems on 6-7 February 2010 using the Long Slit Spectroscopy (LSS) mode of FORS2, before and after the primary science program. These systems are referred to as DD-07A+B, DD-08A+B, DD-09A+B, DD-10A+B, and DD-11A+B for the purposes of this thesis. The program ID for this observing run was 084.D-1097(A). The slit of FORS2 was also aligned to capture the light of both component stars simultaneously. The observations were made using the 600B grating, a  $1.3'$  slit width, using 2x600s, 1x500+1x360s, 2x600s, 2x300s, and 2x300s exposures respectively. 2x250s+2x180s exposures of DC LHS-2333 were taken such that I could remove the instrument response. During our observations at the VLT it became apparent that one of my DD targets featured both low and a high mass

components. At first glance, SDSS 1159+1344 (DD-09A+B) appears to be an ideal system for the purposes of refining the IFMR.

TABLE 2.6: Double-Degenerate Data - Observations and Signal to Noise

WD	Observation Run Target Name	Observatory	Spectrograph	Date	Exposure Time(s)	Slit ( $''$ )	Grating	R (fwhm channels)	Arc Lamp Type	DC WD	S/N
DD-01A	SDSS0052	WHT 4.2m	Long Slit	[25/07/2008]	5x2.4 ks	1	R300B	3	Cu-Ne + Cu-Ar	WD1918+38	12.2
DD-01B	SDSS0052	WHT 4.2m	Long Slit	[25/07/2008]	5x2.4 ks	1	R300B	3	Cu-Ne + Cu-Ar	WD1918+38	32.3
DD-02A	SDSS1507	WHT 4.2m	Long Slit	[24/07/2008]	3x1.8 ks	1	R300B	3	Cu-Ne + Cu-Ar	WD1918+38	64.3
DD-02B	SDSS1507	WHT 4.2m	Long Slit	[24/07/2008]	3x1.8 ks	1	R300B	3	Cu-Ne + Cu-Ar	WD1918+38	37.8
DD-03A	SDSS1703	WHT 4.2m	Long Slit	[24+25/07/2008]	4x1.8+3x1.8 ks	1	R300B	3	Cu-Ne + Cu-Ar	WD1918+38	26.8
DD-03B	SDSS1703	WHT 4.2m	Long Slit	[24+25/07/2008]	4x1.8+3x1.8 ks	1	R300B	3	Cu-Ne + Cu-Ar	WD1918+38	42
DD-04A	SDSS2259	WHT 4.2m	Long Slit	[24+25/07/2008]	4x1.8+1.8+1.7+1.2 ks	1	R300B	3	Cu-Ne + Cu-Ar	WD1918+38	31.8
DD-04B	SDSS2259	WHT 4.2m	Long Slit	[24+25/07/2008]	4x1.8+1.8+1.7+1.2 ks	1	R300B	3	Cu-Ne + Cu-Ar	WD1918+38	105.3
DD-05A	DD-08A+B	Gemini North	Long Slit	[20/07/2009]	3x0.75 ks	2	B600	4.5	Cu-Ar	WD1918+38	136.9
DD-05B	DD-08A+B	Gemini North	Long Slit	[20/07/2009]	3x0.75 ks	2	B600	4.5	Cu-Ar	WD1918+38	133.6
DD-06A	DD-20A+B	Gemini North	Long Slit	[20+25/07/2009]	3x2.0 ks	2	B600	4.5	Cu-Ar	WD1918+38	148.3
DD-06B	DD-20A+B	Gemini North	Long Slit	[20+25/07/2009]	3x2.0 ks	2	B600	4.5	Cu-Ar	WD1918+38	90.2
DD-07A	WDB02	VLT-ANTU	LSS	[02/07/2010]	2x0.6 ks	1.3	600B	3.5	He-HgCd	LHS-2333	89.5
DD-07B	WDB02	VLT-ANTU	LSS	[02/07/2010]	2x0.6 ks	1.3	600B	3.5	He-HgCd	LHS-2333	26.9
DD-08A	WDB04	VLT-ANTU	LSS	[02/07/2010]	1x0.5+1x0.36 ks	1.3	600B	3.5	He-HgCd	LHS-2333	32.1
DD-08B	WDB04	VLT-ANTU	LSS	[02/07/2010]	1x0.5+1x0.36 ks	1.3	600B	3.5	He-HgCd	LHS-2333	45.7
DD-09A	WDB10	VLT-ANTU	LSS	[02/06/2010]	2x0.6 ks	1.3	600B	3.5	He-HgCd	LHS-2333	23.4
DD-09B	WDB10	VLT-ANTU	LSS	[02/06/2010]	2x0.6 ks	1.3	600B	3.5	He-HgCd	LHS-2333	33.1
DD-10A	WDB11	VLT-ANTU	LSS	[02/07/2010]	2x0.3 ks	1.3	600B	3.5	He-HgCd	LHS-2333	43.2
DD-10B	WDB11	VLT-ANTU	LSS	[02/07/2010]	2x0.3 ks	1.3	600B	3.5	He-HgCd	LHS-2333	57.2
DD-11A	WDB12	VLT-ANTU	LSS	[02/07/2010]	2x0.3 ks	1.3	600B	3.5	He-HgCd	LHS-2333	81.2
DD-11B	WDB12	VLT-ANTU	LSS	[02/07/2010]	2x0.3 ks	1.3	600B	3.5	He-HgCd	LHS-2333	55.8
DD-12A	DD-07A+B	Gemini South	Long Slit	[11/05/2010]	3x1.8 ks	2	B600	4.5	Cu-Ar	WD0000+345	99.7
DD-12B	DD-07A+B	Gemini South	Long Slit	[11/05/2010]	3x1.8 ks	2	B600	4.5	Cu-Ar	WD0000+345	94.7



## 2.3 Data Reduction

### 2.3.1 Spectroscopic Data Reduction

Spectroscopic data was reduced using IRAF to follow a common methodology. Scripts were used to drive this process in each case. The specifics of all reduction scripts and external software are outlined in the Appendix Section A.4. However, in brief, the following reduction steps were applied to the data:

1. Bias Subtraction, to account for the ramp level added to the CCD (to prevent negative levels being fed to the analogue-to-digital converter). This was achieved by subtracting a stack of zero exposure time frames from the data.
2. Flat Fielding, to account for CCD pixel to pixel sensitivity variations. This was achieved by dividing the data by a normalised version of the image produced when illuminating the CCD with a quartz continuum lamp. CCD frames were debiased and flat-fielded using the IRAF procedure CCDPROC.
3. Cosmic ray removal using the LAplacian-COSmic ray remover, *lacos\_spec.cl* created by Pieter van Dokkum, April 2001 (van Dokkum 2001).
4. 1D spectra were extracted using the APEXTRACT IRAF procedure.
5. Wavelength calibration using arc lamp exposures. The arc lamps used depended upon the particular spectrograph. On Gemini N+S Cu-Ar lamps were used, on the WHT Cu-Ne + Cu-Ar lamps were used, and on the VLT He-HgCd lamps were used.
6. A first order flux calibration was performed independently using a DC standard star of known effective temperature (see Appendix Section A.4.6).

### Spectroscopic Flux Calibration Method

The flux calibration of my spectra was performed using observations of DC WDs. Three He atmosphere (no Balmer lines) DCs of known effective temperature were used for this purpose. For the northern hemisphere observations, the WHT and Gemini North, I adopted WD1918+38. For the southern hemisphere observations, I used WD0000-345 and WD LHS-2333 to calibrate the data from Gemini South and the VLT, respectively. The effective temperatures of WD0000-345 ( $6240 \pm 140K$ ) and LHS-2333/WD1055-072 ( $7420 \pm 200K$ ) were obtained from Bergeron et al. (2001) and that of WD1918+38 ( $6470K$ ) was taken from Bergeron et al. (1997). Note that I specifically chose stars in the middle and towards the hotter end of the DC range because across the wavelength range of interest (between  $3700\text{\AA}$  and  $5200\text{\AA}$ ) they have more even flux levels, allowing high signal-to-noise data to be acquired right across this regime in relatively short integration times.

The observed spectrum of each DC was fitted with a cubic spline in IRAF *splot*. This allowed me to efficiently eliminate the Calcium H and K lines ( $3968.5\text{\AA}$  and  $3933.7\text{\AA}$

TABLE 2.7: Standard WD Stars

WD	RA ( <i>J2000</i> )	Dec ( <i>J2000</i> )	
WD1918	19 18 58.0	38 43 35.0	6470 $K$
WD0000-345	00 02 40.08	-34 13 38.7	6240 $\pm$ 140 $K$
WD1055-072 (LHS-2333)	10 57 35	-07 31.4	7420 $\pm$ 200 $K$

respectively) and any poor data channels, in the case of the failure in cosmic ray removal or bad CCD columns. Calcium H+K absorption is often seen in the spectra of He atmosphere WDs since the time scales for metals to diffuse below their photospheres are much larger than for DAs of similar effective temperature. Subsequently, each science spectrum was divided by this interpolating spline before being multiplied by a black body function with the same effective temperature as the DC WD. I performed this step using a custom written Perl script, where the details of this are provided in Appendix Section A.4.6. Figures 2.15, 2.16, 2.17, and 2.18 display my normalised flux calibrated spectra. Measurements of signal-to-noise were made on each of these spectra, where the code used to perform these calculations is outlined in the Appendix Section A.4.7

It should be made clear that the use of DC standards and blackbody spectral distributions yielded relative fluxes, not absolute fluxes. The flux calibration performed here was designed to compensate for variations in flux across wavelength due to imperfect calibration of the instruments (gradients in throughput).

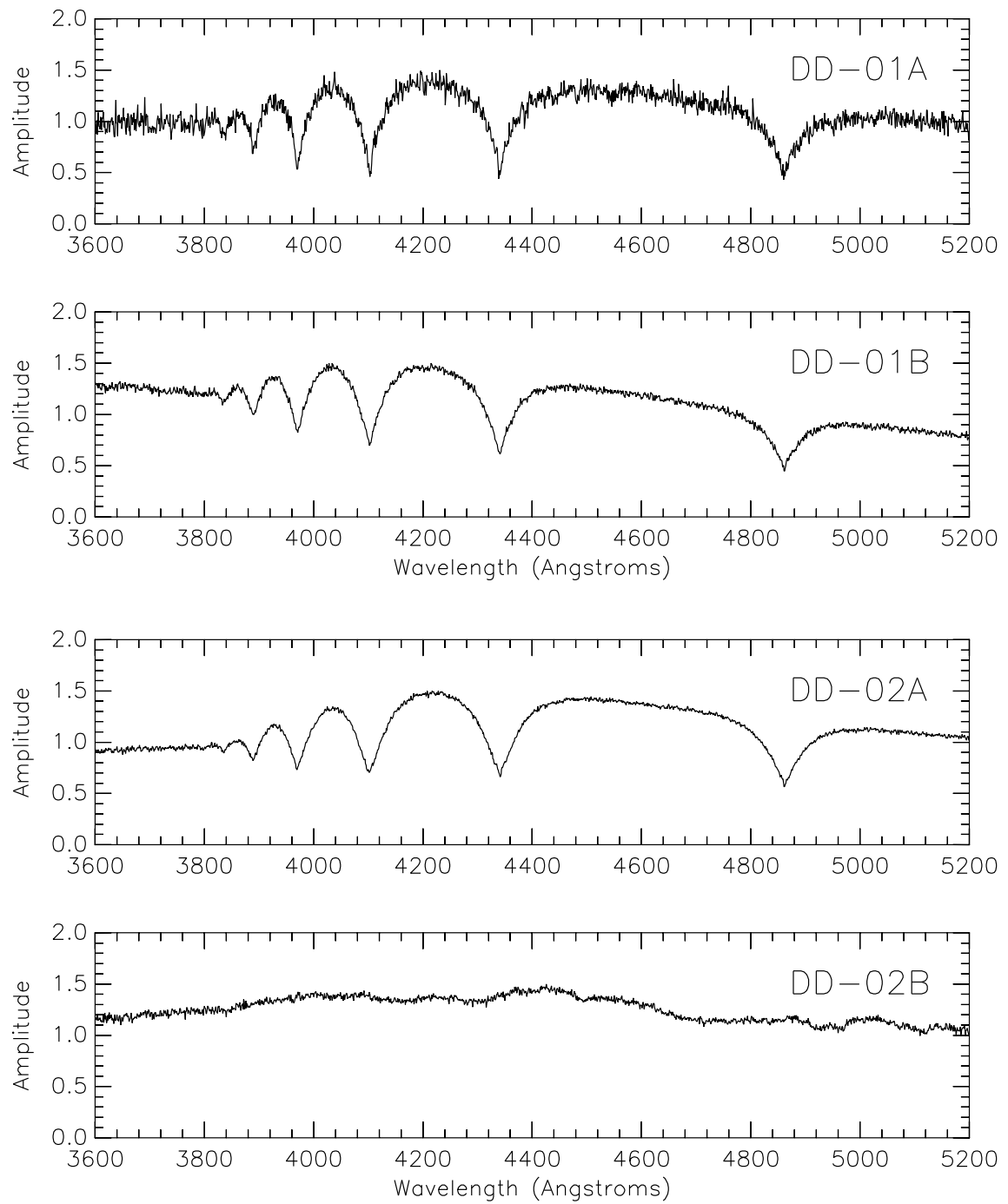


FIGURE 2.15: Flux Calibrated Spectrum - DD01 to DD02

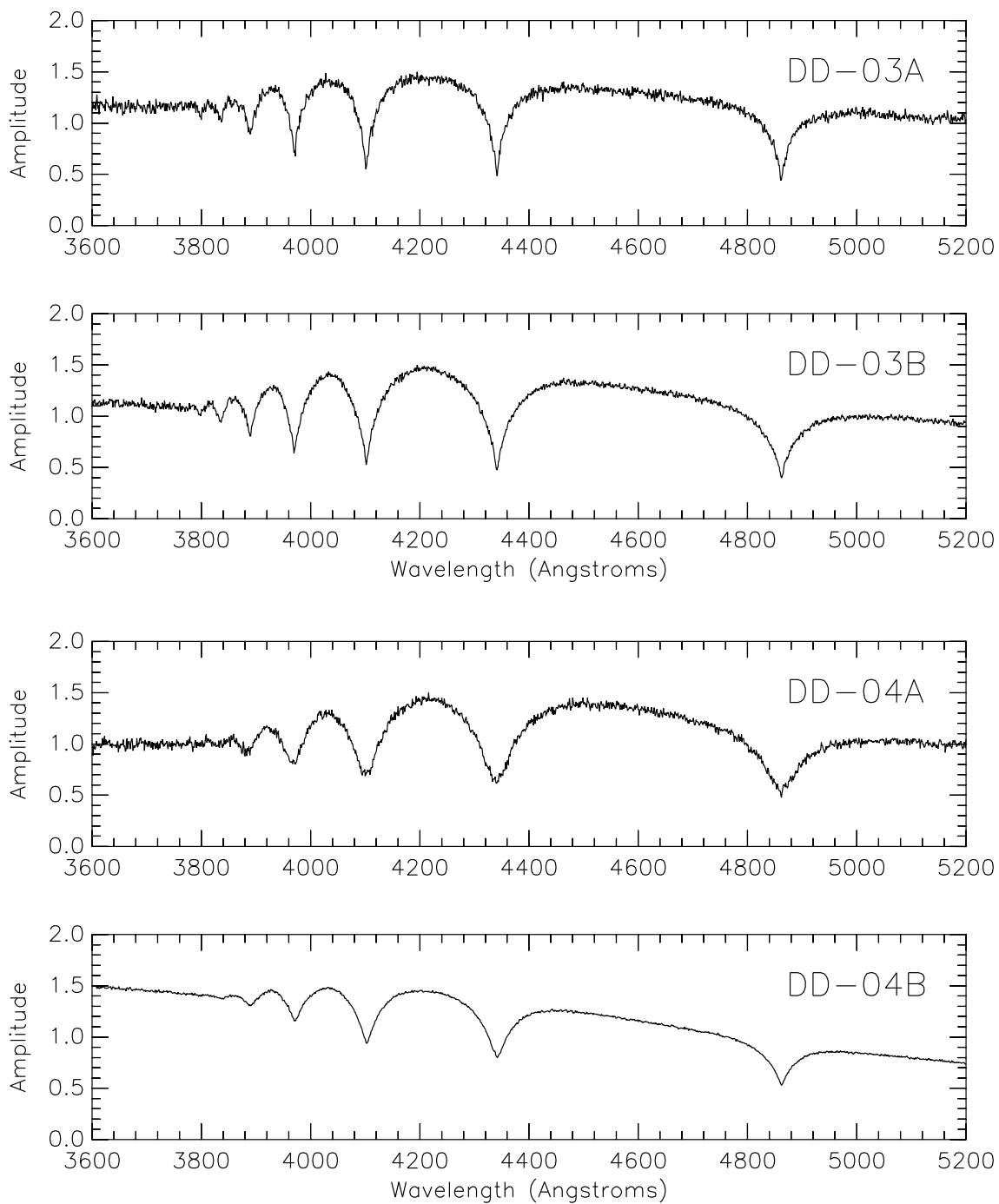


FIGURE 2.16: Flux Calibrated Spectrum - DD03 to DD04

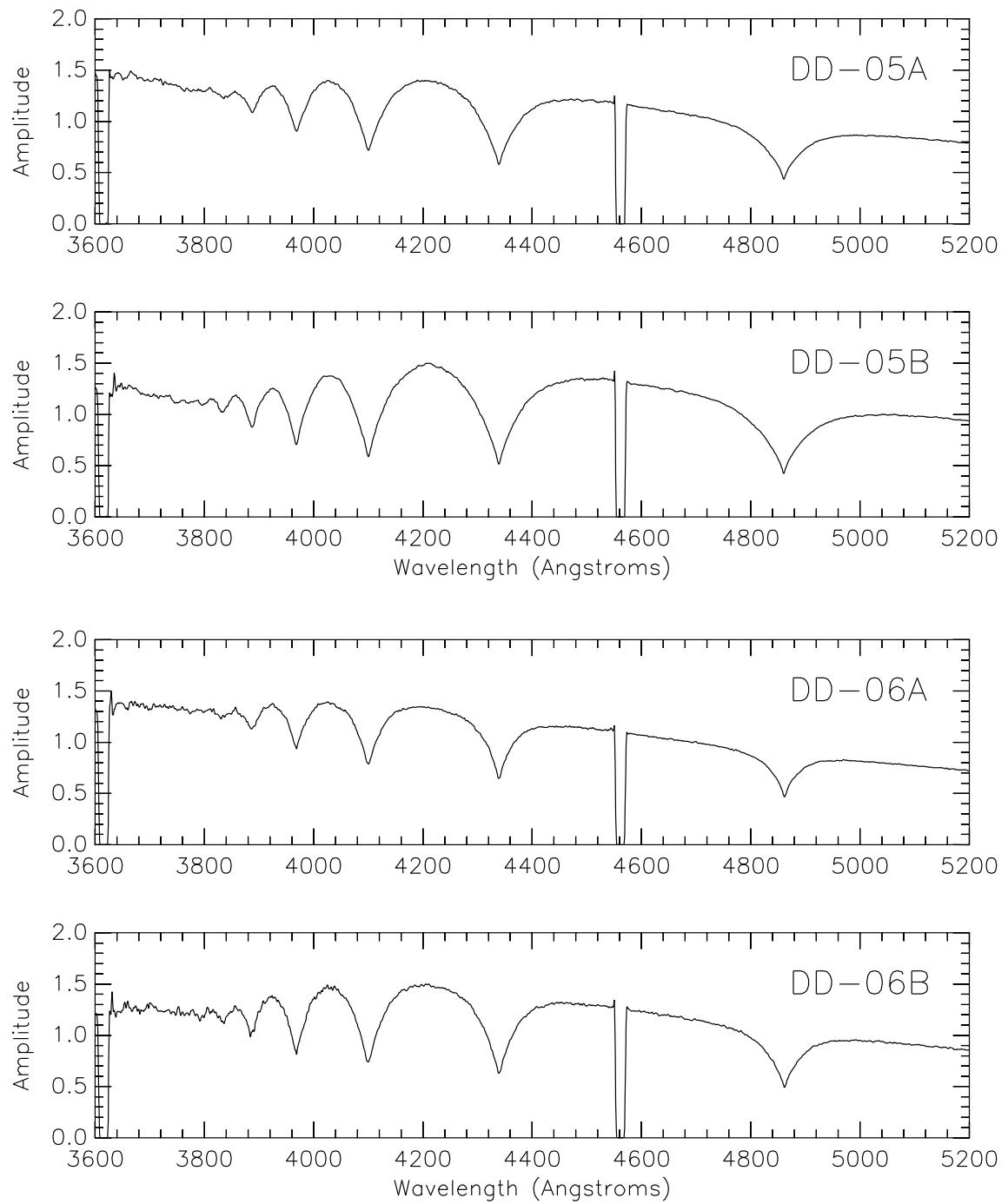


FIGURE 2.17: Flux Calibrated Spectrum - DD05 to DD06

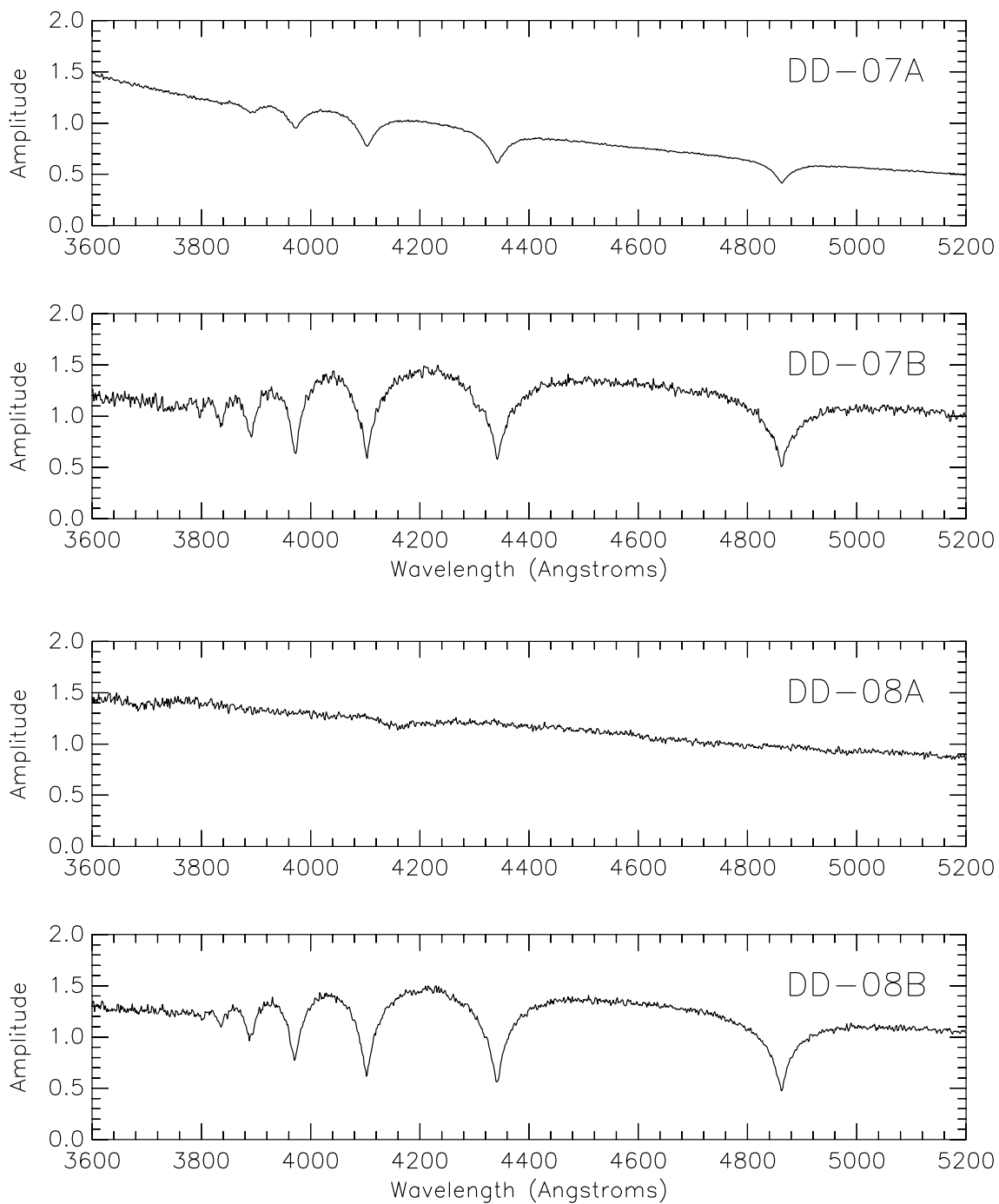


FIGURE 2.18: Flux Calibrated Spectrum - DD07 to DD08

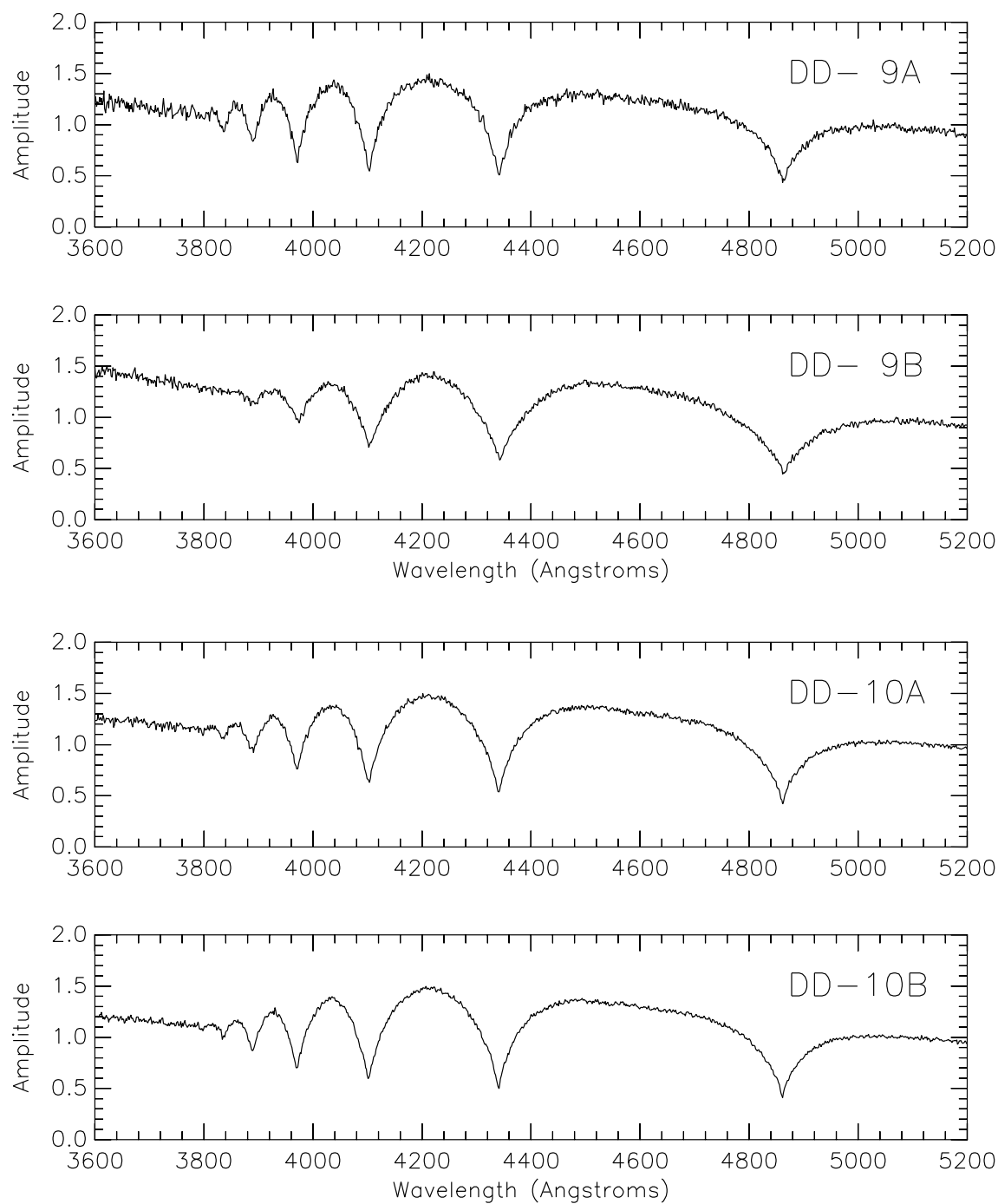


FIGURE 2.19: Flux Calibrated Spectrum - DD09 to DD10

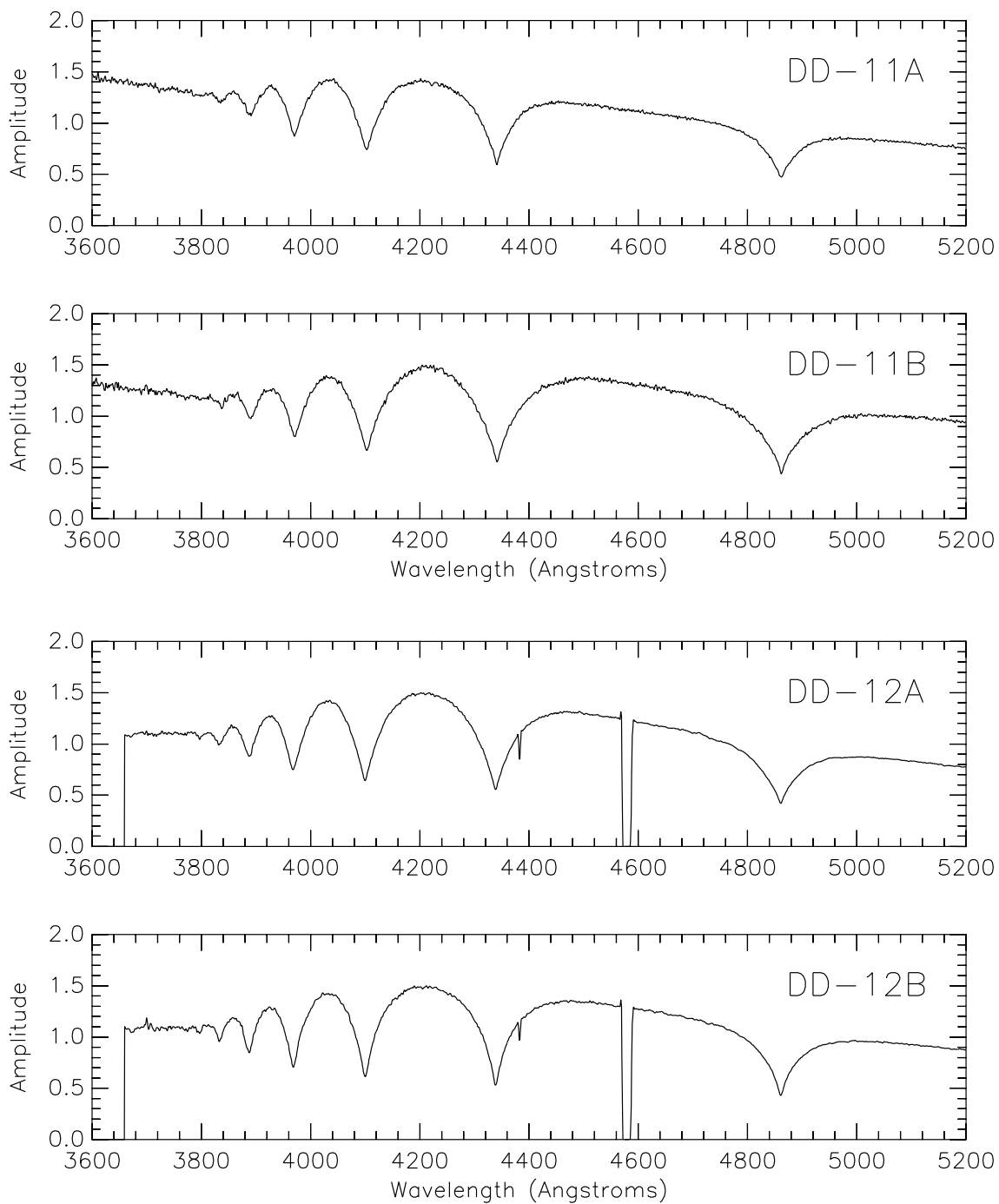


FIGURE 2.20: Flux Calibrated Spectrum - DD11 to DD12



## 2.4 Data modelling

The effective temperature and the surface gravity values for each WD were obtained using grids of pure-H synthetic spectra. These measurements are essential for determining the mass, the radius and the cooling age of the WD from evolutionary tracks. In the next sections I provide a brief guide to these models.

### 2.4.1 Atmospheric modelling

#### Atmospheric Models of DA white dwarfs

Atmospheric models allow the emergent spectrum of a WD star to be predicted as a function of effective temperature ( $T_{\text{eff}}$ ), surface gravity ( $\log g$ ), and elemental composition. Codes for the construction of these models are publicly available (Hubeny and Lanz 1995, Werner 1986), as are pre-calculated tables containing solutions at select  $T_{\text{eff}}$ ,  $\log g$ , and elemental composition values. All WDs with  $T_{\text{eff}} > 20000\text{K}$  modelled in this thesis utilised TLUSTY v200 (Hubeny 1988, Hubeny and Lanz 1995), where the spectral synthesis code SYNSPEC v48 (Hubeny and Lanz 2001) was used to predict the emergent spectra from these model atmosphere structures. The grids of models based on TLUSTY and SYNSPEC used in this thesis were generated by Paul Dobbie. For WDs with  $T_{\text{eff}} \leq 20000\text{K}$ , I used a grid of synthetic spectra supplied by Detlev Koester. The version of the TLUSTY code in hand is not optimised for objects with ( $T_{\text{eff}} \lesssim 12000 - 14000\text{K}$ ) since it was originally written to deal with purely radiative atmospheres.

A variety of simplifying assumptions are adopted in the computation of model atmospheres and synthetic spectra (Auer and Mihalas 1969, Hubeny 1988). The stellar atmosphere is generally represented as a series of plane parallel layers, where the observable portion, the photosphere, represents only a fraction of the radius of the WD, for example  $\frac{R_{\text{atm}}}{R} \approx 0.0011$  (Kubat 1995). Moreover, the photosphere is taken to be horizontally homogeneous (or uniform in  $x$  and  $y$ ) with variations only in depth,  $z$ , reducing the problem to solving the physical and structural equations in a single dimension.

As these objects are generally stable over long periods of time, it is assumed that an equilibrium exists between the gas+radiation pressure and the weight of the atmosphere due to the star's own gravity. The surface gravity is assumed to be constant throughout the layers of the atmosphere, where the pressure derivative,  $dp$ , is taken with respect to mass column ( $m$ , Equation 2.3 with units  $g\text{cm}^{-2}$ ), and not the depth value,  $z$ , since the gas pressure is close to linear in  $m$  (Mihalas 1978). Both stellar characteristics suggest all energy flux radiated from the atmosphere must come from the interior of the star, with the amount entering any given layer equaling the amount exiting that layer, and delineates constancy of flux  $F$  with optical depth,  $\tau$ , or a state of radiative equilibrium, Equation 2.4

$$\frac{dp}{dm} = g \quad (2.3)$$

$$\frac{dF}{d\tau} = 0 \quad (2.4)$$

The radiative energy from the boundary layer between the non-observable atmosphere and observable atmosphere interacts with ions and electrons, and is absorbed, emitted, and scattered frequently, as it approaches the surface of the WD star. The interaction between the radiation field and the constituent material of the atmosphere is expressed in the equation of radiative transfer (Equation 2.5), where  $I_\nu$  is the intensity of the radiation field at frequency  $\nu$  (or the amount of energy,  $dE$ , passing across a surface of area  $dS$ , in a direction  $\mu = \cos \theta$  with respect to the surface normal, into a solid angle  $d\omega$ , in the frequency interval  $d\nu$ , per unit time at the frequency  $\nu$ ),  $\eta$  is the emission coefficient, and  $\chi$  is the absorption co-efficient.

$$\mu \frac{dI_\nu}{dz} = -\chi(z, \nu)I(z, \mu, \nu) + \eta(z, \nu) \quad (2.5)$$

The absorption and emission coefficients represent the efficiency with which radiation at frequency  $\nu$  can pass through the material of the stellar atmosphere, and both depend heavily on the electron occupation numbers of the atomic energy levels of the material. The opacity to radiation and emission of radiation is described as arising from a combination of the continuum and spectral lines for the purposes of the models. The continuum opacity to radiation is produced by a combination of a) bound-free absorption where an electron, bound to a nucleus, is removed by a photon with energy greater than the ionization energy of the ion, b) free-free absorption where an electron absorbs radiation, while the electron briefly interacts with the electric field of an ion, and c) electron scattering, where radiation interacts with an unbound electron, and is scattered - or isotropically redistributed (Hubeny 1988, Mihalas 1978).

The observed radiation arises from a region at an optical depth  $\tau \approx \frac{2}{3}$ , where  $\tau$  is defined by  $d\tau = \chi dz$ , running from the top of the photosphere ( $\tau = 0$ ) towards the deepest layers ( $\tau \rightarrow \infty$ ). Bound-free absorption from HI is an important source of opacity in a DA WD atmosphere. The cross sections for HI are calculated using the “hydrogenic formula” (Mihalas 1978). As these are proportional to  $\nu^{-3}$ , with increasing frequency (ie. towards the blue end of the spectrum) light emerges from deeper (and therefore hotter) layers of the stellar atmosphere, resulting in a harder spectral shape of a DA WD as compared with a black body of the same effective temperature (Shipman 1976).

The processes of absorption and emission have a large effect on the temperature and structure of the atmosphere. In bound-free absorption, any energy excess of ionisation energy (versus the energy of the instigator photon) contributes to the kinetic energy of the electron, which, through elastic collisions, is redistributed amongst neighbouring particles, allowing this energy to be transferred to the thermal pool of semi-opaque gas. Line opacity leads to a warming of the deeper atmospheric layers compared to the upper atmospheric layers where the flux is screened from reaching (Mihalas 1978). However if flux is suppressed in one spectral region, it must be emitted in another.

In a Local Thermal Equilibrium (LTE) model calculation, which is generally a good approximation for the high density atmospheres of WDs, both the electron populations

of the levels of an ion, and the relative ionisation fractions are described by the Boltzmann and Saha distribution functions respectively. The temperature of particles is the same as the temperature of the approximately isotropic radiation field. However, departures from LTE creep in when the atmospheres are extremely hot ( $T_{\text{eff}} > 40000K$ ) or are of low surface gravity ( $\log g < 7.0$ ) and therefore are of lower density. When non-LTE effects become important, radiative rates begin to dominate over collisional rates and the radiation field departs strongly from an near isotropic black body. All WDs studied here have  $T_{\text{eff}} < 40000K$  and  $\log g > 7.5$  so I have considered only LTE models in this work.

### Model Grid Generation

A grid of hot ( $T_{\text{eff}} > 20000K$ ) pure-H LTE model spectra was generated using TLUSTY v200 (Hubeny 1988, Hubeny and Lanz 1995) and SYNSPEC v48 (Hubeny and Lanz 2001). The calculations adopt a model H-atom which incorporates explicitly the eight lowest energy levels and represents levels  $n = 9$  to 80 by a single superlevel. The dissolution of the high-lying levels was taken into account with the occupation formalism of (Hummer and Mihalas 1988). All calculations were carried out under the assumption of radiative equilibrium, including bound-free and free-free opacities of the  $H^-$  ion and incorporated a full treatment for the blanketing effects of  $HI$  lines and the Lyman  $-\alpha$ ,  $-\beta$ , and  $-\gamma$  satellite opacities as computed by N. Allard (Allard et al. 2004). During the calculation of the model structure, the lines of the Lyman and Balmer series were treated using an approximate Stark profile, but in the spectral synthesis step detailed profiles for the Balmer lines were calculated from the Stark broadening tables of Lemke (1997).

The TLUSTY grid extends from  $18000K \leq T_{\text{eff}} \leq 47500K$  and  $7.25 \leq \log g \leq 8.75$ . A model grid extending to lower effective temperatures ( $6000K \leq T_{\text{eff}} \leq 20000K$ ) was provided to us by Detlev Koester and covered surface gravities of  $7.00 \leq \log g \leq 9.50$ . I verified that the synthetic spectra from the two sources were comparable, at least in the overlap region  $18000K \leq T_{\text{eff}} \leq 20000K$  (See Appendix Section A.5.3). The Koester models were preferred upto  $T_{\text{eff}} \approx 20000K$  since they included a more physically realistic treatment of the high order Balmer lines (Tremblay et al. 2008).

### Fitting the data to the model grid

The spectral fitting program XSPEC (version 11.3) (provided personally by Bryan Irby at NASA) was used to perform the comparison between my data and the synthetic spectra. This version was chosen as it most closely matched the version of XSPEC used in previous work (11.2), and could be compiled to operate on a 64-bit (x86\_64) Linux system. Before utilising XSPEC, the individual lines in the model grids were cut-out and converted to fits format as were the lines in the observed data. This was accomplished using the Perl scripts outlined in the Appendix Section A.5.9.

XSPEC operates by folding the model spectrum through a predefined instrument response function (to account for the spectral resolution of the data). The result is then compared to the data using a  $\chi^2$  statistic, where  $\chi^2 = \sum_{i=1}^n \left\{ \frac{1}{\sigma_i^2} [y_i - y(x_i)]^2 \right\}$ ,  $\sigma_i^2$  is the uncertainty in the flux of each data point (e.g.  $1\sigma$ ),  $y_i$  is the observed flux,  $y(x_i)$

is the model predicted flux for the wavelength  $x_i$  and  $n$  is the total number of spectral data points.

The best fit model representation of the data is found by calculating the  $\chi^2$  statistic for different models, and stepping in small increments through the model grid, linearly interpolating between calculated grid points. Care must be taken by the user to ensure a true global minimum is found, and not simply a local minima.

After finding the global minimum in  $\chi^2$ , confidence limits are placed on the free parameters ( $\log g$ ,  $T_{\text{eff}}$ , line scaling, and wavelength shifts). This is performed by applying another iterative procedure, whereby the parameter in question is stepped further and further away from its optimum value and each time finding a new minimum  $\chi^2$ , until the difference between this and the original “best fit”  $\chi^2$  value,  $\delta\chi^2$ , corresponds to the  $1\sigma$  (68%) confidence level (for the particular number of free parameters). All errors (limits) derived in this way are formal  $1\sigma$  (68%) confidence bounds only and do not factor in systematic issues with the models or the data.

Simultaneous fitting of the hydrogen Balmer lines has been performed as in Bergeron et al. (1992). The H-Balmer lines,  $\beta$ ,  $\gamma$ ,  $\delta$ ,  $\epsilon$  and 8, were cut out of the optical spectrum of each WD, where limits are chosen such that the majority of the feature is included, but regions of severe overlap are excluded (in particular for the higher order balmer lines). The synthetic model profiles were then simultaneously fitted to the lines, allowing for variation of  $T_{\text{eff}}$ ,  $\log g$ , and wavelength shift, and utilising independent model normalisations for each spectral region.

In this project I use  $\log g$  error of 0.07 and  $T_{\text{eff}}$  error of 2.3% to compensate for uncertainties in the line profiles used in the synthetic spectral calculations (which are much greater than the model fit errors calculated by XSPEC). Napiwotzki et al. (1999) found that for  $T_{\text{eff}} < 30000\text{K}$ , the mean scatter in temperature and surface gravity for their sample was  $\sigma(T_{\text{eff}}) = 2.3\%$  and  $\sigma(\log g) = 0.07$  dex respectively. See also Section 1.4.4.

The comparatively weaker (yet formally still high field) DAH WDs that were unable to be modelled externally using magnetic models (DD02A and DD4A), were remodelled in XSPEC with my non-magnetic model grid, ignoring their line centres to prevent an overestimate of their masses. This was required as for these magnetic WDs, the peaks of their balmer line decrements are contaminated as product of their magnetic fields. The modelling accuracy using this method of ignoring the centres of the balmer lines was verified using the hot companion, DD-04B. The values of its output parameters  $T_{\text{eff}}$  and  $\log g$  when modelled using the same method (ignoring the balmer line centres) were calculated to be within the error limits of their original derivation (including balmer line centres), ie  $T_{\text{eff}} = 27545.2 \pm 633.5$ ,  $\log g = 8.38 \pm 0.07$  (ignoring centres) versus  $T_{\text{eff}} = 28066.6 \pm 645.5$ ,  $\log g = 8.45 \pm 0.07$  (original).

Figures 2.22, 2.23, 2.24, and 2.25 display “Christmas Tree” graphs of my spectra with models overlayed. Note DD-02B and DD-08A are missing from all plots as they have been modeled externally using magnetic models.

### Magnetic WD Atmospheric Modelling

Although several of my WD components appeared to be high field magnetic white dwarfs (HFMWDs; DD-02A, DD-02B, DD-04A, DD-08A - see Results Chapter), not all of these systems were actually modelled using synthetic spectra for magnetic atmospheres. Those systems which have been compared to magnetic models to date are the objects DD-02B and DD-08A which have  $B > 50\text{MG}$ . These models were calculated with a radiative transfer code for magnetised, high gravity atmospheres (see Jordan 1993; 1992) and this part of the analysis was performed by Baybars Kulebi (e.g Klebi et al. 2009).

Fine flux calibration (or “flux re-calibration”) was performed before magnetic models were fit to DD-02B and DD-08A, so as to improve the accuracy of the fitting. This was achieved by dividing the spectra of their alternate components (DD-02A and DD-08B) with their best fit (non-magnetic) spectroscopic models, and fitting a curve (polynomial function) to the result. The flux calibrated spectra of DD-02B and DD-08A was then multiplied by this fitted curve. The software used to perform this flux re-calibration is outlined in the Appendix Section [A.5.6](#).

### 2.4.2 Evolutionary modelling

Once  $\log g$  and  $T_{\text{eff}}$  values had been determined for a WD using the atmospheric models, I used evolutionary models from the Montreal Group (Fontaine et al. 2001, Holberg and Bergeron 2006) to determine the cooling age, the mass and the absolute magnitude values. These models are available from <http://www.astro.umontreal.ca/~bergeron/-CoolingModels> where a description of them is also provided. I show examples of the theoretical cooling sequences of two WDs of different masses in Figure [2.21](#). The code used to perform these calculations is referenced in Appendix Section [A.5.2](#).

The evolutionary sequence fitting requires apparent magnitude data for the components, and this is taken from the SDSS. It should be noted here that interstellar reddening is assumed to be negligible. This is a reasonable assumption since these are in general high galactic latitude systems within  $\sim 200\text{pc}$ . In any case, these objects share very similar lines of sight so reddening levels towards the components of a given system are likely to be comparable.

For temperatures  $< 30000\text{K}$  the theoretical mass-radius relations are based upon the *CO* (carbon-oxygen) core, thick H-layer evolutionary models of Fontaine et al. (2001) but with  $q_H = 10^{-4}$  of Bergeron et al. (2001).

Colour calculations are described in Holberg and Bergeron (2006), which is an extension of the work by Bergeron et al. (1995b).

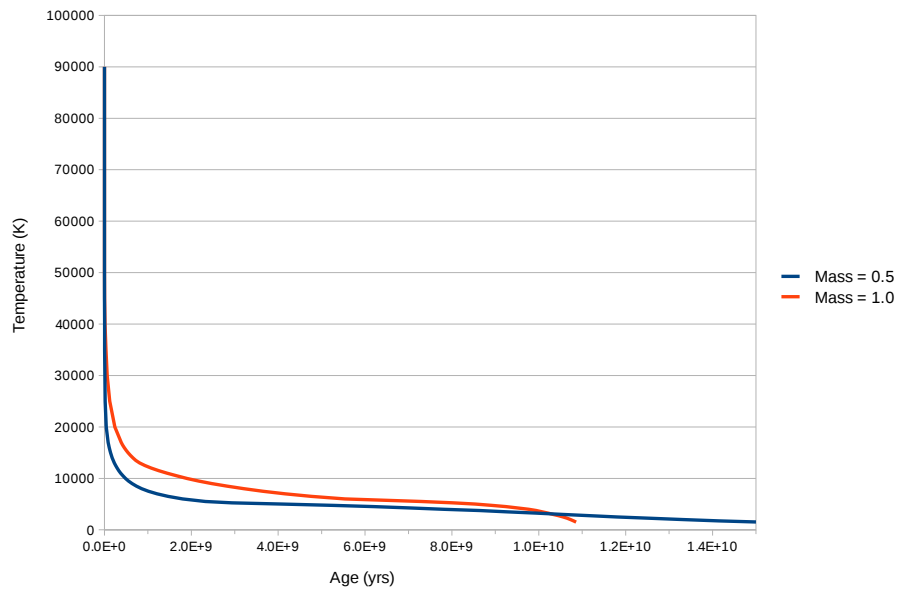


FIGURE 2.21: Bergeron Theoretical WD Cooling Tracts - Temperature versus Age for a given mass. The cooling tracts for both a low mass ( $0.5M_{\odot}$ ) and a high mass ( $1.0M_{\odot}$ ) WD are shown.

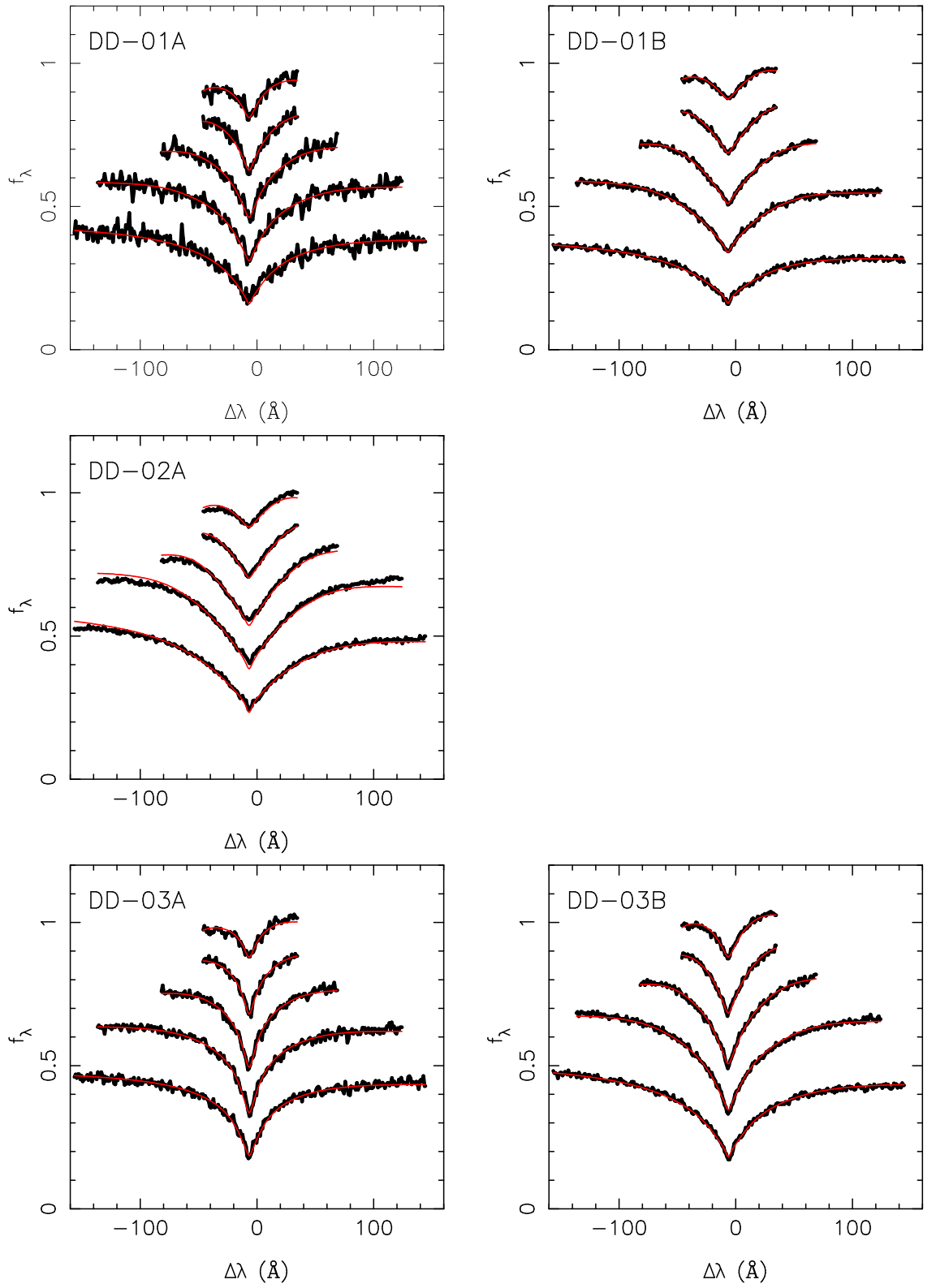


FIGURE 2.22: “Christmas Tree” graphs of my spectra with models overlayed (DD-01 to DD-03). Note DD-02B and DD-08A are missing (as they have been modeled externally using magnetic models).

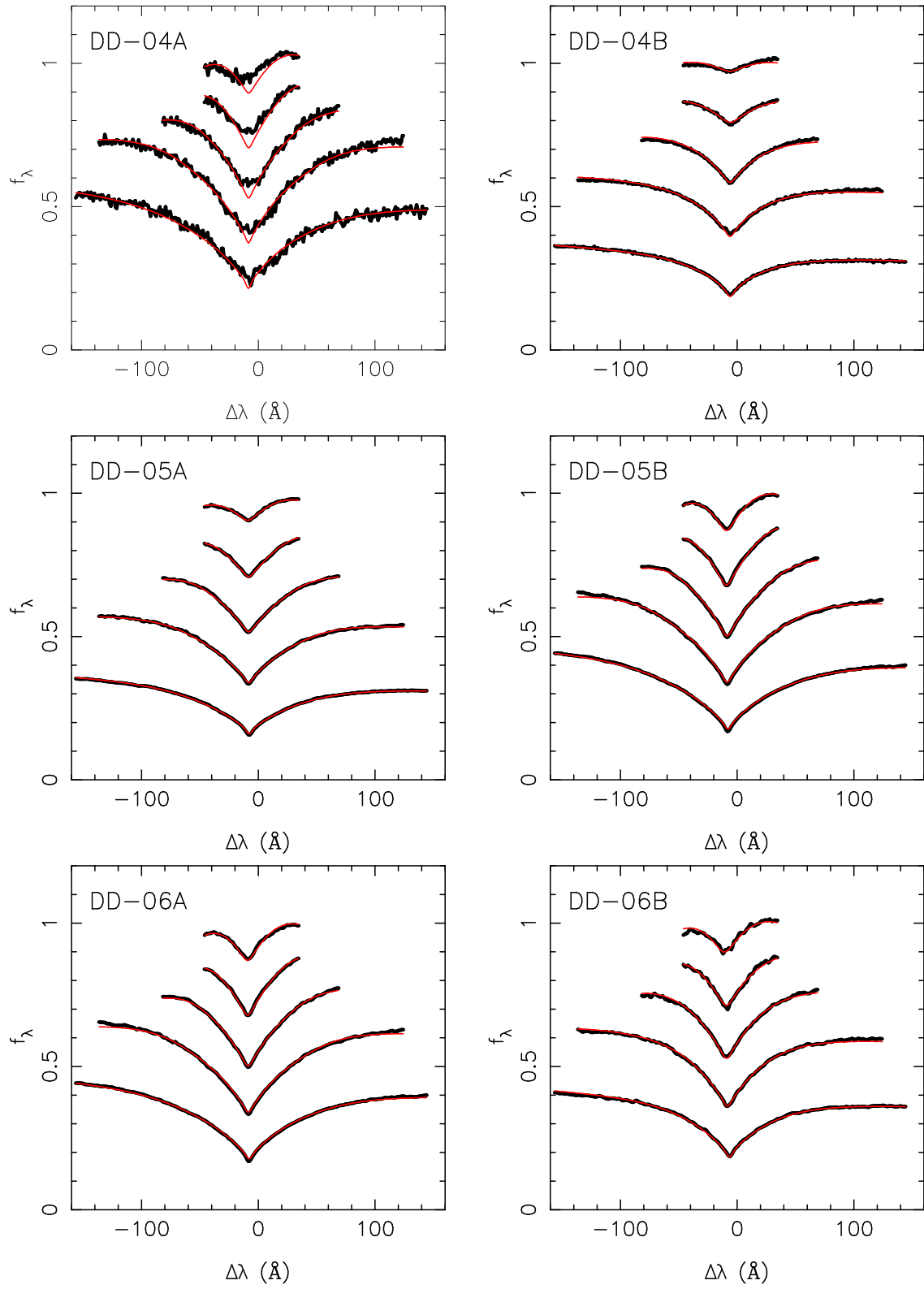


FIGURE 2.23: “Christmas Tree” graphs of my spectra with models overlaid (DD-04 to DD-06).



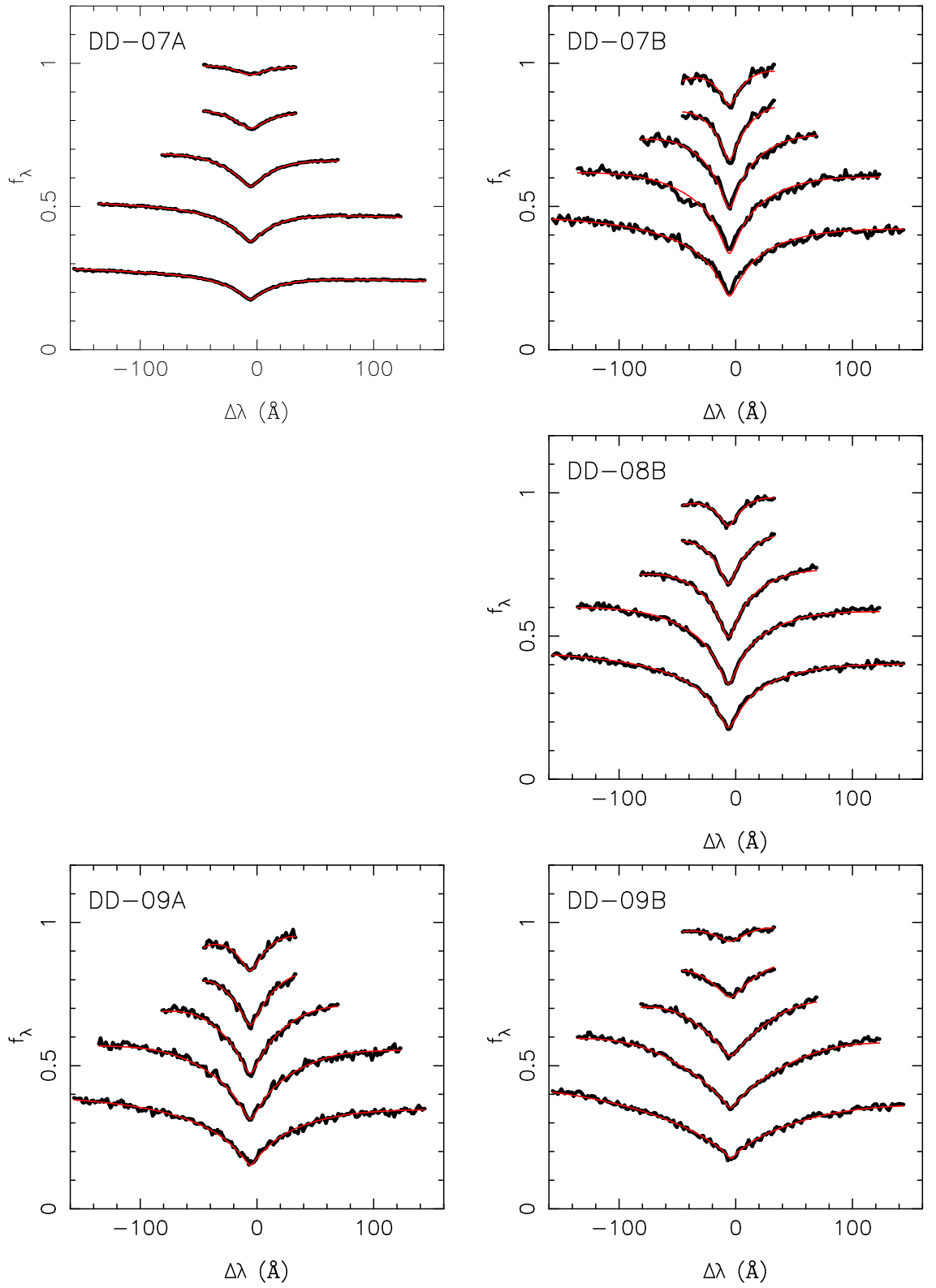


FIGURE 2.24: “Christmas Tree” graphs of my spectra with models overlaid (DD-07 to DD-09). Note DD-02B and DD-08A are missing (as they have been modeled externally using magnetic models).

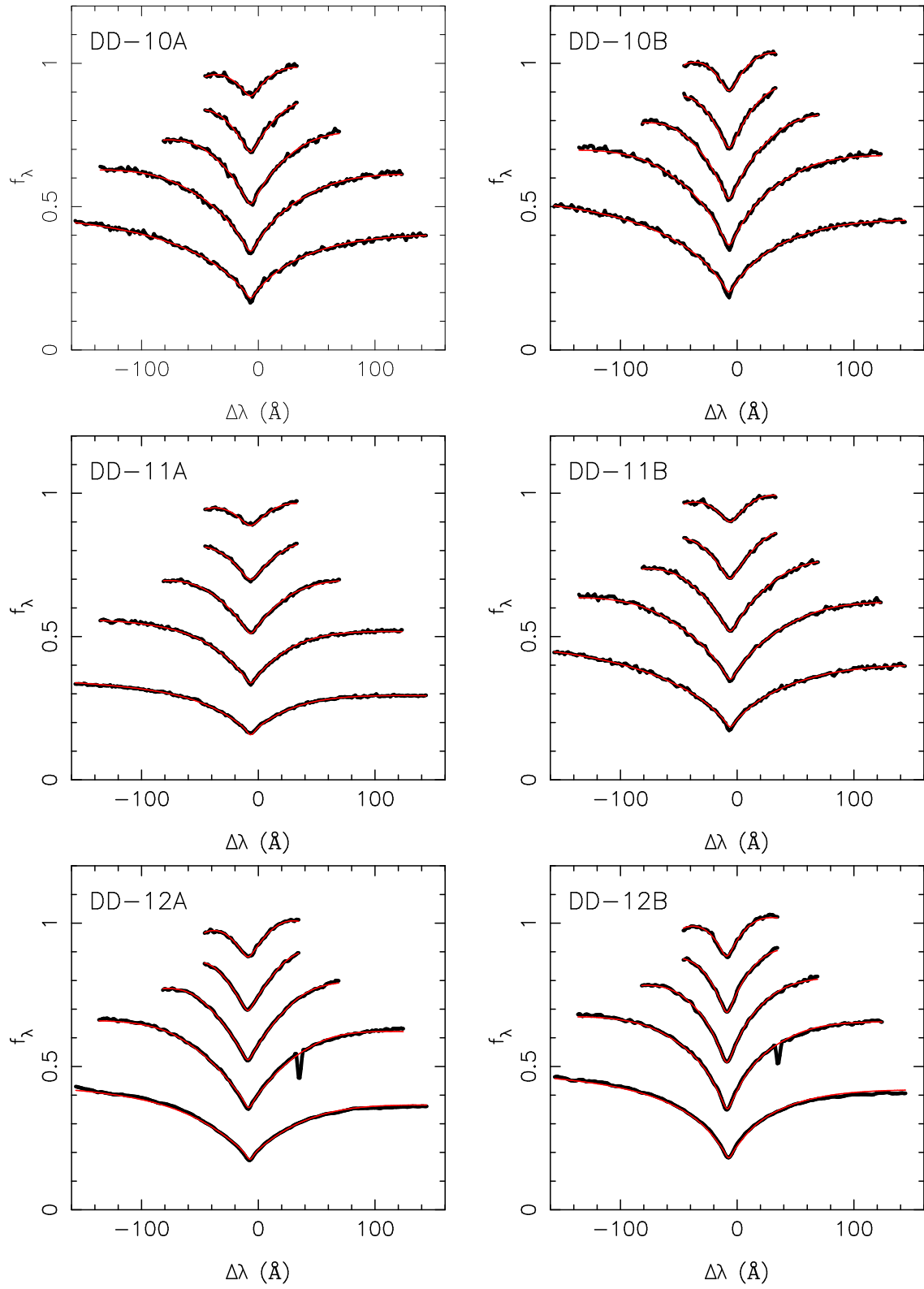


FIGURE 2.25: “Christmas Tree” graphs of my spectra with models overlaid (DD-10 to DD-12).

### 2.4.3 Proper motion verification of physical association

While I have estimated the probability of chance alignment for pairs of objects within 5", 10", 20", and 30" to be 5%, 10%, 25%, and 40% respectively, in my sample of 53 candidate systems this still translates to a non-negligible fraction of these being random alignments. Therefore for objects which were followed-up spectroscopically, I performed proper motion measurements to obtain a strong independent confirmation (or otherwise) on a case by case basis that system components were physically associated. These were performed using an implementation of the method outlined in Casewell et al. (2007) and Moraux et al. (2001). The full procedure is outlined in the Appendix Section A.3. It is dependent upon the software code *pmx - t.f* but can be summarised as follows:-

For each candidate pairing I determined the X,Y positions within the frames of surrounding objects of comparable or greater brightness within 4.0'. The detection of these objects was performed in the **SExtractor** under **GAIA** and provided on average > 20 suitable reference sources. Next, I cross matched on RA and DEC the lists of reference star positions using the **STARLINK TOPCAT** software. Subsequently, I employed routines in the **STARLINK SLALIB** library to construct six co-efficient linear transforms ( $x_1 = Ax_2 + By_2 + C, y_1 = Dx_2 + Ey_2 + F$ ) between the two images, epoch 1, POSS-I blue and epoch 2, SDSS *g*, of the putative systems, where  $>3\sigma$  outliers were iteratively clipped from the fits ( $1\sigma$  was calculated by taking  $1.48\times$  the median of the absolute residuals of the reference stars). The proper motions, in pixels, were then determined by taking the differences between the observed and predicted locations of candidates in the 2nd epoch imaging. These were converted into milli-arcseconds per year in right ascension and declination using the world co-ordinate systems of the 1st epoch datasets and dividing by the time baseline between the two observations.

As WDs are intrinsically faint and therefore typically nearby, it is likely that they will also lie quite far away from the average displacement ( $\sim 0, \sim 0$ ) of the generally more distant reference stars within the field. If the WD components of any given BOCP are associated, then it is expected that they will have the same relative proper motions within the measurement uncertainties. These errors have been estimated by combining quadratically the **GAIA** object detection fit errors for both epochs (SDSS and POSS-I) and the RMS residue of the reference field star correlation as calculated by *pmx - t.f*. The proper motion error calculation procedure has been included in the Appendix Section A.3.1, along with the xy to RA-Dec calibration procedure in Section A.3.3.

Figures 2.26 and 2.27 display proper motions vector point diagrams for the components of my candidate wide DD systems. Additionally, the proper motions are listed in Table 2.8.

I found the proper motion measurements within the SDSS database to be unreliable for these systems. It is suspected that the low angular separation of the components has led to unreliable determinations of their centroids in the photographic data. Indeed, those systems with the highest angular separation have SDSS proper motion measurements with the highest level of correspondence to my own proper motion measurements, i.e. DD-03 and DD-04 at 11.16" and 9.14", respectively (although it is

worth noting that DD-07 at 18.91" does not show a clear correspondence with its SDSS proper motion measurements).

The differences in the proper motions between the components of some systems are substantially larger than their estimated  $1\sigma$  statistical errors. While it should be expected, for the case of normally distributed errors, that with a sample of twelve pairings that are genuinely physically associated,  $\sim 4$  will lie beyond  $1\sigma$ , the proper motions of the components of two systems are in discord at  $>4$  sigma (i.e. DD-05 and DD-08). However, as the components of these pairs each have proper motions that are measured as  $>50$  mas yr $^{-1}$  and lie in the same general region of the vector point diagram, I suspect that these discrepancies are not indicative of these being visual binaries but are instead due to systematic uncertainties in the **GAIA SExtractor** object centroiding calculations. **SExtractor** was designed for low density, high Galactic latitude fields and has difficulty in determining the centroids of objects in pairs with very low angular separations (ie. blended). This is particularly relevant when working with the rather low resolution POSS-I blue photographic data. This suspected systematic error in the centroid calculation due to the blending of sources could be reduced using a more sophisticated modelling of the point spread function, but this was not attempted here. Instead, I recalculated the proper motions of the components of DD-08 using the SDSS  $r$  band image and the POSS-I red plate in which these sources are fainter but slightly better resolved. In this case, the proper motion estimates are much closer to each other (to within or near the extent of their calculated uncertainties), supporting my suspicions that there are systematic errors in my first proper motion measurements for these two systems. Indeed, it is apparent from a visual inspection that for DD-05, in the POSS-I blue frame the centroid calculations result in a very large  $\sim 3$  pixel deviation between components (which corresponds exactly to their calculated difference in proper motion).

With astrometry for these twelve systems in hand, two methods were then employed to estimate the likelihood of their components exhibiting common proper motions by chance. In a first approach, the probability of a BOCP exhibiting the observed proper motion without being associated was calculated based upon the probability of a generated circular field containing the BOCP proper motions (including their errors) lying within a generated circular area containing both the BOCP and the astrometric reference stars. This basic statistical calculation is implemented under the assumption that the BOCP components are most likely WDs, and therefore are likely to have higher proper motions than all of the observed targets within the field, making it realistic to assume that they could lie anywhere in the field (not just within the main field distribution of astrometric reference stars) regardless of their association. The code used in this method has been referenced in the Appendix Section [A.3.5](#).

In an alternative approach, the probability of chance common proper motion alignment was calculated by counting the number of M stars at approximately the same distance as the DD system within  $\approx 5'$  which would have been flagged as having a common proper motion with the DD system - i.e., have proper motions within an artificial two dimensional range bounded by the proper motions (plus proper motion errors) of each WD component. The proper motions of  $\approx 150$  nearest Red Dwarfs ( $< 3^\circ$ ,  $> 5'$ ) at the same distance as the DD system were obtained using an SDSS SQL

query. The distance of the M stars were calculated using an empirical low mass star colour-magnitude relationship discussed by Fuchs et al. (2009) and shown in Equation 2.6, using photometric data from the SDSS. This method should indicate that solar reflex has not significantly influenced/biased these proper motion values. The code used to perform this method has been referenced in the Appendix Section A.3.4.

$$M_r = 4.0 + 11.86(r - i) - 10.74(r - i)^2 + 5.99(r - i)^3 - 1.20(r - i)^4 \quad (2.6)$$

In a variant on the second approach, the astrometry of spectroscopically identified WDs from the SDSS lying within  $10^\circ$  of the double-degenerate pair is examined to determine what proportion of these would have been flagged as having a common proper motion. The code used to perform this method is also referenced in the Appendix Section A.3.4.

The probabilities of chance proper motion alignment were then combined with the probabilities of chance spatial alignment derived from by the Monte-Carlo like simulations. These results are presented in Table 2.9. All seem to indicate a low probability of a chance spatial+astrometric alignment. Note that the probability of having a chance alignment in my sample based on combining these statistics is calculated as 0.0089 ( $\sim 1\%$ ), as per Equation 2.2.

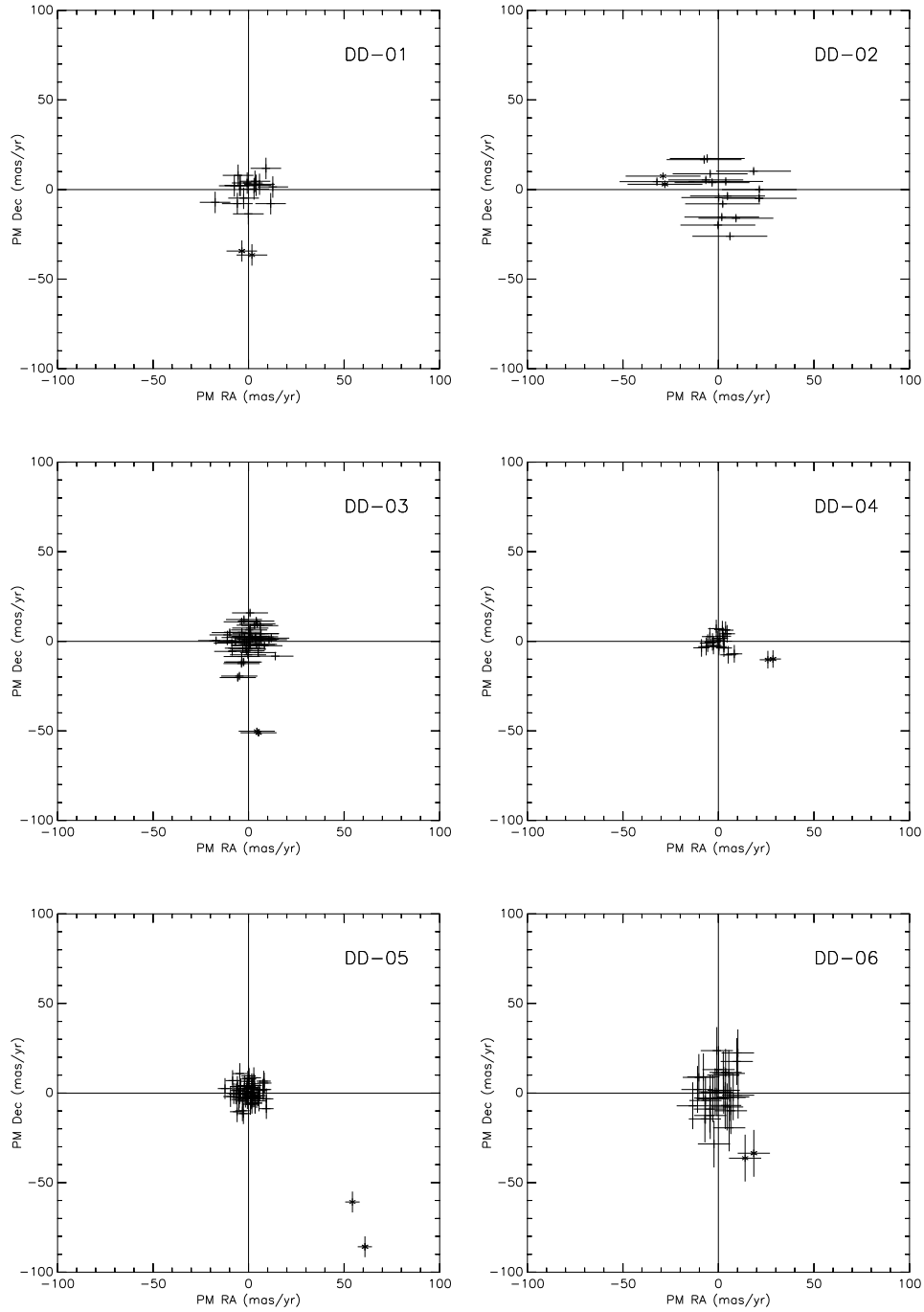


FIGURE 2.26: Proper motion diagrams for the 12 blue object close pairs for which I observed spectroscopic follow-up data (DD01 to DD06). The DD system components are marked as stars.

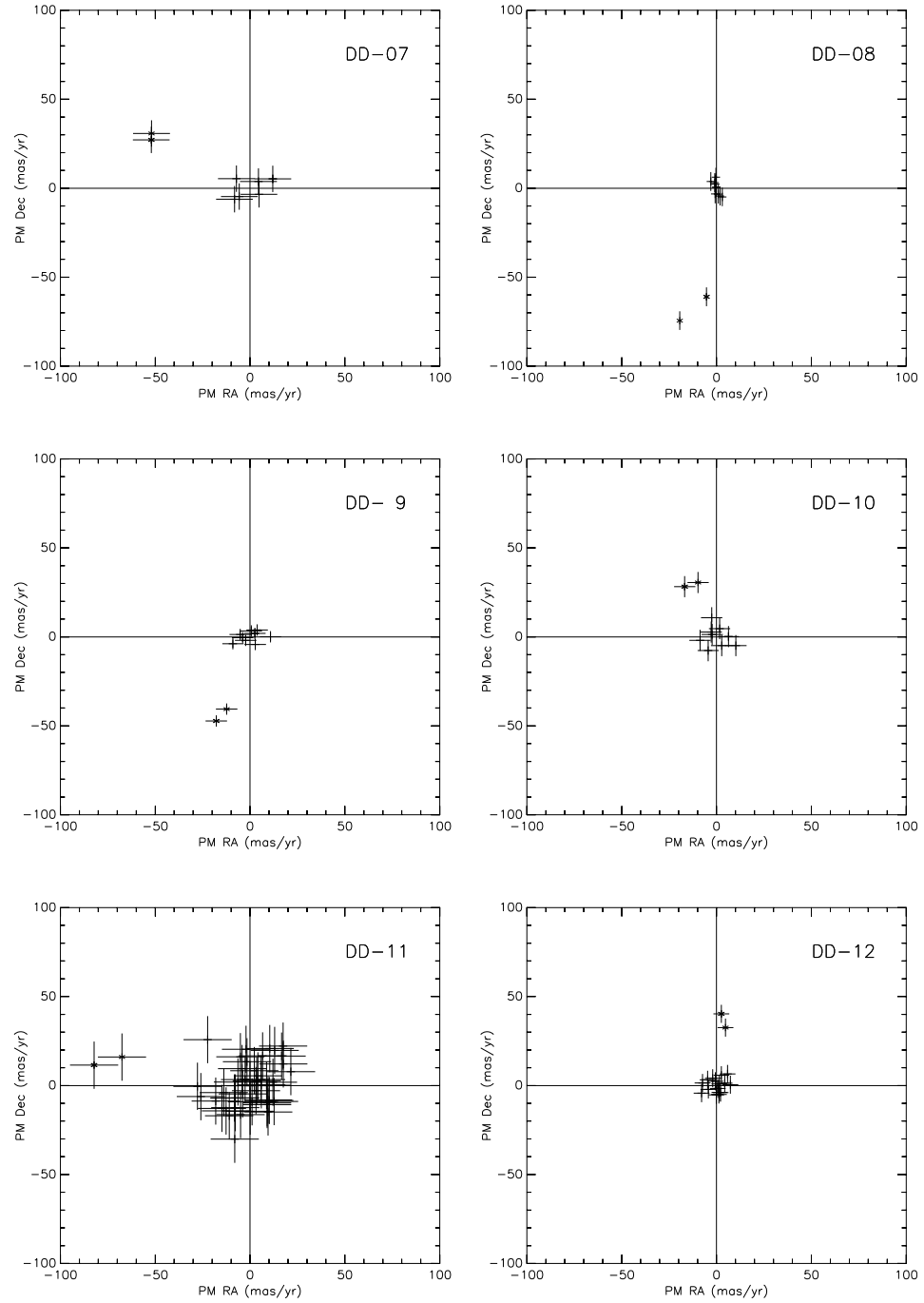


FIGURE 2.27: Proper motion diagrams for the 12 blue object close pairs for which I observed spectroscopic follow-up data (DD07 to DD12). The DD system components are marked as stars.

TABLE 2.8: Double-Degenerate Data - Proper Motions

WD	PM RA (mas/yr)	PM Dec (mas/yr)	$\delta$ PM RA (mas/yr)	$\delta$ PM Dec (mas/yr)	Avg PM RA nearby Red Dwarfs	Avg PM Dec nearby Red Dwarfs	Prob of PM Chance Align (PDD)	Prob of PM Chance Align (RBB)	SDSS PM RA (mas/yr)	SDSS PM Dec (mas/yr)	SDSS $\delta$ PM RA (mas/yr)	SDSS $\delta$ PM Dec (mas/yr)
DD-01A	1.74	-36.55	8.02	5.96	-4.38	6.86	0	0.02	18.25	-39.65	3.54	3.54
DD-01B	-3.56	-34.34	8.01	6	0	0	0	0	-2.98	-38.47	3.14	3.14
DD-02A	-28.01	2.91	19.59	1.54	-6.23	-1.64	0.02	0.01	-73.94	66.73	3.74	3.74
DD-02B	-29.01	7.51	19.59	1.61	0	0	0	0	0	0	0	0
DD-03A	4.29	-50.2	9.46	1.82	-2.76	-3.6	0	0	-1.79	-51.17	3.41	3.41
DD-03B	5.22	-51.13	9.45	1.7	0	0	0	0	0.32	-50.52	3.13	3.13
DD-04A	25.84	-10.3	4.21	4.91	2.75	-7.28	0.04	0.01	28.09	-14.32	3.26	3.26
DD-04B	28.54	-9.89	4.22	4.86	0	0	0	0	28.57	-16.32	2.75	2.75
DD-05A	60.85	-85.85	3.76	5.82	0.88	-1.71	0	0.07	0	0	0	0
DD-05B	54.35	-60.86	3.75	5.82	0	0	0	0	23.9	-5.01	2.44	2.44
DD-06A	18.56	-33.66	8.44	13.08	4.25	-4.62	0.03	0.02	0	0	0	0
DD-06B	13.92	-36.33	9.04	13.5	0	0	0	0	0	0	0	0
DD-07A	-51.97	30.75	9.7	7.42	6.2	-5.57	0	0	-30.91	-23.31	4.48	4.48
DD-07B	-52.09	27.16	9.68	7.4	0	0	0	0	-24.79	-23.63	5.39	5.39
DD-08A	-19.41	-74.43	0.7	5.29	-5.02	-4.53	0	0.06	-50.89	-142.99	3.88	3.88
DD-08B	-5.27	-61.05	0.88	5.28	0	0	0	0	11.46	-5.05	2.68	2.68
DD-09A	-17.81	-47.27	5.65	3.17	-8.88	-7.47	0	0.02	-22.42	-26.25	2.89	2.89
DD-09B	-12.34	-40.57	5.68	3.2	0	0	0	0	-19.23	-77.07	2.87	2.87
DD-10A	-9.76	30.56	5.6	5.94	-12.21	-3.7	0	0.04	-37.72	34.74	3.99	3.99
DD-10B	-16.79	28.26	5.67	5.93	0	0	0	0	-32.05	24.88	4.66	4.66
DD-11A	-82.2	11.45	12.71	13.26	-6.28	-4.4	0	0.04	-84.01	23.29	2.32	2.32
DD-11B	-67.5	16	12.76	13.31	0	0	0	0	0	0	0	0
DD-12A	4.7	32.6	4.15	5.07	5.58	-9.62	0	0.04	0	0	0	0
DD-12B	2.56	40.26	4.14	5.07	0	0	0	0	0	0	0	0



TABLE 2.9: Double-Degenerate Data - Probability of Chance Alignment

WD	Prob of MC Chance Align	Prob of PM Chance Align	Prob of Chance Align
DD-01	0.01	0.01	0.0001
DD-02	0.03	0.02	0.0006
DD-03	0.09	0.01	0.0009
DD-04	0.02	0.04	0.0007
DD-05	0.01	0.01	0.0001
DD-06	0.03	0.03	0.0012
DD-07	0.74	0.01	0.0074
DD-08	0.04	0.01	0.0004
DD-09	0.03	0.01	0.0003
DD-10	0.02	0.01	0.0002
DD-11	0.01	0.01	0.0001
DD-12	0.04	0.01	0.0004

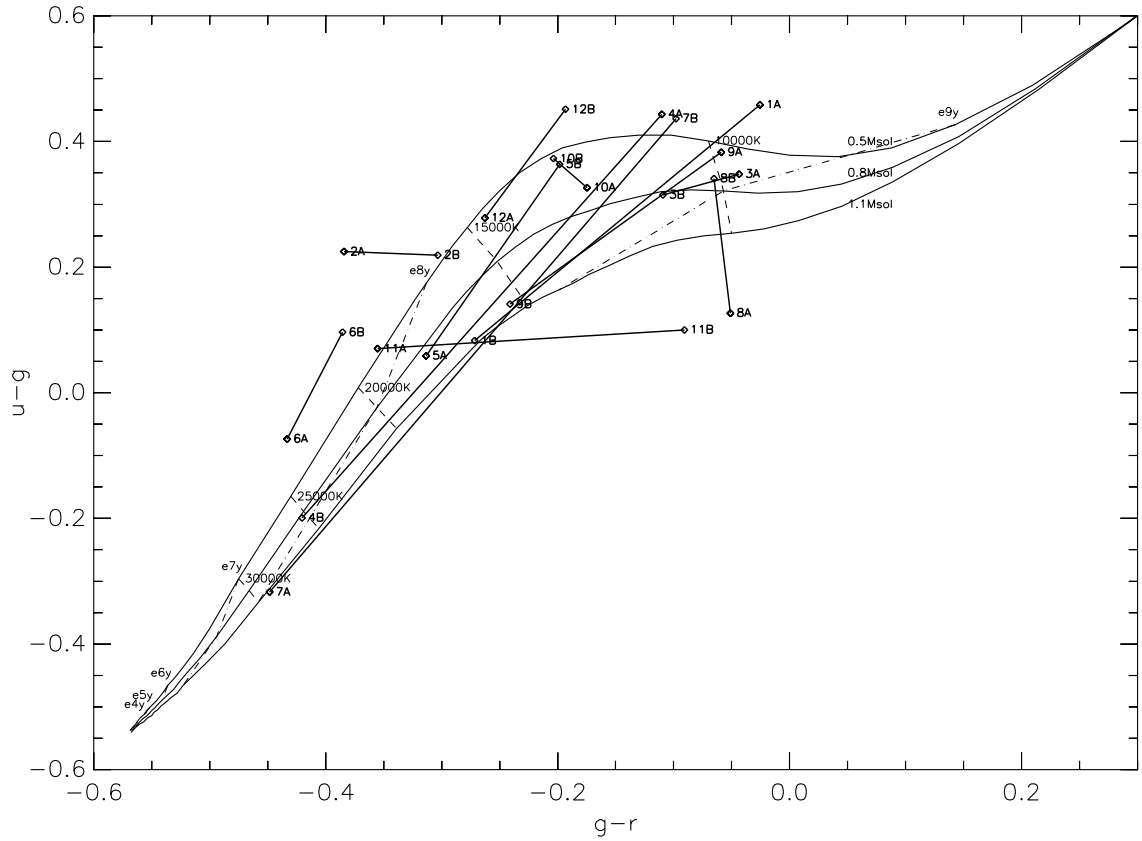


FIGURE 2.28: Colour-Colour for my 12 DD candidates ( $u-g$  vs  $g-r$ ). Bergeron cooling tracts are shown with specific ages ( $t_{cool} = 1 \times 10^4 yrs - t_{cool} = 1 \times 10^9 yrs$ ) and temperatures ( $T_{eff} = 30000K - T_{eff} = 5000K$ ).



*“Further: Wish has for its object the End rather, but Moral Choice  
the means to the End”*

from Aristotle’s Nicomachean Ethics

# 3

## Results

### 3.1 Properties of the components of the wide double-degenerate systems.

The masses, the cooling times and the absolute magnitudes for the WDs presented here were in general obtained by comparing my spectroscopic effective temperature ( $T_{\text{eff}}$ ) and surface gravity ( $\log g$ ) estimates to grids of synthetic photometry (Holberg and Bergeron 2006) and evolutionary models (Fontaine et al. 2001). Custom written IDL routines (see Appendix), were used to perform bi-cubic spline interpolation between points in these grids. As these binaries consisted of WDs with different spectral characteristics, I had to follow a number of different approaches to determine their component properties. I outline each of these in turn below. My results are shown in Table 3.1.

#### 3.1.1 Hot DA + hot DA systems

Here I define a hot DA as a H-rich object with no obvious sign of a magnetic field (i.e. no Zeeman splitting or broadening apparent in the line cores) and with an effective temperature,  $T_{\text{eff}} > 12000K$ . For systems containing two such WDs, the component parameters were calculated completely independently. Absolute magnitudes, masses, cooling ages and distances were calculated by interpolating within the DA evolutionary grids to their measured spectroscopic temperatures and surface gravities. For each system (component), the uncertainties were calculated for the output parameters following the method outlined in Section 3.1.6. The systems which I found to contain two hot DA WDs are DD-05, DD-06, DD-10 and DD-11.

### 3.1.2 Cool DA + hot DA systems

Here I define a cool DA as a H-rich object with no obvious sign of a magnetic field (i.e. no Zeeman splitting or broadening apparent in the line cores) and with an effective temperature,  $T_{\text{eff}} \leq 12000K$ . Spectroscopic mass determinations are known to be systematically larger in this regime than at higher effective temperatures where they agree well with those derived from gravitational redshifts (e.g. Bergeron et al. 1995a). This trend is most likely due to shortcomings in the treatment of convection within the model atmosphere calculations (Koester 2010, Tremblay et al. 2011). Hence for systems containing both a cool DA and a hot DA, I first determined the mass, the cooling time and the absolute magnitude of the latter component, as outlined above in Section 3.1.1. I then derived the distance modulus for the system from the apparent and the absolute  $g$  magnitudes of the hot DA. Subsequently, the parameters of the cool DA were calculated using the spectroscopic effective temperature estimate, the system distance and the apparent  $g$  magnitude of this component. While the same underlying evolutionary model grid was used in this case, the input parameters used here were the effective temperature, the system distance and the apparent  $g$  magnitude (as opposed to effective temperature and surface gravity). For each component, the uncertainties on the derived parameters are calculated following the method outlined in Section 3.1.6. The systems I found to contain a hot DA and a cool DA are DD-01, DD-07, DD-09 and DD-12.

### 3.1.3 Cool DA + cool DA systems

I have defined what I mean by a cool DA and outlined the issue with spectroscopic mass estimates for these objects in Section 3.1.2 above. Therefore, after following the prescription outlined in Section 3.1.1 to obtain a preliminary estimate of the masses of the cool components in these systems, I apply a (downward) correction of  $dM = -0.17 \pm 0.04M_{\odot}$ , derived from the systems in my sample containing both a hot and a cool DA, to account for the spectroscopic overestimate. Based on my revised mass estimates, the parameters for each cool DA are recalculated (e.g. surface gravity and cooling time) using the same underlying evolutionary model grid but where the input parameters in these cases are effective temperature and mass. The uncertainties are calculated for all output parameters following the method outlined in section 3.1.6. These are larger than for systems containing at least one hot DA. The larger uncertainties in mass result in higher errors in the derived cooling times. DD-03 is the only system in my sample where both components are cool DA WDs.

### 3.1.4 HFMWD (DAH) + hot DA systems

The spectra of high field magnetic WDs (HFMWDs) are generally characterised by absorption lines which are very strongly broadened and shifted in wavelength and/or show Zeeman splitting (Schmidt et al. 2003). As detailed Stark line profile calculations do not yet exist for the high field regime, it is not possible to accurately determine the surface gravities and hence masses of these objects using the ‘standard’ spectroscopic

approach. Therefore, for my two systems which were found to contain a DAH and a hot DA (DD-02 and DD-04) I have followed the method described in Section 3.1.2, where the effective temperature of the DAH was obtained from the modelling undertaken by Baybars Kulebi. The larger errors in the effective temperature determinations for these DAHs (relative to a cool DA) propagate as greater uncertainties in the estimates of their masses.

### 3.1.5 HFMWD (DAH) + cool DA systems

For systems containing a cool DA and a DAH I first followed the procedure outlined in Section 3.1.3 to derive preliminary parameters of the former component. Next, I estimated the distance to the system using the apparent  $g$  magnitude and the absolute  $g$  magnitude predicted on the basis of the downward revised mass estimate for the DA. Subsequently, the parameters of the DAH were determined as for those in the systems described in Section 3.1.4. The errors in the mass of the cool DAs and therefore the estimated system distances lead to greater errors in the masses determined for these DAHs relative to those paired with hot DAs. Only one of the systems in my sample, DD-08, was found to contain a cool DA and a HFMWD.

### 3.1.6 Estimation of the uncertainties in derived parameters

The uncertainties in the derived parameters of the WDs (distances, masses, cooling times, progenitor masses, progenitor lifetimes and system ages) were estimated using custom written IDL routines. After I had calculated the most likely value for each of these “derived” parameters, I generated 25000 realisations of the WD pairing, allowing for normally distributed errors in the “measured” parameters of these objects (effective temperatures, surface gravities, observed magnitudes, IFMR linear coefficients). Following Napiwotzki et al. (1999), for effective temperatures and surface gravities I assumed uncertainties of at least 2.3% and 0.07dex respectively, while for the SDSS photometry I assumed a minimum uncertainty of at least 0.02 magnitudes (Abazajian et al. 2009). The errors on the linear coefficients were obtained from the relevant papers. Each of these realisations was propagated through the interpolation routines written to determine the most likely values to build up distributions for these “derived” parameters. After sorting the arrays holding the 25000 estimates of these parameters, I selected the values in these distributions above and below which 16% of these data lay, which represent, approximately,  $1\sigma$  upper and lower bounds.

## 3.2 The double-degenerate systems on a case-by-case basis

My estimates of the masses, the cooling times, the absolute magnitudes and the distances for the components of the twelve systems studied here are shown in Table 3.1. In determining the distances to my objects, I chose to ignore interstellar reddening since these targets are generally at relatively high galactic latitudes and are fairly close

to the Sun (typically  $\lesssim 200\text{pc}$ ). Moreover, as these pairings have very small angular separations, they share similar lines of sight so any low level extinction towards the components of a particular system is likely to be comparable and result in a small systematic overestimate of the binary's distance.

I have plotted the distances to the components of each system in Figure 3.2. Figures 3.3 and 3.4 show the matching of distance moduli for DD systems with at least one cool component. Figures 3.5 and 3.6 show the matching of distance moduli for DD systems with two cool components or a HFMWD system. Figure 3.7 shows the distances of the components within systems comprising only hot components.

I have used the components of these systems to probe three recent (independent) determinations of the form of the IFMR which are based largely on WD members of young and intermediate age open clusters ie.  $\tau < 1\text{Gyr}$ , ie. (e.g Dobbie et al. 2006), (Kalirai et al. 2008) and (Williams et al. 2009). In each of these cases the IFMR has been modelled using a simple linear function, with co-efficients of  $a_0=0.289\pm0.051$   $a_1=0.133\pm0.015$ ,  $a_0=0.394\pm0.025$   $a_1=0.109\pm0.007$  and  $a_0=0.339\pm0.015$   $a_1=0.129\pm0.004$ , respectively.

I have used these relations to calculate the initial (progenitor) mass of each degenerate and then appealed to the solar metallicity stellar evolutionary models of Girardi et al. (2000) to determine their stellar lifetimes. By combining these with the WD cooling times I have obtained two estimates of the total age of each binary. If the published IFMRs are a good representation of the transformation of these objects from stars to WDs then it could be expected that for each system these two age estimates are consistent with one and other. However, if discord is found between the age estimates, this would suggest that these IFMRs do not reflect well the past evolution of the objects in question and for these cases I have proposed some possible reasons for this. These calculations have been performed using the codes listed in Appendix Section A.6.1, and my data spreadsheet referenced in Appendix Section A.7.1. I will now discuss the results of this process for each system on a case-by-case basis.

### 3.2.1 DD-01

Optical spectroscopy of the components of this binary indicates both to be hydrogen rich WDs and reveals no evidence for the presence of magnetic fields. Component A is a cool DA and component B is a hot DA thus it has been analysed following the method I outlined in 3.1.2. These objects are separated on sky by  $6.78 \pm 0.1''$  and have consistent proper motions in RA, Dec of  $1.7 \pm 8, -36.6 \pm 8 \text{ mas yr}^{-1}$  and  $-3.6 \pm 8, -34.3 \pm 8 \text{ mas yr}^{-1}$ , respectively. I have estimated, based on the observed properties, that there is less than a 1 in 10000 probability that these objects merely form a visual binary. I have determined DD-01A and DD-01B to have effective temperatures of  $T_{\text{eff}} = 10648 \pm 245\text{K}$  and  $T_{\text{eff}} = 19199 \pm 442\text{K}$ , respectively, and derived their masses and cooling times to be  $M=0.51^{+0.09}_{-0.05}\text{M}_{\odot}$ ,  $\tau_{\text{cool}}=419^{+79}_{-38}\text{Myr}$  and  $M=0.61^{+0.04}_{-0.04}\text{M}_{\odot}$ ,  $\tau_{\text{cool}}=76^{+16}_{-13}\text{Myr}$ , respectively. Subsequently, from the characteristics of the hot DA, I have estimated the distance modulus of this system to be  $m_g - M_g = 7.06 \pm 0.12$ .

Adopting the recent Dobbie et al. (2006), Kalirai et al. (2008) and Williams et al.

(2009) determinations of the IFMR, in turn, I estimate the progenitor mass of component A to be  $M_{\text{init}}=1.66^{+1.04}_{-0.51}M_{\odot}$ ,  $1.07^{+0.93}_{-0.48}M_{\odot}$  or  $1.33^{+0.72}_{-0.38}M_{\odot}$ , respectively. The corresponding stellar lifetimes as predicted by the solar metallicity model grid of Girardi et al. (2000) are  $\tau=2149^{+4089}_{-1584}$  Myr,  $9756^{+5604}_{-9569}$  Myr or  $4313^{+7997}_{-3119}$  Myr, resulting in total system age estimates of  $\tau=2568^{+4108}_{-1410}$  Myr,  $10170^{+5610}_{-9136}$  Myr or  $4731^{+8019}_{-3033}$  Myr, respectively. Similarly, for component B I calculate initial masses of  $M_{\text{init}}=2.38^{+0.6}_{-0.52}M_{\odot}$ ,  $1.94^{+0.46}_{-0.43}M_{\odot}$  or  $2.06^{+0.34}_{-0.33}M_{\odot}$ , leading to estimates of the total system age from this component of  $\tau=989^{+732}_{-417}$  Myr,  $1627^{+1382}_{-650}$  Myr or  $1450^{+529}_{-476}$  Myr, for Dobbie et al. (2006), Kalirai et al. (2008) and Williams et al. (2009) respectively.

I find that my system age determinations from the two components are not formally consistent within their error bounds. This suggests that the simple models I adopt for mapping the masses of stars, from the main sequence to the WD stage, may not be a particularly good description of reality, at least in the case of this particular system. It is possible that none of the three IFMRs adopted here accurately reflects the mass loss history of one or both of these stars. The relation may not be very well represented in this initial mass regime by the simple linear fits which have been largely defined by studies of open cluster WDs, the majority of which are from stars of higher initial masses (ie.  $M_{\text{init}} \gtrsim 2\text{--}3M_{\odot}$ ) or possibly there is substantial scatter in the relation here. Alternatively, perhaps as a consequence of having a close companion, component A has endured greater mass loss than is predicted by my models. Studies of stellar multiplicity have revealed that at least 10% of stars are members of triple or higher order systems (Abt and Levy 1976, Raghavan et al. 2010). For reasons of dynamical stability, these systems are frequently hierarchically structured with triples often consisting of a body in a relatively wide orbit around a much closer pairing (Harrington 1972). DD-01A and DD-01B perhaps trace what was the wider orbit of a putative triple system, with component A possibly having been, or perhaps still being, part of a tighter pairing. A  $M_{\text{init}} \sim 2.5M_{\odot}$  star that experiences Roche Lobe overflow while it ascends the thermally pulsing AGB can lead to the formation of a CO WD with a mass which is  $\lesssim 0.15M_{\odot}$  less than that from a single object of this mass (e.g. Iben and Tutukov 1985).

### 3.2.2 DD-02

The components of this system are separated on sky by  $5.05 \pm 0.1''$  and display comparable proper motions in RA, Dec of  $-28 \pm 19.6, 2.9 \pm 19.6 \text{ mas yr}^{-1}$  and  $-29 \pm 19.6, 7.5 \pm 19.6 \text{ mas yr}^{-1}$  for A and B, respectively. I estimate that there is less than a 1 in 1500 probability that these objects form a visual binary. My spectroscopy reveals the components of this system to be a hot DA (A) and a high field magnetic hydrogen rich (B) WD, so it has been analysed following the method I outlined in 3.1.4. I have measured the effective temperatures of DD-02A and DD-02B to be  $T_{\text{eff}} = 17622 \pm 405 K$  and  $T_{\text{eff}} = 18000 \pm 1000 K$ , respectively. I have estimated the mass and the cooling time of DD-02A to be  $0.69^{+0.04}_{-0.04}M_{\odot}$ , and  $157^{+25}_{-22}$  Myr, and the distance modulus of the system to be  $m_g - M_g = 5.81 \pm 0.12$ . Subsequently, I have derived the mass and the cooling time of DD-02B to be  $1.03^{+0.04}_{-0.05}M_{\odot}$ , and  $354^{+50}_{-45}$  Myr. Given the distance of this system and the observed angular separation of the components, I find that DD-02A and DD-02B are separated by at least  $a \sim 750 \text{ AU}$ . Even if it is assumed that the original orbital

separation of this binary was substantially smaller, the Roche lobes of the components have likely always been much larger than the dimensions of an asymptotic giant branch (AGB) star ( $r \lesssim 4\text{--}5\text{AU}$ ; Iben and Livio 1993).

In terms of mass and cooling time, component A is comparable to several of the Hyades WDs (e.g. WD 0352+098, WD 0421+162, Claver et al. 2001), whereas component B ( $M=1.01\pm0.05M_\odot$ ) is similar in mass to the Pleiades WD LB 1497 ( $M=1.02^{+0.04}_{-0.05}M_\odot$ ,  $\tau_{\text{cool}}\sim 50\text{Myr}$ , Bergeron et al. 1992, Dobbie et al. 2006, Wegner et al. 1991). Notably, LB 1497 is descended from a star with a lifetime shorter than the current age of this cluster ( $\tau=125\pm 8\text{Myr}$ , Stauffer et al. 1998) ie.  $M_{\text{init}}\gtrsim 4.8M_\odot$ . The parameters of the DA argue that this system is likely to have a similar total age to the Hyades ( $\tau=625\pm 50\text{Myr}$ , Perryman et al. 1998). Using the stellar lifetimes predicted by solar metallicity models of Girardi et al. (2000) and my determinations of the progenitor mass of component A ( $M_{\text{init}}=3.05^{+0.66}_{-0.57}M_\odot$ ,  $2.76^{+0.5}_{-0.47}M_\odot$  or  $2.76^{+0.37}_{-0.36}M_\odot$ ), I calculate the age of the binary to be  $\tau=611^{+357}_{-181}\text{Myr}$ ,  $766^{+391}_{-219}\text{Myr}$  or  $767^{+261}_{-166}\text{Myr}$ . The parameters of the latter object, which from my model of stellar evolution is the progeny of a star of  $M_{\text{init}}=5.55^{+0.88}_{-0.77}M_\odot$ ,  $5.8^{+0.63}_{-0.62}M_\odot$  or  $5.33^{+0.4}_{-0.44}M_\odot$ , lead to estimates of the total age of the binary of  $\tau=448^{+66}_{-46}\text{Myr}$ ,  $438^{+54}_{-41}\text{Myr}$  or  $457^{+52}_{-40}\text{Myr}$  for Dobbie et al. (2006), Kalirai et al. (2008) and Williams et al. (2009) respectively.

I find that the estimates from the two components are only formally consistent within their quoted ( $1\sigma$ ) error bounds when the oldest, least well constrained of the three approximations to the IFMR (Dobbie et al. 2006) is adopted. While the slight discord between some of the age estimates for this system alone do not constitute a significant result, it is notable for being similar in case to other HFMDs, RE J0317-853 and EG 59, with that derived from the magnetic component being somewhat lower ( $\sim 160\text{--}310\text{Myr}$ ).

### 3.2.3 DD-03

My optical spectroscopy for the stars in this system indicates both to be hydrogen rich WDs. There is no evidence for the presence of magnetic fields. These two cool DAs are separated on sky by  $11.16 \pm 0.1''$  and have “common” proper motions in RA, Dec of  $4.3 \pm 9.5, -50.2 \pm 9.5 \text{ mas yr}^{-1}$  and  $5.2 \pm 9.5, -51.1 \pm 9.5 \text{ mas yr}^{-1}$  for A and B, respectively. I estimate, based on these observed properties, that there is less than a 1 in 1000 likelihood that these stars are not physically associated. This system has been analysed following the method I outlined in 3.1.3.

I determine DD-03A and DD-03B to have effective temperatures of  $T_{\text{eff}} = 10008 \pm 230\text{K}$  and  $T_{\text{eff}} = 11222 \pm 258\text{K}$ , respectively. I estimate their masses and cooling times to be  $M = 0.72^{+0.05}_{-0.05}M_\odot$ ,  $\tau_{\text{cool}} = 795^{+116}_{-101}\text{Myr}$  and  $M = 0.6^{+0.05}_{-0.05}M_\odot$ ,  $\tau_{\text{cool}} = 440^{+65}_{-53}\text{Myr}$ , respectively and find the distance moduli of the two components to be fully consistent with one and other (A:  $m_g - M_g = 6.32 \pm 0.16$ , B:  $m_g - M_g = 6.36 \pm 0.14$ ).

Adopting the recent Dobbie et al. (2006), Kalirai et al. (2008) and Williams et al. (2009) determinations of the IFMR, in turn, I estimate the progenitor mass of component A to be  $M_{\text{init}}=3.22^{+0.71}_{-0.62}M_\odot$ ,  $2.97^{+0.57}_{-0.54}M_\odot$  or  $2.93^{+0.43}_{-0.42}M_\odot$ , respectively. The corresponding stellar lifetimes as predicted by the solar metallicity model grid of Girardi et al. (2000) are  $\tau=388^{+330}_{-164}\text{Myr}$ ,  $492^{+374}_{-194}\text{Myr}$  or  $509^{+276}_{-167}\text{Myr}$  for Dobbie et al. (2006),



Kalirai et al. (2008) and Williams et al. (2009) respectively, resulting in total system age estimates of  $\tau=1182_{-127}^{+296}$  Myr,  $1287_{-116}^{+311}$  Myr or  $1304_{-82}^{+201}$  Myr, respectively. Similarly, for component B I calculate initial masses of  $M_{\text{init}}=2.32_{-0.58}^{+0.66}M_{\odot}$ ,  $1.87_{-0.53}^{+0.56}M_{\odot}$  or  $2.01_{-0.42}^{+0.45}M_{\odot}$ , leading to estimates of the total system age from this component of  $\tau=1411_{-442}^{+887}$  Myr,  $2073_{-732}^{+2435}$  Myr or  $1900_{-566}^{+966}$  Myr, respectively. I find my estimates of the binary age from these two WDs are consistent with each other, indicating that the three IFMRs I adopt here may offer a satisfactory description of the massloss history of the components of this particular system.

### 3.2.4 DD-04

The components of this system are separated on sky by  $9.14 \pm 0.1''$  and display similar but small proper motions in RA,Dec of  $25.8 \pm 4.2, -10.3 \pm 4.2$  mas yr $^{-1}$  and  $28.5 \pm 4.2, -9.9 \pm 4.2$  mas yr $^{-1}$  for A and B respectively. I estimate, based on these observed properties, that there is less than a 1 in 1000 probability that these objects are not physically related. Optical spectroscopy of this pairing reveals DD-04 to consist of two hydrogen rich WDs, one a high field magnetic (DD-04A) and the other non-magnetic (DD-04B). I have estimated the effective temperatures of DD-04B to be  $T_{\text{eff}} = 28067 \pm 646 K$ . I have also estimated the effective temperature (and surface gravity) of DD-04A to be  $T_{\text{eff}} = 16018 \pm 368 K$ , by excluding the central Zeeman split portions of the Balmer line cores from the spectral fitting process. As this system consists of a (comparatively) lower field DAH (DD-04A) and a hot DA (DD-04B), it has been analysed following the method I outlined in 3.1.1.

I have determined the mass and the cooling time of DD-04A to be  $0.71_{-0.04}^{+0.04}M_{\odot}$ , and  $310_{-36}^{+42}$  Myr, and the mass and the cooling time of DD-04B to be  $0.91_{-0.04}^{+0.04}M_{\odot}$ , and  $54_{-12}^{+14}$  Myr. I have calculated the distance moduli of DD-04A and DD-04B to be  $m_g - M_g = 6.99 \pm 0.12$  and  $m_g - M_g = 5.74 \pm 0.14$ , respectively and I find them to be substantially different (1.26 magnitudes,  $\sim 6\sigma$ ). Even if DD-04B was itself a multi system, which can result in objects appearing up to 0.75 magnitude closer, there would still be a discrepancy of 0.5 magnitudes. Thus, I am forced to conclude that these objects do not constitute a physical system.

### 3.2.5 DD-05

The components of DD-05 are separated on sky by  $6.56 \pm 0.1''$  and display proper motions in RA,Dec of  $60.9 \pm 3.8, -85.9 \pm 3.8$  mas yr $^{-1}$  and  $54.3 \pm 3.7, -60.9 \pm 3.7$  mas yr $^{-1}$  for A and B respectively, which I consider to be in accord (see Section 2.4.3). I estimate, based on these observed properties, that there is less than a 1 in 8000 probability that these objects are not physically associated. My spectroscopy reveals this system to consist of two hot DAs. There is no evidence for the presence of magnetic fields so this system has been analysed following the method I outlined in Section 3.1.1.

I have estimated DD-05A and DD-05B to have effective temperatures of  $T_{\text{eff}} = 19020 \pm 438 K$  and  $T_{\text{eff}} = 13950 \pm 321 K$  and have determined their masses and cooling times to be  $0.85_{-0.04}^{+0.04}M_{\odot}$ ,  $180_{-25}^{+29}$  Myr and  $0.65_{-0.04}^{+0.04}M_{\odot}$ ,  $273_{-31}^{+36}$  Myr, respectively. I find the distance moduli of these two objects to be consistent since the error bounds

on my measurements overlap at the  $\sim 1.5\sigma$  level (A:  $m_g - M_g = 4.30 \pm 0.13$ , B:  $m_g - M_g = 4.55 \pm 0.12$ ). Given my distance estimate and the observed angular separation of the components, I determine that DD-05A and DD-05B are separated by at least  $\sim 475$  AU and thus unlikely to have ever exchanged mass as a result of Roche Lobe overflow (Girardi et al. 2000). However, based on my estimates of the progenitor masses of these WDs (A:  $M_{\text{init}} = 4.21^{+0.76}_{-0.65} M_{\odot}$ ,  $4.17^{+0.56}_{-0.53} M_{\odot}$  or  $3.95^{+0.39}_{-0.38} M_{\odot}$  and B:  $M_{\text{init}} = 2.73^{+0.63}_{-0.55} M_{\odot}$ ,  $2.36^{+0.49}_{-0.46} M_{\odot}$  or  $2.42^{+0.36}_{-0.35} M_{\odot}$ ) and their corresponding predicted stellar lifetimes  $\tau = 187^{+106}_{-64}$  Myr,  $191^{+85}_{-53}$  Myr or  $221^{+70}_{-49}$  Myr and B:  $\tau = 630^{+540}_{-284}$  Myr,  $926^{+666}_{-374}$  Myr or  $867^{+486}_{-275}$  Myr I find the total system ages derived from these two components to be discordant, A:  $\tau = 367^{+101}_{-55}$  Myr,  $371^{+72}_{-37}$  Myr or  $401^{+54}_{-29}$  Myr and B:  $\tau = 903^{+527}_{-266}$  Myr,  $1199^{+648}_{-350}$  Myr or  $1139^{+462}_{-246}$  Myr (for Dobbie et al. (2006), Kalirai et al. (2008) and Williams et al. (2009) respectively).

Despite both these WDs having masses which are comparable to those of the objects seen in the young/intermediate age open clusters which dominate current estimates of the form the IFMR, this system does not fit well with the simple assumptions I have made about stellar evolution. It is possible that the level of scatter in the IFMR has been somewhat underestimated by the open cluster studies, with DD-05B lying well below the general pattern (see Section 3.2.13). Alternatively, I note that LB 5893, which is a member of Praesepe, sits well above the trend defined by the other nine WD members of the cluster (e.g Dobbie et al. 2006). It has been proposed that this object is the progeny of a blue straggler (Casewell et al. 2009), a type of star whose evolution appears to have been retarded. It is conceivable that DD-05A has similar origins and thus appears substantially younger than the binary age as estimated from DD-05B.

Further higher resolution spectroscopy of this pair of WDs would be useful. At effective temperatures comparable to those of these objects the narrow, non-LTE core of the  $H\alpha$  line is rather prominent in absorption, permitting its wavelength displacement to be determined to a few  $\text{km s}^{-1}$  with data of moderate resolution ( $R \sim 6000$ ). This would allow measurements of their relative radial velocities so that the small possibility that they are not associated can be ruled out and/or to search for evidence of velocity variation which would betray the presence of a close companion object.

### 3.2.6 DD-06

The components of this system are separated on sky by  $2.04 \pm 0.1''$  and have proper motions that are consistent with one and other (ie.  $RA = 18.6 \pm 8.4$ ,  $Dec = -33.7 \pm 8.4$  mas  $\text{yr}^{-1}$  and  $RA = 13.9 \pm 9$ ,  $Dec = -36.3 \pm 9$  mas  $\text{yr}^{-1}$  for A and B, respectively). I estimate, based on these observed properties, that there is less than a 1 in 800 probability that these objects are merely a visual binary. My optical spectroscopy reveals both objects to be hot, hydrogen rich WDs, with neither displaying any evidence for the presence of magnetic fields. I have analysed the components of this system following the method I outlined in 3.1.1.

I have estimated DD-06A and DD-06B to have effective temperatures of  $T_{\text{eff}} = 24788 \pm 570 K$  and  $T_{\text{eff}} = 18502 \pm 426 K$  respectively. I have determined the mass and the cooling time of DD-06A to be  $0.67^{+0.04}_{-0.04} M_{\odot}$ , and  $27^{+8}_{-5}$  Myr, and the mass and the cooling time of DD-06B to be  $0.66^{+0.04}_{-0.04} M_{\odot}$ , and  $108^{+20}_{-17}$  Myr. I find the distance

modulii of DD-06A and DD-06B ( $m_g - M_g = 6.49 \pm 0.12$  and  $m_g - M_g = 6.41 \pm 0.15$ , respectively) to be fully consistent. Given the system distance and the observed angular separation of the components, I find that DD-06A and DD-06B are separated by at least  $\sim 390$  AU. Thus it is unlikely that the Roche lobes of the progenitors of these WDs too have even been smaller than the dimensions of an AGB star (Iben and Livio 1993).

Based on the recent Dobbie et al. (2006), Kalirai et al. (2008) and Williams et al. (2009) determinations of the IFMR, I estimate the progenitor mass of component A to be  $M_{\text{init}} = 2.85_{-0.55}^{+0.63} M_{\odot}$ ,  $2.52_{-0.45}^{+0.48} M_{\odot}$  or  $2.55_{-0.33}^{+0.35} M_{\odot}$ , respectively. The corresponding stellar lifetimes as predicted by the solar metallicity model grid of Girardi et al. (2000) are  $\tau = 554_{-241}^{+444}$  Myr,  $786_{-307}^{+587}$  Myr or  $756_{-231}^{+351}$  Myr (for Dobbie et al. (2006), Kalirai et al. (2008) and Williams et al. (2009) respectively), resulting in total system age estimates of  $\tau = 581_{-238}^{+442}$  Myr,  $813_{-301}^{+583}$  Myr or  $784_{-225}^{+348}$  Myr, respectively. Similarly, for component B I calculate initial masses of  $M_{\text{init}} = 2.75_{-0.54}^{+0.63} M_{\odot}$ ,  $2.4_{-0.45}^{+0.48} M_{\odot}$  or  $2.45_{-0.34}^{+0.35} M_{\odot}$ , leading to estimates of the total system age from this component of  $\tau = 721_{-265}^{+502}$  Myr,  $1002_{-338}^{+641}$  Myr or  $950_{-245}^{+434}$  Myr, respectively. The agreement I find between these binary age determinations indicate that DD-06A and DD-06B have characteristic which are consistent with current estimates of the form of the IFMR.

### 3.2.7 DD-07

The components of this system are separated on sky by  $18.91 \pm 0.1''$  and have proper motions in RA, Dec of  $-52 \pm 9.7, 30.8 \pm 9.7$  mas yr $^{-1}$  and  $-52.1 \pm 9.7, 27.2 \pm 9.7$  mas yr $^{-1}$  for A and B, respectively. I estimate, based on these observed properties, that there is approximately a 1 in 135 probability that these objects are not physically associated. My follow-up spectroscopy has revealed both stars to be hydrogen rich WDs but no evidence for the presence of magnetic fields. I have estimated DD-07A and DD-07B to have effective temperatures of  $T_{\text{eff}} = 33444 \pm 769$  K and  $T_{\text{eff}} = 10393 \pm 239$  K respectively. Consequently, this system has been analysed following the method I outlined in 3.1.2.

I have determined the mass and the cooling time of DD-07A to be  $0.65_{-0.04}^{+0.04} M_{\odot}$ , and  $6_0^+3$  Myr, and the distance modulus of the system to be  $m_g - M_g = 6.17 \pm 0.13$ . Subsequently I have determined the mass and the cooling time of DD-07B to be  $0.6_{-0.05}^{+0.08} M_{\odot}$ , and  $540_{-54}^{+104}$  Myr. I estimate the progenitor mass of component A to be  $M_{\text{init}} = 2.74_{-0.53}^{+0.61} M_{\odot}$ ,  $2.38_{-0.43}^{+0.47} M_{\odot}$  or  $2.43_{-0.32}^{+0.33} M_{\odot}$ , using the IFMRs of Dobbie et al. (2006), Kalirai et al. (2008) and Williams et al. (2009), respectively and similarly, for component B I calculate initial masses of  $M_{\text{init}} = 2.31_{-0.58}^{+0.95} M_{\odot}$ ,  $1.86_{-0.55}^{+0.88} M_{\odot}$  or  $2_{-0.44}^{+0.69} M_{\odot}$ . The corresponding stellar lifetimes for component A as predicted by the solar metallicity model grid of Girardi et al. (2000) are  $\tau = 623_{-275}^{+511}$  Myr,  $913_{-354}^{+628}$  Myr or  $857_{-253}^{+419}$  Myr, resulting in total system age estimates of  $\tau = 630_{-268}^{+632}$  Myr,  $919_{-346}^{+706}$  Myr or  $863_{-249}^{+511}$  Myr, respectively. From component B I estimate the total system age to be  $\tau = 1520_{-454}^{+902}$  Myr,  $2188_{-935}^{+2633}$  Myr or  $2012_{-717}^{+1128}$  Myr, respectively.

I find my system age estimates from these two components to be discordant at  $\sim 3\sigma$ . This argues that the simple models I have adopted for mapping the masses of stars, from the main sequence to the WD stage, are not an appropriate description of the evolutionary history of this particular system. As I have suggested for DD-01A, it could

be that as consequence of having a close companion, component B has suffered heavier massloss than predicted by the three IFMRs. However, in terms of their masses, these WDs lie at and beyond the lower end of the range of the IFMR which has been mapped using the members of open clusters. Thus an alternative explanation could be that a simple linear extrapolation of the form the IFMR observed at higher masses into this regime does not adequately represent reality. These data are consistent with a relation which is substantially flatter (ie.  $a_1 \rightarrow 0$ ) in this mass regime.

### 3.2.8 DD-08

The components of this system are separated on sky by  $4.35 \pm 0.1''$  and display proper motions in RA,Dec of  $-19.4 \pm 0.7, -74.4 \pm 0.7 \text{ mas yr}^{-1}$  and  $-5.3 \pm 0.9, -61.1 \pm 0.9 \text{ mas yr}^{-1}$  for A and B, respectively. I estimate on grounds of these observed properties, that there is less than a 1 in  $\sim 2500$  probability that these objects are a mere visual binary. My follow-up optical spectroscopy reveals this system to contain a high field magnetic DA (DD-08A) and a cool DA (DD-08B) so it has been analysed following the method I outlined in 3.1.5.

I have estimated components A and B to have effective temperatures of  $T_{\text{eff}} = 9500 \pm 500 \text{ K}$  and  $T_{\text{eff}} = 10492 \pm 241 \text{ K}$ , respectively. I have determined the mass and the cooling time of DD-08B to be  $0.8^{+0.05}_{-0.05} M_{\odot}$  and  $849^{+114}_{-106} \text{ Myr}$ , and the distance modulus of the system to be  $m_g - M_g = 5.89 \pm 0.16$ . Subsequently I have derived the mass and the cooling time of DD-08A to be  $0.61^{+0.14}_{-0.09} M_{\odot}$ , and  $715^{+183}_{-91} \text{ Myr}$ . Following again my procedure above, using the three different IFMRs, I estimate the progenitor mass for DD-08B as  $M_{\text{init}} = 3.81^{+0.76}_{-0.65} M_{\odot}$ ,  $3.69^{+0.6}_{-0.56} M_{\odot}$  or  $3.54^{+0.44}_{-0.42} M_{\odot}$  and calculate the total age of this binary to be  $\tau = 1092^{+179}_{-92} \text{ Myr}$ ,  $1115^{+146}_{-62} \text{ Myr}$  or  $1146^{+109}_{-48} \text{ Myr}$  (for Dobbie et al. (2006), Kalirai et al. (2008) and Williams et al. (2009) respectively). From the parameters of the DAH component, which, from my modelling, is expected to be the progeny of a star of  $M_{\text{init}} = 2.44^{+1.17}_{-0.78} M_{\odot}$ ,  $2.02^{+1.31}_{-0.85} M_{\odot}$  or  $2.13^{+1.08}_{-0.7} M_{\odot}$ , I infer a total system age of  $\tau = 1562^{+1159}_{-405} \text{ Myr}$ ,  $2158^{+2986}_{-899} \text{ Myr}$  or  $1967^{+1819}_{-637} \text{ Myr}$  (again, for Dobbie et al. (2006), Kalirai et al. (2008) and Williams et al. (2009) respectively). These two sets of estimates are not formally consistent within their  $1\sigma$  errors for any of the three adopted IFMRs, although, admittedly the discrepancy is not overwhelming, statistically. However, the variance suggested here is in the opposite sense to that observed for DD-02, RE J0317-853 and EG 59 with DD-08A appearing “too old” for its mass or, alternatively, too “low in mass” for its cooling time. It could be expected, on the basis of my simple model, that since the WDs in this system have similar cooling times, they should have comparable masses, having descended from stars with similar initial masses. Component A appears to have experienced greater massloss than would be expected for a single star. As was suggested for DD-01B, this could be a consequence of having a close companion, if this system was a primordial triple. A  $M_{\text{init}} \sim 3.5 M_{\odot}$  star that experiences Roche Lobe overflow around the time of central helium ignition can lead to the formation of a CO white dwarf with a mass towards the lower end of the range estimated for this HFMDWD (e.g. Iben and Tutukov 1985). However, I note that there is an observed lack of HFMDWDs with close detached companions (Liebert et al. 2005b). Nevertheless, the intermediate temperature of the non-magnetic component

in this system, coupled with its comparatively high mass suggests that this HFMWD is linked to an early-type star,  $M_{\text{init}} > 2.1 M_{\odot}$ .

### 3.2.9 DD-09

The proper motions I determine for the components of this system are consistent with one and other,  $\text{RA, Dec} = -17.8 \pm 5.6, -47.3 \pm 5.6 \text{ mas yr}^{-1}$  and  $-12.3 \pm 5.7, -40.6 \pm 5.7 \text{ mas yr}^{-1}$  for A and B respectively. These sources are separated on sky by  $5.18 \pm 0.1''$ . On grounds of these observed properties, I estimate that there is less than a 1 in 3500 probability that these objects are not physically associated. My optical spectroscopy of these stars indicates both to be hydrogen rich WDs and reveals no evidence for the presence of magnetic fields. I have estimated DD-09A and DD-09B to have effective temperatures of  $T_{\text{eff}} = 11543 \pm 266 K$  and  $T_{\text{eff}} = 16037 \pm 369 K$  respectively. As this system consists of a cool DA (DD-09A) and a normal DA (DD-09B) WD, it has been analysed following the method I outlined in 3.1.2.

I have determined the mass and the cooling time of DD-09B to be  $1.17^{+0.03}_{-0.03} M_{\odot}$ , and  $893^{+111}_{-136} \text{ Myr}$ , and the distance modulus of the system to be  $m_g - M_g = 5.56 \pm 0.15$ .

Close scrutiny of DD-09A reveals that it is unlike the cooler components in the three other cool DA + hot DA systems in my sample, where the spectroscopic mass determinations are larger by  $\sim 0.17 M_{\odot}$  than those calculated by assuming that the objects in each pairing have a common distance (the binary method). I find the spectroscopic mass of DD-09A is smaller by  $\sim 0.20 M_{\odot}$  than that determined by the binary method. As the results of several studies of field WDs also point to spectroscopic determinations overestimating the true mass at  $T_{\text{eff}} < 12000 K$ , I am led to conclude that my mass estimate for this star might be in error. Therefore, I have also explored the parameters of this system by applying the spectroscopic mass offset as calculated for cool components ( $\sim 0.17 M_{\odot}$ ). In this case, the mass of component A is set to  $0.54^{+0.05}_{-0.05} M_{\odot}$  (with a corresponding cooling time of  $360^{+49}_{-42} \text{ Myr}$ ). I find determinations of the system age from this object of  $\tau = 1950^{+2328}_{-792} \text{ Myr}$ ,  $4356^{+8794}_{-2485} \text{ Myr}$  or  $2894^{+3649}_{-1015} \text{ Myr}$ . These are not consistent with the ages estimates from component B. The revised distance moduli of component A is  $m_g - M_g = 6.47 \pm 0.14$  and also appears to be discrepant with respect to that of component B.

It can be seen in Figures 3.3 and 3.4 that the cooler component of DD-09 (DD-09A) actually has a higher apparent distance modulus than its hot companion before mass correction (distance matching) - where as the opposite is the case for all other Cool+Hot Systems. This discrepancy can also be seen in Figure 3.1, in which my effective spectroscopic mass offsets (to align cool component distances with their respective hot components) are compared to that of Tremblay et al. (2011) across temperature.

Thus the obvious conclusion on this basis is that these objects do not form a physical binary. However, their proximity to each other on sky and relatively large and similar proper motions seem to point rather strongly to a physical association. It is interesting to note that the disparity between the distance moduli of these two objects is within  $1\sigma$  of  $\sim 0.75$  magnitudes and in the sense that the distances would be in accord if DD-09B, which appears to be unusually massive, actually consists of a spatially unresolved pairing of WDs with similar masses and effective temperatures.

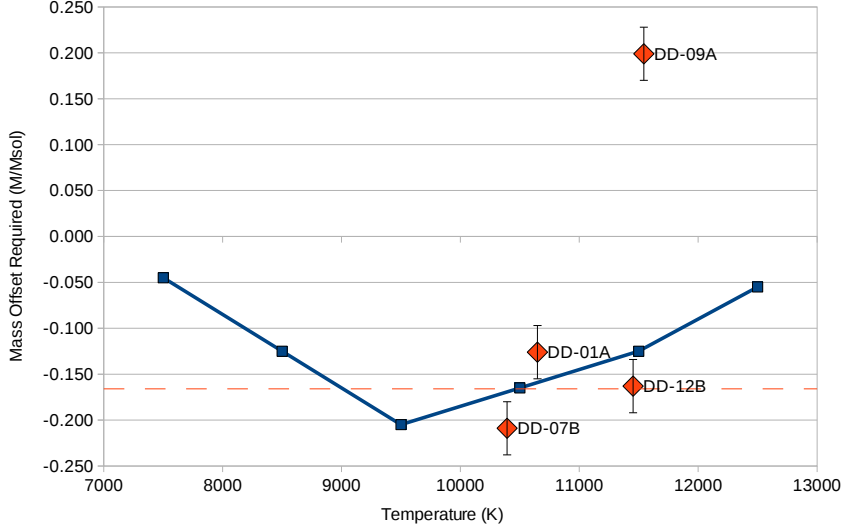


FIGURE 3.1: A plot in which my effective spectroscopic mass offsets (to align cool component distances with their hot components) are compared to that of Tremblay et al. (2011) across temperature. The blue curve is that of Tremblay et al. (2011), while the red data points are calculated from my Double Degenerate survey. The error in my derived mass offset is displayed with error bars, while my derived mass offset itself is displayed as a dashed red line about  $dM = -0.17 \pm 0.04 M_{\odot}$ .

This is an intriguing system and clearly one which warrants further detailed follow-up study e.g. as proposed for DD-05, higher resolution spectroscopy extending over the  $H\alpha$  line to permit measurements of the radial velocities of these objects. For the rest of my analysis, I assume that this pair of objects is not associated.

### 3.2.10 DD-10

The components of this system are separated on sky by  $5.93 \pm 0.1''$  and have proper motions in RA, Dec of  $-9.8 \pm 5.6, 30.6 \pm 5.6 \text{ mas yr}^{-1}$  and  $-16.8 \pm 5.7, 28.3 \pm 5.7 \text{ mas yr}^{-1}$  for A and B respectively. I estimate, based on these observed properties, that there is less than a 1 in 5000 probability that these objects are only a visual binary. From my follow-up spectroscopy I find these stars to both be hydrogen rich WDs, with neither displaying any evidence for the presence of magnetic fields. I have estimated DD-10A and DD-10B to have effective temperatures of  $T_{\text{eff}} = 13072 \pm 301 K$  and



$T_{\text{eff}} = 12758 \pm 293K$  respectively. As this system consists of a normal DA (DD-10A) and a normal DA (DD-10B) WD, it has been analysed following the method I outlined in 3.1.1.

I have determined the masses and the cooling times of DD-10A and DD-10B to be  $0.88^{+0.04}_{-0.05}M_{\odot}$ ,  $574^{+82}_{-70}\text{Myr}$  and  $0.76^{+0.05}_{-0.04}M_{\odot}$ ,  $450^{+62}_{-52}\text{Myr}$ , respectively. Subsequently, I have calculated the distance moduli of DD-10A and DD-10B to be  $m_g - M_g = 5.66 \pm 0.12$  and  $m_g - M_g = 5.59 \pm 0.12$ , respectively, which I note are in accord with one and other. Based on the IFMRs of Dobbie et al. (2006), Kalirai et al. (2008) and Williams et al. (2009), I have derived the progenitor masses of components A and B to be  $M_{\text{init}}=4.43^{+0.79}_{-0.67}M_{\odot}$ ,  $4.45^{+0.57}_{-0.54}M_{\odot}$  or  $4.18^{+0.4}_{-0.39}M_{\odot}$  and  $M_{\text{init}}=3.51^{+0.7}_{-0.6}M_{\odot}$ ,  $3.31^{+0.53}_{-0.5}M_{\odot}$  or  $3.23^{+0.39}_{-0.37}M_{\odot}$ , respectively. These lead to estimates of the total system age from component A of  $\tau=737^{+106}_{-61}\text{Myr}$ ,  $736^{+79}_{-43}\text{Myr}$  or  $763^{+65}_{-36}\text{Myr}$  and from component B of  $\tau=756^{+206}_{-99}\text{Myr}$ ,  $808^{+190}_{-83}\text{Myr}$  or  $836^{+130}_{-62}\text{Myr}$ , respectively.

I find that the two binary age determinations are in excellent agreement for all three of the adopted IFMRs. I note that these two WDs have masses which are typical of those studied in young/intermediate age open clusters and that largely dominate current estimates of the form the relation. The components of DD-10 appear to lend support to the results derived from the open cluster investigations.

### 3.2.11 DD-11

Components A and B in this pairing have consistent proper motions in RA,Dec of  $-82.2 \pm 12.7, 11.4 \pm 12.7 \text{ mas yr}^{-1}$  and  $-67.5 \pm 12.8, 16 \pm 12.8 \text{ mas yr}^{-1}$ , respectively. They are separated on sky by only  $1.32 \pm 0.1''$ . Based on these observed properties, I estimate that there is only a 1 in 10500 probability that these objects are not physically associated. Optical spectroscopy of these stars indicates both to be hydrogen rich WDs and in neither case reveals evidence for the presence of magnetic fields. I have measured DD-11A and DD-11B to have effective temperatures of  $T_{\text{eff}} = 20000 \pm 460K$  and  $T_{\text{eff}} = 14037 \pm 323K$  respectively. As this system consists of two hot DAs, it has been analysed following the method I outlined in 3.1.1.

I have estimated the masses and the cooling times of DD-11A and DD-11B to be  $0.74^{+0.04}_{-0.04}M_{\odot}$ ,  $107^{+20}_{-18}\text{Myr}$  and  $0.89^{+0.04}_{-0.05}M_{\odot}$ ,  $489^{+70}_{-60}\text{Myr}$ , respectively and I find their distance moduli to be consistent (A:  $m_g - M_g = 5.37 \pm 0.12$  and B:  $m_g - M_g = 5.61 \pm 0.27$ ). From this distance determination and the observed angular separation of these sources, I calculate that the minimum separation is  $\sim 175\text{AU}$ . Thus even allowing for orbital expansion by a factor 5-10 as a result of the loss of primordial mass from the system, it is unlikely that either of these objects has exchanged gas as the result of Roche Lobe overflow. I derive progenitor masses for components A and B, based on the IFMRs used in previous sections, of  $M_{\text{init}}=3.36^{+0.69}_{-0.58}M_{\odot}$ ,  $3.14^{+0.52}_{-0.49}M_{\odot}$  or  $3.08^{+0.38}_{-0.37}M_{\odot}$  and  $M_{\text{init}}=4.54^{+0.79}_{-0.67}M_{\odot}$ ,  $4.58^{+0.58}_{-0.54}M_{\odot}$  or  $4.29^{+0.39}_{-0.39}M_{\odot}$ , respectively. These lead to estimates of the total system age from component A of  $\tau=450^{+244}_{-127}\text{Myr}$ ,  $524^{+251}_{-131}\text{Myr}$  or  $548^{+183}_{-108}\text{Myr}$  and from component B of  $\tau=643^{+93}_{-54}\text{Myr}$ ,  $640^{+69}_{-38}\text{Myr}$  or  $666^{+56}_{-31}\text{Myr}$ , respectively.

I find that the binary age determinations from these two components are fully consistent with each other for all models of the IFMR considered. This argues that for DD-11 these can be a good representation of the massloss history of the component

stars. As was the case for DD-10, this result is not entirely surprising since these two WDs also have masses which are typical of those studied in young/intermediate age open clusters and that largely dominate current estimates of the form the IFMR. Indeed, I note that the estimates of system age, from model to model are all very similar, highlighting this point.

### 3.2.12 DD-12

My follow-up spectroscopy for these stars has revealed both to be hydrogen rich WDs. I also find no evidence for the presence of magnetic fields in these datasets. The components of this system are separated on sky by  $4.29 \pm 0.1''$  and have proper motions in RA, Dec of  $4.7 \pm 4.2, 32.6 \pm 4.2 \text{ mas yr}^{-1}$  and  $2.6 \pm 4.1, 40.3 \pm 4.1 \text{ mas yr}^{-1}$  for A and B respectively, which I consider to be consistent (see Section 2.4.3). I estimate, based on these properties, that there is less than a 1 in 2500 probability that these objects are merely a visual binary. From an analysis of the spectra I determine the effective temperatures of component A and component B to be  $T_{\text{eff}} = 15834 \pm 364K$  and  $T_{\text{eff}} = 11453 \pm 263K$  respectively. As this system consists of a hot DA (DD-12A) and a cool DA (DD-12B), it has been analysed following the method I outlined in 3.1.2.

I have estimated the mass and the cooling time of DD-12A to be  $0.63^{+0.04}_{-0.04}M_{\odot}$ , and  $172^{+26}_{-22}\text{Myr}$ , and the distance modulus of the system to be  $m_g - M_g = 5.30 \pm 0.12$ . Subsequently I have calculated the mass and the cooling time of DD-12B to be  $0.63^{+0.12}_{-0.04}M_{\odot}$ , and  $449^{+144}_{-41}\text{Myr}$ . Using the three IFMRs discussed in the Sections above, I have determined the progenitor masses of component A and component B to be  $M_{\text{init}}=2.54^{+0.6}_{-0.54}M_{\odot}$ ,  $2.13^{+0.47}_{-0.45}M_{\odot}$  or  $2.23^{+0.35}_{-0.34}M_{\odot}$  and  $M_{\text{init}}=2.57^{+1.08}_{-0.54}M_{\odot}$ ,  $2.17^{+1.23}_{-0.47}M_{\odot}$  or  $2.26^{+0.99}_{-0.37}M_{\odot}$ , respectively. These lead to estimates of the total system age from component A of  $\tau=942^{+691}_{-339}\text{Myr}$ ,  $1429^{+807}_{-524}\text{Myr}$  or  $1270^{+496}_{-344}\text{Myr}$  and from component B of  $\tau=1190^{+655}_{-325}\text{Myr}$ ,  $1629^{+807}_{-655}\text{Myr}$  or  $1494^{+531}_{-480}\text{Myr}$ , respectively. I find general agreement between these binary age determinations, with only the ages stemming from the use of the oldest IFMR not being formally consistent within the  $1\sigma$  error bounds. I am led to conclude that the observed properties of DD-12A and DD-12B are consistent with current estimates of the form of the IFMR.

### 3.2.13 My systems overall and understanding of the IFMR

The derived parameters of half of the pairs which I find to be physically associated are consistent with recent estimates of the IFMR that are based largely on open cluster WDs. However, I find that three of my systems, DD-01, DD-05 and DD-07, do not conform to predictions based on these same estimates of the IFMR. I note that the WDs in these three binaries all have  $M \lesssim 0.65M_{\odot}$ . While open clusters now provide more than 50 data points for the IFMR which span a broad range of initial masses ( $1.5\text{-}6M_{\odot}$ ), they are largely concentrated within the range  $M_{\text{init}}=2.8\text{-}5M_{\odot}$ . These data suggest that the bulk of stars follow relatively closely a monotonic relation which can be adequately represented by a simple linear function at least down to  $M_{\text{init}}\approx 2.5M_{\odot}$  (e.g. Williams et al. 2009).



That the three discordant systems contain WDs with  $M \lesssim 0.65M_{\odot}$  might be taken as an indication that the IFMR may not be very well represented at lower initial/final masses by these linear functions. Theoretical considerations suggest that the relation is likely to become flatter at  $M_{\text{init}} \approx 2\text{--}2.5M_{\odot}$  than it is at higher masses (Weidemann 2000). Nevertheless, three of the systems which have parameters that appear to be consistent with the cluster dominated IFMRs also contain at least one WD with  $M \lesssim 0.65M_{\odot}$ , although the masses of the components of DD-06 and DD-12 are very similar to one and other and could be expected to, in my approach here, be little affected by erroneous assumptions about the relations form.

A small number of points in the open clusters are known to deviate from the general trend delineated by the bulk of the data, including LB 5893, LB 390 and half a dozen WDs towards the intermediate age population NGC 2099 (Kalirai et al. 2008). This latter dataset may not be reliable since the spectroscopy for these WDs was of rather low signal-to-noise towards the blue end of the optical where the gravity sensitive high order Balmer lines reside. Nevertheless, a recent investigation of the IFMR based on wide stellar + WD binaries, which probes relatively lower masses, has found some evidence of greater scatter in the IFMR than indicated by the cluster studies (Catalan et al. 2008). It seems plausible that the level of scatter in the IFMR maybe mass dependent. Dobbie et al. (2009) argue that the IFMR at  $M_{\text{init}} > 2.5M_{\odot}$ , where third dredge-up is expected to be rather efficient at preventing further growth of the degenerate core during the AGB, resembles the  $M_{\text{init}}$  versus core mass at the time of the first thermal-pulse relation. At lower initial masses third dredge-up is expected to be less efficient with the core growing significantly during this phase. Thus any factor that can substantially influence the rate of mass loss during the AGB (e.g. the presence of a close companion), when a star attains its maximum radius, could impact the final mass of the resulting WD.

Alternatively, it could be that at least some of the open cluster studies have been slightly biased against finding WDs of lower mass that form from recently deceased stars. Generally, “young” degenerates are identified in colour-magnitude diagrams by their blue colours which often cleanly separate them from the bulk of field stars. However, as WDs of lower mass have larger radii and cool more quickly, they will generally be redder in colour and reside closer to the field star population. Since the 8m class telescope time required to obtain spectra of these objects is at a premium, this part of colour-magnitude space is less likely to be targeted for follow-up observations.

In summary, my analysis of these twelve systems suggests that recent estimates of the form of the IFMR provide a fair description of the transformation of intermediate mass stars into WDs ( $M_{\text{init}} > 2.5M_{\odot}$ ), but it is likely that there is more scatter in the relation than assumed from the results of recent open cluster based studies, at least at lower initial/final masses (ie.  $M_{\text{init}} < 2.5M_{\odot}$ ).

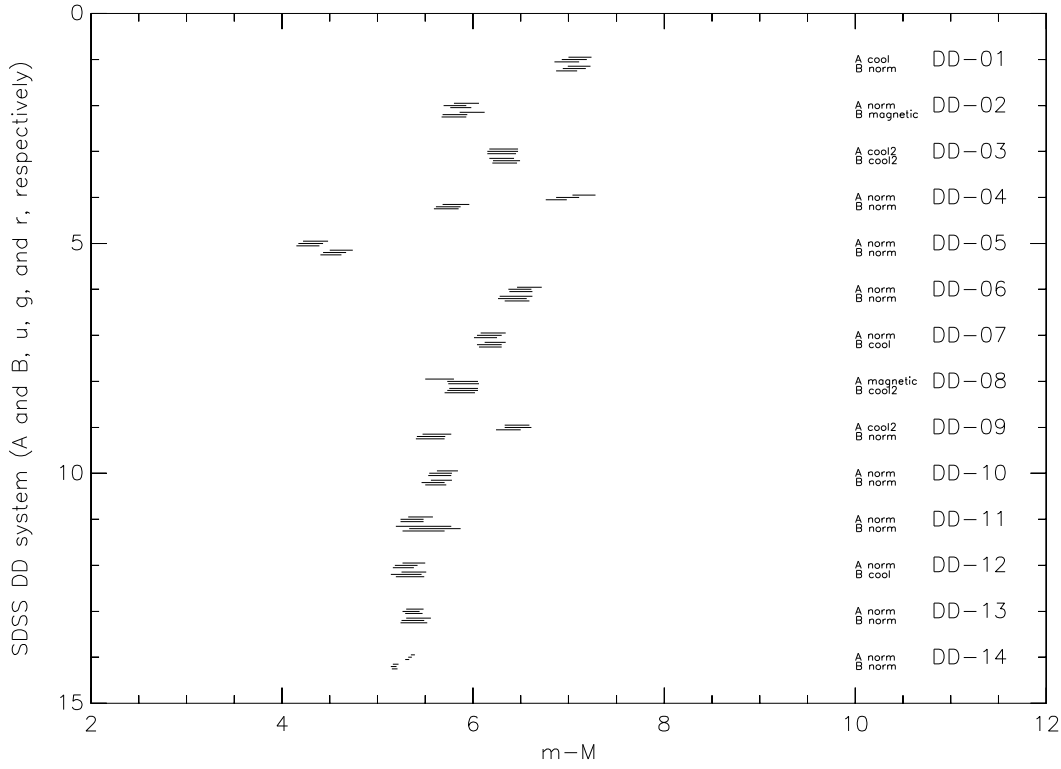


FIGURE 3.2: Distance Modulii ( $m - M$ ) for all DD systems (u, g, r), with cool component mass corrections / distance matching

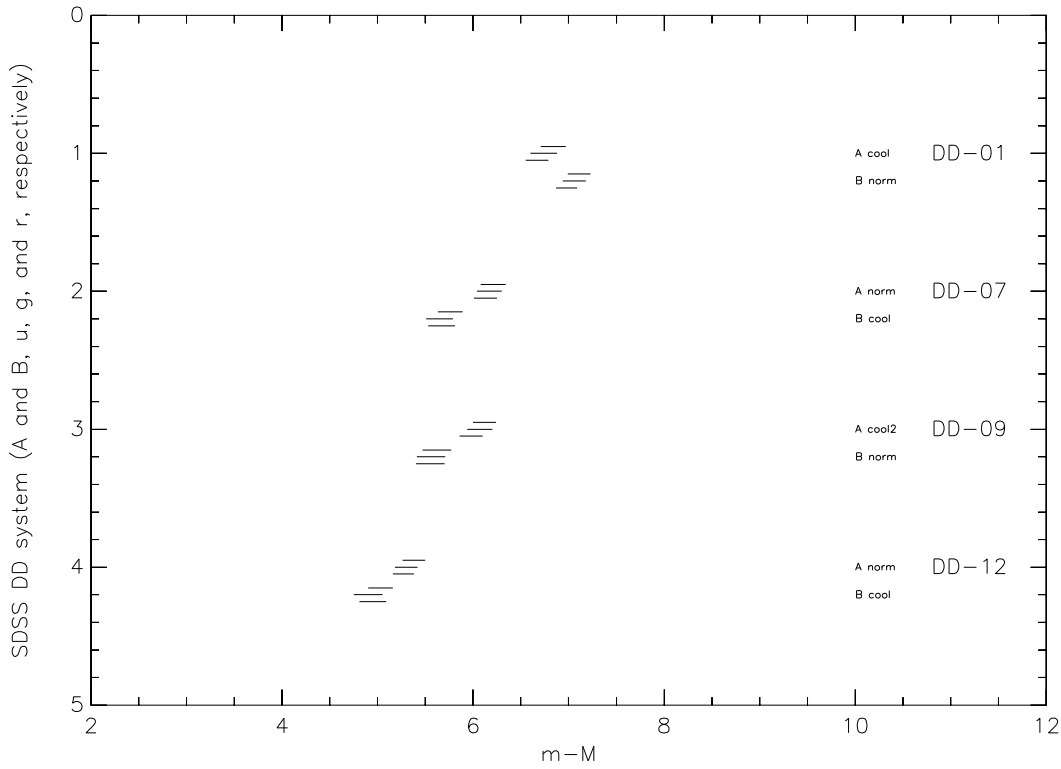


FIGURE 3.3: Distance Modulii ( $m - M$ ) for DD systems with at least one cool component (u, g, r), without cool component mass corrections / distance matching

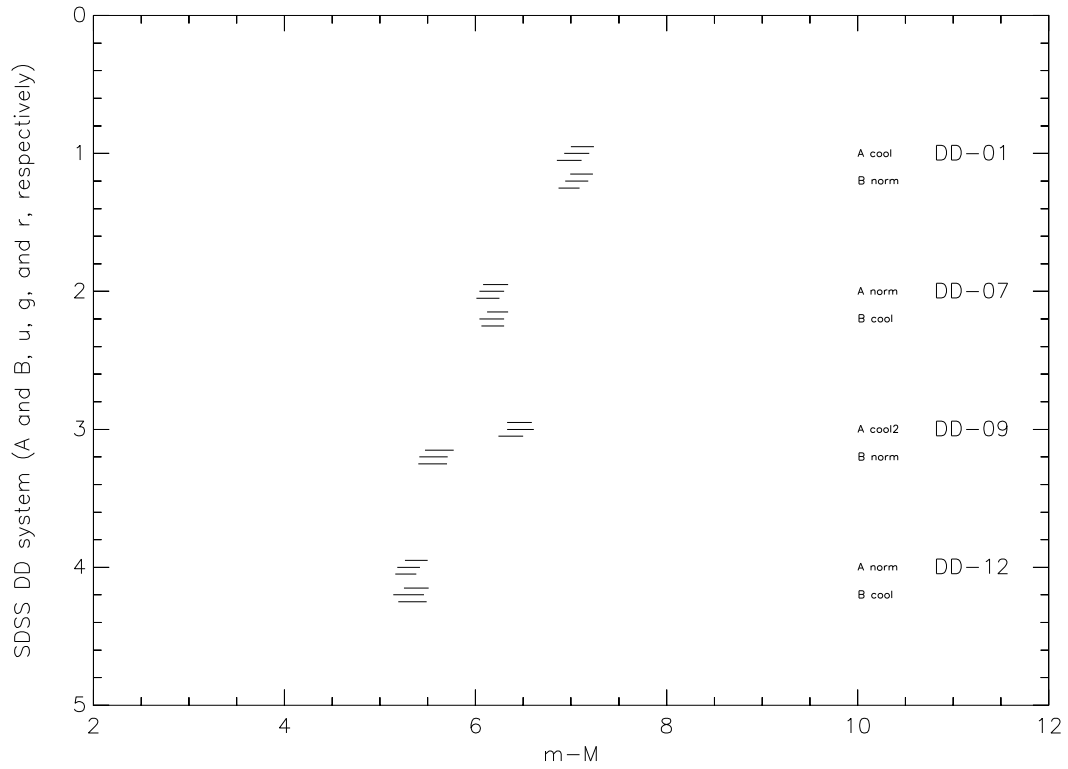


FIGURE 3.4: Distance Modulii ( $m - M$ ) for DD systems with at least one cool component (u, g, r), with cool component mass corrections / distance matching

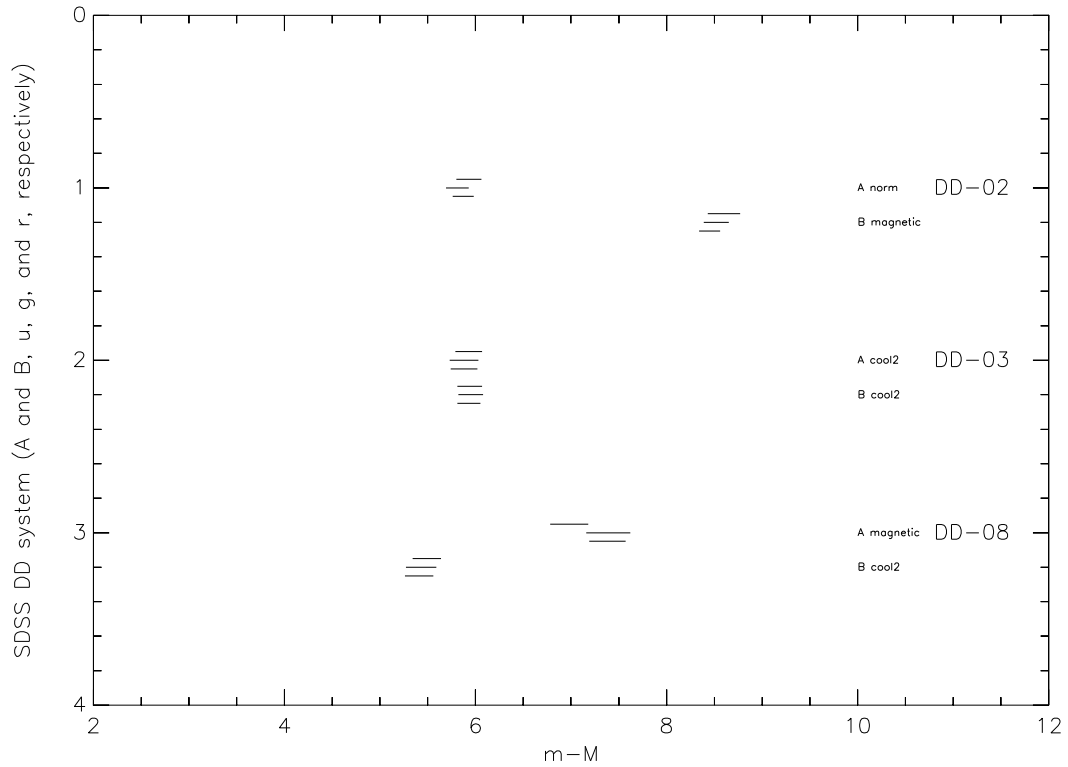


FIGURE 3.5: Distance Modulii ( $m - M$ ) for DD systems with two cool components or a HFMWD system (u, g, r), without cool component mass corrections / distance matching

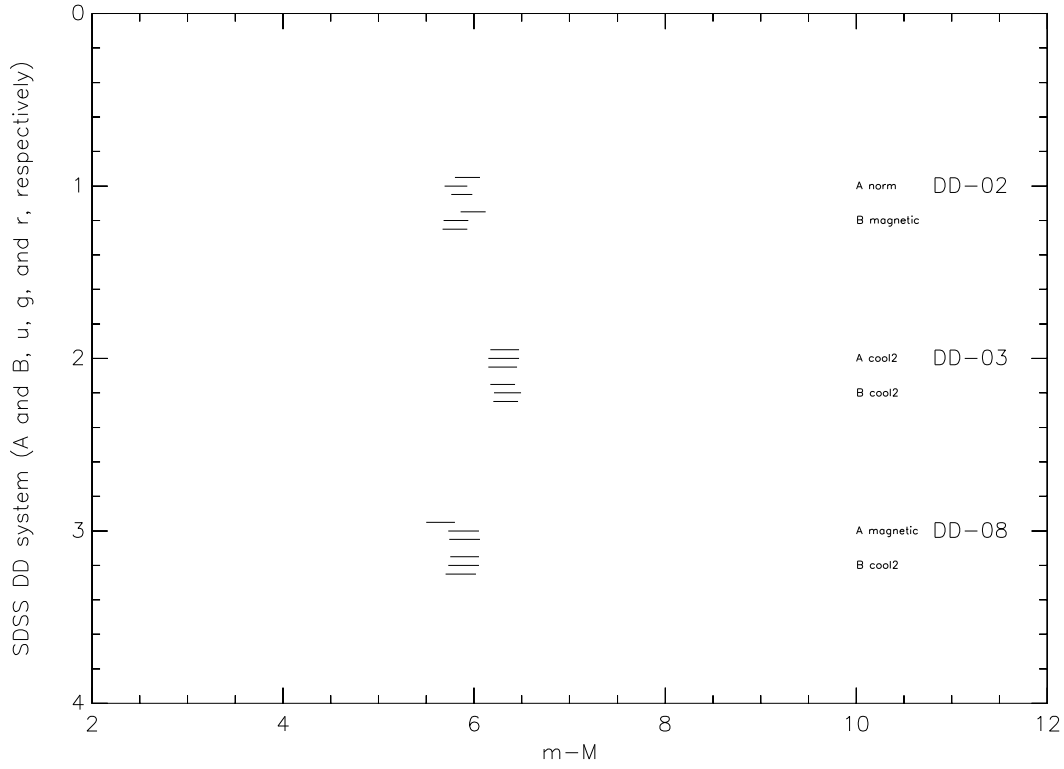


FIGURE 3.6: Distance Modulii ( $m - M$ ) for DD systems with two cool components or a HFMWD system (u, g, r), with cool component mass corrections / distance matching

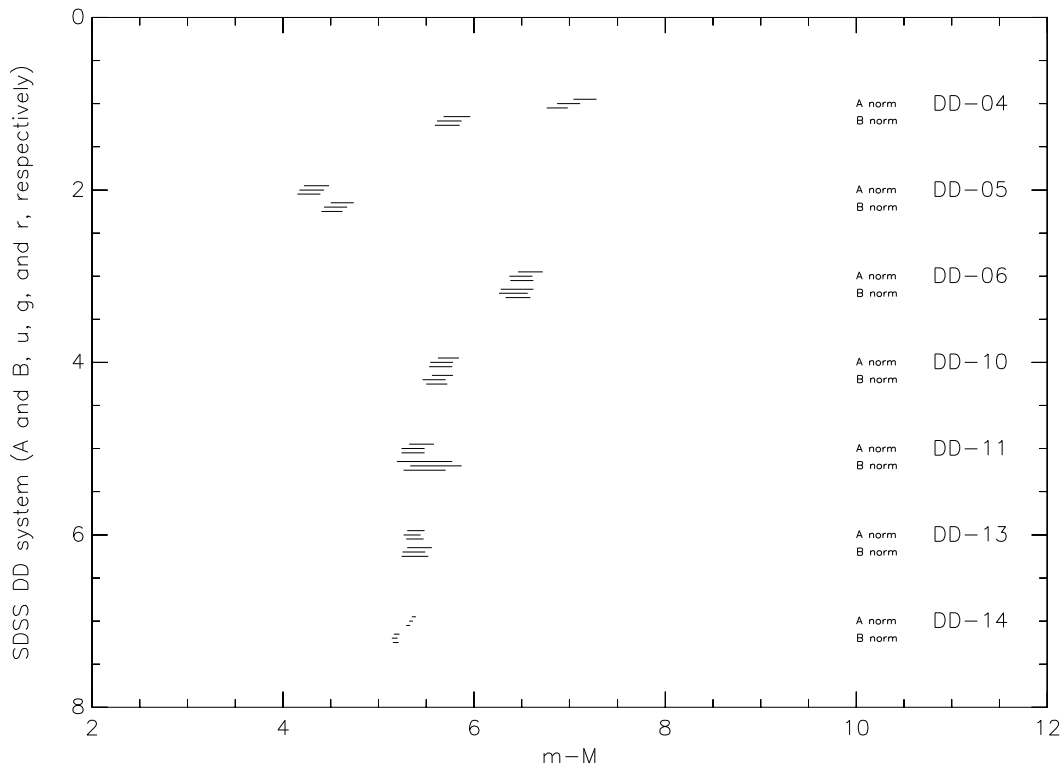


FIGURE 3.7: Distance Modulii ( $m - M$ ) for DD systems with hot components (u, g, r)

TABLE 3.1: Double Degenerate Data - Results

WD	$\log g$	$\log g$ err	$T_{eff}$ (K)	$T_{eff}$ (K) err	$\tau_c$ (Myr)	$\tau_c$ (Myr) err	$M_{final}$ ( $M_{\odot}$ )	$M_{final}$ ( $M_{\odot}$ ) err	abs u	abs g	abs r	abs u err	abs g err	abs r err	dist	dist err	tang vel (km/s)	tang vel (km/s) err
DD-01A	7.90	0.10	10648	245	419	59	0.510	0.068	12.23	11.83	11.94	0.11	0.13	0.13	7.06	0.12	44.8	9.1
DD-01B	7.97	0.07	19199	442	76	14	0.605	0.039	10.68	10.65	11.00	0.12	0.12	0.11	7.06	0.12	42.3	9.3
DD-02A	8.13	0.07	17285	398	157	23	0.695	0.042	11.21	11.1	11.42	0.12	0.12	0.11	5.81	0.12	19.4	11.7
DD-02B	8.67	0.09	18000	1000	354	48	1.027	0.047	11.99	11.95	12.26	0.13	0.13	0.13	5.81	0.13	20.6	11.6
DD-03A	8.19	0.08	10008	230	795	108	0.717	0.051	12.84	12.5	12.56	0.15	0.16	0.15	6.32	0.16	43.8	4.7
DD-03B	7.99	0.09	11222	258	440	59	0.598	0.052	12.18	11.81	11.94	0.13	0.14	0.13	6.36	0.14	45.5	5.1
DD-04A	8.16	0.07	13987	322	310	39	0.707	0.044	11.86	11.58	11.81	0.12	0.12	0.11	6.99	0.12	33.0	5.5
DD-04B	8.45	0.07	28067	646	54	13	0.911	0.044	10.34	10.62	11.06	0.14	0.13	0.13	5.74	0.14	20.2	2.8
DD-05A	8.37	0.07	19020	438	180	27	0.849	0.045	11.31	11.30	11.64	0.13	0.13	0.12	4.30	0.13	36.1	0.2
DD-05B	8.07	0.07	13950	321	273	34	0.652	0.042	11.75	11.46	11.69	0.12	0.12	0.11	4.55	0.12	31.5	0.8
DD-06A	8.06	0.07	24788	570	27	7	0.668	0.040	10.10	10.27	10.69	0.13	0.12	0.12	6.49	0.12	36.2	11.8
DD-06B	8.06	0.07	18502	426	108	19	0.655	0.041	10.91	10.85	11.19	0.12	0.12	0.11	6.41	0.15	35.3	11.4
DD-07A	8.00	0.07	33444	769	6	1	0.653	0.038	9.11	9.47	9.96	0.13	0.12	0.12	6.17	0.13	49.1	6.6
DD-07B	7.98	0.10	10393	239	540	79	0.597	0.069	12.41	12.03	12.12	0.11	0.12	0.12	6.17	0.12	47.7	6.8
DD-08A	8.03	0.18	9500	500	715	137	0.614	0.113	12.81	12.45	12.49	0.15	0.16	0.16	5.89	0.16	54.8	0.4
DD-08B	8.31	0.08	10492	241	849	110	0.796	0.052	12.84	12.51	12.60	0.15	0.16	0.15	5.89	0.16	43.7	0.4
DD-09A	7.89	0.09	11543	266	360	45	0.542	0.049	11.99	11.60	11.75	0.13	0.14	0.13	6.47	0.14	47.1	2.6
DD-09B	8.94	0.07	16037	369	893	123	1.173	0.032	12.80	12.72	12.97	0.15	0.15	0.15	5.56	0.15	26.1	2.0
DD-10A	8.43	0.07	13072	301	574	76	0.879	0.045	12.40	12.14	12.33	0.11	0.12	0.12	5.66	0.12	20.6	3.8
DD-10B	8.24	0.07	12758	293	450	57	0.755	0.045	12.19	11.90	12.08	0.11	0.12	0.11	5.59	0.12	20.5	3.8
DD-11A	8.19	0.07	20000	460	107	19	0.737	0.044	10.89	10.91	11.27	0.13	0.12	0.12	5.37	0.12	46.6	7.2
DD-11B	8.45	0.07	14037	323	489	65	0.893	0.045	12.27	12.05	12.26	0.12	0.13	0.12	5.61	0.27	43.5	5.2
DD-12A	8.02	0.07	15834	364	172	24	0.626	0.041	11.30	11.11	11.40	0.12	0.12	0.11	5.30	0.12	17.9	2.4
DD-12B	8.03	0.10	11453	263	449	93	0.631	0.083	12.18	11.81	11.96	0.12	0.14	0.14	5.30	0.12	21.9	2.2

### 3.3 IFMR probing

Systems with one or more magnetic components, which are less accurately modelled, have been isolated in the analysis of system age conformance. DD-04 and DD-09, which result in noticable distance age discrepancies have also been isolated in this analysis.

See Table 3.2 for a list of the published IFMR forms used for this comparison (including their linear gradient  $m$  and  $y$  intersection  $c$  parameters). This table also contains a summary of the DD system age conformance resultant from their respective forms, as described in the following paragraphs.

This table displays statistics calculated from a monte carlo generated distribution of 25000 hypothetical WDs with parameters selected within their error limits, as discussed in Section 3.1.6. These results rely upon a numerical (rather than analytical) propagation of their errors in derivation of their initial (main sequence progenitor) age/masses and therefore system age estimates. The code used to perform this method is described in Appendix Section A.6.2.

Firstly, this table displays the number of DD systems determined to have components with a common system age; [1] using an independent system age comparison, and [2] using an interdependent/covariant system age difference derivation. This section of the table was generated using my DD Data spreadsheet referenced in Appendix Section A.7.1. Secondly, this table displays the median system age difference, averaged across all systems, and the number of DD systems best satisfied by the published IFMR (i.e. having the lowest system age difference with the given published IFMR).

Figures 3.12 and 3.13 show plots of the system age difference distribution for each DD system, based on the generated monte carlo distribution of 25000 hypothetical WDs where parameters are selected within their error limits. For each plot a number of published IFMR forms are assumed; solid (Dobbie et al. 2006), dotted (Kalirai et al. 2008), and dashed (Williams et al. 2009). Figures 3.15, 3.16, and 3.17 each show plots of the system age difference distributions for all DD systems based on a particular published IFMR (Dobbie et al. (2006), Kalirai et al. (2008), and Williams et al. (2009) respectively). Plots of the systems ages are shown in Figures 3.9, 3.10, and 3.11, each assuming a unique form of the IFMR published in the literature.

For reference, plots of the published IFMRs used in this analysis are given in Figure 3.8.

TABLE 3.2: Published forms of the IFMR (linear gradient  $m$  and  $y$  intersection  $c$  parameters). It displays statistics calculated from a monte carlo generated distribution of 25000 hypothetical WDs with parameters selected within their error limits. Firstly it displays the number of DD systems determined to have components with a common system age; [1] using an independent system age comparison, and [2] using the interdependent/covariant system age difference derivation - from Figures 3.9, 3.10, and 3.11. Secondly, it displays the median system age difference, averaged across all systems, and the number of DD systems best satisfied by the published IFMR (i.e. having the lowest system age difference with the given published IFMR).

IFMR	$m$	$m$ err	$c$	$c$ err	DD $t_{sys}$ common ([1])	DD $t_{sys}$ common [2]	average $t_{sys}$ diff	DD $t_{sys}$ diff low
Dobbie et al. (2006)	0.133	0.01	0.289	0.051	11	5	438.72821	7
Kalirai et al. (2008)	0.109	0.007	0.394	0.025	9	6	971.28286	7
Williams et al. (2009)	0.129	0.004	0.339	0.015	8	5	734.30429	0

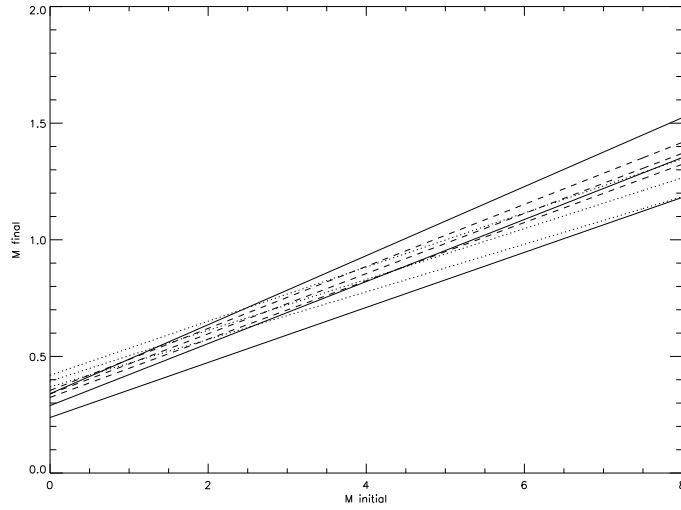


FIGURE 3.8: Plots of all published IFMRs used in this analysis; solid (Dobbie et al. 2006), dotted (Kalirai et al. 2008), dashed (Williams et al. 2009).

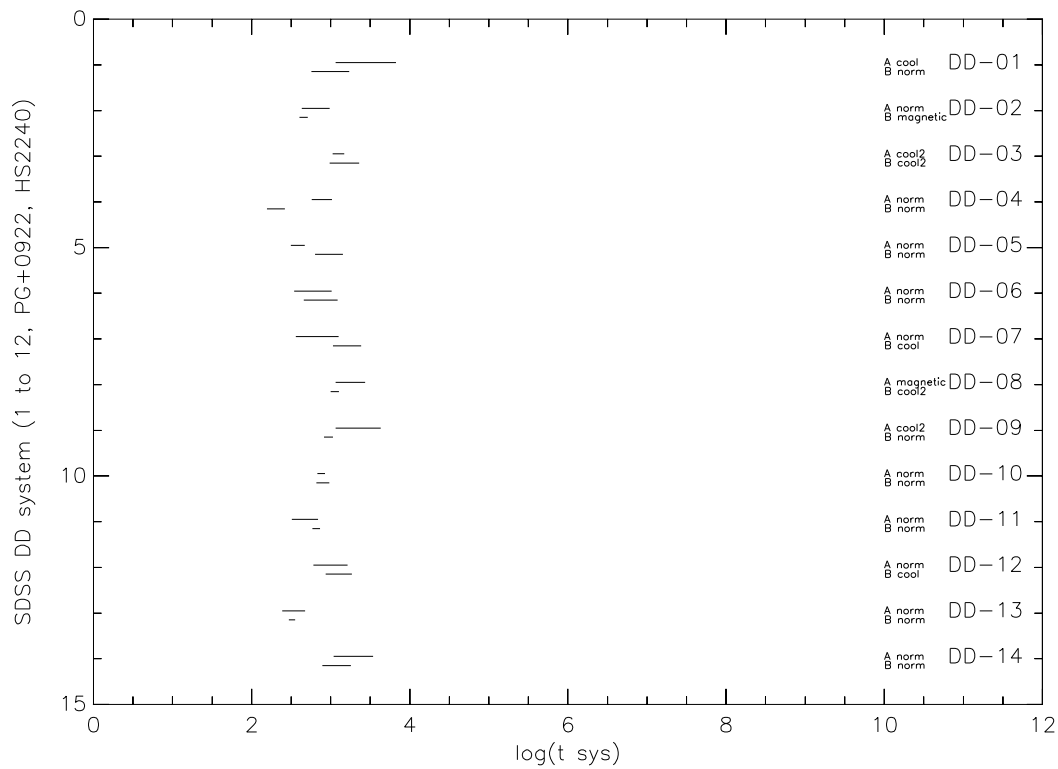


FIGURE 3.9: Calculated System Age for SDSS DD systems, using known IFMR from Dobbie et al. (2006).



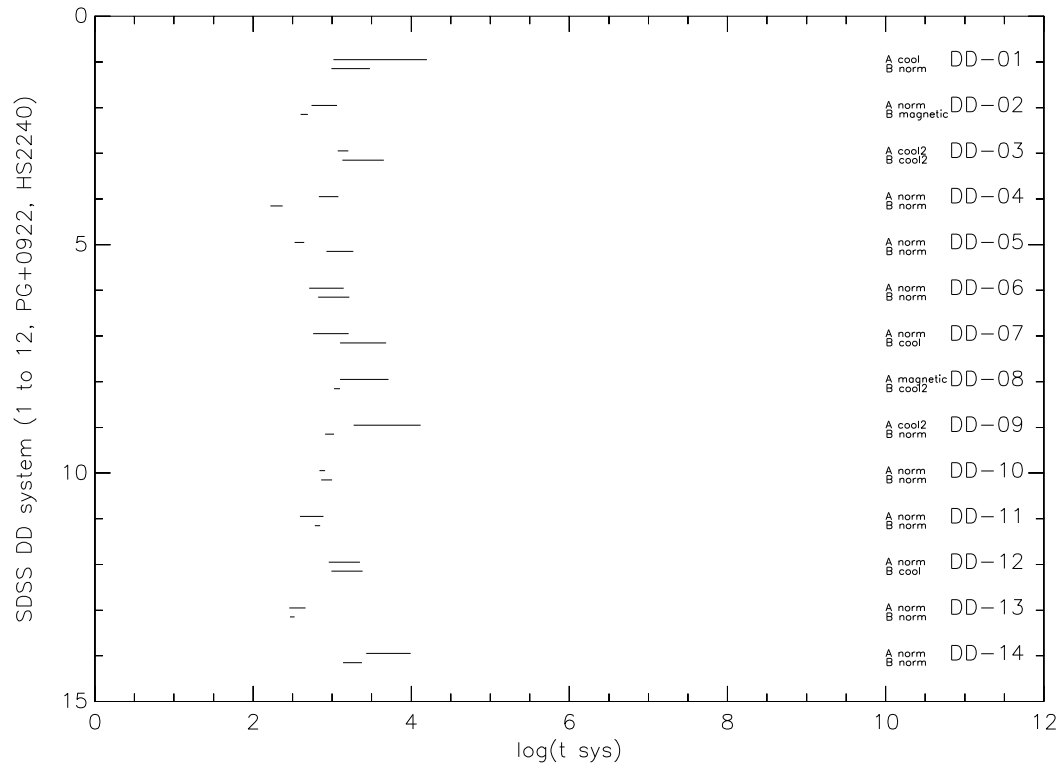


FIGURE 3.10: Calculated System Age for SDSS DD systems, using known IFMR from Kalirai et al. (2008).

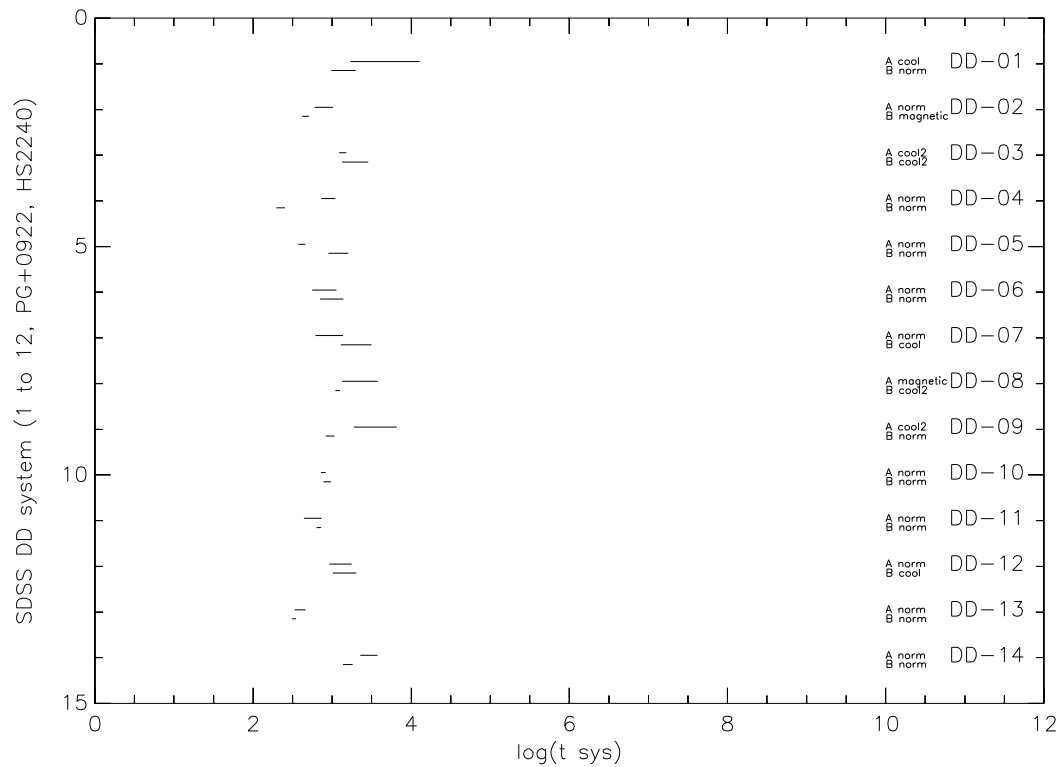


FIGURE 3.11: Calculated System Age for SDSS DD systems, using known IFMR from Williams et al. (2009).

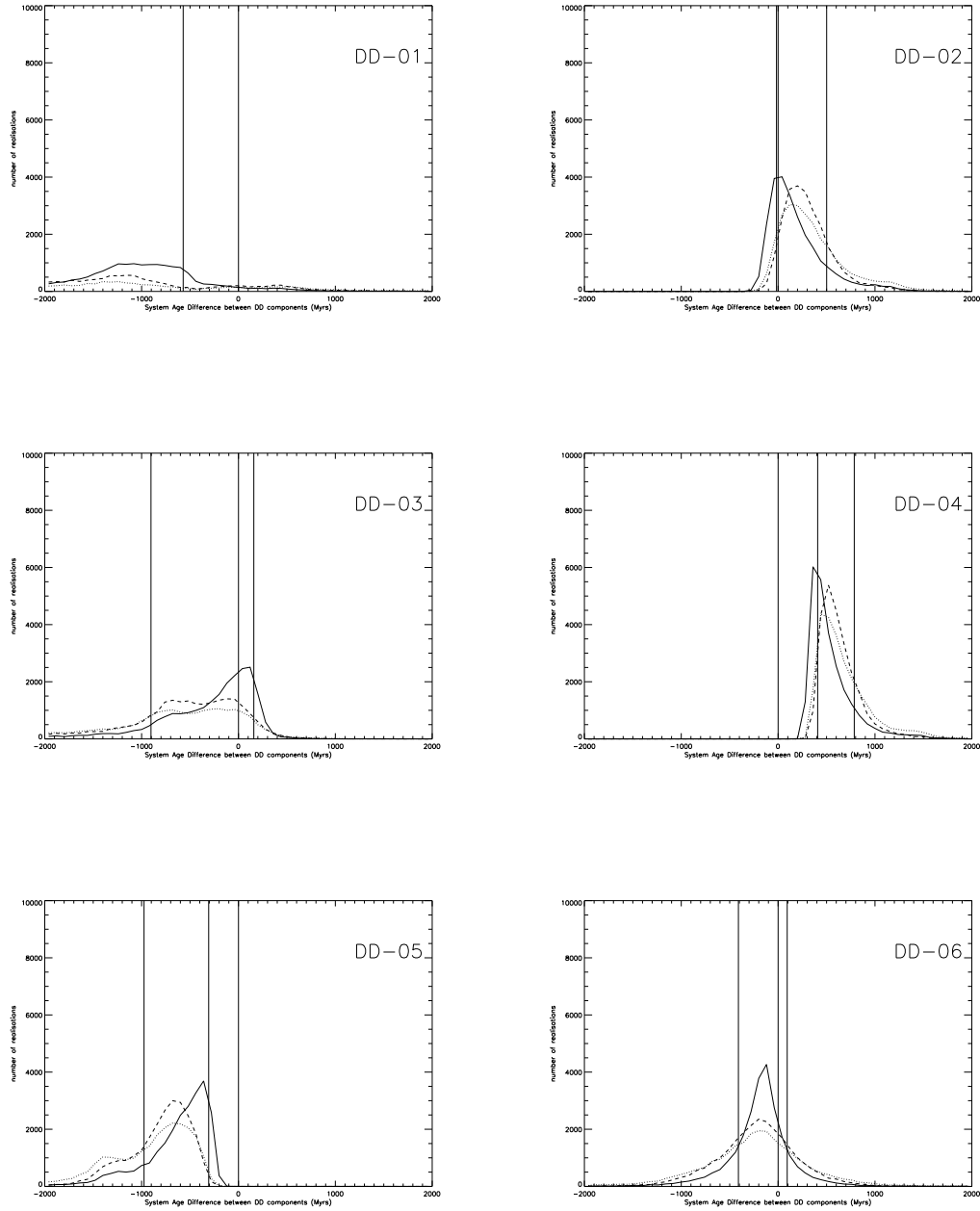


FIGURE 3.12: Plots of the system age difference distribution for DD-01 to DD-06, based upon a generated monte carlo distribution of 25000 hypothetical WDs with parameters selected within their error limits. For each plot a number of published IFMR forms are assumed; solid (Dobbie et al. 2006), dotted (Kalirai et al. 2008), dashed (Williams et al. 2009).

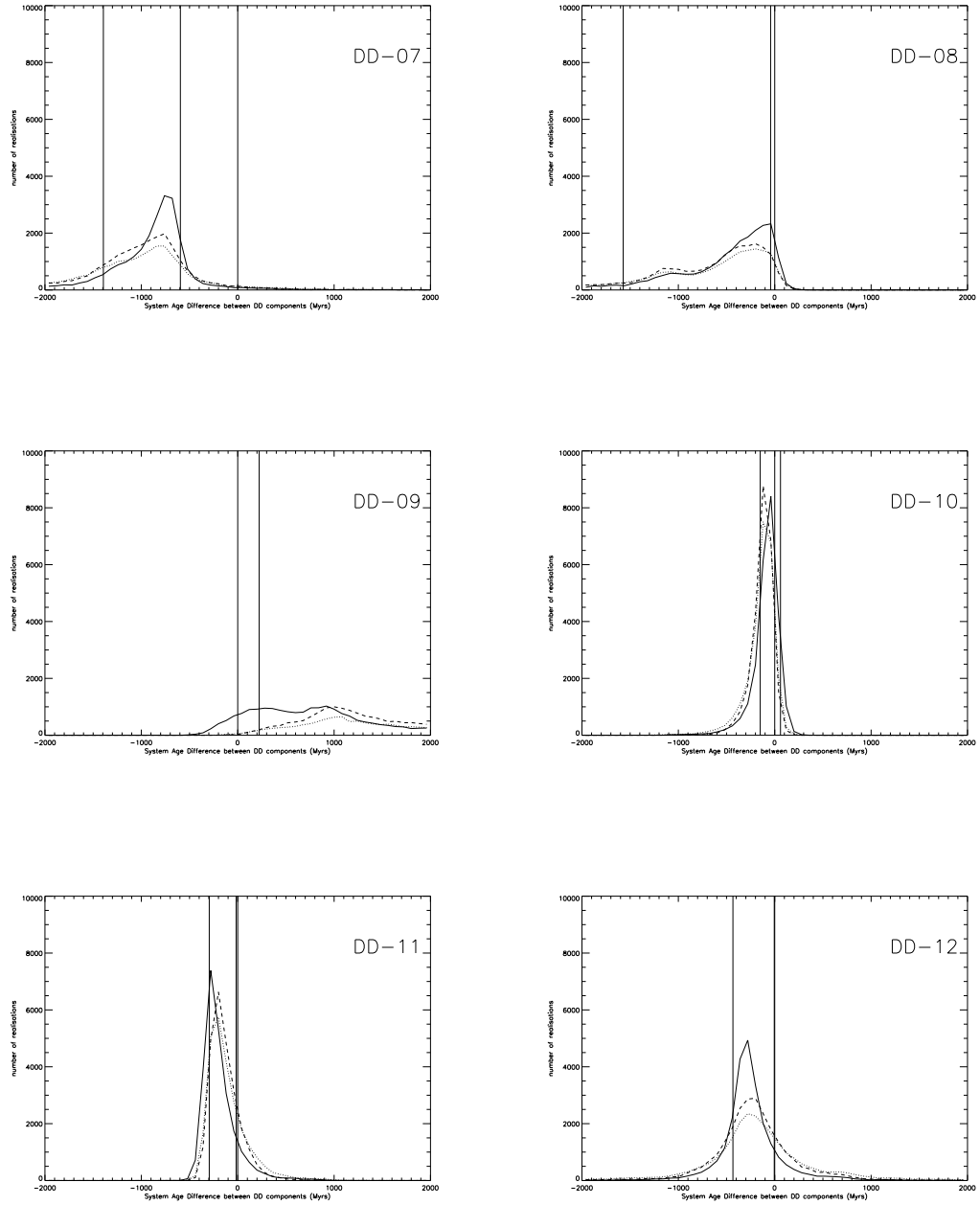


FIGURE 3.13: Plots of the system age difference distribution for DD-07 to DD-12, based upon a generated monte carlo distribution of 25000 hypothetical WDs with parameters selected within their error limits. For each plot a number of published IFMR forms are assumed; solid (Dobbie et al. 2006), dotted (Kalirai et al. 2008), dashed (Williams et al. 2009).

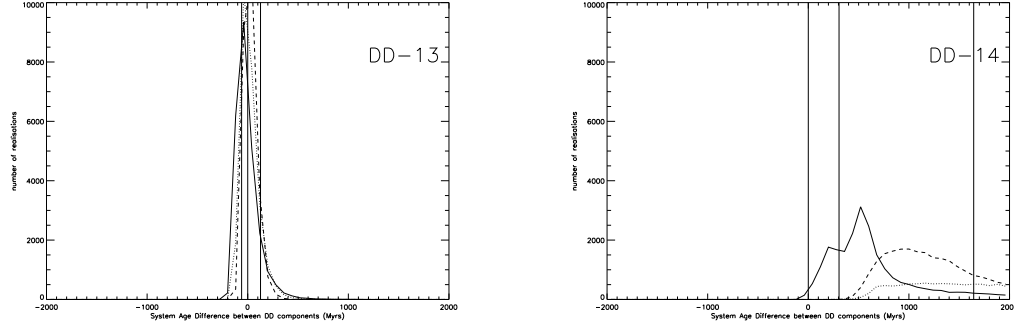


FIGURE 3.14: Plots of the system age difference distribution for external WDs PG0922+162 (DD-13) and HS2240+125A (DD-14) respectively, based upon a generated monte carlo distribution of 25000 hypothetical WDs with parameters selected within their error limits. For each plot a number of published IFMR forms are assumed; solid (Dobbie et al. 2006), dotted (Kalirai et al. 2008), dashed (Williams et al. 2009).

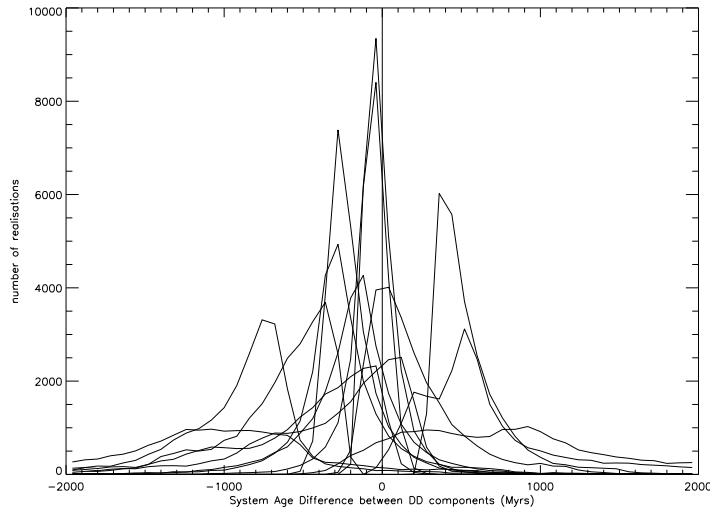


FIGURE 3.15: Plots of the system age difference distributions for all DD systems, based upon a generated monte carlo distribution of 25000 hypothetical WDs with parameters selected within their error limits. For this plot the following published IFMR form has been assumed; Dobbie et al. (2006).

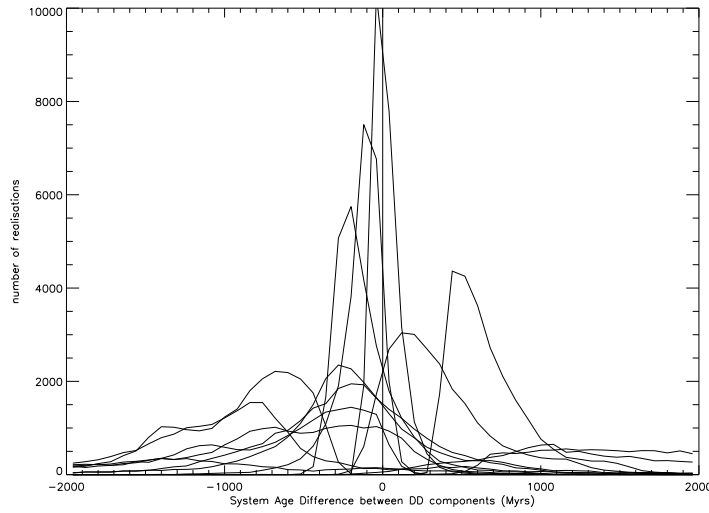


FIGURE 3.16: Plots of the system age difference distributions for all DD systems, based upon a generated monte carlo distribution of 25000 hypothetical WDs with parameters selected within their error limits. For this plot the following published IFMR form has been assumed; Kalirai et al. (2008).

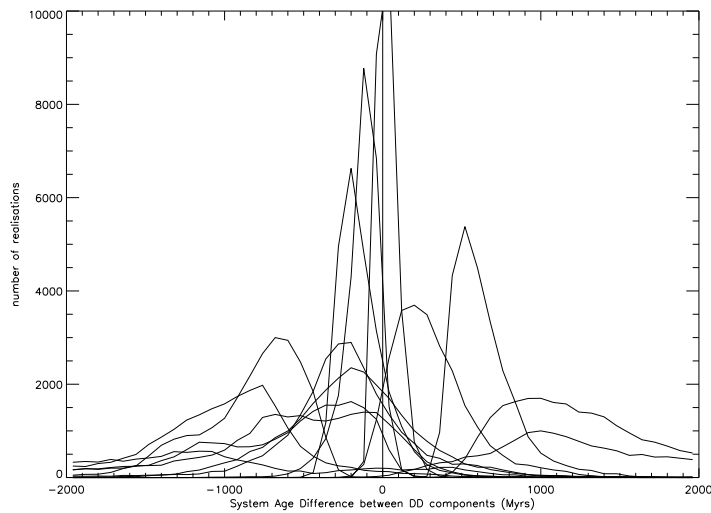


FIGURE 3.17: Plots of the system age difference distributions for all DD systems, based upon a generated monte carlo distribution of 25000 hypothetical WDs with parameters selected within their error limits. For this plot the following published IFMR form has been assumed; Williams et al. (2009).

Figures 3.18 and 3.19 show the WD component initial-final mass according to Dobbie et al. (2006) (A/B), for each DD system respectively.

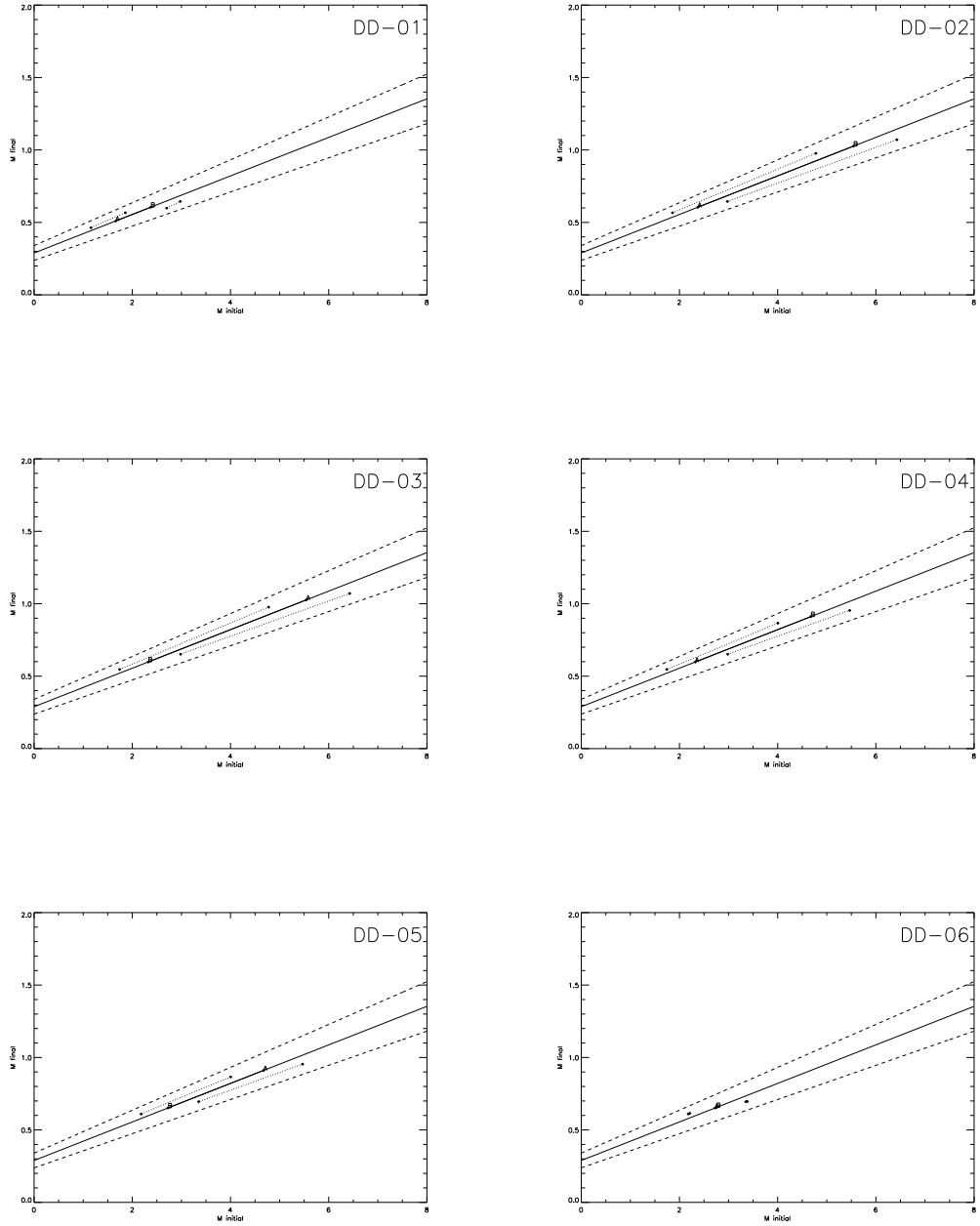


FIGURE 3.18: Plots of the initial-final mass for each component WD (of DD-01 through to DD-06) according to the (Dobbie et al. 2006) IFMR (A/B).

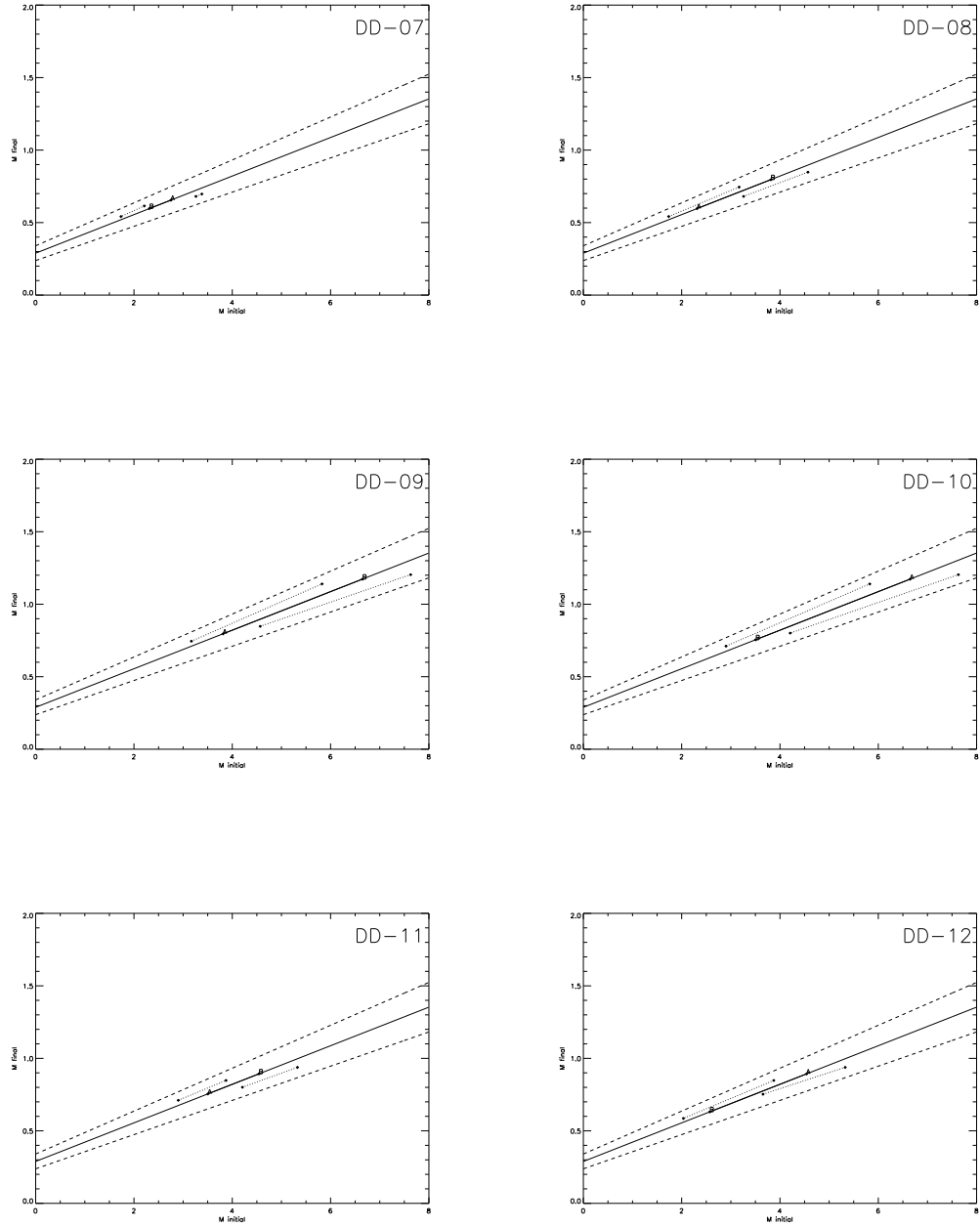


FIGURE 3.19: Plots of the initial-final mass for each component WD (of DD-07 through to DD-12) according to the (Dobbie et al. 2006) IFMR (A/B).



### 3.4 A preliminary investigation of the double degenerate mass distribution

The field WD mass distribution has been determined several times during the last few decades. These studies have applied corrections to account for the mass dependence of the volume being probed in a magnitude limited survey. If these corrections are not applied, mass distributions assembled from magnitude limited samples tend to over represent low mass WDs and under represent high mass WDs. The recent field WD mass distribution obtained by Kepler et al. (2007) using the SDSS DR4 and Liebert et al. (2005a) using the Palomar-Green (PG) Bright Quasar Survey both include  $1/V_{\max}$  corrections, which are shown in Figures 3.20 and 3.21 respectively. The SDSS field WD mass distribution was compiled from 1733 WDs with  $T_{\text{eff}} > 12000K$ ,  $g < 19$ , while the PG based distribution was constructed from 347 WD stars with  $T_{\text{eff}} > 13000K$ . These effective temperature limits are designed to negate the documented discrepancy in the reliability of the WD  $\log g$  determinations at lower effective temperatures.

In generating my DD mass distribution, I have used all known spectroscopically studied DD systems that lie within the SDSS DR7 footprint and that pass my selection criteria (ie. separation, colour and magnitude limits). This includes binaries which were omitted from my follow-up work because they had already been observed spectroscopically and have had their parameters determined by other investigators ie. PG 0922 + 162A+B from the Palomar-Green Bright Quasar Survey (Finley and Koester 1997) and HS 2240 + 125A+B from the Hamburg Quasar Survey (Jordan et al. 1998a). Details on these additional DD systems are shown in Table 3.3. My distribution contains the 24 WDs from the double degenerate pairing which after detailed analysis I believe to be physically associated (ie, excluding DD-04 and DD-09), and has been binned at  $0.1M_{\odot}$  intervals. This fits best with the uncertainties in my individual mass calculations, provides a number of reasonably well populated bins and at the same time provides fair resolution in mass. I have made no attempt to model the impact of WD mass on my sampling volume (ie. I have not applied a  $1/V_{\max}$  correction) so if anything, high mass WDs should be under represented in my preliminary mass distribution.

I have plotted my mass distribution for WDs in wide double-degenerate systems in Figure 3.22. I have overplotted in this figure, the raw SDSS field WD mass distribution of Kepler et al. (2007), the  $1/V_{\max}$  corrected SDSS WD mass distribution of the same investigators and also the volume corrected field WD mass distribution of Liebert et al. (2005a). A glance at this figure suggests that my sample is skewed towards higher WD masses than the field studies.

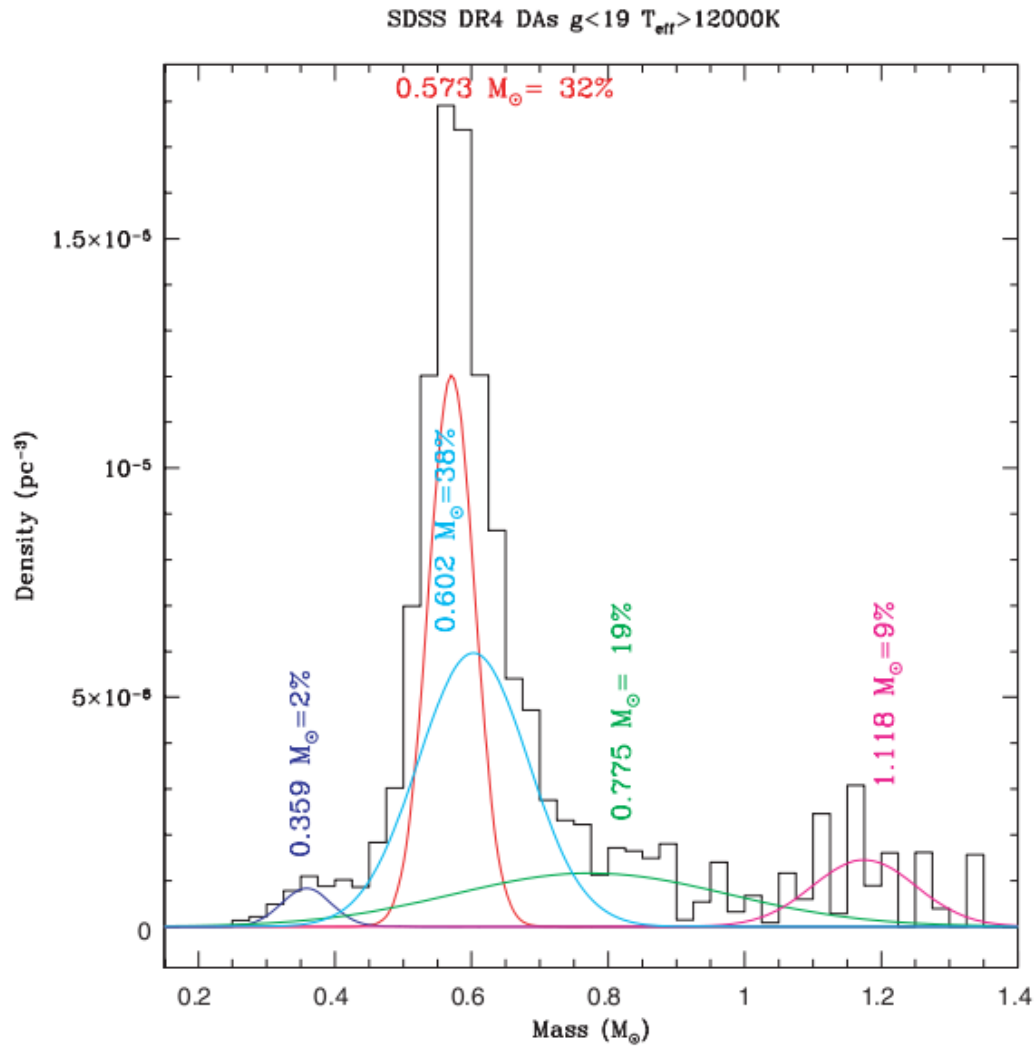


FIGURE 3.20: Kepler SDSS  $V_{\text{max}}$  Corrected Mass Distribution (Kepler et al. 2007)

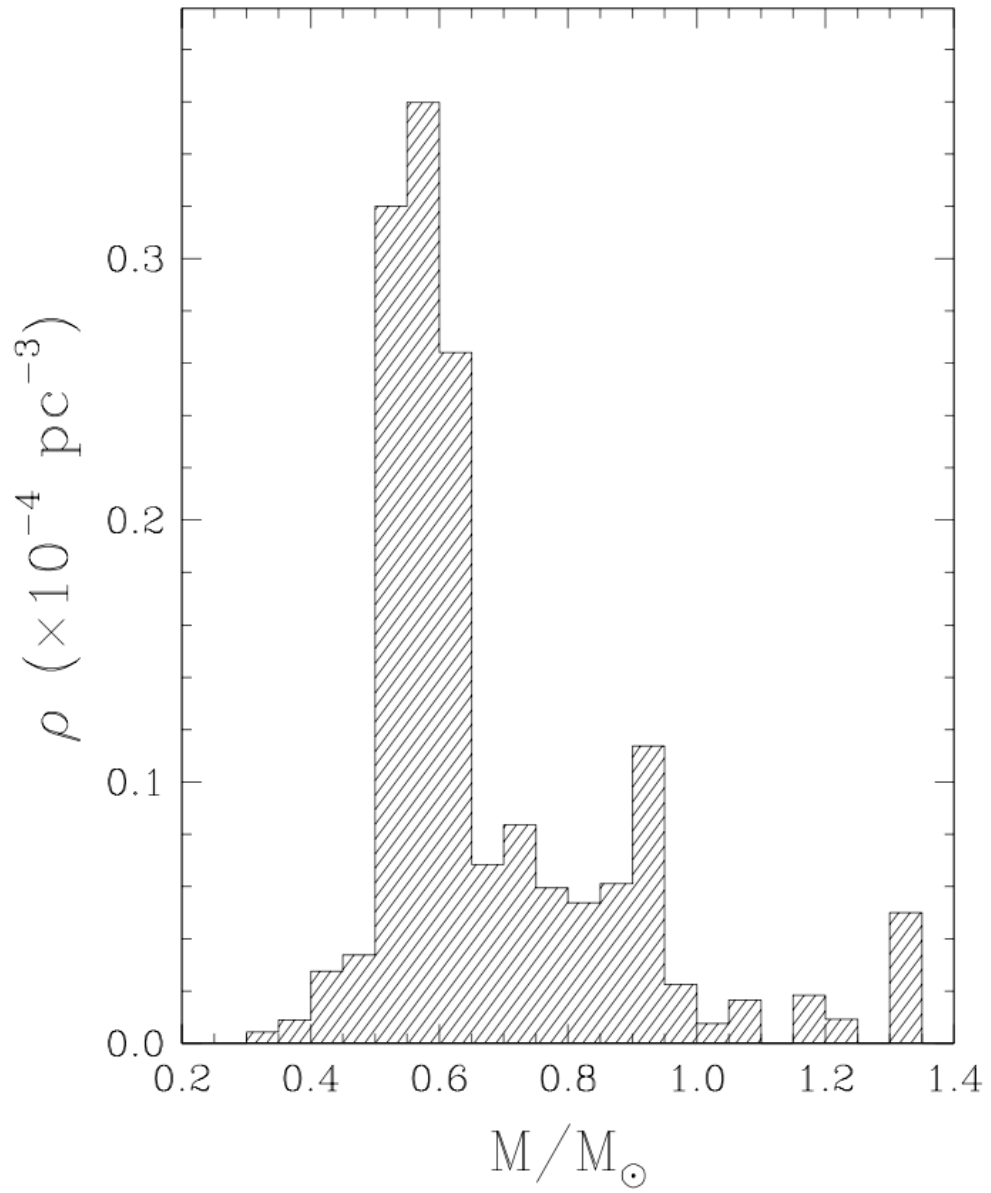


FIGURE 3.21: Liebert PG Survey  $V_{max}$  Corrected Mass Distribution (Liebert et al. 2005a)

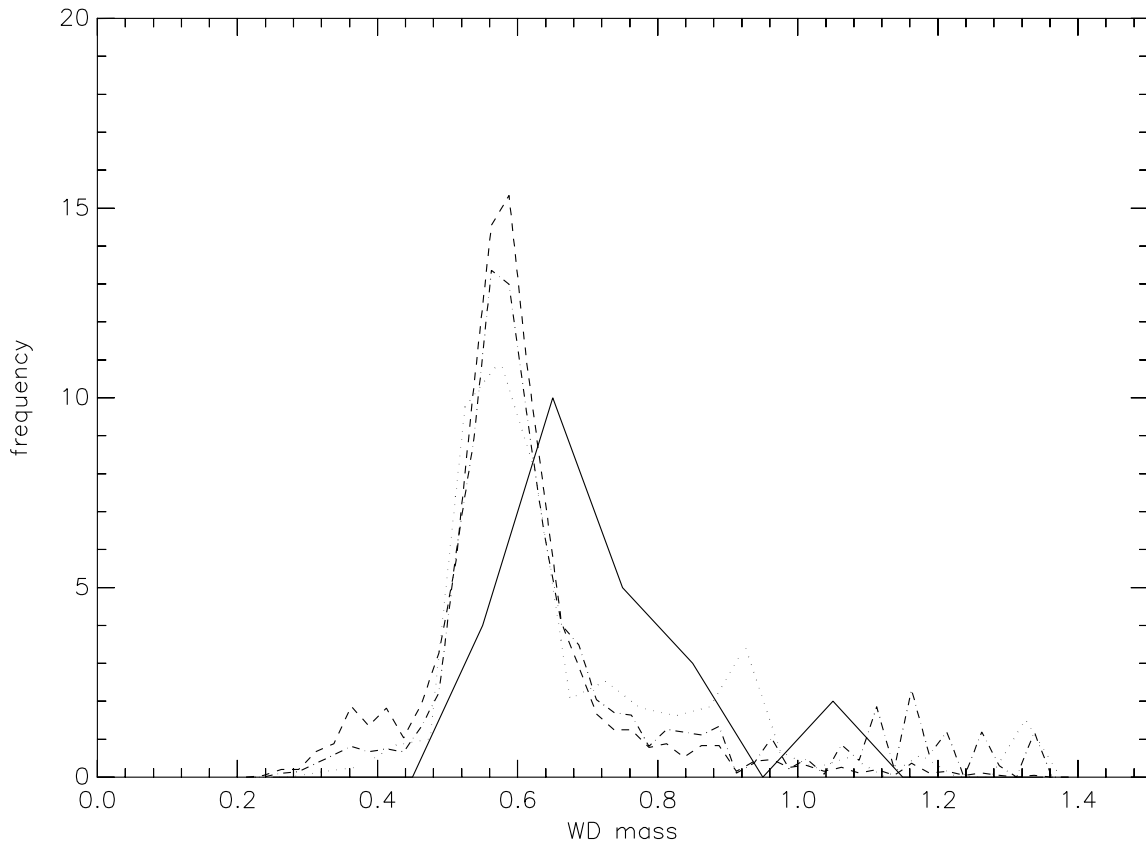


FIGURE 3.22: DD mass distribution (Solid) versus the PG Survey Vmax corrected mass distribution (Dotted), the Kepler SDSS DR4 WD mass distribution (Kepler et al. 2007) (Dashed), and the Kepler SDSS DR4 WD Vmax corrected mass distribution (Kepler et al. 2007) (Dash Dot)

TABLE 3.3: Additional (third party) Double Degenerate systems added to my mass distribution

WD	$\log g$	$\log g$ err	$T_{eff}$ (K)	$T_{eff}$ (K) err	$\tau_c$ (Myr)	$\tau_c$ (Myr) err	$M_{final}$ ( $M_{\odot}$ )	$M_{final}$ ( $M_{\odot}$ ) err	abs u	abs g	abs r	abs u err	abs g err	abs r err	dist	dist err
PG0922+162A	8.27	0.05	22740	230	78	10	0.792	0.031	10.66	10.78	11.17	0.08	0.09	0.08	5.35	0.09
PG0922+162B	8.78	0.05	22130	220	248	24	1.094	0.026	11.62	11.76	12.13	0.1	0.1	0.1	5.38	0.12
HS2240+125A	7.86	0.01	15636	9	146	1	0.536	0.004	11.11	10.89	11.19	0.01	0.01	0.01	5.33	0.02
HS2240+125B	7.99	0.01	13935	112	244	7	0.604	0.007	11.64	11.33	11.57	0.03	0.03	0.02	5.17	0.03

### 3.4.1 Comparing the DD mass distribution to the field WD mass distribution

To calculate the likelihood that the mass distribution I obtain from the DD systems and the field WD mass distribution are drawn from the same underlying population, I have performed Kolmogorov-Smirnov (K-S) tests. In order to perform these comparisons I first took the respective field WD mass distributions (Kepler SDSS Survey WD mass distribution, Kepler SDSS Survey  $V_{\max}$  corrected WD mass distribution and Liebert PG Survey  $V_{\max}$  corrected WD mass distribution) and created a model of them using combinations of gaussians (or in the case of the SDSS distributions I lifted the gaussian model parameters directly from the Kepler paper). I then formed a set of “hypothetical” mass values representing WDs within the distribution using the number of WDs used to create the distribution originally (1733, 1733, and 347 respectively). I then compared this set of data with the observed WD masses from my survey using a K-S test routine written in IDL. This code is provided in the Appendix (Section A.6.4). I calculated the probabilities of the DD and the field WD mass distributions being the same as  $P \sim 2.11E - 6$ , 0.00068, and 0.00371 for the Kepler SDSS Survey WD mass distribution, Kepler SDSS Survey  $V_{\max}$  corrected WD mass distribution, and Liebert PG Survey  $V_{\max}$  corrected WD mass distribution respectively. Thus considering that I have not applied  $1/V_{\max}$  corrections, I conclude that the masses of my WDs in wide DD systems are generally higher than those of field WDs.

In my sample, one component (DD-09B) has a very high mass of  $1.17M_{\odot}$ , and 6 components have  $M > 0.82M_{\odot}$ . 25% of my components have high masses whereas only 5% of the Gianninas et al. (2011) white dwarfs have similar high masses.

It is also evident that all of my high mass components also have  $T_{eff} > 13000K$ . The 9 cool components in the sample ( $T_{eff} < 13000K$ ) have an average mass of  $0.64M_{\odot}$ , whereas the 15 hot components ( $T_{eff} > 13000K$ ) have an average mass of  $0.78M_{\odot}$ . Hotter white dwarfs should however have lower mass than cooler white dwarfs (Kleinman et al. 2004). Gianninas et al. (2011) has found that hot white dwarfs ( $T_{eff} > 13000K$ ) have an average mass of  $0.661M_{\odot}$ , with a dispersion of  $0.160M_{\odot}$ , whereas cool white dwarfs ( $T_{eff} < 13000K$ ) have an average mass of  $0.638M_{\odot}$ , with a dispersion of  $0.145M_{\odot}$ .

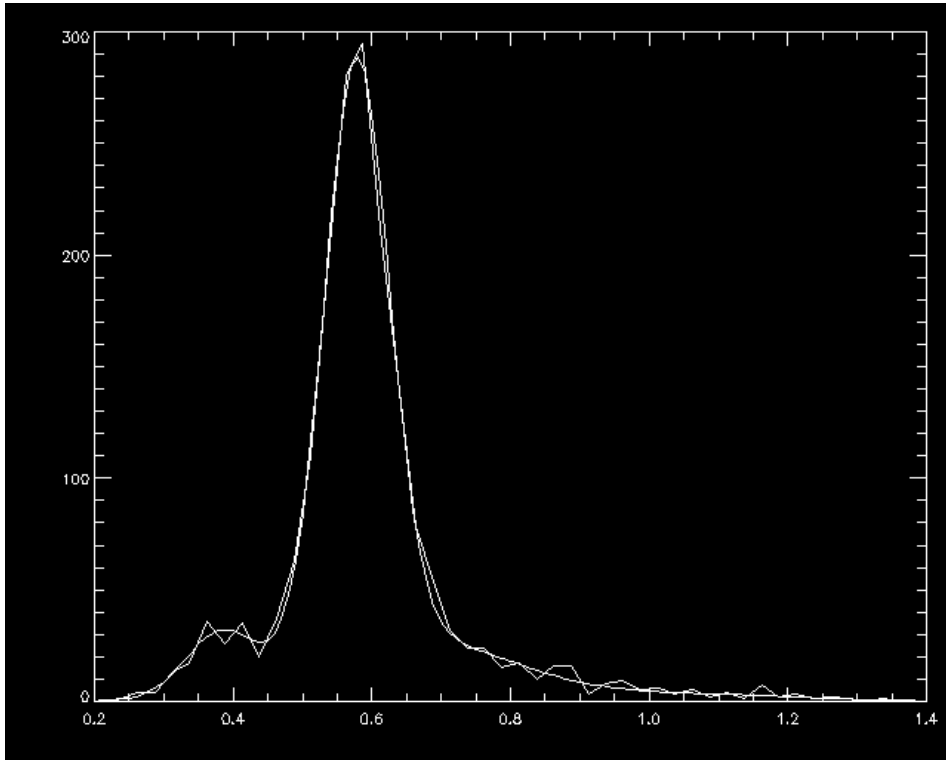


FIGURE 3.23: Kepler SDSS Survey Mass Distribution Modelled With Gaussians

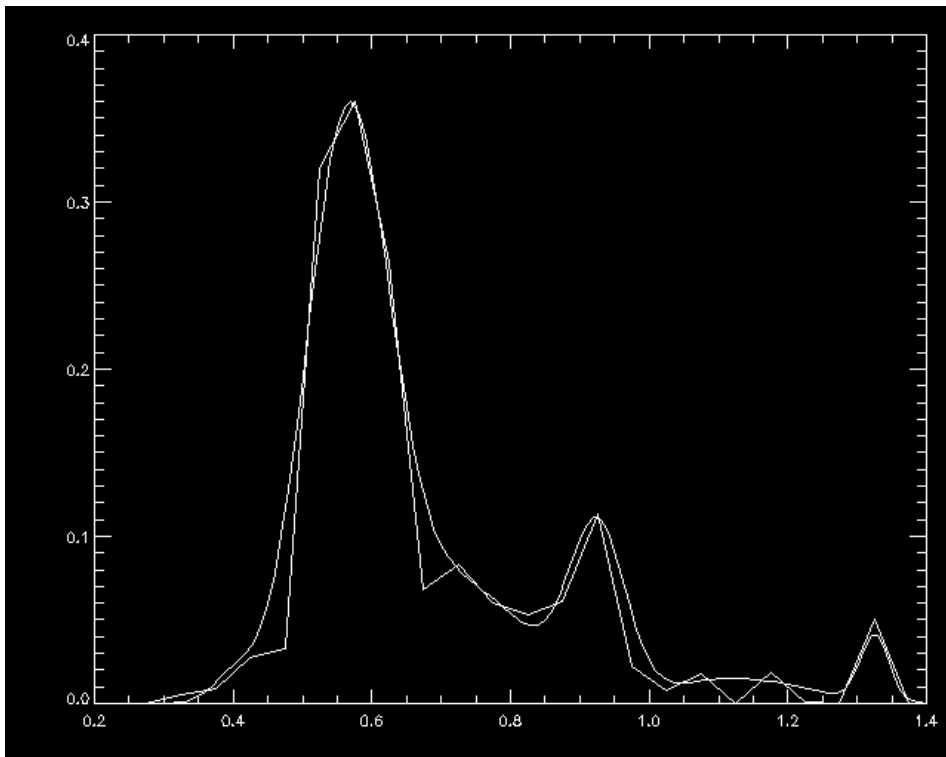


FIGURE 3.24: PG Survey  $V_{\text{max}}$  Corrected Mass Distribution Modelled With Gaussians

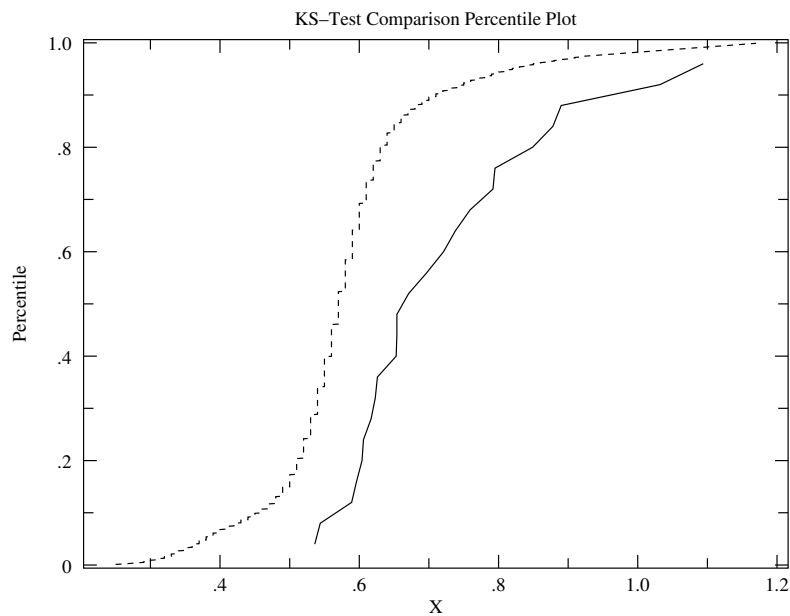


FIGURE 3.25: KS Test Method 2 - Comparison of DD masses with masses derived from Kepler theoretical SDSS WD mass distribution modelled with Gaussians

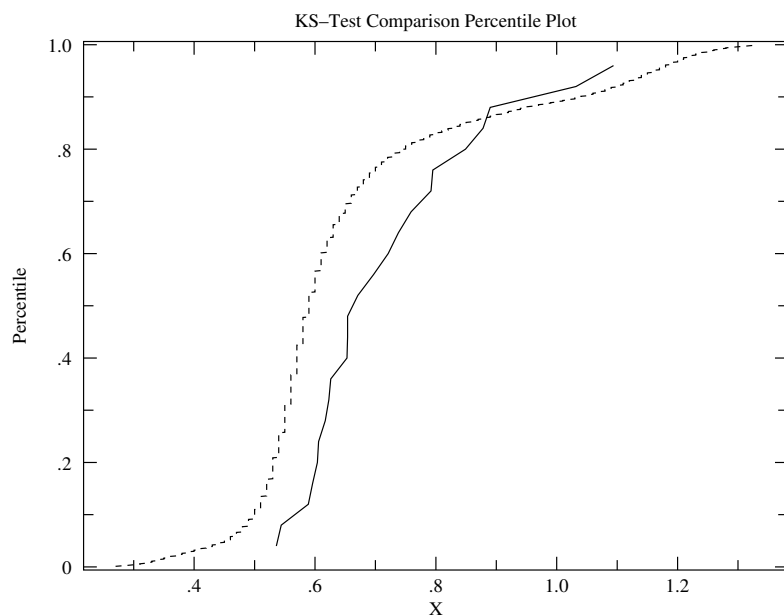


FIGURE 3.26: KS Test Method 6 - Comparison of DD masses with masses derived from Kepler theoretical  $V_{\max}$  corrected SDSS WD mass distribution modelled with Gaussians



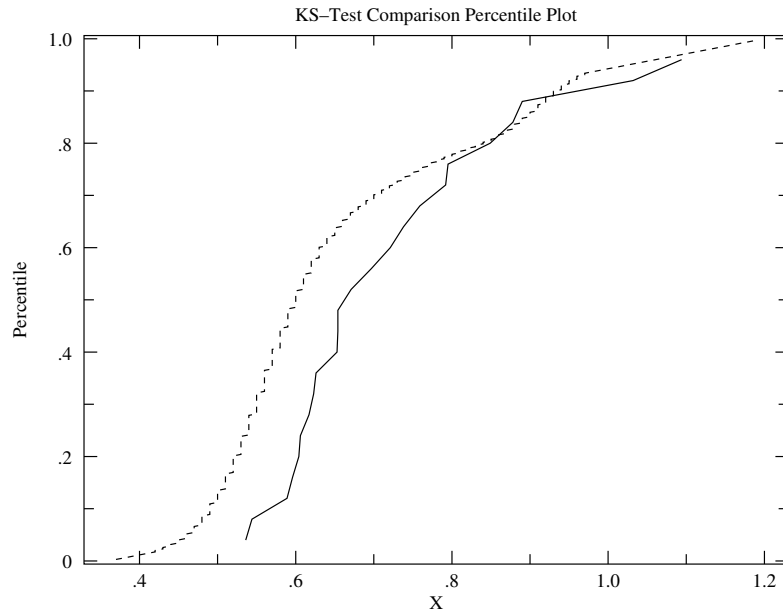


FIGURE 3.27: KS Test Method 5 - Comparison of DD masses with masses derived from Liebert theoretical PG Survey  $V_{\max}$  corrected mass distribution modelled with Gaussians

### 3.4.2 Why might the DD mass distribution be skewed to higher mass?

There are a number of possible reasons as to why my preliminary mass distribution for the components of wide DD systems may be skewed to higher mass than that of the field WD population. First, there are differences in the binary fraction of main sequence stars as a function of mass. Stars of earlier spectral types are observed to occur more often in binary systems than those of later spectral type (e.g Sterzik and Durisen 2004). For example, Kouwenhoven et al. (2005) have determined the binary fraction of B, A and F stars in the Upper Scorpius Association to be  $\sim 60\%$ ,  $\sim 40\%$  and  $\sim 20\%$ , respectively. Thus since in general, higher mass stars lead to more massive WDs, the binary fraction of WDs may also show this mass dependence. Second, it could be expected that for my systems there are proportionately fewer close primordial pairings ( $\approx 10 - 20\%$  percent of my DD systems could be triple systems) than for a sample of apparently single field objects where the overall binary fraction is typically  $\sim 40-50\%$  (e.g Kouwenhoven et al. 2005). Therefore within the field population, a higher fraction of these systems may have interacted with a companion and experienced enhanced massloss at earlier evolutionary phases, which can lead to the formation of a WD of lower mass than that from a single star of corresponding initial mass. A third possible reason is that orbital separation likely increases due to the loss of mass from the system as stars become WDs. Since intermediate mass stars, which produce high mass WDs, lose a much higher proportion of their initial mass during their evolution than lower mass stars, primordial binaries with components of this mass likely lead to on average, WD pairs with larger final separations. For example, by applying Jean's theorem which states that the product of the total mass and the semi-major axis of the orbit remain constant (e.g. Iben 2000), I find that the transformation of a  $M_i = 1.8M_\odot$  main sequence star into a  $M_f = 0.6M_\odot$  WD would result in an orbital expansion factor of  $\sim 3$ , whereas a  $M_i = 4.5M_\odot$  main sequence star evolving into a  $M_f = 0.9M_\odot$  WD (based on the recent Casewell et al. (2009) IFMR), would lead to an expansion in the orbital separation by a factor of  $\sim 5$ . Thus assuming a similar primordial distribution of orbital separations, I estimate that on an object by object basis a double degenerate system containing two  $0.9M_\odot$  components is  $\sim 3$  times more likely to be unearthed by my target selection criteria than a binary containing two  $0.6M_\odot$  components.

## 3.5 A preliminary investigation of the double degenerate magnetic WD distribution

I also found an unusually high percentage of magnetic stars. Gianninas et al. (2011) found 25 magnetic (or suspected magnetic) stars out of about 1300 stars studied (2%). In my sample, 4 out of 24 of my stars were found to be magnetic (DD-02A, DD-02B, DD-04A, and DD-08A), an order of magnitude higher.

*"So it is plain that Science must mean the most accurate of all Knowledge; but if so, then the Scientific man must not merely know the deductions from the First Principles but be in possession of truth respecting the First Principles.."*

from Aristotle's Nicomachean Ethics

# 4

## Moving forward

### 4.1 Further optical spectroscopy

#### 4.1.1 Non-magnetic systems

While I have secured long-slit optical spectroscopy for 12 systems, there are 25 further pairs with angular separations  $<10''$  awaiting follow-up observations. A key goal of this further work is to identify systems with extreme mass ratios e.g.  $M_1=0.7M_\odot$ ,  $M_2=1.3M_\odot$ . Unfortunately I have not yet confirmed a physical system in which one component has a mass  $M>1.1M_\odot$ , the theoretical dividing line between CO and ONe core WDs. A substantial population of these ultramassive ( $M_{WD}\gtrsim 1.05M_\odot$ ) WDs has been recognised in the field for well over a decade (e.g. Fleming et al. 1986, Marsh et al. 1997, Vennes et al. 1997) but their origins remain a matter of considerable debate. The results of population synthesis calculations suggest that the majority of these objects might be produced through the merging of the lower mass components of close binary systems, at least at the higher galactic latitudes typical of the Palomar Green and Sloan Digital Sky surveys (Liebert et al. 2005a). However, models of this merging process encounter difficulties in explaining the observed space density of nearby, hot, ultramassive white dwarfs unless they assume the formation rate of close binaries in the Galaxy is somewhat higher than expected and the viscosity of the merger interior is very low (Segretain et al. 1997). Liebert et al. (2005a) have noted that the spatial distribution of the 28 most massive white dwarfs detected in the extreme ultraviolet (EUV) sky surveys displays similarities with that of the younger stellar populations in the vicinity of Gould's Belt (with the caveat that the EUV source distribution is affected by the patchy opacity of the local ISM). The identification of these objects in wide double-degenerate systems would allow me to constrain their pre-WD lifetimes and examine whether these are consistent (or otherwise) with them having formed from single heavy-weight intermediate mass stars.

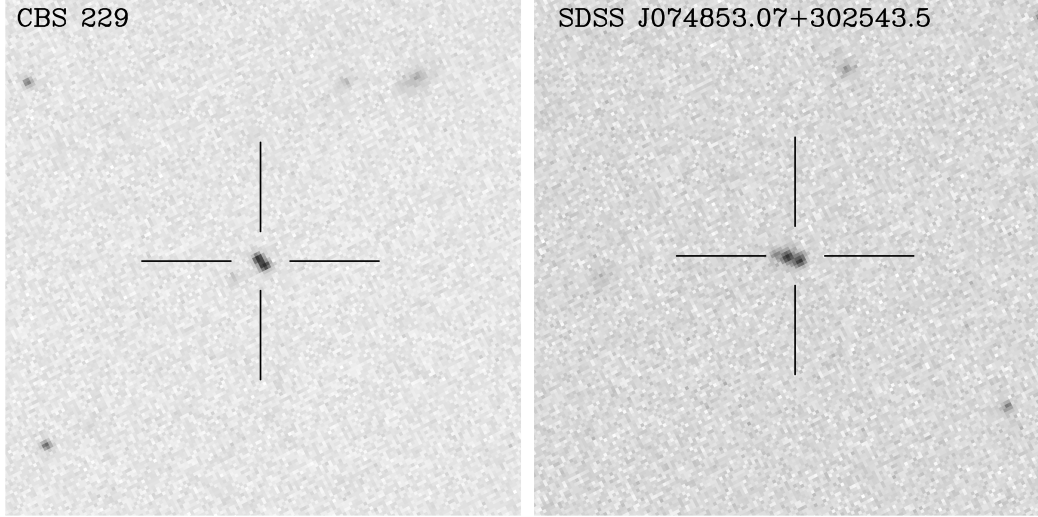


FIGURE 4.1: SDSS  $z$  band image of two candidate spatially resolved magnetic/non-magnetic double-degenerate systems, CBS 229 (Gianninas et al. 2009) and SDSS J074853.07+302543.5. Images are approximately  $1' \times 1'$  with N at the top and E to the left.

An enlarged sample of spectroscopically studied wide double-degenerate systems would also be useful for searching for WDs with atmospheres dominated by elements other than hydrogen e.g. helium or carbon. There is a suggestion from open clusters that helium dominated atmospheres are extremely rare in young and intermediate age populations,  $\tau \lesssim 1\text{Gyr}$  (Kalirai et al. 2005b). WDs of this atmospheric composition are believed to form as a result of a late-helium shell flash during the final phases of the AGB, which consumes all hydrogen rich material. The possibility that this mechanism is mass dependent can be tested by studying DB WDs in wide binaries, where constraints on the system age are available from the companion star.

#### 4.1.2 Systems containing HFMWDs

To help shed further light on the formation of HFMWDs and the impact of magnetic fields on stellar evolution, it is also desirable to enlarge the sample of these objects that are located in wide double-degenerate binaries (or in nearby open clusters) so that any trends in their cooling times (with respect to non-magnetic WDs) can be clearly identified. At least one of my candidate systems awaiting detailed spectroscopic follow-up,

SDSS J074853.07+302543.5 and SDSS J074852.95+302543, which have an angular separation of  $\sim 1.6''$  (see Figure 4.1, right), seems likely to be a DAH+WD system, since the SDSS spectrum of the former shows clear evidence of Zeeman split Balmer lines. I also note that the previously known hot DA+DAH system CBS 229, which lies within the SDSS DR7 footprint, is probably a wide binary. It was identified as an unresolved pairing during the course of a spectroscopic survey of bright WDs ( $V \leq 17.5$ ) drawn from the catalogue of McCook and Sion (1999). Gianninas et al. (2009) have performed a preliminary analysis of a composite spectrum of this system and find that the non-magnetic component has  $T_{\text{eff}} \approx 15000\text{K}$  and  $\log g \approx 8.5$ , corresponding to a mass of  $M \approx 0.9M_{\odot}$ . The shape of their deblended spectrum of the DAH suggests that the two objects have similar effective temperatures. My examination of the SDSS imaging reveals that the components are resolved into two photocenters with a projected separation of  $\sim 1.3''$  (see Figure 4.1, left). From the Gianninas et al. (2009) parameters for the DA and its magnitude from the SDSS  $z$  imaging (the band in which the objects are most clearly resolved), I provisionally estimate a distance to this binary of  $d \sim 140\text{pc}$  and a projected orbital separation of  $a \sim 180\text{AU}$ . Thus, despite both components having  $T_{\text{eff}} \gtrsim 9000\text{K}$ , CBS 229 appears to be a wide magnetic/non-magnetic double-degenerate system which escaped detection by my survey. This is probably due to the  $u$  band magnitude measurement for the NE component which appears to be anomalous. Undoubtedly further magnetic/non-magnetic pairings remain to be identified within my existing sample of candidate DD systems.

Thus I find a number of scientific reasons for obtaining spectroscopy of more of my candidate DD systems. A number of the systems for which I have already secured spectroscopy were observed during “band 3” weather conditions, ie. poorer seeing and poorer sky transparency. A significant proportion of the remaining systems will require better observing conditions since they are fainter and/or of lower angular separation. The number of candidate wide DD systems available for follow-up will shortly increase when southern sky survey imaging datasets such as Skymapper and VST ATLAS become publicly available. As part of a preliminary investigation, I have performed a basic replication of the target selection process on the SDSS DR8 dataset. Due to time constraints, detailed error checking has not been performed as yet on this initial collection of additional DD candidate data. See Figure 4.2 for a list of these DR8 specific candidates.

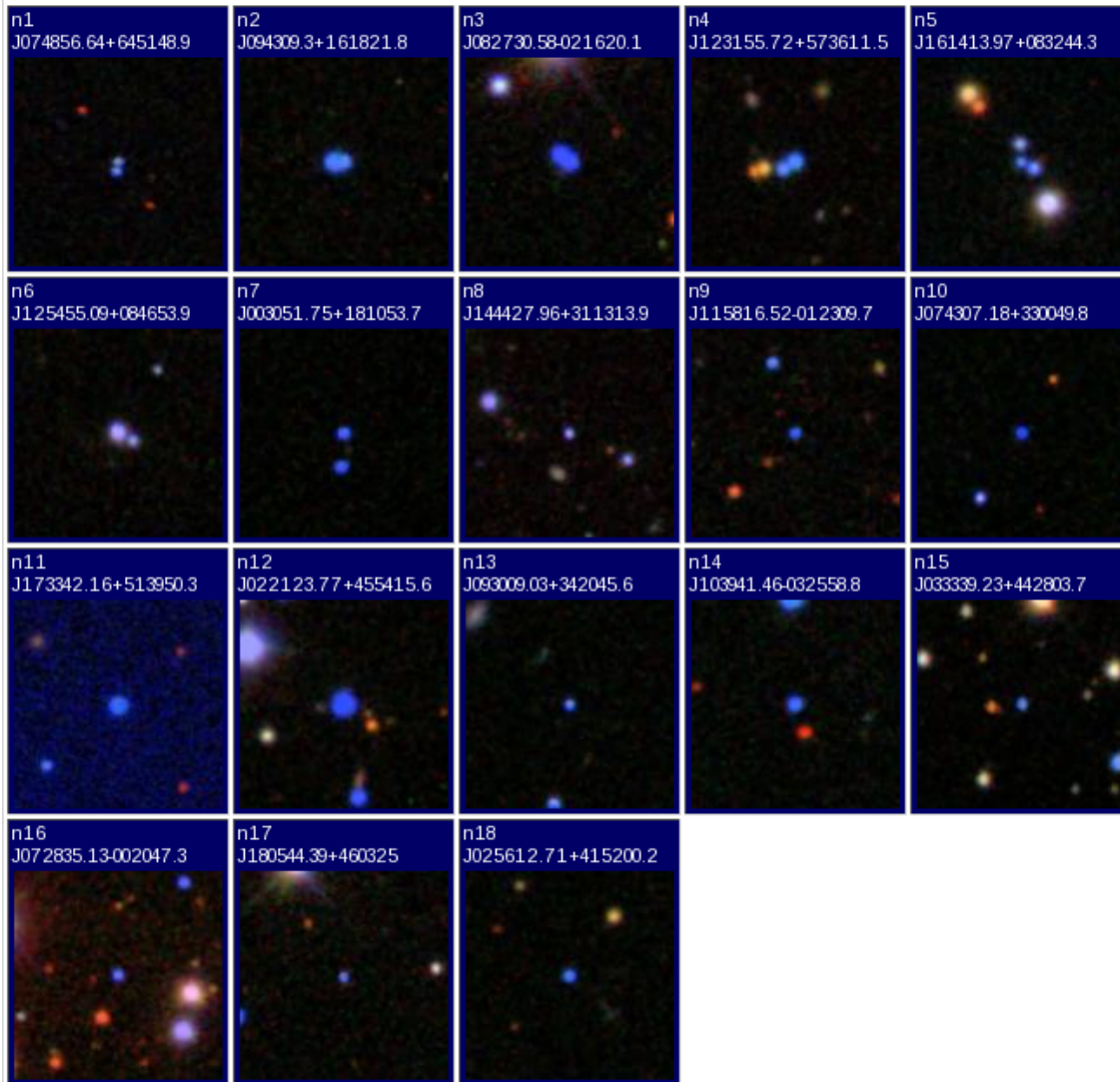


FIGURE 4.2: DR8 Only DD Candidates

TABLE 4.1: A table of my preliminary IFMR linear parameter derivations, [1] for all systems, and [2] excluding systems with an uncommon distance between components (DD-04 and DD-09)

IFMR	m	m err	c	c err
Dobbie et al. (2006)	0.133	0.015	0.289	0.051
DD IFMR derivation (all systems [1])	0.155	0.017	0.167	0.037
DD IFMR derivation (excluding [2])	0.159	0.018	0.149	0.03

## 4.2 Preliminary investigation of IFMR form derivation

In addition to probing the IFMR, where system ages were confirmed as consistent (or inconsistent) with established forms of the IFMR, a preliminary investigation was made into the ability to independently derive the form of the IFMR using DD systems. A basic constraint of the form of the IFMR was derived using my DD data, by equalising the system age of each system across a range of linear IFMR forms (m and c parameters).

Figure 4.3 shows the derivation of the form of the IFMR for each DD system individually, by selecting a linear IFMR form (m and c parameters) resulting in a common system age. These plots also include derivations taking into account the errors in the masses and cooling ages of the components, although they have not been formally treated at present (they are interdependent). A statistical derivation of the form of the IFMR is shown by averaging these parameters (with error bars showing min/max mass assumption extremes). This graph also shows the Dobbie et al. (2006) linear IFMR form for comparison (with cited errors).

Figure 4.4 shows another derivation of the form of the IFMR by selecting a linear IFMR form (m and c parameters) resulting in a common system age, excluding systems with an uncommon distance between components (DD-04 and DD-09).

Table 4.1 displays my preliminary IFMR linear parameter derivations, [1] for all systems, and [2] excluding systems with an uncommon distance between components (DD-04 and DD-09).

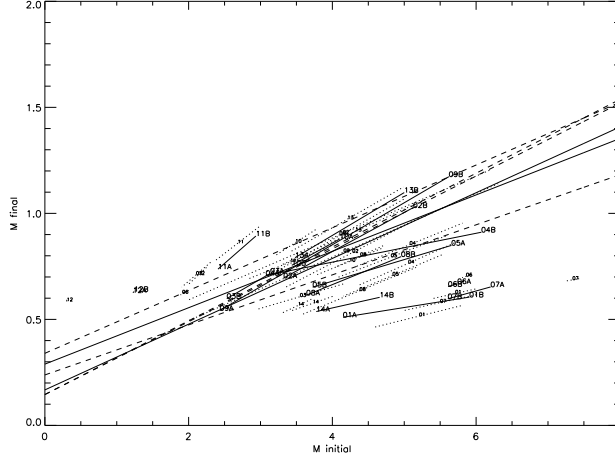


FIGURE 4.3: A plot of the derivation of the form of the IFMR for each DD system individually, by selecting a linear IFMR form ( $m$  and  $c$  parameters) resulting in a common system age. A statistical derivation of the form of the IFMR is shown by averaging these parameters (with error bars showing min/max mass/cooling age assumption extremes). This graph also shows the Dobbie et al. (2006) linear IFMR form for comparison (with cited errors).

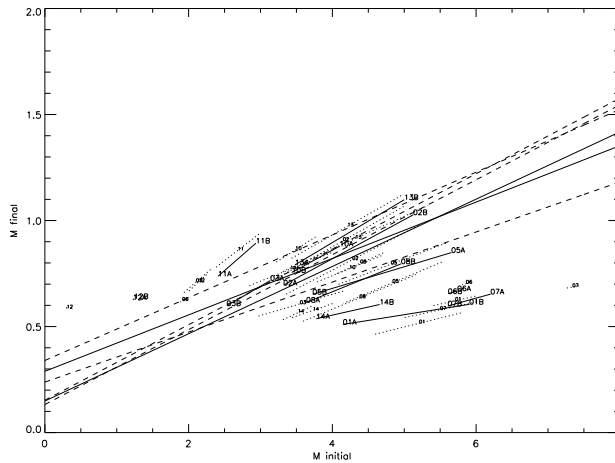


FIGURE 4.4: A second plot of the derivation of the form of the IFMR as in Figure 4.3 - excluding systems with an uncommon distance between components (DD-04 and DD-09).



### 4.3 Conclusion

In conclusion, I have performed a preliminary study of twelve candidate double-degenerate binaries. Blue Object Close Pairs (BOCPs) were identified from the Sloan Digital Sky Survey (SDSS) imaging data by applying selection criteria in software. Monte Carlo like simulations were performed to estimate the probability of BOCPs being mere chance alignments as a function of angular separation. Targets were prioritised for spectroscopic follow-up based upon weather, RA, magnitude and angular separation constraints, and astrometric analysis was performed on all these targets to determine if the components had (or did not have) consistent proper motions.

Spectroscopic data were obtained from a variety of telescopes, including the WHT, Gemini North, Gemini South, and the VLT ANTU, and reduced using IRAF scripts. I used existing WD model atmospheres, and grids of evolutionary models to analyse these data. The WD parameters of mass,  $M_f$ , and cooling time,  $t_{\text{cool}}$ , were used to probe the form of the stellar initial-final mass relation (IFMR). I have used existing estimates of the IFMR to confirm that binary components within the majority of my DD systems indicate a common system age. For those systems where these age estimates are inconsistent, allowing for uncertainties, I have suggested reasons for the disparity. I have concluded on the basis of distance estimates that the components in two out of the twelve systems are unlikely to be physically associated. For those systems which appear to be associated I have examined them in the context of recent estimates of the IFMR, finding that these provide a fair description of the transformation of intermediate mass stars into WDs ( $M_{\text{init}} > 2.5M_{\odot}$ ), but that there is likely more scatter in the relation than assumed from the results of recent open cluster based studies, at least at lower initial/final masses (ie.  $M_{\text{init}} < 2.5M_{\odot}$ ).

I have also generated a preliminary DD mass distribution containing all systems within my target selection with follow-up spectroscopic data (DD-01 through to DD-12, with PG0922+162 and HS2240+125 also), excluding systems unlikely to be physically associated based on my present data (DD-04 and DD-09). This distribution reveals a slight bias towards higher mass, even without a volume correction being applied to my sample. Although further analysis is required, a number of ideas have been presented to provide a possible explanation for this variation. I have also concluded that DD systems could be useful for studying ultramassive WDs, and may therefore help in establishing more firmly the lower limits on Type II supernovae progenitors.



FIGURE 4.5: La Palma - Cloud Valley



FIGURE 4.6: La Palma - Volcano



FIGURE 4.7: La Palma - INT



FIGURE 4.8: La Palma - From Top





FIGURE 4.9: La Palma - Sunset



FIGURE 4.10: La Palma - Forest Mountain



FIGURE 4.11: Cerro Paranal in Chile - Accomodation Paronama



FIGURE 4.12: Cerro Paranal in Chile - From Top





FIGURE 4.13: VLT Unit Telescope view 1

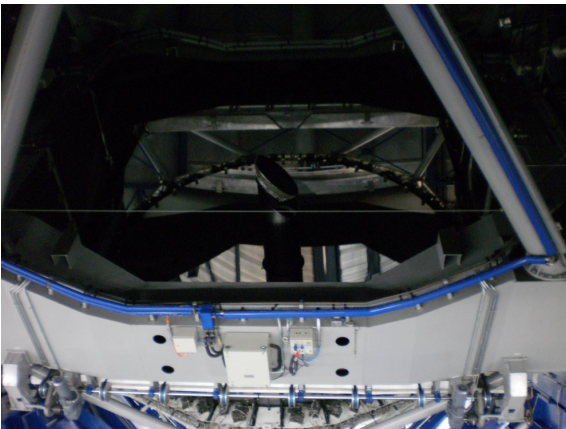


FIGURE 4.14: VLT Unit Telescope view 2

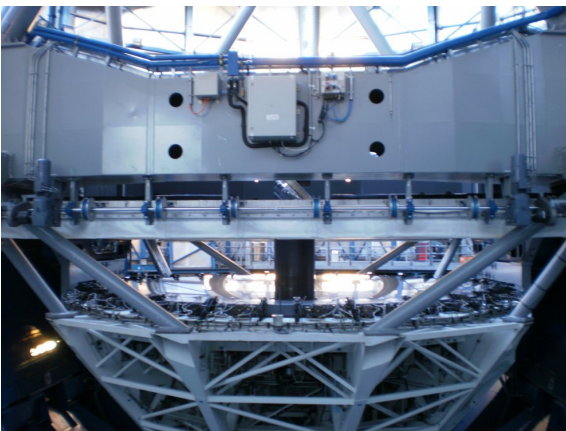


FIGURE 4.15: VLT Unit Telescope view 3



FIGURE 4.16: VLT Unit Telescope view 4

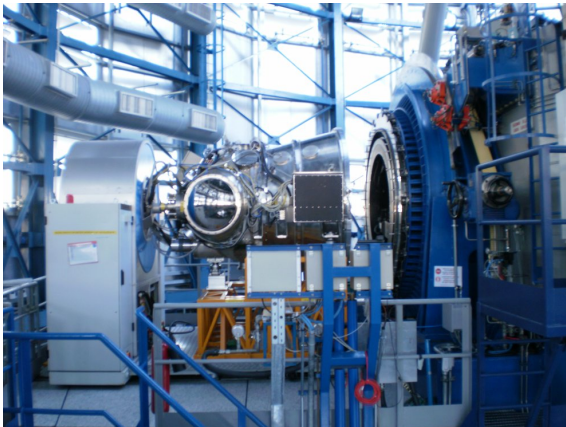


FIGURE 4.17: VLT Unit Telescope view 5

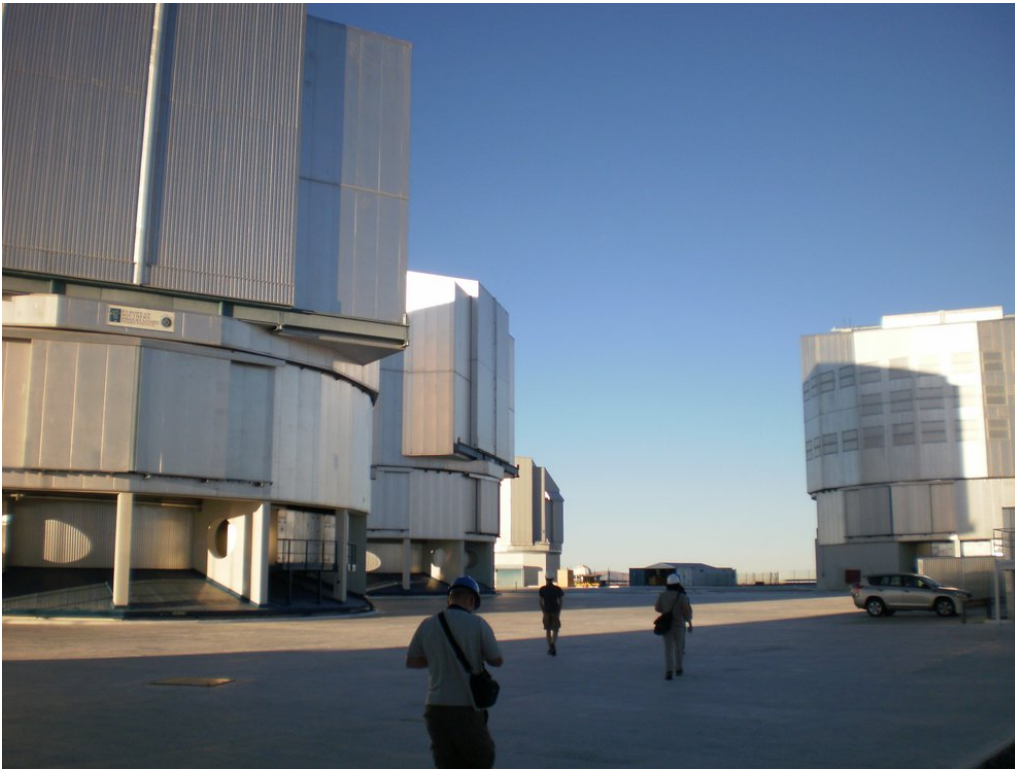


FIGURE 4.18: VLT Platform 1



FIGURE 4.19: VLT Platform 2





FIGURE 4.20: VLT Platform 3



FIGURE 4.21: Cerro Paranal in Chile - Sunset

*“people, for instance, who eat sweetmeats in the theatre do so most when the performance is indifferent..”*

from Aristotle’s Nicomachean Ethics



# Appendix

## A.1 Overview

This appendix references over 12000 lines of code written specifically for this project. As such, only the headers of source files have been included in the Appendix. Additional routines have been written but have since been discarded and are not required for the replication of this project. This Appendix also references the names of routines not written specifically for this project, but used in this project. An example IDL routine has been attached at the end of the Appendix in Section A.9 for reference.

### A.1.1 Standard Libraries

The IDL (/GDL) code written for this project requires the following standard libraries (or modifications thereof).

```
; repchr.pro [NASA]
; gettok.pro [NASA]
; readcol64bitvars.pro [RBB – modified NASA pro for 64bit unsigned longs {ID}]
; remchar.pro [NASA]
; skip_lun.pro [required for GDL]
; strsplit.pro [GDL library]
; strnumber64bitvars.pro [RBB – modified NASA pro for 64bit unsigned longs {ID}]
```

## A.2 Target Selection Code and Data

### A.2.1 SDSS SQL Scripts for blue object list generation

The following SQL script may be used in conjunction with the SDSS Skyserver (<http://cas.sdss.org/>) to extract a list of blue objects (SDSSblueObjectsDR7detailed.txt) under the a set of magnitude/colour criteria;

## resultsDR7detailed.sql

<http://cas.sdss.org/astrodr7/en/tools/search/sql.asp>

```
SELECT P.ObjID as SDSSID, P.ra as RIGHT_ASCENSION, P.dec as DECLINATION, P.b as GALATIC_LATITUDE, P.
l as GALATIC_LONGITUDE, P.psfmag_u as u, P.psfmag_g as g, P.psfmag_r as r, P.clean as pok
FROM Star P
WHERE
  P.clean > 0
  and (P.psfmag_u-P.psfmag_g)<=0.5
  and (P.psfmag_u-P.psfmag_g)>=-0.7
  and (P.psfmag_g-P.psfmag_r)<=0.0
  and (P.psfmag_g-P.psfmag_r)>=-0.7
  and P.psfmag_g<=20
  and P.psfmag_r<=20
  and P.psfmag_i<=20.5
  and P.psfmag_g>=15.3
```

## A.2.2 Count Close Pairs within a BO List Code

This program generates a list of blue object pairs within a given angular separation from SDSS blue object data

BOCPmonteCarloStats-01June11a.zip

## CCPtest.pro

This code calculates the probability of a close pair existing within a set of BOs at a given angular separations.

```
; Title: Count Close Pairs
; File: CCPtest.pro
; Version: 9 March 09 6:00pm
;
; Preconditions;
;
; Assumes a file SDSSblueObjects.csv, containing 4 columns of data and 56587 rows (56587 stars
; within a total 11663 square degree field)
;
; Column 1 = RIGHT_ASCENSION, Column 2 = DECLINATION, Column 3 = GALATIC_LATITUDE, Column 4 =
; GALATIC_LONGITUDE
;
; Postconditions;
;
; Estimates the number of close pairs within a maximum radius of
; maxDistanceForConsideredPairInArcDegrees (Eg 30 Arc Seconds)
;
```

## CCPtestsweep.pro

This code calculates the probability of a close pair existing within a set of BOs across a range of angular separations.

```
; Title: Count Close Pairs (across multiple separations)
; File: CCPtestsweep.pro
; Version: 10 March 09 12pm
; Summary:
;
; Preconditions;
;
; Assumes a file SDSSblueObjects.csv, containing 4 columns of data and 56587 rows (56587 stars
; within a total 11663 square degree field)
;
; Column 1 = RIGHT_ASCENSION, Column 2 = DECLINATION, Column 3 = GALATIC_LATITUDE, Column 4 =
; GALATIC_LONGITUDE
;
; Postconditions;
;
; Estimates the number of close pairs within a maximum radius of
; maxDistanceForConsideredPairInArcDegrees (Eg 30 Arc Seconds)
;
```

### A.2.3 Count Close Pairs within a Random Distribution Code

Forms a random distribution of stars (monte-carlo simulation), and calculates the number of close pairs found at a given separation (note it is a parabolic distribution;  $x^2$ ).

#### CCP.pro

This code calculates the probability of a close pair existing within a random distribution at a given angular separations.

```
; Title: Count Close Pairs
; File: CCP.pro
; Version: 9 March 09 10pm
;
;   Preconditions;
;
;   Assumes a random distribution of stars within a field of fieldSquareDegrees (Eg 1000 sqr deg)
;   with fieldNumberOfStars (Eg 4852).
;
;   Postconditions;
;
;   Estimates the number of close pairs within a maximum radius of
;   maxDistanceForConsideredPairInArcDegrees (Eg 30 Arc Seconds)
```

#### CCPsweep.pro

This code calculates the probability of a close pair existing within a random distribution across a range of angular separations.

```
; Title: Count Close Pairs (across multiple separations)
; File: CCPsweep.pro
; Version: 10 March 09 12pm
;
;   Preconditions;
;
;   Assumes a random distribution of stars within a field of fieldSquareDegrees (Eg 1000 sqr deg)
;   with fieldNumberOfStars (Eg 4852).
;
;   Postconditions;
;
;   Estimates the number of close pairs within a maximum radius of
;   maxDistanceForConsideredPairInArcDegrees (Eg 30 Arc Seconds)
```

### A.2.4 Plot Clustering Code

Plots a list of Blue Objects in a galactic coordinate system

#### PBO19Mar09.pro

WD candidate clustering IDL Plot (DR7) - galactic coord - normalised.zip

```
; Title: Plot SDSS Blue Objects
; File: PBO.pro
; Version: 19 March 09 1pm
;
;   Preconditions;
;
;   Assumes a file SDSSblueObjects.csv, containing 4 columns of data and 56587 rows (56587 stars
;   within a total 11663 square degree field)
;   Column 1 = RIGHT_ASCENSION, Column 2 = DECLINATION, Column 3 = GALATIC.LATITUDE, Column 4 =
;   GALATIC.LONGITUDE
;
;   Postconditions;
;
;   Plots the Blue Objects
```

### A.2.5 Create Blue Object Close Pair List (BOCPL)

This program generates a list of blue object pairs within a given angular separation.

#### BOCPL1createBlueObjectClosePairList.pro

```
; Title: Blue Object Close Pair List - create Blue Object Close Pair List.pro
; File: BOCPLcreateBlueObjectClosePairList.pro [old file name; CCPTtestDetailed.pro]
; Version: 8 April 09 3pm
;
; Postconditions;
;
; This program generates a list of blue object pairs within a given angular separation. In the
; output list each close pair is listed twice, A with B and B with A. The list has been ordered
; in terms of pair distance, DISTANCE.BETWEEN_PAIR. The output files are of the following format;
;
; BOCPLPart1.txt [RIGHT_ASCENSION A, DECLINATION A, GALATIC_LATITUDE A, GALATIC_LONGITUDE A, U A,
; G A, R A, POK A, DISTANCE.BETWEEN_PAIR, RIGHT_ASCENSION B, DECLINATION B, GALATIC_LATITUDE B,
; GALATIC_LONGITUDE B, U B, G B, R B, POK B]
; BOCPLPart2.txt [ID A, ID B]
;
; Preconditions;
;
; The input files are of the following format;
;
; BOCPLSDSSblueObjectsDR7detailed.txt [ID, RIGHT_ASCENSION, DECLINATION, GALATIC_LATITUDE,
; GALATIC_LONGITUDE, ID, U, G, R, POK] for 56587 blue objects, tab delimited
```

### A.2.6 Create BOCPL Subset using Is Quasar Data

This program generates a list of blue object pairs from a BOCPL which do not match with objects from a quasar database within a given angular separation.

See Section ??

### A.2.7 create BOCPL Subset using Visual Check Bad List

This program generates a list of blue object pairs from a BOCPL which do not match with objects from a visual check bad database within a given angular separation.

See Section ??

### A.2.8 create BO Subset Using Generic Ra and Dec Data

This program generates a subset of a BO list based upon a list of arbitrary Ra and Dec values.

BOCPL2createBOsubsetusingRaDecList-01June11a.zip

#### BOCPL2createBOsubsetusingRaDecList.pro

```
; Title: Blue Object Close Pair List - create BO Subset using Ra Dec List
; File: BOCPL2createBOsubsetusingRaDecList.pro
; Version: 21 Mar 11 5:30pm (updated 12 April 11 5:30pm)
;
; Postconditions;
;
; This program generates a list of blue object pairs from database 1 which DO NOT match with
; objects from database 2 within a given angular separation. The output files are of the
; following format;
;
; BOCPLSDSSconfirmedMatches.txt [RIGHT_ASCENSION A, DECLINATION A, GALATIC_LATITUDE A,
; GALATIC_LONGITUDE A, U A, G A, R A, POK A, DISTANCE.BETWEEN_PAIR, RIGHT_ASCENSION B,
; DECLINATION B, GALATIC_LATITUDE B, GALATIC_LONGITUDE B, U B, G B, R B, POK B]
; BOCPLSDSSconfirmedMatches.txt [ID A, ID B]
; BOCPLSDSSconfirmedNonMatches.txt [RIGHT_ASCENSION A, DECLINATION A, GALATIC_LATITUDE A,
; GALATIC_LONGITUDE A, U A, G A, R A, POK A, DISTANCE.BETWEEN_PAIR, RIGHT_ASCENSION B,
; DECLINATION B, GALATIC_LATITUDE B, GALATIC_LONGITUDE B, U B, G B, R B, POK B]
; BOCPLSDSSconfirmedNonMatches.txt [ID A, ID B]
```

```

;
; Preconditions
;
; The input files are of the following format;
;
; default: BOCPLSDSSblueObjectsDR7detailed.txt [ID A, RIGHT_ASCENSION A, DECLINATION A,
; GALATIC_LATITUDE A, GALATIC_LONGITUDE A, U A, G A, R A, POK A] for X blue objects, tab
; delimited
; alternate: BOCPLSDSSBOconfirmedNotQuasarsData.txt [RIGHT_ASCENSION A, DECLINATION A,
; GALATIC_LATITUDE A, GALATIC_LONGITUDE A, U A, G A, R A, POK A, DISTANCE_BETWEEN_PAIR,
; RIGHT_ASCENSION B, DECLINATION B, GALATIC_LATITUDE B, GALATIC_LONGITUDE B, U B, G B, R B, POK B
; ] for X blue objects Pairs, tab delimited
; BOCPLSDSSBOconfirmedNotQuasarsIDs.txt [ID A, ID B] for X blue objects Pairs, tab
; delimited
; SDSSsubset.txt, Eg BOCPLVisualCheckBad.txt, BOCPLHarrisSDSSDR4WDDataSmall.txt,
; SDSSDR7QuasarCatalogDataSmall.txt [RIGHT_ASCENSION, DECLINATION] for z blue objects, space
; delimited

```

### A.2.9 create BOCPL Subset Using Generic Ra and Dec Data

This program generates a subset of a BOCPL list based upon a list of arbitrary Ra and Dec values.

BOCPL2createBOsubsetusingRaDecList-01June11a.zip

#### BOCPL2createBOCPsubsetusingRaDecList.pro

```

; Title: Blue Object Close Pair List - create BOCPL Subset using Ra Dec List
; File: BOCPL2createBOCPsubsetusingRaDecList.pro
; Version: 10 Apr 11 11:50pm (updated 11 April 11 11:50pm)
; Summary:
;
; Postconditions;
;
; This program generates a list of blue object pairs from database 1 which DO NOT match with
; objects from database 2 within a given angular separation. The output files are of the
; following format;
;
; BOCPLSDSSconfirmedMatches.txt [RIGHT_ASCENSION A, DECLINATION A, GALATIC_LATITUDE A,
; GALATIC_LONGITUDE A, U A, G A, R A, POK A, DISTANCE_BETWEEN_PAIR, RIGHT_ASCENSION B,
; DECLINATION B, GALATIC_LATITUDE B, GALATIC_LONGITUDE B, U B, G B, R B, POK B]
; BOCPLSDSSconfirmedMatches.txt [ID A, ID B]
; BOCPLSDSSconfirmedNonMatches.txt [RIGHT_ASCENSION A, DECLINATION A, GALATIC_LATITUDE A,
; GALATIC_LONGITUDE A, U A, G A, R A, POK A, DISTANCE_BETWEEN_PAIR, RIGHT_ASCENSION B,
; DECLINATION B, GALATIC_LATITUDE B, GALATIC_LONGITUDE B, U B, G B, R B, POK B]
; BOCPLSDSSconfirmedNonMatches.txt [ID A, ID B]
;
; Preconditions
;
; The input files are of the following format;
;
; BOCPLPart1.txt/BOCPLSDSSBOCPconfirmedNotBadData.txt [RIGHT_ASCENSION A, DECLINATION A,
; GALATIC_LATITUDE A, GALATIC_LONGITUDE A, U A, G A, R A, POK A, DISTANCE_BETWEEN_PAIR,
; RIGHT_ASCENSION B, DECLINATION B, GALATIC_LATITUDE B, GALATIC_LONGITUDE B, U B, G B, R B, POK B
; ] for X blue objects Pairs, tab delimited
; BOCPLPart2.txt/BOCPLSDSSBOCPconfirmedNotBadIDs.txt [ID A, ID B] for X blue objects Pairs, tab
; delimited
; SDSSsubset.txt, Eg BOCPLVisualCheckBad.txt, BOCPLHarrisSDSSDR4WDDataSmall.txt,
; SDSSDR7QuasarCatalogDataSmall.txt [RIGHT_ASCENSION, DECLINATION] for z blue objects, space
; delimited

```

### A.2.10 create BOCPL Subset Using Bergeron Theoretical Data

This program generates a list of blue object pairs from a BOCPL which have a high mass ratio based upon bergeron theoretical DA WD data. This code was not used, as I did not wish to bias my target selection towards particular estimated masses (such that I could form a mass distribution).

A subset was create using Bergeron Theoretical Data to select those candidates estimated to have a significant difference in mass between their binary components. Their mass difference was estimated by either requiring a) significant magnitude difference but same temperature, or b) significant theoretical magnitude difference at a given arbitrary temperature derived from a theoretical cooling tract of arbitrary mass based on their current photometric derived temperatures (assuming this arbitrary mass

in both cases). Ideally, this meant ideally selecting BOCs with similar colours ( $u - g$  and  $g - r$ ) / temperatures, therefore any apparent luminosity difference being a product of a significant difference in mass. An alternative, theory dependent, method was applied as follows;

1. For both objects, in Bergeron theoretical database (DA WD  $M_{\odot} = 0.6$  table, Table\_Mass\_0.6, <http://www.astro.umontreal.ca/~bergeron/CoolingModels/>), located the hypothetical WDs with the closest matching  $u - r$  value (NB  $u - g$  and  $g - r$  can also be used).
2. For both objects, obtained the corresponding theoretical absolute  $r$  magnitude
3. calculated the theoretical  $r$  absolute magnitude difference between the binary WDs
4. calculated the measured  $r$  apparent magnitude difference between the binary WDs
5. the difference between 3. and 4. corresponds to differences in WD mass/radii, so if this difference is greater than some threshold (eg 0.5) I assumed this represented a binary system with a significant mass

The following code was created to execute this method.

### BOCPL4createSubsetUsingBergeronTheoreticalData.pro

```
; Title: Blue Object Close Pair List - create Subset Using Bergeron Theoretical Data
; File: BOCPL4createSubsetUsingBergeronTheoreticalData.pro
; Version: 6 October 09 2pm
;
; Postconditions;
;
; This program plots u-g vs g-r for each blue object pair, and provides the apparent magnitudes (r
; ) for both objects
;
; For every binary pair, calculate u-g and g-r
; 0. require binary WD pair to have similar colours (u-g and g-r)
; 1. In Bergeron theoretical database (DA WD solar mass 0.6 table), locate the hyp WD with
; closest matching u-g [or g-r] value ]
; 2. obtain the corresponding theoretical absolute r magnitude (and theoretical
; temperature, although not currently used)
; 3. calculate the theoretical r absolute magnitude difference between the binary WDs
; 4. calculate the measured r apparent magnitude difference between the binary WDs
; 5. the difference between 3. and 4. must correspond to differences in WD mass/radii, so
; if this difference is > some threshold, we can assume a binary system (assuming it actually is
; a real binary system - requiring proper motions for confirmation) with a low and a high mass WD
;
; The output files are of the following format;
; BOCPLBergeronTheoreticalComparisonPart1.txt [RIGHT_ASCENSION A, DECLINATION A,
; GALATIC.LATITUDE A, GALATIC.LONGITUDE A, U A, G A, R A, POK A, DISTANCE.BETWEEN_PAIR,
; RIGHT_ASCENSION B, DECLINATION B, GALATIC.LATITUDE B, GALATIC.LONGITUDE B, U B, G B, R B, POK B
; ] for X blue objects Pairs, tab delimited
; BOCPLBergeronTheoreticalComparisonPart2.txt [ID A, ID B] for Y blue objects Pairs, tab
; delimited
;
; Preconditions;
;
; The input files are of the following format;
;
; BOCPLSDSSDR5QuasarCatalogConfirmedStarsVisualCheckPart1.txt [RIGHT_ASCENSION A, DECLINATION A,
; GALATIC.LATITUDE A, GALATIC.LONGITUDE A, U A, G A, R A, POK A, DISTANCE.BETWEEN_PAIR,
; RIGHT_ASCENSION B, DECLINATION B, GALATIC.LATITUDE B, GALATIC.LONGITUDE B, U B, G B, R B, POK B
; ] for X blue objects Pairs, tab delimited
; BOCPLSDSSDR5QuasarCatalogConfirmedStarsVisualCheckPart2.txt [ID A, ID B] for X blue objects
; Pairs, tab delimited
;
; Table_Mass_0.6 [from http://www.astro.umontreal.ca/~bergeron/CoolingModels/, Teff, log g,
; Mbol, BC, U, B, V, R, I, J, H, K, u, g, r {not Teff, log g, Mbol, BC, U, B, V, R, I, J, H, K, u
; , g, r, i, z, y, b-y, u-b, v-y, V-I, G-R, U-V, U-G, B-V, Age}]
```



### A.2.11 Calculate probability of chance alignment using distance limited volume method

This calculates the probability of chance alignment of each DD system using a distance limited volume method

probabilityOfChanceAlignmentUsingDistanceLimitedVolume-15Dec10a.ods

## A.3 Proper Motions Code and Data (Target Selection Part II)

### A.3.1 Proper Motion Calculation Procedure

The full proper motion calculation procedure is outlined here.

#### propermotions calculations.txt

```
//NB changes;
error columns have been added
the formal SDSS gain (from SDSS plates data on internet) is used during object detection(set to 1.0
in POSSI object detection)
the same mexhat 3.0_9x9 kernel is used for both POSSI and SDSS object detection.
a slightly greater detection radius is used for small database generation [4 arc min]
NB DD3/12 use a 600 pixel radius for 4arcmin extraction calculations
2.5sigma pmx-t cull
pmx-t.f bug correction

//do: Proper motion measurement instructions for DD systems (using SDSS r+b and POSSI/POSSII r+b
data);

repeat the following for each DD system and for each colour band (ie, for POSSII blue and SDSS g,
POSSII r and SDSS r, POSSI blue and SDSS g, and POSSI r and SDSS r);

0.
extract .tar/.gz image files to .fits

1.

? go to AAO (with a working version of gaia)
ssh -X rbaxter@aaolxa
source /star/etc/login
source /star/etc/cshrc
gaia

OR

add the following to /home/rich/star/gaia/gaia.sh;
if test "$EXTRACTOR_DIR" = ""; then
    EXTRACTOR_DIR="/$HOME/star/bin/extractor"
    export EXTRACTOR_DIR
fi
/usr/bin/gaia

2.
open up SDSS image file of scene containing DD system
Run Image Analysis - object Detection;
set catalogue name to something local, eg /home/aaossz/rbaxter/working/trialgaiaonsERVER/
propermotionconfirmation/DD01/SDSS/catalog/rbb_sdss_g_werrors_cat
Detector - set the detector gain to the formal SDSS values (from SDSS plates data on internet)
Catalogue - select X.WORLD, Y.WORLD, X.IMAGE, Y.IMAGE, ERRX2.IMAGE, ERRY2.IMAGE, ERRXY.IMAGE,
ERRX2.WORLD, ERRY2.WORLD, ERRXY.WORLD
Set Detection Filter to mexhat 3.0_9x9 {OLD: gauss 3.0_7x7} for SDSS images, set contrast
parameter to 0.005 [NO; or 0.00], set detection threshold and analysis thresholds to 1.5 [
NO; or 2.0]
set object size 5
Detect Objects
verify correct objects have been detected
in catalogue box;
set central position to the coordinates to either component of the DD system (see SDSS object
table)
set max radius to >4.0, eg 8.0 {OLD: ~3.0 [2.0 -> 3.0 depending upon number of objects around,
such that ~20 objects are selected]}
Save as ascii file list of 10 objects, eg /home/aaossz/rbaxter/working/trialgaiaonsERVER/
propermotionconfirmation/DD01/SDSS/catalog/rbb_sdss_g_werrors_cat_small
```

```

including their ra+dec coord (col 2+3), and their x+y coord (col 4+5)
verify files saved include ra+dec coord (col 2+3), and their x+y coord (col 4+5)

open up a POSSI/POSSI image file of scene containing DD system
Run Image Analysis - object Detection;
set catalogue name to something local, eg /home/aaossz/rbaxter/working/trialgaiaonserver/
propermotionconfirmation/DD01/SUPERCosmos-POSS-I/catalog/rbb_poss1_b_werrors_cat
Detector - set the detector gain to 1.0 for POSSI object detection
Catalogue - select X.WORLD, Y.WORLD, X.IMAGE, Y.IMAGE, ERRX2.IMAGE, ERRY2.IMAGE, ERRXY.IMAGE,
ERRX2.WORLD, ERRY2.WORLD, ERRXY.WORLD
Set Detection Filter to mexhat.3.0.9x9 {OLD: gauss.3.0.7x7} for POSSI images
set object size 5
Run Image Analysis - object Detection
verify parameters as above
Detect Objects
verify correct objects have been detected
in catalogue box;
verify central position is set to the coordinates to either component of the DD system (see SDSS
object table)
set max radius to 4.0 [or 5.0 if less than 20 eg DD10?] {OLD: ~4.0, ~3.0 [2.0 -> 3.0 depending
upon number of objects around, such that ~20 objects are selected]}
Save as ascii file list of 10 objects, eg /home/aaossz/rbaxter/working/trialgaiaonserver/
propermotionconfirmation/DD01/SUPERCosmos-POSS-I/catalog/rbb_poss1_b_werrors_cat_small
verify files saved include ra+dec coord (col 2+3), and their x+y coord (col 4+5)

B. topcat
cd '/home/rich/utls/extrautilscentos5.3x64/21 topcat'/
java -jar topcat-full.jar
i. For DD-03 and DD-12 only - whose world coordinates could not be established by GAIA/extractor;
0.
download revised SDSS FITS catalog from SDSS website for a given photometric frame; eg drObj
-002328-5-40-0113[-revised].fit
open in GAIA, and save as ascii, DD-03catalogDownloadFits-revised.ASC
open in nedit
preferences - tab stops - 20
trim off extra columns (shift ctrl - click and hold down) [NB there should only be 117
columns]
Save as DD-03catalogDownloadFits-revised2.ASC
1. perform a pair match [2d-cartesian, not sky, error=6.0/7.0 respectively] of
rbb_sdss_g_werrors_cat_small.ASC and DD-03/12catalogDownloadFits-revised2.ASC using their
fits image pixel xy coordinates columns [col2+col3, col23+col21 respectively]
this will determine the RA Dec coordinates of rbb_sdss_g_werrors_cat_small.ASC
save this matched table as rbb_sdss_g_werrors_cat_small-withCoordinates-6pixMatch.ASC
2. perform a pair match [2d-cartesian, not sky, error=1.0 respectively] of
rbb_poss1_b_werrors_cat_small.ASC and rbb_poss1_b_werrors_cat.ASC using their fits image
pixel xy coordinates columns [col4+5, col4+5 respectively]
this will determine the RA Dec coordinates of rbb_poss1_b_werrors_cat_small.ASC in formats
which match rbb_sdss_g_werrors_cat_small-withCoordinates-6pixMatch.ASC [ie, RA in hours
, Dec in degrees decimal]
save this matched table as rbb_poss1_b_werrors_cat_small-
withCoordinatesInSDSSdownloadedCatalogFormat.ASC
3. perform a pair match [sky, error=3.0arcsec] comparison of rbb_sdss_g_werrors_cat_small-
withCoordinates-6pixMatch.ASC and rbb_poss1_b_werrors_cat_small-
withCoordinatesInSDSSdownloadedCatalogFormat.ASC using their hours RA + decimal degrees Dec
columns [col104+col105, col2_1+col3_2 respectively] {but note must set all matches to "
degrees"; this is required for some reason, regardless of the fact the RA columns are in
hours not degrees...}
this will map the fits image xy pixels of the SDSS and POSSI data together
save this matched table as POSSIversusSDSS.dat
ii. Or for all other DD systems;
Load Table - select ascii - select rbb_sdss_g_werrors_cat_small.ASC
Load Table - select ascii - select rbb_poss1_b_werrors_cat_small.ASC
OR [for DD-06 and DD-11];
Load Table - select ascii - select rbb_sdss_i_werrors_cat_small.ASC {NB I actually used
small for these calculations, in anticipation of reverting from 2011C medium/8as to
2011B small/4as for all DD system proper motion calculations}
Load Table - select ascii - select rbb_int_i_werrors_cat_small.ASC {NB I actually used small
for these calculations, in anticipation of reverting from 2011C medium/8as to 2011B
small/4as for all DD system proper motion calculations}
Joins - Pair Match [match tables]
max error 3.0 arc seconds
type/algorithm = sky
1.
Col2 degrees
Col3 degrees
rbb_sdss_cat_small.ASC [OR int]
2.
Col2 degrees
Col3 degrees
rbb_poss1_b_cat_small.ASC [OR sdss]

select 'Best Match only'
Select join type '1 and 2'
Go
[should get >= ~30 matches]
Select 'Match(1,2)', File - save table -
create output ascii file called POSSIbversusSDSSg.dat (POSSIb/r/versusSDSSg/r.dat) [OR
SDSSiversusINTi.dat]
This matches/aligns the ra/dec coordinates of the matching objects, now use x,y (not ra,dec)
coordinates from the matched data.

```

C.

```
Trim out all data except x/y columns from POSSIbversusSDSSg.dat, and create POSSIbversusSDSSgA.dat
remove DD data (2 rows) and create POSSIbversusSDSSgB.dat
edit pmx-t.f, and change the names of the two input files (POSSIbversusSDSSgB.dat for global
transformation function fit [average RMS], and POSSIbversusSDSSgA.dat for individual residual
fitting)
```

```
gfortran -c pmx-t.f
gfortran pmx-t.o -L$HOME/star/lib -lsla -o nige
setenv LD_LIBRARY_PATH $HOME/star/lib
./nige
OR;
bash
export LD_LIBRARY_PATH=$HOME/star/lib
```

```
This prints out a list of x+y deviations between expected positions (without any real proper motions
, just noise) and observed positions - highlighting therefore the large and similar direction
of the DD component proper motions.
```

### A.3.2 Proper Motion Calculations in Pixels

This code has been used during target selection to confirm common proper motions between components. It requires ASCII files to be previously calculated using GAIA and Topcat, indicating CCD frame relative positions of double degenerate candidate WDs along with a selection of nearby stars.

pmx-t.f is written by PDD (and updated by RBB) - it is used to calculate proper motions in pixels of one or more stars (eg a DD system) based upon astrometric reference field star list, where for each star, pixel positions are given for two photometric frames (eg SDSS and POSS-I).

#### pmx-t.f

pmx-t.f

#### Results

SDSSDDproperMotionMeasurements-pmx-t-xy2xylog-28May11a.zip

Graphs indicating the relative displacement of WD double degenerate candidates and nearby stars over an epoch.

POSS-I[blue] : SDSS epoch;

- xy2xylogDD01.ods
- xy2xylogDD02.ods
- xy2xylogDD03.ods
- xy2xylogDD04.ods
- xy2xylogDD05.ods
- xy2xylogDD06.ods
- xy2xylogDD07.ods
- xy2xylogDD08.ods
- xy2xylogDD09.ods
- xy2xylogDD10.ods
- xy2xylogDD11.ods
- xy2xylogDD12.ods

SDSS : INT La Palma 12 February 2011 epoch;

- xy2xylogDD06.ods
- xy2xylogDD11.ods

### A.3.3 Proper Motion Calculations in RA/Dec (Calibration of pixel values)

DDproperMotionWCScalibration-01June11a-2011B.ods

### A.3.4 Calculation Probability of Chance Proper Motion Alignment - PDD Method

calcAveragePMofDDNearest150MDwarfObjects-19May11a.zip calcAveragePMofDDNearest150WDwarfObjects-19May11a.zip

#### calcAveragePMofNearest150MDwarfObjects.pro

```
; Title: calculate Average Proper Motion of Nearest 150 M Dwarf Objects
; File: calcAveragePMofNearest150MDwarfObjects.pro
; Version: 7 Jan 11 2pm
; Updated: 1 Feb 11b 8pm [Added errors; to be considered a chance pm alignment, the MD has to be
;         within the bounds of not only the rectangle formed by the proper motions (plus the pm errors) of
;         the two WD components
;
; Postconditions;
;
; This program calculates the Average Proper Motion of Nearest 150 M Dwarf Objects
;
; For each component/system; NearestMDs-DDX.csv [SDSSID,RIGHT_ASCENSION,DECLINATION,
; GALATIC_LATITUDE,GALATIC_LONGITUDE,u,g,r,i,z,pok,RIGHT_ASCENSION, DECLINATION, PMRA, PMDEC,
; PMRAErr, PMDECErr] [X = DD component/system index]
;
; Preconditions;
;
; The input files are of the following format;
;
; DDpropermotionsA/B.txt [RIGHT_ASCENSION,DECLINATION,PMRA,PMDEC,PMRAERR,PMDECERR] for X blue
; objects pair A/B components, tab delimited [this list was generated using GAIA/Topcat]
; NearestMDs-DDX.csv [SDSSID,RIGHT_ASCENSION,DECLINATION,GALATIC_LATITUDE,GALATIC_LONGITUDE,u,g,r,
; i,z,pok,PMRA,PMDEC,PMRAERR,PMDECERR,SIGRA,SIGDEC] for X DD components, comma delimited
```

#### findNearest150WDOBJECTS-usingEisensteinSDSSDR4WDDData.pro

```
; Title: Blue Object Close Pair List - create Subset using Eisenstein SDSS DR4 WD Data
; File: BOCPLcreateSubsetusingEisensteinSDSSDR4WDDData.pro
; Version: 8 April 09 3pm
;
; Postconditions;
;
; This program compares RA and Dec data from rows 49 and 50 [48 and 49] of
; EisensteinSDSSDR4WDDDataSmall.txt to find matching stars with RA and Dec data from rows 10 and
; 11 [9 and 10] of BOCPLPart1.txt data
;
; This program generates a list of blue object pairs from database 1 which match with objects from
; database 2 within a given angular separation. The output files are of the following format;
;
; For each component/system; BOCPEisensteinABNearestWDsX.txt [RIGHT_ASCENSION A, DECLINATION A,
; proper motion magnitude, proper motion angle] [X = component/system index]
;
; Preconditions;
;
; The input files are of the following format;
;
; DDtargetList.txt [RIGHT_ASCENSION A, DECLINATION A] for X blue objects Pairs, tab delimited
; BOCPEisensteinSDSSDR4WDDDataSmallWithProperMotions.txt [RIGHT_ASCENSION A, DECLINATION A, proper
; motion magnitude, proper motion angle]
; SDSSblueObjectsDR7detailedWithProperMotions.txt [ID, RIGHT_ASCENSION, DECLINATION,
; GALATIC_LATITUDE, GALATIC_LONGITUDE, ID, U, G, R, POK, PMRA, PMDEC, PMRAERR, PMDECERR, SIGRA,
; SIGDEC] for ~56587 blue objects, tab delimited
```

#### calcAveragePMofNearest150WDwarfObjects.pro

```
; Title: calculate Average Proper Motion of Nearest 150 W Dwarf Objects
; File: calcAveragePMofNearest150WDwarfObjects.pro
; Version: 19 May 11 9am [based on calcAveragePMofNearest150MDwarfObjects.pro]
;
; Postconditions;
;
; This program calculates the Average Proper Motion of Nearest 150 M Dwarf Objects
;
; For each component/system; NearestMDs-DDX.csv [SDSSID,RIGHT_ASCENSION,DECLINATION,
; GALATIC.LATITUDE,GALATIC.LONGITUDE,u,g,r,i,z,pok,RIGHT_ASCENSION, DECLINATION, PMRA, PMDEC,
; PMRAErr, PMDECErr] [X = DD component/system index]
;
; Preconditions;
;
; The input files are of the following format;
;
; DDpropermotionsA/B.txt [RIGHT_ASCENSION,DECLINATION,PMRA,PMDEC,PMRAERR,PMDECERR] for X blue
; objects pair A/B components, tab delimited [this list was generated using GAIA/Topcat]
; BOCPLEisensteinABNearestWDsPart1-DDX.csv [RIGHT_ASCENSION,DECLINATION,GALATIC.LATITUDE,
; GALATIC.LONGITUDE,u,g,r,pok,PMRA,PMDEC,PMRAERR,PMDECERR,SIGRA,SIGDEC] for X DD components,
; space delimited
```

### A.3.5 Calculation Probability of Chance Proper Motion Alignment - RBB Method

calculateRBBprobabilityOfChanceAlignment-13April11a.zip

calculateRBBprobabilityOfChanceAlignment.pro

```
; Title: calculate RBB probability Of Chance Alignment
; File: calculateRBBprobabilityOfChanceAlignment.pro
; Version: 14 April 11a 5am
; Summary:
;
; Postconditions;
;
; This program calculates probability Of Chance Alignment (of proper motions)
;
; Preconditions
;
; The input files are of the following format;
;
; plotASCIITableUsingGDL.pro [NASA]
; asciiTable.txt [X Axis, Y Axis 1, Y Axis 2] for X variables, tab delimited
```

## A.4 Observations Code and Data

### A.4.1 calculate the angle between WD components in double degenerate system (for aligning slit)

bearing-23Aug10a.ods

(bearing.pro, although used for many calculations in this project - is no longer used, as it's printed values cannot be relied upon to a high degree of accuracy due to an IDL/GDL print function limitation).

### A.4.2 Flux Calibrated WD Data

WHT Flux calibrated Data

.zip PDWHTJuly08ReducedData15Nov09c-usingNewfcBB.zip:

- SSWD01Aw.dat - szbc1dwfcSDSS0052a.dat
- SSWD01Bw.dat - szbc1dwfcSDSS0052b.dat
- SSWD02Aw.dat - szbc1dwfcSDSS1507a.dat

- SSWD02Bw.dat - szbc1dwcfcdSDSS1507b.dat
- SSWD03Aw.dat - szbc1dwcfcdSDSS1703a.dat
- SSWD03Bw.dat - szbc1dwcfcdSDSS1703b.dat
- SSWD04Aw.dat - szbc1dwcfcdSDSS2259a.dat
- SSWD04Bw.dat - szbc1dwcfcdSDSS2259b.dat

### **WHT Flux Re-calibrated Magnetic WD Candidate Data**

SDSSDDmagneticWDdata-30Aug10a.zip:

- fcSDSS1507a-SSWD02Aw.dat.FluxRecalibratedUsingModel
- fcSDSS1507b-SSWD02Bw.dat.FluxRecalibratedUsingModel
- fcSDSS2259a-SSWD04Aw.dat.FluxRecalibratedUsingModel

### **Gemini North Flux calibrated Data**

geminiN2009Bdatafluxcalibrated23Sept09c-usingNewfcBB.zip:

- SSWD05Ag.dat - fcde1stgsN20090720S0083.dat
- SSWD05Bg.dat - fcde2stgsN20090720S0083.dat
- SSWD06Ag.dat - fcde1stgsN20090720S0094.dat
- SSWD06Bg.dat - fcde2stgsN20090720S0094.dat

### **Gemini South Flux calibrated Data**

geminiS2010Adatafluxcalibrated-15June10a.zip:

- SSWD12Ag.dat - f2010A-DD-07A.dat
- SSWD12Bg.dat - f2010A-DD-07B.dat

### **VLT Flux calibrated Data**

IRAFreducedVLTDDataByPDD-richard.tar.gz:

- SSWD07Av.dat - WD2-T-WAV-FLX-A.dat
- SSWD07Bv.dat - WD2-T-WAV-FLX-B.dat
- SSWD08Av.dat - WD4-T-WAV-FLX-A.dat
- SSWD08Bv.dat - WD4-T-WAV-FLX-B.dat
- SSWD09Av.dat - WD10-T-A-WAV-FLX.dat
- SSWD09Bv.dat - WD10-T-B-WAV-FLX.dat
- SSWD10Av.dat - WD11-T-WAV-FLX-A.dat
- SSWD10Bv.dat - WD11-T-WAV-FLX-B.dat
- SSWD11Av.dat - WD12-T-WAV-FLX-A.dat
- SSWD11Bv.dat - WD12-T-WAV-FLX-B.dat

## WiFeS Flux Re-calibrated Magnetic WD Candidate Data - low S/N - NOT USED

N/A

### A.4.3 WHT Data Reduction

WHT Data was reduced using IRAF scripts.

#### IRAF Software Installation

IRAF Software (version 2.14.1);

- as.pcix.gen.gz
- ib.rhux.x86.gz
- nb.rhux.x86.gz
- tcsh-6.15-7.fc10.x86\_64.rpm
- iraf\_install.sh.centos5

Instructions for IRAF software installation on Centos 5 are found here;

//how to install iraf using the script iraf\_install.sh;

IRAF README

```

1. The script used to install IRAF creates a user account named iraf. It has no password set so it
   is advised to set one of your own.
After installation IRAF can be run from any user account, instructions are given below.

2. During installation the script will perform a trial installation, after that it will return a
   prompt. At this point you must type "exit" and it will proceed to the full installation.
When the install configuration asks for default locations for folders keep hitting enter to accept
   the default locations.

2.a.      Post install configuration
The default options are enclosed in () while the option i chose is given after

   Configure IRAF Networking on this machine? (yes): no
Unless you are installing this on a networked machine choose no

   Create a default tapecap file? (yes): no      / Do you wish to create a default dev$tapecap link?
   (yes): no

   Do you wish to delete these unused HSI binaries? (yes): yes
This deletes the binaries used in Mac OS, Cygwin (Windows compatability), and other Linux
   architectures

   Do you wish to strip the system of sources? (no): no
Unless you are planning on developing the code then select yes to free up disk space

2b. install X11 libraries using [optional - can use skycat/gaia instead]
   x11iraf-v2.0BETA-bin.redhat/install
2e. System - Administration - Users and Groups - change iraf password to something secure

3. To set up IRAF on your user account it is first recommended that you make a directory in your
   home folder named iraf (mkdir ~/iraf).
The following steps must be done in a command line terminal
Go into the folder (cd iraf) and type in the command "mkiraf". When it asks for preferred terminal
   type select xterm, this will have been installed along with IRAF.
Two objects should be created in your iraf folder, a directory named uparm and file named login.cl

4. To start IRAF open an xgterm window (this can done by typing "xgterm &" into a command line
   terminal) and type "cd iraf" followed by "cl"
This will start IRAF

```

#### Lacos Spec Software Installation

Laplacian Cosmic Ray Removal Software created by Pieter van Dokkum, April 2001  
(van Dokkum 2001);

lacos.spec.cl

## Reduction Archive Files

Reduced Files: PDWHTJuly08ReducedData15Nov09c-usingNewfcBB.zip

Raw and Reduced Files: backupIRAFWHT08workingDir15Nov09c.zip

WHT Reduced Files:

- 24july08WHTlog.txt
- 25july08WHTlog.txt
- biaslistblue.txt
- caliblamplistblue0.6.txt
- caliblamplistblue0.6zerocorrectedMappedToScience1d.0001.txt
- caliblamplistblue0.6zerocorrectedMappedToScience1d.txt
- caliblamplistblue0.6zerocorrectedMappedToScience.txt
- caliblamplistblue0.6zerocorrected.txt
- caliblamplistblue1.0.txt
- caliblamplistblue1.0zerocorrectedMappedToScience1d.0001.txt
- caliblamplistblue1.0zerocorrectedMappedToScience1d.0002.txt
- caliblamplistblue1.0zerocorrectedMappedToScience1d.txt
- caliblamplistblue1.0zerocorrectedMappedToScience.txt
- caliblamplistblue1.0zerocorrected.txt
- flatlistblue0.6.txt
- flatlistblue0.6zerocorrected.txt
- flatlistblue1.0.txt
- flatlistblue1.0zerocorrected.txt
- fluxCalDemo.ods
- fluxCalibrationUsingDCWD.perl
- listAllObjectsExceptForFluxCalDCCWDdat.txt
- listAllObjectsExceptForFluxCalDCCWDfits.txt
- listszbc1dwcComaWD.txt
- listszbc1dwcSDSS0052a.txt
- listszbc1dwcSDSS0052b.txt
- listszbc1dwcSDSS1507a.txt
- listszbc1dwcSDSS1507b.txt
- listszbc1dwcSDSS1703a-24July.txt
- listszbc1dwcSDSS1703a-25July.txt
- listszbc1dwcSDSS1703a.txt
- listszbc1dwcSDSS1703b-24July.txt
- listszbc1dwcSDSS1703b-25July.txt
- listszbc1dwcSDSS1703b.txt
- listszbc1dwcSDSS2259a-24July.txt
- listszbc1dwcSDSS2259a-25July.txt
- listszbc1dwcSDSS2259a.txt
- listszbc1dwcSDSS2259b-24July.txt
- listszbc1dwcSDSS2259b-25July.txt
- listszbc1dwcSDSS2259b.txt
- listszbc1dwcSP2157-24July.txt



- listszbc1dwcSP2157-25July.txt
- listszbc1dwcWD1918-24July.txt
- listszbc1dwcWD1918-25July.txt
- login.cl
- sciencelistblue0.6.txt
- sciencelistblue0.6zeroandbadpixcorrected1d.0001.txt
- sciencelistblue0.6zeroandbadpixcorrected1dS.0001.txt
- sciencelistblue0.6zeroandbadpixcorrected1dS.txt
- sciencelistblue0.6zeroandbadpixcorrected1dwavelengthCalibrated.0001.txt
- sciencelistblue0.6zeroandbadpixcorrected1dwavelengthCalibrated.txt
- sciencelistblue0.6zeroandbadpixcorrectedS.txt
- sciencelistblue0.6zeroandbadpixcorrected.txt
- sciencelistblue0.6zerocorrected.txt
- sciencelistblue1.0.txt
- sciencelistblue1.0zeroandbadpixcorrected1d.0001.txt
- sciencelistblue1.0zeroandbadpixcorrected1d.0002.txt
- sciencelistblue1.0zeroandbadpixcorrected1d.000x.txt
- sciencelistblue1.0zeroandbadpixcorrected1dDD.0001.txt
- sciencelistblue1.0zeroandbadpixcorrected1dDD.0002.txt
- sciencelistblue1.0zeroandbadpixcorrected1dDD.txt
- sciencelistblue1.0zeroandbadpixcorrected1dS.0001.txt
- sciencelistblue1.0zeroandbadpixcorrected1dS.txt
- sciencelistblue1.0zeroandbadpixcorrected1d.txt
- sciencelistblue1.0zeroandbadpixcorrected1dwavelengthCalibrated.0001.txt
- sciencelistblue1.0zeroandbadpixcorrected1dwavelengthCalibrated.0002.txt
- sciencelistblue1.0zeroandbadpixcorrectedDD.txt
- sciencelistblue1.0zeroandbadpixcorrectedS.txt
- sciencelistblue1.0zeroandbadpixcorrected.txt
- sciencelistblue1.0zerocorrected.txt
- spectraReductionMethod13Nov09b.txt
- szbc1dwcComaWD.dat
- szbc1dwcComaWD.fits
- szbc1dwfcComaWD.dat
- szbc1dwfcSDSS0052a.dat
- szbc1dwfcSDSS0052b.dat
- szbc1dwfcSDSS1507a.dat
- szbc1dwfcSDSS1507b.dat
- szbc1dwfcSDSS1703a-24July.dat
- szbc1dwfcSDSS1703a-25July.dat
- szbc1dwfcSDSS1703a.dat
- szbc1dwfcSDSS1703b-24July.dat
- szbc1dwfcSDSS1703b-25July.dat
- szbc1dwfcSDSS1703b.dat
- szbc1dwfcSDSS2259a-24July.dat
- szbc1dwfcSDSS2259a-25July.dat

- szbc1dwcfcSDSS2259a.dat
- szbc1dwcfcSDSS2259b-24July.dat
- szbc1dwcfcSDSS2259b-25July.dat
- szbc1dwcfcSDSS2259b.dat
- szbc1dwcfcSP2157-24July.dat
- szbc1dwcfcSP2157-25July.dat
- szbc1dwcSDSS0052a.dat
- szbc1dwcSDSS0052a.fits
- szbc1dwcSDSS0052b.dat
- szbc1dwcSDSS0052b.fits
- szbc1dwcSDSS1507a.dat
- szbc1dwcSDSS1507a.fits
- szbc1dwcSDSS1507b.dat
- szbc1dwcSDSS1507b.fits
- szbc1dwcSDSS1703a-24July.dat
- szbc1dwcSDSS1703a-24July.fits
- szbc1dwcSDSS1703a-25July.dat
- szbc1dwcSDSS1703a-25July.fits
- szbc1dwcSDSS1703a.dat
- szbc1dwcSDSS1703a.fits
- szbc1dwcSDSS1703b-24July.dat
- szbc1dwcSDSS1703b-24July.fits
- szbc1dwcSDSS1703b-25July.dat
- szbc1dwcSDSS1703b-25July.fits
- szbc1dwcSDSS1703b.dat
- szbc1dwcSDSS1703b.fits
- szbc1dwcSDSS2259a-24July.dat
- szbc1dwcSDSS2259a-24July.fits
- szbc1dwcSDSS2259a-25July.dat
- szbc1dwcSDSS2259a-25July..fits
- szbc1dwcSDSS2259a.dat
- szbc1dwcSDSS2259a.fits
- szbc1dwcSDSS2259b-24July.dat
- szbc1dwcSDSS2259b-24July.fits
- szbc1dwcSDSS2259b-25July.dat
- szbc1dwcSDSS2259b-25July..fits
- szbc1dwcSDSS2259b.dat
- szbc1dwcSDSS2259b.fits
- szbc1dwcSP2157-24July.dat
- szbc1dwcSP2157-24July.fits
- szbc1dwcSP2157-25July.dat
- szbc1dwcSP2157-25July.fits
- szbc1dwcWD1918-24July.fits
- szbc1dwcWD1918-25July.fits
- szbc1dwcWD1918-25JulyInterpolated.dat

- WHTfileListCreationRecord.txt
- whtreduce15Nov09b.cl
- whtreduce15Nov09c.cl
- whtreduce.cl
- zerolistblue.txt

### whtreduce.cl

```
# RBB wht reduction script 15 Nov 09c [cosmic rays removal using lacos_spec.cl];
# instructions;
#   cd /home/rich/iraf
#   delete all files in /home/rich/iraf/uparm
#   delete all temporary files in /home/rich/iraf/database/
#   delete all temporary files in /home/rich/iraf/
#   add to /home/rich/iraf/login.cl;
#       task whtreduce = /home/rich/iraf/whtreduce.cl
#       task lacos_spec = /home/rich/iraf/lacos_spec.cl
#   cl
#   whtreduce
#
# IRAF Reduction Process for Paul Dobbie WHT July 08 Data;
#   "IRAF V2.14.1 September 2008"
# preconditions;
#   Arc + Flat + Bias; ensure window sizes are the same for each file.
#   ensure to use the correct flat field slit date
#       (0.6 = high res, 0.1 = low res)
#   biassec/trimsec values - see fits header for exact parameters and modify accordingly
#
# notes:
#   1. regarding apall background subtraction - ensure background subtraction areas are correct (
#       currently use +interac here),
#   2. apall fit - ensure rejection is applied and the correct fit order is applied (currently use +
#       interac here),
#   3. have not separated flat (and bias) data from 24 July and 25 July (currently they are all
#       combined together)
#   4. flux calibration is currently done manually by executing a separate perl script
```

## A.4.4 Gemini South/North Data Reduction

Gemini Data was reduced using IRAF scripts (implementing Gemini GMOS IRAF software).

### Gemini Reduction Software Installation

GMOS Software (version 1.10);

gemini\_v110.tar.gz

GMOS Software additional IRAF packages required;

- color-bin.redhat.tar.gz
- color.tar.Z
- extern.pkg
- fitsutil-bin.redhat.tar.gz
- fitsutil.tar.gz
- gmisc-bin.redhat.tar.gz
- gmisc.tar.Z
- nmisc-bin.redhat.tgz
- nmisc.tar.Z
- stsdas3.10.bin.redhat.tar.gz
- stsdas3.10.tar.gz
- tables3.10.bin.redhat.tar.gz

- tables3.10.tar.gz

Instructions for Gemini software installation are found here;

```
for all packages x;
    extract extern source data for package x to /iraf/extern/x/
    extract extern bin data for package x to /iraf/extern/x/bin/
su iraf
cd $hlib      /    cd /iraf/iraf/unix/hlib
su root
chmod 777 extern.pkg
su rich
nedit extern.pkg; [and update the file's contents with the following]

# External (non core-system) packages.  To install a new package, add the
# two statements to define the package root directory and package task,
# then add the package helpdb to the 'helpdb' list.

reset    noao          = iraf$noao/
task     noao.pkg      = noao$noao.cl

reset    tables        = /iraf/extern/tables/
task     tables.pkg    = tables$tables.cl

reset    stsdas        = /iraf/extern/stsdas/
task     stsdas.pkg    = stsdas$stsdas.cl

reset    color         = /iraf/extern/color/
task     color.pkg     = color$color.cl

reset    fitsutil      = /iraf/extern/fitsutil/
task     fitsutil.pkg  = fitsutil$fitsutil.cl

reset    gemini        = /iraf/extern/gemini/
task     gemini.pkg    = gemini$gemini.cl

reset    gmisc         = /iraf/extern/gmisc/
task     gmisc.pkg     = gmisc$gmisc.cl

reset    nmisc         = /iraf/extern/nmisc/
task     nmisc.pkg     = nmisc$nmisc.cl

reset    helpdb        = " lib$helpdb.mip\
                        ,noao$lib/helpdb.mip\
                        ,tables$lib/helpdb.mip\
                        ,stsdas$lib/helpdb.mip\
                        ,color$lib/helpdb.mip\
                        ,fitsutil$lib/helpdb.mip\
                        ,gemini$lib/helpdb.mip\
                        ,gmisc$lib/helpdb.mip\
                        ,nmisc$lib/helpdb.mip\
                        "

keep

copy lacos_spec.cl to /home/rich/iraf/lacos_spec.cl
```

## Reduction Archive Files

Reduced Files: geminiN2009Bdatafluxcalibrated23Sept09c-usingNewfcBB.zip Reduced Files: geminiS2010Adatafluxcalibrated-15June10a.zip Raw and Reduced Files: backupIRAFGeminiN2009BworkingDir23Sept09a (with CuAr\_GMOS.dat.rbbmod5).zip Raw and Reduced Files: backupIRAFGeminiS2010AworkingDir15June10a.zip

Gemini North Reduced Files:

- cde1stgsN20090720S0067.dat
- cde1stgsN20090720S0067.fits
- cde1stgsN20090720S0067interpolated.dat
- cde1stgsN20090720S0083.dat
- cde1stgsN20090720S0083.fits
- cde1stgsN20090720S0094.dat
- cde1stgsN20090720S0094.fits

- cde2stgsN20090720S0067.dat
- cde2stgsN20090720S0067.fits
- cde2stgsN20090720S0083.dat
- cde2stgsN20090720S0083.fits
- cde2stgsN20090720S0094.dat
- cde2stgsN20090720S0094.fits
- CuAr\_GMOS.dat.orig
- CuAr\_GMOS.dat.rbbmod5
- fcde1stgsN20090720S0083.dat
- fcde1stgsN20090720S0094.dat
- fcde2stgsN20090720S0083.dat
- fcde2stgsN20090720S0094.dat
- flux\_cal\_example1.ods
- flux\_cal\_example2.ods
- fluxCalibrationUsingDCWD.perl
- geminireduce15Sept09a.cl
- gsextractmulti.cl

Gemini South Reduced Files:

- 2010A-DD-07A.dat
- 2010A-DD-07A.fits
- 2010A-DD-07B.dat
- 2010A-DD-07B.fits
- 2010A-WD0000-345A.dat
- 2010A-WD0000-345A.fits
- 2010A-WD0000-345Ainterpolated.dat
- 2010A-WD0000-345Atemp1interp.dat
- 2010A-WD0000-345Atemp2interp.dat
- 2010A-WD0000-345Atempinterp.dat
- 2010A-WD0000-345B.dat
- 2010A-WD0000-345B.fits
- CuAr\_GMOS.dat.orig
- CuAr\_GMOS.dat.rbbmod5
- f2010A-DD-07A.dat
- f2010A-DD-07A.ods
- f2010A-DD-07B.dat
- f2010A-DD-07B.ods
- fluxCalibrationUsingDCWD.perl
- geminireduce.cl
- geminireduce.cl.backup15June10a
- gsextractmulti.cl

Gemini North Raw File List:

Raw files available on a data disk.

Gemini South Raw File List:

Raw files available on a data disk.

## geminireduce.cl

```
# RBB gemini reduction script 27 May 10a[supports gemini 1.10] [cosmic rays removal using lacos_spec
.cl];
# instructions;
# install iraf with gemini 1.10 and all required packages [http://www.gemini.edu/sciops/data-and-
results/processing-software]
# cd /home/rich/iraf
# delete all files in /home/rich/iraf/uparm
# delete all temporary files in /home/rich/iraf/database/
# delete all temporary files in /home/rich/iraf/
# add to /home/rich/iraf/login.cl;
#
# gemini
# gmos
# noao
# onedspec
# task geminireduce=/home/rich/iraf/geminireduce.cl
# task lacos_spec=/home/rich/iraf/lacos_spec.cl
# task gsextractmulti=/home/rich/iraf/gsextractmulti.cl
# cp /iraf/extern/gemini/gmos/data/CuAr_GMOS.dat /iraf/extern/gemini/gmos/data/CuAr_GMOS.dat .
# backup
# cp CuAr_GMOS.dat.rbbmod5 /iraf/extern/gemini/gmos/data/CuAr_GMOS.dat
# cl
# geminireduce
# use cosmic ray removal method 5 (lacos spec after bias subtraction, flat field)
# not 1 (gemini gsrej),
# not 2 (lacos spec after bias subtraction, flat field and combined),
# not 3 (lacos spec before bias subtraction)
# not 4 (lacos spec after bias subtraction)
#
# cp
```

## gsextractmulti.cl

gsextractmulti.cl is a modified version of gsextract.cl enabling the extraction of multiple spectral lines from a single long slit image.

## A.4.5 VLT Data Reduction

VLT Data reduced using IRAF by PDD. RBB VLT data reductions not used due to Gasgano pipeline lacos\_spec cosmic ray removal integration difficulties.

### Reduction Archive Files

richard.tar.gz

## A.4.6 Flux Calibration

Flux Calibration using DC WD (PDD Code).

### fluxCalibrationUsingDCWD.perl

## A.4.7 Signal to Noise Calculations

This program calculates the signal to noise of a set of reduced 1D WD spectra.

### calculateSignalToNoise.perl

```
; Title: Calculate Signal to Noise
; File: calculateSignalToNoise.pro
; Version: 12 November 10 6pm (updated 15 Mar 11)
; Summary:
;
;
; Postconditions;
;
; This program calculates the signal to noise of a set of ASCII Tables Using GDL
```

```

;
;   Preconditions;
;
;   The input files are of the following format;
;
;   calculateSignalToNoise.pro [NASA]
;   SSWDOXA/B.txt [Wavelength, Flux] for 12 WDs (A/B), tab delimited
;   instrumentResolution.txt for X WDs

```

## A.5 Stellar Modelling Scripts

### A.5.1 Balmer Line Extraction

The Balmer Line Extraction software is used to verify the wavelength calibration of reduced (spectroscopic) WD data. It also serves for some basic normalisation purposes (NOT USED).

**'RBBBalmerLineExtraction11Sept09a.pro'**

RBBBalmerLineExtraction 13 Sept 09a.zip

```

; Title: RBB Balmer Line Extraction
; File: RBBBalmerLineExtraction.pro
; Version: 31 July 09 3:00pm
;
;   Postconditions;
;
;   This program calculates the X positions of the balmer lines for a WD flux calibrated .dat file -
;   such that normalisation can be applied and models can be fitted [2 step process]
;
;   Preconditions;
;
;   The input files are of the following format;
;
;   szbc1dwcfcdSS0052a.dat [wavelengthArray, amplitudeArray], space delimited
;
;

```

### A.5.2 White Dwarf Parameter Extraction

This software is otherwise known as the "Bergeron" code.

This code has been used to interpolate and derive a best fit WD model from Bergeron DA/DB WD colour-magnitude / evolutionary grids, and a given set of WD match criteria (parameters).

The PDD Bergeron grid interpolation code (pda\_wd\_mag\_sigma.f) has been generalised and extended to support the following operational modes;

#### Mode Norm

input filename; loggtempmag.dat (PDD cooler component mass calculations) replaces pda\_wd\_mag\_sigma.f/pda\_wd\_Vmag.f + fontaine g2m\_fbbCO.f [minus gravitational redshift and radius parameters] inputs; logg + temperature

#### Mode Cool

input filename; teffdistmag.dat (RBB cooler component calculations) replaces pda\_wd\_dd\_cool\_n\_hot.f / rbb\_wd\_dd\_cool\_n\_hot.f) inputs; temperature + distance

## Mode Cool 2

input filename; masstempmag.dat (PDD cooler component mass calculations) inputs;  
mass + temperature

## Mode DC

input filename; distmag.dat (PDD cooler component mass calculations) replaces rbb\_dd\_DC.f  
inputs; distance + observed mag

## 'rbb\_wd\_dd\_param.f'

rbb\_wd\_dd\_param-08Nov10d.zip

```

c
c      Title: Calculate White Dwarf Parameters
c      File: rbb_wd_dd_param.f
c      Version: 9 Aug 10a (updated 08 Nov 10a)
c      Description: bicubic spline interpolation of Bergeron WD model grid
c      Summary:
c
c      par_DC; [distMag.dat]
c      input: distance modulus, distance modulus error, observed u_mag, observed g_mag, observed
r_mag, observed i_mag, observed z_mag, observed u_mag error, observed g_mag error, observed
r_mag error, observed i_mag error, observed z_mag error
c      output: distance modulus, observed g_mag, mass, mass error, age, age error, logg, logg error
, abs u_mag, abs g_mag, abs r_mag, abs i_mag, abs z_mag, abs u_mag error, abs g_mag error, abs
r_mag error, abs i_mag error, abs z_mag error, Teff, Teff error
c
c      par_cool; [teffdistmag.dat]
c      input: Teff, distance modulus, distance modulus error, observed u_mag, observed g_mag,
observed r_mag, observed i_mag, observed z_mag, observed u_mag error, observed g_mag error,
observed r_mag error, observed i_mag error, observed z_mag error
c      output: Teff, distance modulus, observed g_mag, mass, mass error, age, age error, logg, logg
error, abs u_mag, abs g_mag, abs r_mag, abs i_mag, abs z_mag, abs u_mag error, abs g_mag error
, abs r_mag error, abs i_mag error, abs z_mag error
c
c      par_norm; [loggtempmag.dat]
c      input: logg, logg error, temp, temp error, observed u_mag, observed g_mag, observed r_mag,
observed i_mag, observed z_mag, observed u_mag error, observed g_mag error, observed r_mag
error, observed i_mag error, observed z_mag error
c      output: observed g_mag, mass, mass error, age, age error, logg, logg error, abs u_mag, abs
g_mag, abs r_mag, abs i_mag, abs z_mag, abs u_mag error, abs g_mag error, abs r_mag error, abs
i_mag error, abs z_mag error
c
c      par_cool_2; [masstempmag.dat] - required for DD system with both a DC and a low
temperature component (where the low temperature component's spectroscopic mass has been
corrected for estimated offset in low temp spectroscopic determination [~0.15Msol])
c      input: mass, mass error, temp, temp error, observed u_mag, observed g_mag, observed r_mag,
observed i_mag, observed z_mag, observed u_mag error, observed g_mag error, observed r_mag
error, observed i_mag error, observed z_mag error
c      output: observed g_mag, mass, mass error, age, age error, logg, logg error, abs u_mag, abs
g_mag, abs r_mag, abs i_mag, abs z_mag, abs u_mag error, abs g_mag error, abs r_mag error, abs
i_mag error, abs z_mag error
c
c      par_DC_3/par_cool; [teffdistmag.dat]
c      input: Teff, distance modulus, distance modulus error, observed u_mag, observed g_mag,
observed r_mag, observed i_mag, observed z_mag, observed u_mag error, observed g_mag error,
observed r_mag error, observed i_mag error, observed z_mag error
c      output: Teff, distance modulus, observed g_mag, mass, mass error, age, age error, logg, logg
error, abs u_mag, abs g_mag, abs r_mag, abs i_mag, abs z_mag, abs u_mag error, abs g_mag error
, abs r_mag error, abs i_mag error, abs z_mag error
c

```

## A.5.3 Tlusty And Koester ASCII Model Grid Comparison Using GDL

This code has been used to verify that the PDD calculated Tlusty and Koester WD ASCII WD model grids align.



**compareTlustyAndKoesterModelGrid**

tlustyAndKoesterASCIIModelGridComparisonUsingGDL-26May10a-includingModelGrids.zip

```
; Title: compare Tlusty And Koester Model Grid
; File: compareTlustyAndKoesterModelGrid.pro
; Version: 26 May 10 2:00pm
; Summary:
;
;   Postconditions;
;
;   This program flux normalises and compares Tlusty And Koester Model Grid files
;
;   Preconditions;
;
;   The input files are of the following format;
;
;   ngc3532-11s300750.dat [wavelengthArray, amplitudeArray], space delimited
;   da15000-900.dk_tr_rg [wavelengthArray, amplitudeArray], space delimited
```

### A.5.4 Interpolate ASCII Spectroscopic Model Grid and create ASCII model using Best Fit Temperature and Surface Gravity values

This code has been used to create ASCII WD spectroscopic models using the temperature and surface gravity values derived from Xspec modelling and the ASCII model grids.

**interpolateTlustyOrKoesterASCIIModelGrid.pro**

interpolateTlustyOrKoesterASCIIModelGrid-29Aug10a.zip

```
; Title: interpolate Tlusty Or Koester ASCII Model Grid
; File: interpolateTlustyOrKoesterASCIIModelGrid.pro
; Version: 28 August 10 5:00pm
;
;   Postconditions;
;
;   This program interpolates Tlusty Or Koester ASCII Model Grid for an ideallogg and teff value,
;   and outputs the interpolated model grid
;
;   Preconditions;
;
;   The input files are of the following format;
;
;   ngc3532-11s300750.dat [wavelengthArray, amplitudeArray], space delimited
;   da15000-900.dk_tr_rg [wavelengthArray, amplitudeArray], space delimited
```

### A.5.5 White Dwarf Parameter Extraction - including gravitational redshift values - NOT USED

This software is otherwise known as the "Fontaine" code. It has been replaced for the most part by the RBB Bergeron grid interpolation code (rbb\_wd\_dd\_param.pro) - except for gravitational redshift and radius determination purposes.

**Compilation Instructions**

```
'g77 -c *.f [need to recompile *.f into .o objectfiles]'
'g77 g2m_fbbC.o hunt.o interpralf.o loadvec.o readt1C.o spline.o spl2.o interp.o
splint.o spl2.o [only C related] [link them all into an executable]'
'g77 g2m_fbbCO.o hunt.o interpralf.o loadvec.o readt1CO.o spline.o spl2.o interp.o
splint.o spl2.o [only CO related] [link them all into an executable]'
```

## Execution Instructions

./g2m.fbbCO

## Inputs

hyad.in [created based upon output of XSPEC] A or B specify name irr irr opttemp  
low high gopt glow ghigh flag[1,0]-gravitationalredshiftinfo?

## Outputs

hyad.out NB GR - Km/s

### A.5.6 Flux Recalibration using Best Fit ASCII Spectroscopic Model

This code has been used to recalibrate the flux of a set of magnetic WD candidates before having modelling performed externally by a Magnetic WD expert.

#### fitPolyToDataModelRatio.pro

fitPolyToDataModelRatio-30Aug10a.zip

```
; Title: fit Poly To Data:Model Ratio
; File: fitPolyToDataModelRatio.pro
; Version: 28 August 10 9:00pm
;
; Postconditions;
;
; This program fits a poly to a data model ratio
;
; Preconditions;
;
; The input files are of the following format;
;
; WDMModelFile: DD-0Xqmodel.dat [wavelengthArray, amplitudeArray], space delimited
; WDDataFile: SSWD0Xqw.dat [wavelengthArray, amplitudeArray], space delimited
; make sure that data file's last amplitude value is correct (not set to 0.0)
```

### A.5.7 Interpolate ASCII Main Sequence Stellar evolutionary model grid using theoretical main sequence mass or age values to calculate a best fit main sequence age or mass

This code has been used during IFMR refinement for both (binary/open cluster) system age calculations (Interpolate ASCII Main Sequence Stellar evolutionary model grid using theoretical main sequence mass to calculate a best fit main sequence age) and initial mass calculations (Interpolate ASCII Main Sequence Stellar evolutionary model grid using theoretical main sequence age value to calculate a best fit main sequence mass).

### A.5.8 ASCII Model Grid Creation Software - performed by PDD and Koester

synspec43.tar.gz  
tlusty200.tar.gz

#### Organisation of ASCII Tlusty Model Grid Files

tlustyModelgridOrganise.csh

#### Organisation of ASCII Koester Model Grid Files

koesterModelgridOrganise.csh

### A.5.9 XSpec Software

xspec11.3.2ag-src.tar.gz

Xspec requires data files and model grid to be converted to Fits.

#### Conversion of ASCII WD Model Grid to Xspec Fits Format - performed by PDD - sag2xam\_mp.pl

PDD's ASCII WD Model Grid to Xspec Fits Format software.  
sag2xam\_mp.pl

```
#!/usr/bin/perl
#####
#
# grid of ascii SYNSPEC output --> XSPEC atable model file , OGIP (like) FITS
#
#####
```

#### Conversion of ASCII WD Data to Xspec Fits Format - lin2xspB.pl

PDD's ASCII WD data to Xspec fits WD data conversion software.

lin2xspB.pl (based on lin2xsp.pl - but a work around has been applied to compensate for an Astro CFITSIO boolean to string conversion bug)

```
#!/usr/bin/perl
#####
#
# based on opt2xsp.f and lin2xsp.f
#
# in:  ascii data file with APPROXIMATELY the following form :
#
# lambda (in ang.), flux (ergs cm-2 s-1 ang-1), fluxerror (ergs cm-2 s-1 ang-1).
#
# out: OGIP FITS pha and rsp files suitable for xspec.
#
#####
```

Note for reversion back to version A in the event the bug in Astro CFITSIO is corrected sometime in the future;

diff lin2xspB.pl lin2xsp.pl gives;

```
'515c515'
```

```
'i $fptr->write_key(TLOGICAL, 'POISSERR', $pois, 'poissonians errors', $status);
'__'
```

```
'& $fptr-&update_key(TLOGICAL, 'POISSERR',$pois, 'poissonian errors', $status);'
```

### lin2xspB.pl prerequisites

**CFITSIO** Astro-FITS-CFITSIO-1.05.tar.gz

**Astro-FITS-CFITSIO** Astro-FITS-CFITSIO-1.05.tar.gz

### Pgplot

Pgplot is difficult to compile and install on a modern Linux System, so it is recommended that a precompiled version of pgplot from starlink is used (precompiled and tested for one's system).

## A.5.10 PDD IDL ASCII Model Interpolation Software Prerequisites - NOT USED

### IDL Astro Lib

astroLib - astron.zip

## A.5.11 Model Grids

### Koester Low-Mid Temperature WD Spectroscopic Model Grid (T=6000K - 20000K)

kmod.tar.gz (ASCII)  
KOESTERDA (Xspec Fits)

**Intervals** logg interval = 0.25  
Teff interval = 1000K

**File Name Format** "'da" + teffString + "-" + STRMID(loggString,0,1) + STRMID(loggString,2,2) + ".dk\_tr\_rg"'  
(Eg da16000\_775.dk\_tr\_rg)

**Format** Wavelength Flux

### PDD Mid-High Temperature WD Spectroscopic Model Grid (T=15000K - 47500K)

tlmod.tar.gz (ASCII)  
TLUSTY10v2 (Xspec Fits)

**Intervals** logg interval = 0.25  
 Teff interval = 2500K

**File Name Format** tlustyModelFileName = "ngc3532-lls" + STRMID(teffString,0,3)  
 + STRMID(loggString,0,1) + STRMID(loggString,2,2) + ".dat"  
 (Eg ngc3532-lls160775.dat)

**Format** Wavelength Flux

## A.5.12 Xspec Model Files

xspecWorkingFolder-30June10a.zip

### Flux Calibrated Data Files

WDname.dat (Eg SSWD01A.dat)

### Xspec workspace files

WDname.xcm (Eg SSWD01A.xcm)

```
cpd /xw
data 1:1 "SSWD01Bwhb.pha"
data 2:2 "SSWD01Bwhg.pha"
data 3:3 "SSWD01Bwhd.pha"
data 4:4 "SSWD01Bwhe.pha"
data 5:5 "SSWD01Bwh8.pha"
  statistic chi
  abund angr
  xsect bcmc
  xset forcecalc off
  cosmo 70.000 0.000 0.730
model atable{/home/rich/tasks/atmosphericmodelfitting/working/modelgrid/KOESTERDA}
  7.9689 7.00000E-03 7.0000 7.0000 9.5000 9.5000
  19217. 6.0000 6000.0 6000.0 20000. 20000.
  6.44005E-05 1.00000E-06 -1.00000E-03 -1.00000E-03 1.00000E-03 1.00000E-03
  320.75 5.0000 0.0000 0.0000 1.00000E+24 1.00000E+24
=
= 1
= 2
= 3
  306.38 5.0000 0.0000 0.0000 1.00000E+24 1.00000E+24
= 1
= 2
= 3
  293.99 5.0000 0.0000 0.0000 1.00000E+24 1.00000E+24
= 1
= 2
= 3
  287.75 5.0000 0.0000 0.0000 1.00000E+24 1.00000E+24
= 1
= 2
= 3
  282.88 5.0000 0.0000 0.0000 1.00000E+24 1.00000E+24
fit
ipl
```

```
cpd /xw
data 1:1 "SSWD01Bwhb.pha"
data 2:2 "SSWD01Bwhg.pha"
data 3:3 "SSWD01Bwhd.pha"
data 4:4 "SSWD01Bwhe.pha"
data 5:5 "SSWD01Bwh8.pha"
  statistic chi
  abund angr
  xsect bcmc
```

```

xset forcecalc off
cosmo 70.000 0.000 0.730
model atable{/home/rich/tasks/atmosphericmodelfitting/working/modelgrid/TLUSTY10v2}
19217. 6.0000 15000. 15000. 45000. 45000.
7.9689 7.00000E-03 7.2500 7.2500 8.7500 8.7500
6.44005E-05 1.00000E-06 -1.00000E-03 -1.00000E-03 1.00000E-03 1.00000E-03
320.75 1.0E+8 0.0000 0.0000 1.00000E+24 1.00000E+24
= 1
= 2
= 3
306.38 1.0E+8 0.0000 0.0000 1.00000E+24 1.00000E+24
= 1
= 2
= 3
293.99 1.0E+8 0.0000 0.0000 1.00000E+24 1.00000E+24
= 1
= 2
= 3
287.75 1.0E+8 0.0000 0.0000 1.00000E+24 1.00000E+24
= 1
= 2
= 3
282.88 1.0E+8 0.0000 0.0000 1.00000E+24 1.00000E+24

```

### 'Fits Model Files generated using lin2xspect.pl'

- WDnameha.pha (Eg SSWD01Aha.pha)
- WDnameha.rsp
- WDnamehb.pha
- WDnamehb.rsp
- WDnamehg.pha
- WDnamehg.rsp
- WDnamehd.pha
- WDnamehd.rsp
- WDnamehe.pha
- WDnamehe.rsp
- WDnameh8.pha
- WDnameh8.rsp
- WDnameh9.pha
- WDnameh9.rsp

## A.5.13 Operational Manuals

All data processing procedures have been documented in operational manuals.

### Spectroscopic Modelling Instructions

```

//do: WD model fitting software installation and usage instructions;
1. 1 WD Model Grid Creation utils [PDD generates models]

A. synspec43
cannot compile on linux

B. tlusty200
cd tlusty200
g77 -O3 -static -fno-automatic -o tlusty200 tlusty200.f

```

```

2. astrolib
   install astrofits idl/gdl library
   - if idl on server, copy pro files to working directory? use gftp.
   - if gdl, copy pro files to /usr/share/gdl/

3. IDL normalisation using model grid - IDL Software [IDL preliminary T and log g model grid fitting
   process: Normalises Mell11-WD.dat data using model grid producing spectralfile0/Mell11-WD.
   dat.m/norm (first two columns of this data may be used by lin2xsp.pl/xspec), and calculates
   basic estimate of g and Teff using the model grid]
1. place MODELS folder somewhere, nedit loadmodarr0.pro,
   (eg in IDL model grid working folder, somewhere = /home/rich/tasks/
   atmosphericmodelfitting/utls/1modelgridgenerationUsingIDL/home/pdd/IDL-WD/)
   and change
   modfilename='/MODELS/'+resstring+'/'+tstring+'/'+gstring+'/'+H090717.dat'
   to;
       modfilename='somewhere/MODELS/'+resstring+'/'+tstring+'/'+gstring+'/'+H090717.dat'
2. nedit in_0.FRC and change dat file [eg Mell11-WD.dat]
   filename must be <= 8 characters.
   nedit in_1.dat, and set min/max temp and logg parameters
   nedit loadmodarr0.pro
   set the following;
   ntmax= number of temperature folders in model grid LRES folder
   nlmax= number of logg folders in model grid LRES/temp folder
   teffs=[all temp folder names in model grid LRES folder]
   logg=[all logg folder names in model grid LRES/temp folder]
   modfilename='/disks/etna/home/science/staff/rbaxter/modelgrid/
   koestermodegridORtlustymodegridOR/'+resstring+'/'+tstring+'/'+gstring+'/'+TLUSTYDA.
   dat'
3. use idl [NOT gdl; too slow]
   or to use IDL;
   ssh rbaxter@137.111.88.18 -X
   cd idl
   idl

{/home/rich/tasks/atmosphericmodelfitting/}

.run loadmodarr0.pro
.run read_in
read_in [to perform model grid fitting using idl, and to produce a continuum normalised output
   file with extension .dat.m]

.run inter.pro
inter_0 [to calc values without producing a poly/continuum normalised output file with extension
   n.dat, for a single redshift value]
filename
1
5
poly

4. cfitsio [install CFITSIO]
su rich
cd utls/cfitsio [v3.x]
./configure --prefix=/usr/local
make
su root
make install

5. Astro-FITS-CFITSIO-1.05 [Perl Modules - Astro:Fits:CFITSIO (and required or fortan I, libraries)]
su rich
cd utls/Astro-FITS-CFITSIO-1.05 [v1.05]
nedit Makefile.PL, and set -I/usr/local/include and -L/usr/local/lib -lcfitsio -lm
perl Makefile.PL OPTIMIZE=O
make
make test
su root
make install

6. lin2xsp [lin2xsp.pl - what does lin2xsp do? generates pha/phm files used by xspec (eg referenced
   in COMA-WD.xcm)]
[must use lin2xsp.pl version B {with hack/work around} when using buggy cfitsio v1.05]
cuts the lines out and creates separate files.
[rsp = response files - uses rsp files to blur the model to match the resolution of the data
]

lin2xsp;
Enter the root name of the ascii data file > COMA-WDn
Is there a flux error column in this file (y/n) ? > n
Estimate the fractional flux error on the data > 0.02 {signal to noise 50:1 [so
insert 0.02]}
Isolate H-(1)yman, H-(b)almer or H(e)lium line series ? > b
Correct slopes of lines (y/n) ? > n
Enter instrument resolution (fwhm channels) > 2.5 {fwhm in channels?
deltaLambda/RBBfitsfileresl[1.0A] = }

Coma WD:
[NB COMA = 0.6arc with R300B grating, most likely has been binned every 1.0 arc seconds
- use WHT blue arm website - PDD had matched the slit width and the seeing on the
night - ; as 1" will project to 4pixels, therefore 0.6" will project to 2.4 pixels,
then * 0.86 gives ~2.064 fwhm]
divide spec res by image res, so if image res is 1.7 [should be 1.0 with myGemini/myWHT
data], then enter into Lw2xsp 2.0/1.7 = 2.5

```

```

instrument resolution = spec res / image res

http://en.wikipedia.org/wiki/Spectral_resolution
spectral resolution (R) = lambda[4400] / delta lambda
delta lambda = lambda[4400] / spectral resolution [R]

Gemini GMOS:
http://www.gemini.edu/?q=node/10375

Enter name of source > coma {??????}

7. pgplot
pgplot 5.x insallation instructions;
install starlink [http://starlink.jach.hawaii.edu/starlink]
[create a link in /usr/bin to /home/rich/star/manifests/pgplot]
su root
ln -s /home/rich/star/manifests/pgplot /usr/bin/pgplot

8. XSPEC (HEASARC) version 11.3 [what does xspec do? Performs formal T and log g model grid fitting.
Creates a file similar to hyad.in for fontaine?]

what xpsec does? reads in model grid [dont need to smooth the model]

instructions to install XSPEC 11;
download xspecv11.3 source, xspec11.3.2ag-src.tar [MB I had to obtain this in person
from Bryan Irby (irby@milkyway.gsfc.nasa.gov) as only v12 is available online at
the moment]
cd xspecv11.3/heasoft-6.6.3/BUILD_DIR
./configure
make
su root
make install

instructions to run XSPEC 11;
https://astrophysics.gsfc.nasa.gov/XSPECwiki/XSPECPage
http://heasarc.gsfc.nasa.gov/docs/xanadu/xspec/index.html
http://heasarc.gsfc.nasa.gov/docs/xanadu/index.html#quicklink
http://heasarc.gsfc.nasa.gov/docs/software/lheasoft/install.html

su rich
cd /home/rich/tasks/atmosphericmodelfitting/working/xspec
HEADAS=/home/rich/tasks/atmosphericmodelfitting/utis/xspecv11.3/heasoft-6.6.3/x86_64-
unknown-linux-gnu-libc2.5
export HEADAS
alias heainit=". $HEADAS/headas-init.sh"
heainit
xspec11

manual operations (without using pre-existing xcm file);

configure plot device;

set plotting device to pgplot (http://heasarc.gsfc.nasa.gov/docs/xanadu/
xspec/manual/XScpd.html);

A?
cpd /GIF
exit

B?
[p1]
ipl
dev /xw

configure balmer line models

da 1:1 W2T-WAV-FLX-Ahb 2:2 W2T-WAV-FLX-Ahg 3:3 W2T-WAV-FLX-Ahd 4:4 W2T-
WAV-FLX-Ahe 5:5 W2T-WAV-FLX-Ah8

what it does;
findsthe optimum fit
test it out on a dataset already analysed
PDD supply a anormalised COMA-WDn.dat file

modify SSWD08Bv.xcm with appropriate file names (including model grid)
model atable{/home/rich/tasks/atmosphericmodelfitting/modelgrid/TLUSTY10}
OR
model atable{/home/rich/tasks/atmosphericmodelfitting/modelgrid/BAXTERDA}
xspec11

EITHER; (if xcm file exists);

@SSWD08Bv.xcm [or @COMA-WD.xcm]
thaw 3 {I don't know why this is required, but for some reason the redshift always
happens to be frozen upon load of the xcm file}
ipl [only required if initial estimate not good enough and xcm fit reference
triggered interactive fit autoenabled]
fit [only required if initial estimate not good enough and xcm fit reference
triggered interactive fit autoenabled]
ign 5:1-** [only required if balmer line 8 gives bad fit]

```



```

error 3.5 stopat 200000,,1,2

OR; (if xcm file does not exist);

data 1:1 "SSWD08Bvhh.pha" 2:2 "SSWD08Bvhg.pha" 3:3 "SSWD08Bvhd.pha" 4:4 "SSWD08Bvhe.
pha" 5:5 "SSWD08Bvh8.pha"
fit
ipl
thaw 3 [unfreeze redshift]
new 3
1e-4 1e-6 -1e-3 -1e-3 1e-3 1e-3
1e-6 1e-6 -1e-3 -1e-3 1e-3 1e-3
untie 4 8 12 16 20
ign 5:1-** [only required if balmer line 8 gives bad fit]
fit
error 3.5 stopat 200000,,1,2
[reduced ch sq <= 2.0]
[delta chi sq ^= 3.5]
exit
save all SSWD08Bv

reduce chi squared to ^3.5;
if >>1 , then under estimate error , in lin2xspect increase the fraction
if <<1 , then over estimate error , in lin2xspect reduce the fraction

As for the fractional error...you will likely need to make a couple of
iterations of the lin2xsp.pl -> fitting process to tune this to give a
reduced chi^2 of ^1.0

ask Quentin about it g - XSPEC

```

#### 9. fontaine [Matt Wood Software; calculates WD cooling times and masses]

```

http://astro.fit.edu/wood/wd.html
[in folder called "Fontaine" - feb 92; bergeron tracks differ from MW tracks; very hottest/
coolest[crystallise] end differences]
rpm -i compat-gcc-34-g77-3.4.6-4.x86_64.rpm
g77 -c *.f [need to recompile *.f into .o objectfiles]
g77 g2m.fbbC.o hunt.o interpralf.o loadvec.o readt1C.o spline.o splt2.o interp.o splint.o splt.o
[only C related] [link them all into an executable]
g77 g2m.fbbCO.o hunt.o interpralf.o loadvec.o readt1CO.o spline.o splt2.o interp.o splint.o splt
.o [only CO related] [link them all into an executable]

yum install libg2c.so.0
./g2m.fbbCO
Note the following files;
sdssdd.in [created based upon output of XSPEC] {A or B specify}
name irr irr opttemp low high gopt glow ghigh flag[1,0] -
gravitationalredshiftinfo?
sdssdd.out
GR - Km/s

```

#### 10. bergeronPDDcode [calculates absolute magnitudes using WD atmospheres - in g/v band? [need to modify this such that it outputs in r, u, g/v bands also]

```

await code from PD (Bergeron)

bergeron code (pda_wd.Vmag.f, fort.55, tefflogg.dat);

g77 -fno-second-underscore -c pda_wd.Vmag.f
g77 pda_wd.Vmag.o /home/rich/star/lib/libpda.a -o pda_wd.Vmag

ie. you'll need starlink to link with...
fort.55 is the bergeron input data,
tefflogg.dat is your temps and gravs...
answers output to fort.21

```

## A.6 Data Analysis

### A.6.1 Calculate Main Sequence Ages

This software is used to calculate the main sequence age of a given main sequence mass (or vice versa). It is also used to plot system age confirmation bar graphs (across a range of published IFMRs). It is also used to perform a statistical IFMR derivation (m/gradient and c/y-intersection parameters of a linear IFMR form) based upon system

age difference optimisation (minimisation). It is also used to plot the initial-final mass of components of each system against a known IFMR form.

## findMainSequenceCoolingTimeOrMassInGirardiModel.pro

### mainSequenceStellarEvolutionModelCalculations-29June11a.zip

```
; Title: find Main Sequence Cooling Time Or Mass In Girardi Model
; File: findMainSequenceCoolingTimeOrMassInGirardiModel.pro
; Version: 11 August 10 6:00pm (Updated 31 July 11)
; Summary:
;
; Postconditions;
;
; This program uses Girardi 2000 main sequence evolution data to either a) find mass based upon
; age or b) find age based upon mass
;
; Preconditions;
;
; The input files are of the following format;
;
; mainSequenceStellarAges-SolarMetallicity.txt [recno, Overshoot, Z yr, age solMass, Mini solMass,
; Mact [solLum], logL, logTeff [K],logg [cm/s2], VMAG mag, U-B mag, B-V mag, V-I mag, Stage],
; tab delimited
; 1. initialMassInput.txt [value], 2. initialAgeInput.txt [value], or 3. finalAgeInput.txt,
; finalMassInput.txt [value, valueMin, valueMax] {NB 3:0 requires initialMassInput.txt,
; initialAgeInput.txt [value, valueMin, valueMax] also}
; for usage 3:0. only: systemAgeConstraints.txt [known IFMR estimated System Age, known IFMR
; estimated max System Age, known IFMR estimated min System Age], tab delimited (in Myrs)
; for usage 3:1 and 3:2 only: systemAgeCommon.txt [whether to use the DD system for final
; calculations]
;
; Only modes still used [all other modes have been replaced with PDD/
; RBBcompareDDSystemAgeDifferenceDistributionAcrossPublishedIFMRS and SDSSDDSystemAgeConfirmation
; >= 31 July 11a];
; 3:0 and 3:1 [ie 1, 2, and 3:2 are no longer used]
;
; Usage GDL [linear interpolation only];
;
; gdl
; .run findMainSequenceCoolingTimeOrMassInGirardiModel.pro
;
; Usage IDL:
; mkdir /home/aaossz/rbaxter/idllib/astron
; cd /home/aaossz/rbaxter/idllib/astron
; tar -xvf astron.tar.gz
; idl
; !PATH = Expand_Path('/home/aaossz/rbaxter/idllib/astron/pro') + ':' + !PATH
; PRINT, !PATH
; .run findMainSequenceCoolingTimeOrMassInGirardiModel.pro
```

## A.6.2 compare DD System Age Difference Distribution Across Published IFMRs

This software is used to compare the DD System Age Difference Distribution Across Published IFMRs (and creates monte carlo distributions of expected component [WD/-final and MS/initial] combinations for each DD system based on final mass/age errors).

## compareDDSystemAgeDifferenceDistributionAcrossPublishedIFMRS.pro

### compareDDSystemAgeDifferenceDistributionAcrossPublishedIFMRS-13July11a.zip

```
; Title: compare DD System Age Difference Distribution Across Published IFMRs
; File: compareDDSystemAgeDifferenceDistributionAcrossPublishedIFMRS.pro
; Version: 09 July 11 10:00am [updated 31 July 11a]
;
; Postconditions;
;
```

```

; This program compares the DD System Age Difference Distribution Across Published IFMRs (and
; creates monte carlo distributions of expected component [WD/final and MS/initial] combinations
; for each DD system based on final mass/age errors)
;
; Preconditions;
;
; compareDDSystemAgeDifferenceDistributionAcrossPublishedIFMRs.pro has been executed
;
; The input files are of the following format;
;
; WDinputParameters.txt [name logg      logg error temp      temp error  observed u_mag  observed
; g_mag  observed r_mag  observed i_mag  observed z_mag  observed u_mag error  observed g_mag
; error      observed r_mag error      observed i_mag error      observed z_mag error  Special Case (
; for the purpose of mass/age SW calculations)]
;
; Usage GDL [linear interpolation only];
;
; gdl
; .comp compareDDSystemAgeDifferenceDistributionAcrossPublishedIFMRs.pro
; compareDDSystemAgeDifferenceDistributionAcrossPublishedIFMRs
;
; Usage IDL:
; mkdir /home/aaossz/useraccount/idllib/astron
; cd /home/aaossz/useraccount/idllib/astron
; tar -xvf astron.tar.gz
; idl
; !PATH = Expand.Path('+/home/aaossz/useraccount/idllib/astron/pro') + ':' + !PATH
; PRINT, !PATH
; .comp compareDDSystemAgeDifferenceDistributionAcrossPublishedIFMRs.pro
; compareDDSystemAgeDifferenceDistributionAcrossPublishedIFMRs
;
; Title: plot DD System Age Difference Distribution Across Published IFMRs
; File: plotDDSystemAgeDifferenceDistributionAcrossPublishedIFMRs.pro
; Version: 09 July 11 10:00am [updated 31 July 11a]
; Summary:
;
; Postconditions;
;
; This program plots the DD System Age Difference Distribution Across Published IFMRs
;
; Preconditions;
;
; compareDDSystemAgeDifferenceDistributionAcrossPublishedIFMRs.pro has been executed
;
; The input files are of the following format;
;
; IFMR0WDoutputParameterSystemAgeDiff.txt [sysAgeDiff] for n WDs
;
; Usage GDL [linear interpolation only];
;
; gdl
; .comp plotDDSystemAgeDifferenceDistributionAcrossPublishedIFMRs.pro
; plotDDSystemAgeDifferenceDistributionAcrossPublishedIFMRs
;
; Usage IDL:
; mkdir /home/aaossz/useraccount/idllib/astron
; cd /home/aaossz/useraccount/idllib/astron
; tar -xvf astron.tar.gz
; idl
; !PATH = Expand.Path('+/home/aaossz/useraccount/idllib/astron/pro') + ':' + !PATH
; PRINT, !PATH
; .comp plotDDSystemAgeDifferenceDistributionAcrossPublishedIFMRs.pro
; plotDDSystemAgeDifferenceDistributionAcrossPublishedIFMRs
;
;

```

### A.6.3 Distance Moduli Comparison of DD components

This software is used to plot the distance moduli of double degenerate WD components based upon their observed apparent magnitudes and theoretical absolute magnitudes (for u, g, r, bands), to confirm that they are associated and that the modelling processes have provided accurate absolute magnitude values.

#### plotToFileDistanceModulus.pro

SDSSDDdistancemoduliconfirmation-29Oct10a.zip

```
; Title: Plot Distance Modulus
; File: plotDistanceModulus.pro
; Version: 1 July 10 10pm [updated 29 July 11a]
;
; Postconditions;
;
; This program plots g vs g-r for each blue object pair
;
; Preconditions;
;
; The input files are of the following format;
;
; DDphotometricBandsx.txt [DD-NUMBER, G app psf, R app psf, U app psf, G abs, R abs, U abs,
; Temperature, G app psf error, R app psf error, U app psf error, delta M g, delta M r, delta M u
; , G m-M error, R m-M error, U m-M error] for X blue objects Pairs, tab delimited
```

## A.6.4 DD Mass Distribution Comparison with Field WD Survey

This software is used to apply a K-S test to my DD Data and a known field WD survey mass distribution.

### cmd.pro

#### compareMassDistributions-08Mar11a.zip

```
; Title: CMD: Compare Mass Distributions (DD systems versus SDSS field WDs)
; File: cmd.pro
; Version: 24 Feb 11 8:00pm (updated 7 Mar 11a)
;
; Postconditions;
;
; This program compare Mass Distributions of DD systems versus SDSS field WDs
;
; Preconditions
;
; The input files are of the following format;
;
; kstwo.pro (NASA)
; PROB.KS.pro (NASA)
; METHOD01; WdmassDistributionPGsurveyVmaxCorrectedWithCoarseBinning.txt [NB this data has been
; rebinned to match binning of DD mass Distribution]
; METHOD01; DDmassDistribution.txt
; METHOD02; (SW generated from predefined gaussians) [uses WdmassDistributionKepler.txt for visual
; comparison]
; METHOD02; DDmasses.txt
; METHOD04; WdmassDistributionPGsurveyVmaxCorrected.txt
; METHOD04; DDmasses.txt
; METHOD05; (SW generated from predefined gaussians) [uses WdmassDistributionPGsurveyVmaxCorrected.
; txt for visual comparison]
; METHOD05; DDmasses.txt
; METHOD06; (SW generated from predefined gaussians) [uses WdmassDistributionVmaxCorrectedKepler.
; txt for visual comparison]
; METHOD06; DDmasses.txt
;
```

## A.7 List of Documentation

### A.7.1 Object Table

All WD parameters from the project are stored in the object table spreadsheet (also serving as a data model process guideline);

SDSSDDObjectTable.ods

## A.7.2 Target Selection Confirmations

### Target Selection Mass Bias Confirmation

estimateTargetSelectionMassBias.ods

### Target Selection Basic WD Population Synthesis

RBB Basic WD Population Synthesis Model B.ods

## A.7.3 Private Projects

### RBB IFMR private project 1

Aim: Derive empirical WD Cooling Model using open cluster data  
empirical WD cooling models using open cluster WD masses.ods  
theoretical WD cooling models.ods  
Results suggest this is not possible due to current errors in data.

### RBB IFMR private project 2

Aim: use the SDSS to calculate a mass distribution of main sequence stars, model, then compare with this with SDSS WD survey. Compare theoretical WD mass distribution (based upon observed main sequence mass distribution and currently defined IFMR) and observed WD mass distribution.  
main sequence luminosity function.ods  
Results suggest this is not possible due to current error in data.

### RBB IFMR private project 3

Aim: use the Initial Mass Function (IMF) to calculate a mass distribution of main sequence stars, model, then compare with this with SDSS WD survey  
mass function derivation.ods  
Results suggest this is not possible due to current error in data.

**RBB IFMR private project 4**

Aim: compare theoretical double degenerate mass distribution (based upon observed WD mass distribution) and observed double degenerate mass distribution

EstimateIFMRusingSDSSDDMassDistributionBias.ods

**A.7.4 WHT Observing Proposals****A.7.5 WHT 2008A Proposal**

Particle Physics and Astronomy Research Council  
Polaris House, North Star Avenue, Swindon, SN2 1SZ  
Telephone 01793 442000 Fax 01793 442002  
**APPLICATION FOR TELESCOPE TIME (OPTICAL AND INFRARED)**

**PATT2**  
Version 02/2003

1 TELESCOPE ( <i>AAT, UKST, WHT, INT or UKIRT</i> )		WHT	Reference:	Date Stamp:
2 SEMESTER		2008A	3 SCIENTIFIC CATEGORY	3
4 COORDINATED PATT PROPOSALS		<i>AAT:</i> <input type="checkbox"/> <i>UKST:</i> <input type="checkbox"/> <i>WHT:</i> <input type="checkbox"/> <i>INT:</i> <input type="checkbox"/> <i>UKIRT:</i> <input type="checkbox"/> <i>JCMT:</i> <input type="checkbox"/> <i>GEMINI:</i> <input type="checkbox"/> <i>LT:</i> <input type="checkbox"/> <i>MERLIN:</i> <input type="checkbox"/>		
5 PRINCIPAL APPLICANT				
Surname:	Dobbie		Title:	Dr
Post held:	Research Astronomer			
Address:	Anglo-Australian Observatories, Epping, NSW 1710			
Telephone:			Fax:	
E-mail:	pdd@aao.gov.au		Is the applicant a possible observer?	Yes
6 COLLABORATORS				
Name:	Institute:		Observer?	
M.R. Burleigh	University of Leicester		Yes	
7 SHORT TITLE OF PROPOSAL ( <i>maximum 12 words</i> )				
Constraining the masses of cool white dwarfs with SDSS candidate wide double degenerates				
8 SUMMARY OF PROPOSED OBSERVATIONS				
<p>We propose to obtain ISIS spectroscopy of the components of a number of spatially resolved candidate WD binary systems where one component has <math>T_{eff} &gt; 12500K</math> and the other <math>T_{eff} \leq 12500K</math>. We will use these data to 1) confirm that these objects are WDs, 2) place stringent constraints on the effective temperatures and (spectroscopic) surface gravities of both members of each system and 3) measure the wavelength shift of the H-<math>\alpha</math> line core to determine the system line of sight velocity. Subsequently, using gravitational redshift we will determine the mass of the cooler WD in each system. We will compare this to the spectroscopic mass estimate to investigate the physics of cool WD model atmospheres. This physics is crucial to interpreting the WD luminosity function which contains information on the local star formation history and the age of the Galactic disk and to constraining the form of initial mass-final mass relation at near solar masses.</p>				
9 FOCAL STATION, INSTRUMENT AND DETECTOR				
Focal station:	Instrument:	Detector(s):	Gratings/Filters:	
Cass	ISIS	EEV12+REDPLUS	R300B+R1200R	
10 OBSERVING TIME REQUESTED THIS SEMESTER				
Time requested this semester	Dark:	Grey:	Bright:	specify nights
		3		or weeks: n
Minimum useful allocation this semester	Dark:	Grey:	Bright:	
		2		
<i>UKIRT applicants requiring dark time must justify this in section 18</i>				
11 COMPLETE THIS SECTION ONLY IF THIS IS A LONG TERM PROPOSAL				
Total time requested	Dark:	Grey:	Bright:	specify nights
				or weeks:
<i>Justification for long term status must be given in section 17</i>				

Text fonts must *not* be smaller than the style-file defaults

<p style="text-align: right;">Preferred dates:</p> <p style="text-align: right;">Impossible dates:</p> <p style="text-align: center;"><i>Give justification for impossible dates</i></p> <p>If observations are to be simultaneous with other telescopes or satellites, give details:</p> <p style="text-align: right;">Any other scheduling constraints:</p> <p style="text-align: center;"><i>Include likely clashes with other time applications, constraints on lunar position or quarter, instrument preparation requirements, etc</i></p>	<div style="border: 1px solid black; height: 25px; margin-bottom: 5px;"></div> <div style="border: 1px solid black; height: 50px; margin-bottom: 5px;"></div> <div style="border: 1px solid black; height: 50px; margin-bottom: 5px;"></div> <div style="border: 1px solid black; height: 50px;"></div>																																																												
<p><b>13 SERVICE OBSERVING</b></p> <div style="display: flex; justify-content: space-around; align-items: center;"> <span>yes: <input style="width: 40px; height: 20px;" type="checkbox"/></span> <span>no: <input checked="" style="width: 40px; height: 20px;" type="checkbox"/></span> <span>maybe: <input style="width: 40px; height: 20px;" type="checkbox"/></span> </div>																																																													
<p><b>14 SUPPORT ASTRONOMER REQUESTED AT TELESCOPE</b></p> <div style="display: flex; justify-content: space-around; align-items: center;"> <span>every night: <input style="width: 40px; height: 20px;" type="checkbox"/></span> <span>no: <input style="width: 40px; height: 20px;" type="checkbox"/></span> <span>first night only: <input checked="" style="width: 40px; height: 20px;" type="checkbox"/></span> </div>																																																													
<p><b>15 LIST OF PRINCIPAL TARGETS</b></p> <table style="width: 100%; border-collapse: collapse;"> <thead> <tr> <th style="text-align: left;">Object(s):</th> <th style="text-align: left;">RA(h,m):</th> <th style="text-align: left;">Dec(degs):</th> <th style="text-align: left;">Mag(type):</th> <th style="text-align: left;">Colour:</th> <th style="text-align: left;">Exp. Time:</th> </tr> </thead> <tbody> <tr><td>SDSS0332-00</td><td>03 32 37</td><td>-00 49 18</td><td>r=18.3</td><td>u-r=0.3</td><td>2hr</td></tr> <tr><td>SDSS0750+30</td><td>07 50 53</td><td>+30 25 44</td><td>r=17.9</td><td>u-r=-0.4</td><td>1.5hr</td></tr> <tr><td>SDSS0851+47</td><td>08 51 53</td><td>+47 12 50</td><td>r=17.8</td><td>u-r=0.3</td><td>1.5hr</td></tr> <tr><td>SDSS1157+13</td><td>11 57 38</td><td>+13 44 14</td><td>r=18.5</td><td>(u-r=0.3)</td><td>3hr</td></tr> <tr><td>SDSS1509+52</td><td>15 09 47</td><td>+52 10 02</td><td>r=18.1</td><td>u-r=-0.1</td><td>1.5hr</td></tr> <tr><td>SDSS1705+33</td><td>17 05 56</td><td>+33 04 38</td><td>r=18.9</td><td>u-r=0.35</td><td>4hr</td></tr> <tr><td>SDSS2224-08</td><td>22 24 36</td><td>-08 28 08</td><td>r=17.3</td><td>u-r=0.25</td><td>0.75hr</td></tr> <tr><td>SDSS2257+14</td><td>22 57 32</td><td>+14 04 39</td><td>r=18.7</td><td>u-r=0.35</td><td>3.5hr</td></tr> <tr><td>SDSS0054+13</td><td>00 54 12</td><td>+13 53 02</td><td>r=18.9</td><td>u-r=0.45</td><td>4hr</td></tr> </tbody> </table>		Object(s):	RA(h,m):	Dec(degs):	Mag(type):	Colour:	Exp. Time:	SDSS0332-00	03 32 37	-00 49 18	r=18.3	u-r=0.3	2hr	SDSS0750+30	07 50 53	+30 25 44	r=17.9	u-r=-0.4	1.5hr	SDSS0851+47	08 51 53	+47 12 50	r=17.8	u-r=0.3	1.5hr	SDSS1157+13	11 57 38	+13 44 14	r=18.5	(u-r=0.3)	3hr	SDSS1509+52	15 09 47	+52 10 02	r=18.1	u-r=-0.1	1.5hr	SDSS1705+33	17 05 56	+33 04 38	r=18.9	u-r=0.35	4hr	SDSS2224-08	22 24 36	-08 28 08	r=17.3	u-r=0.25	0.75hr	SDSS2257+14	22 57 32	+14 04 39	r=18.7	u-r=0.35	3.5hr	SDSS0054+13	00 54 12	+13 53 02	r=18.9	u-r=0.45	4hr
Object(s):	RA(h,m):	Dec(degs):	Mag(type):	Colour:	Exp. Time:																																																								
SDSS0332-00	03 32 37	-00 49 18	r=18.3	u-r=0.3	2hr																																																								
SDSS0750+30	07 50 53	+30 25 44	r=17.9	u-r=-0.4	1.5hr																																																								
SDSS0851+47	08 51 53	+47 12 50	r=17.8	u-r=0.3	1.5hr																																																								
SDSS1157+13	11 57 38	+13 44 14	r=18.5	(u-r=0.3)	3hr																																																								
SDSS1509+52	15 09 47	+52 10 02	r=18.1	u-r=-0.1	1.5hr																																																								
SDSS1705+33	17 05 56	+33 04 38	r=18.9	u-r=0.35	4hr																																																								
SDSS2224-08	22 24 36	-08 28 08	r=17.3	u-r=0.25	0.75hr																																																								
SDSS2257+14	22 57 32	+14 04 39	r=18.7	u-r=0.35	3.5hr																																																								
SDSS0054+13	00 54 12	+13 53 02	r=18.9	u-r=0.45	4hr																																																								
<p><b>16 LIST ALL SIMILAR/SUPPORTING APPLICATIONS TO ANY PATT OR OTHER TIME ASSIGNMENT COMMITTEE</b></p> <p><i>You must include a brief description of any other applications whose targets or science goals are similar to those requested here</i></p> <table style="width: 100%; border-collapse: collapse;"> <thead> <tr> <th style="width: 25%; text-align: left;">Telescope/satellite:</th> <th style="text-align: left;">Title/Description of programme:</th> </tr> </thead> <tbody> <tr> <td style="height: 250px;"></td> <td></td> </tr> </tbody> </table>		Telescope/satellite:	Title/Description of programme:																																																										
Telescope/satellite:	Title/Description of programme:																																																												



**White dwarf masses:** Spectroscopy of samples of young ( $12500\text{K} < T_{\text{eff}} \lesssim 80000\text{K}$ ) H-rich (DA) white dwarfs (WDs) has revealed that their mass distribution has a comparatively sharp peak centered on  $M \sim 0.6M_{\odot}$  (e.g. 129 hot WDs, Bergeron et al. 1992; the ROSAT WDs, Marsh et al. 1997). This contains  $\sim 75\%$  of these objects by number (Liebert et al. 2005) once the dependence of the sampling volume on mass is accounted for (massive WDs have small radii). However, spectroscopy of older, cooler ( $T_{\text{eff}} \leq 12500\text{K}$ ) samples reveal a shift in this peak to larger masses. For example, Kepler et al. (2007) examine 964 DAs with  $8000\text{K} \leq T_{\text{eff}} \leq 12000\text{K}$  and find the peak mass to be  $M = 0.818M_{\odot}$ . It is still not completely settled as to whether this is a real trend in WD masses or a problem with spectroscopic mass determinations. Either way, better characterisation and understanding of the increase in spectroscopic masses at  $T_{\text{eff}} < 12500\text{K}$  is **important for** any astrophysical study which relies on good knowledge of WD masses and cooling times (very sensitive to the former) e.g. **deciphering information on the history of local star formation and the age of the Galactic disk from the WD luminosity function and constraining the form of the initial mass-final mass relation for stars with near solar mass, which is integral to modelling Galactic chemical evolution.**

Willson (2000) argue that cooler WDs, which presumably are generally the descendants of older, more metal poor stars, should have larger masses due to the lower efficiency of mass loss on the AGB. However, Kepler et al. (2007) highlight that recent spectroscopic studies of relatively hot WDs in globular clusters indicate that these have near normal masses ( $M \sim 0.53M_{\odot}$ , Moehler et al. 2004). Bergeron et al. (1991) argue instead that the deepening of the convective zone in the atmospheres of cooler WDs may lead to material from the underlying He layer being mixed into the predominantly H photosphere. The presence of He increases the gas pressure in the photosphere, mimicking a higher surface gravity and hence larger mass. However, astroseismological measurements of the surface H-layer mass ( $M_{\text{H}}$ ) in pulsating WDs have all concluded that  $M_{\text{H}} > 10^{-7}M_{\odot}$  (e.g. Bradley 2006). Thus convection should not protrude into the underlying He layer until  $T_{\text{eff}} \leq 6500\text{K}$ . A seemingly more credible explanation is that there is some shortcoming in the treatment of the pressure dissolution of the excited energy levels of HI. The degree to which these are dissolved in model calculations affects the predicted strength of the high order Balmer lines, which are the primary diagnostic of surface gravity. At  $T_{\text{eff}} > 12500\text{K}$  the perturbation of these energy levels is dominated by interactions with charged ( $e^{-}$ ,  $H^{+}$ ) particles. The good agreement between spectroscopic and gravitational redshift (GR) mass determinations for objects with  $T_{\text{eff}} \gtrsim 12500\text{K}$  (e.g. Bergeron et al. 1995) indicates that the model physics is robust in this  $T_{\text{eff}}$  regime. However, at lower  $T_{\text{eff}}$ , where the quality of the small number of existing GR mass determinations is poor, perturbations by neutral particles become increasingly dominant. These are treated in terms of a simplistic hard sphere model where an HI energy level is assumed to be dissolved if its characteristic interaction radius, which is a fraction,  $f$ , of its hydrogenic radius, is greater than the mean interatomic distance in the gas. Unfortunately,  $f$  is largely unconstrained by theory.

**Proposed observations:** We have recently performed a survey for wide (ie. spatially resolved) double degenerate binaries ( $T_{\text{eff}} > 8000\text{K}$ ), using photometry from the vast SDSS DR6, proper motions and (very) limited spectroscopy. We have identified 25 candidates, recovering two previously known examples of such systems (PG0922+162, HS2240+1234). We wish to obtain follow-up data for the components of a subsample of these with the WHT and ISIS to 1) confirm that those objects lacking spectroscopy (ie. 14/18 WDs) are indeed WDs, 2) where none yet exist place stringent constraints on (spectroscopic)  $T_{\text{eff}}$  and surface gravities using high S/N low resolution blue arm data and 3) using moderate S/N high resolution red arm data measure the shift of the H- $\alpha$  line core of all objects to  $\sim 4\text{kms}^{-1}$ . For the targets we are concentrating on here the SDSS photometry indicates that one component has  $T_{\text{eff}} > 12500\text{K}$ , while the other has  $T_{\text{eff}} < 12500\text{K}$ . We will determine the mass of the hotter WD in each pair by comparing the  $T_{\text{eff}}$  and surface gravity estimate to evolutionary models and then deconvolve the GR and line of sight velocity components of the H- $\alpha$  line shift. Note that the necessary high resolution data currently exists for only one WD in this subsample (SDSS0332-00A). With the system line of sight velocity in hand we will determine the GR component of the H- $\alpha$  line core shift in the spectrum of the cooler member of each binary. From this we will estimate the “true” mass of the second degenerate which can be used to constrain the physics of cool WD model atmospheres.

While the common proper motion of the components of our systems argue that they are physically associated, the combination of velocity constraints from the high resolution red arm data and the SDSS photometry can put this assertion beyond reasonable doubt (or otherwise). Our confirmed double degenerate systems will also be useful for placing constraints on the form of the initial mass-final mass relation, in particular at lower progenitor masses ( $M_{\text{init}} \lesssim 2M_{\odot}$ ) than cannot be accessed through the study of open cluster WDs (e.g. Dobbie et al. 2006). Thus these systems can potentially provide clues to the fate of stars with masses similar to the Sun.

To undertake the proposed work we require high S/N, low resolution blue and moderate S/N red optical spectroscopy of the 18 WDs of our candidate wide double degenerate systems (which all have separations of  $<30''$ ). We propose to use the ISIS spectrograph with EEV12 and REDPLUS CCDs, the “new” dichroic, the R300B and R1200R gratings and a 1.0” wide slit suitably orientated to cover both components of each system simultaneously and provide coverage over the range 3600-5500Å at  $\lambda/\delta\lambda \sim 1000$  and 6240-6875Å at  $\lambda/\delta\lambda \sim 7500$ . The blue arm observations will give us access to the Balmer series members ranging from H- $\beta$ – H-8, coverage of which are necessary to determine robustly effective temperature and **spectroscopic** surface gravity in the temperature range ( $\sim 8000$ -30000K) occupied by our candidate white dwarfs (e.g. Bergeron et al. 1992). Our extensive previous experience of fitting synthetic profiles to the observed hydrogen Balmer lines of DAs indicates that a  $S/N \gtrsim 50$  at the above resolution allows rather tight constraints to be placed on the effective temperature, the surface gravity ( $\pm$  few 100K and a few 0.01 dex respectively) and with reference to state-of-the-art evolutionary models the **spectroscopic** mass ( $\Delta M \lesssim 0.05M_{\odot}$ ) and the cooling time ( $\Delta\tau < 50$  Myrs) of a WD (e.g. see Dobbie et al. 2006). Moreover, using the masses and the radii derived from the evolutionary models, the GR of the hot WDs ( $T_{\text{eff}} > 12500$ K) can be constrained to  $\sim 2\text{kms}^{-1}$ . The red arm observations will give us access to the H- $\alpha$  line, from which we will determine the line shift due to the combination of line of sight velocity and GR. The H- $\alpha$  line profile formed in the atmospheres of DA WDs features a relatively sharp core (see Figure 2). Based on our previous experience with high resolution data covering this part of the spectral energy distribution of WDs (with UVES data at  $\lambda/\delta\lambda \sim 20000$  and a  $S/N \sim 17$  per resolution element it is possible to constrain the line shift to  $\sim 2\text{kms}^{-1}$  by fitting a synthetic profile to the observed line), we estimate that with  $S/N \gtrsim 25$  per resolution element at  $\lambda/\delta\lambda \sim 7500$  we can constrain the line shift to  $\sim 4\text{kms}^{-1}$  and pin down the system line of sight velocity to  $\sim 4.5\text{kms}^{-1}$ . Thus we can determine the “true” mass of the cooler component in each binary to  $\sim 10\%$ . We note that the shift in the peak of the WD mass distribution is  $\sim 0.2M_{\odot}$  at  $T_{\text{eff}} = 10000$ K, which may indicate that the currently adopted value of  $f$  is underestimated by  $\sim 60\%$ . This work offers the chance to constrain  $f$  to  $\sim 15\%$ .

The magnitudes given in Section 15 correspond to the fainter WD of each pair. We have used the SIGNAL exposure time calculator to determine that a 5400s observation will provide  $S/N \approx 25$  per resolution element on a  $r' = 17.8$  (SDSS AB magnitude!) object at H- $\alpha$  in 1.0” seeing and grey moon conditions (1.0” slit, sec z=1.2). This integration time provides ample S/N ( $>50$ ) in the blue arm for our purposes. We find a  $S/N \sim 25$  per resolution element can be achieved at H- $\alpha$  on our faintest 2 candidates ( $r' \approx 18.9$ ) in grey conditions in an exposure time of 14400s. Note that useful S/N cannot be achieved on these fainter candidates during bright time in reasonable integration times. We intend splitting each observation up into a series of shorter exposures to allow the removal of CR hits from the data. Allowing for overheads such as target and guide star acquisition (300s), the readout time of the CCD ( $\sim 30$ s), a number of observations of the arc lamp and a standard star (600s every other target; e.g. sdOC star PG0823+546) we determine that we will need 24 hours in total.

Our targets span a wide range of RAs and are not all observable on a given night. However, 5/9 objects are visible in February (10 hours of darkness) and 5/9 (including the three faintest objects) are visible in July (7.5 hours of darkness). Therefore, we request one grey night in February and two grey nights in July to complete this program.

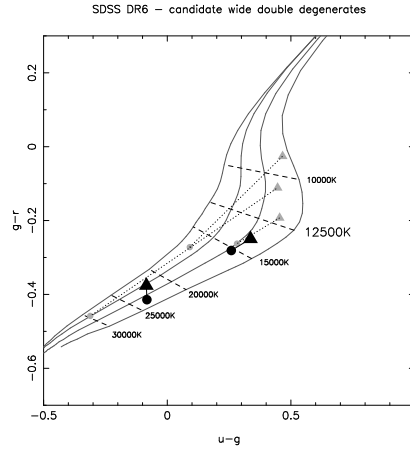


Figure 1. A selection of our candidate wide double degenerate binaries in ugr colour-colour space, with the DA models of Pierre Bergeron overplotted (top to bottom,  $1.2M_{\odot}$ ,  $0.9M_{\odot}$ ,  $0.6M_{\odot}$  and  $0.3M_{\odot}$ ). Two previously known wide double degenerate systems are shown in bold.

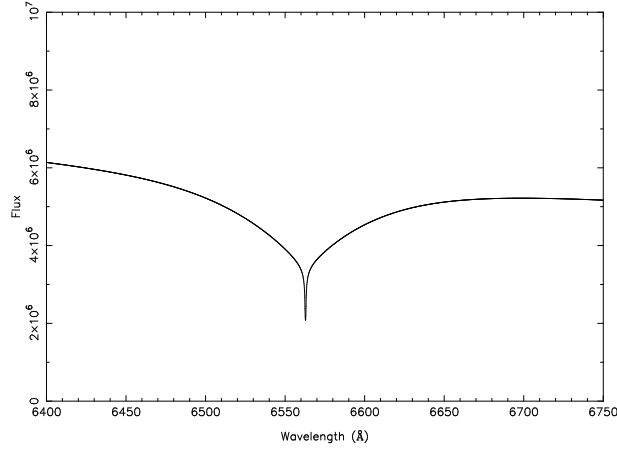


Figure 2. Synthetic white dwarf spectrum ( $T_{\text{eff}}=15000\text{K}$ ,  $\log g = 8.0$ ) showing the H- $\alpha$  line with the pronounced non-LTE core.

### References

- Bergeron, P. et al. 1991, ApJ, 367, 252
- Bergeron, P., et al. 1992, ApJ, 394, 228
- Bergeron, P., et al. 1995, ApJ, 444, 810
- Bradley, P.A., 2006, MmSAI, 77, 437
- Dobbie, P. et al. 2006, MNRAS, 369, 383
- Kepler, S., et al., 2007, MNRAS, 375, 1315
- Liebert, J. et al. 2005, ApJ, 156, 47
- Marsh, M. et al. 1997, MNRAS, 286, 369
- Moehler, S., et al., 2004, A&A, 420, 515
- Willson, L-A., 2000, ARA&A, 38, 573

*If instrumentation or setup differs from main programme, give full details*

20 RELATED PATT APPLICATIONS OVER THE LAST FOUR SEMESTERS *(including unsuccessful applications)*

PATT reference:	Award:	Clear nights:	Comments:
W/2006A/1	3G	3	2 published papers

21 PUBLICATIONS BASED ON PATT TIME PUBLISHED DURING THE LAST FOUR SEMESTERS *(maximum 6)*

Dobbie et al., 2006, MNRAS, 369, 383

22 EXPERIENCE OF INTENDED OBSERVERS WHO HAVE NOT PREVIOUSLY USED THIS TELESCOPE

all are experienced

23 COMPLETE IF THE OBSERVATIONS ARE PRIMARILY FOR A STUDENT RESEARCH TRAINING PROGRAMME

Name of student: \_\_\_\_\_  
Project title: \_\_\_\_\_

24 COMPLETE IF THE OBSERVATIONS ARE ASSOCIATED WITH A CURRENT PPARC/SERC RESEARCH GRANT

Name of principal investigator: \_\_\_\_\_  
Grant title: \_\_\_\_\_  
Grant number: \_\_\_\_\_

25 NON-STANDARD TRAVEL AND SUBSISTENCE REQUIREMENTS *(UK observers only)*

Justify requests for travel and subsistence for more than one person:

Details of any other expenditure (eg freight, remote observing):

### **A.7.6 Gemini Observing Proposals**

#### **Gemini North 2009B Proposal**

# GEMINI OBSERVATORY

## *observing time request summary*

**Semester:** 2009B

**Observing Mode:** queue

**Instruments:**  
GMOS North

**Gemini Reference:**

**Time Awarded:**

**Thesis:**  
no

---

**Title:** Probing the stellar initial mass-final mass relation with wide double-degenerate binaries - the northern systems  
**Principal Investigator:** Paul Dobbie  
**PI institution:** Anglo-Australian Observatory, P.O. Box 296 (167 Vimiera Road), Epping, NSW 2121, Australia  
**PI status:** PhD/Doctorate  
**PI phone/fax/e-mail:** +61 293724846 / +61 293724880 / pdd@aao.gov.au  
**Co-Investigators:** Quentin Parker: Anglo-Australian Observatory, qap@aao.gov.au  
Richard Baxter: Macquarie University, richardbrucebaxter@gmail.com

---

### **Partner Submission Details** (*multiple entries for joint proposals*)

Partner	Partner Lead Scientist	Time Requested	Minimum Time Requested	Reference Number	NTAC		
					Reco-mmended Time	Minimum Time Reco-mmended	Rank
Australia	Dobbie	17.8 hours	8.5 hours		0.0	0.0	
	<i>Total Time</i>	<i>17.8 hours</i>					

### **Abstract** (*118 words*)

*We propose to obtain high S/N low-resolution GMOS spectroscopy of several wide double-degenerate binary systems which will allow us to test and extend our understanding of the fundamentally important stellar initial mass-final mass relation (IFMR). Several parts of this relation remain poorly delineated e.g. at initial masses  $M_{\text{init}} < 2.5\text{-}3.0 M_{\text{solar}}$  and  $M_{\text{init}} > 5\text{-}6 M_{\text{solar}}$ . Our new data will be used 1) to place tight limits on the effective temperatures and surface gravities of the binary components 2) in conjunction with WD evolutionary models to determine their masses and cooling times. Subsequently, we will exploit existing knowledge of the IFMR to estimate the progenitor masses, leading to the provision of extremely valuable additional data points on the IFMR in these initial mass regimes.*

**Science Justification** (996 words)

We propose GMOS spectroscopy of several wide double-degenerate binaries that will allow us to test and extend understanding of the fundamentally important stellar initial mass-final mass relation (IFMR). This is a theoretically predicted positive correlation between the masses of single low/intermediate mass stars ( $M < 10 M_{\text{solar}}$ ) and the remnants left after they have expired. A comprehensive knowledge of its form is important to several areas of astrophysics: it is a key ingredient of galaxy chemical evolution models as it provides an estimate of the amount of gas, enriched with C, N and other metals, these stars return to the ISM; it is crucial to deciphering information locked up in the white dwarf (WD) luminosity functions of stellar populations (Oswalt et al. 1996); the relations upper end can be used to probe directly the maximum mass of a star that will evolve through the planetary nebula phase and thus indirectly the minimum mass of a star that will expire via a Type II SNe (Williams et al. 2009).

The finer details of the IFMR cannot be determined from first principles as the late stages in the lifecycle of a star, while brief, remain extremely challenging to model (e.g. Marigo & Girardi 2007). Observations play a key role in advancing our understanding of the relations form. Most existing empirical data has been obtained via study of open cluster WDs (Weidemann 2000). Here progenitor lifetimes can be determined from the difference between the age of the cluster and the cooling times of WD members. Subsequently, initial masses ( $M_{\text{init}}$ ) can be estimated by referring to stellar evolutionary models. Greater access to mosaic imagers and 8/10m telescopes with blue sensitive spectrographs has led to substantial recent progress in mapping the IFMR (Kalirai et al. 2007). Our latest work (Dobbie et al. 2009), where we compiled data for ~50 open cluster WDs, indicates that the bulk of stars follow closely a monotonic relation. It has also shown that the IFMR is somewhat steeper in the range  $3 M_{\text{solar}} < M_{\text{init}} < 4 M_{\text{solar}}$  than elsewhere (Figure 1). This is consistent with theoretical expectations and the sharp drop seen in the number density of objects on the high mass side of the main peak in the field WD mass distribution (Ferrario et al. 2005).

Despite this headway, the IFMR remains sparsely sampled in several important initial mass regimes. For example, there are only two data points at  $M_{\text{init}} \sim 5\text{--}6 M_{\text{solar}}$ . Thus, the form of the upper IFMR remains substantially uncertain (Figure 1). Furthermore, there are very few objects at  $M_{\text{init}} < 2.5\text{--}3 M_{\text{solar}}$  yet it is crucial to have a good understanding of the fate of the numerous stars with masses more closely resembling that of our Sun. In the open cluster approach, mapping the higher initial mass regime of the IFMR requires targeting young ( $\sim 100\text{--}300 \text{ Myrs}$ ) populations sufficiently rich to have harboured a substantial number of stars with  $M_{\text{init}} \sim 5\text{--}6 M_{\text{solar}}$  and where the progeny of these stars are still relatively young, hot and luminous. Investigation of the lower initial mass regime requires targeting old ( $> 1\text{--}2 \text{ Gyrs}$ ) open clusters, populations sufficiently mature that stars with  $M_{\text{init}} < 2.5\text{--}3 M_{\text{solar}}$  have evolved beyond the main sequence. Such clusters are comparatively rare so it is necessary to probe large volumes to identify good examples. Consequently, while high S/N optical spectroscopy is critical to determining WD masses and cooling times, the great distances involved make it extremely challenging to obtain the necessary data even with today's large telescopes.

We focus here on a novel independent approach to probing the IFMR, involving the exploitation of wide (spatially resolved) double-degenerate field binaries in which the WDs have substantially different masses ( $\Delta M \sim 0.1 M_{\text{solar}}$ ). The components of these co-eval systems have essentially evolved as single stars since they have remained sufficiently well separated that neither object has ever overflowed its Roche Lobe and initiated mass transfer onto the other. If one of the WDs in such a system has a mass ( $M_{\text{final}}$ ) which places it on the part of the IFMR which is reasonably well delineated by existing data ( $M_{\text{final}} \sim 0.65\text{--}1.0 M_{\text{solar}}$ ; Figure 1) then it is possible to estimate the initial mass (and lifetime) of this component and thus the total age of the binary. The progenitor mass of the other component then follows as for a WD cluster member and can be used to probe a different initial mass regime.

We have used SDSS DR7 photometry and SuperCOSMOS proper motions to identify ~70 likely wide double-degenerate binaries containing components with effective temperatures,  $T_{\text{eff}} > \sim 10000 \text{ K}$

(where atmospheres can be reliably modelled). The magnitudes and colours of all systems have been scrutinised to identify those where there appears to be a significant difference in the masses of the components (ie.  $\Delta M > \sim 0.1 M_{\odot}$ ). For example, the components of one system both have  $u-g = -0.08$ , indicating similar effective temperature. However, one WD is 1.0 magnitudes fainter than the other suggesting a smaller radius ( $\sim 65\%$ ) which translates to a larger mass ( $\sim 0.3 M_{\odot}$ ). As the finite age of the Galaxy dictates that single star evolution cannot yet have produced WDs with  $M_{\text{fin}} < 0.5-0.55 M_{\odot}$ , it is highly probable that the mass of at least one component of each system in this subset lies in the range  $M_{\text{fin}} = 0.65-1.0 M_{\odot}$ . Here we propose to obtain high S/N, low resolution spectroscopy spanning 3800-5200 angstroms for the components of the 5 systems visible this semester from Gemini-North. With this data we will measure the effective temperature and the surface gravity for each WD by comparing the observed profiles of H-beta-H-8 lines to the predictions of state-of-the-art model atmospheres. Our extensive experience of the line fitting process indicates that  $S/N > \sim 50$  per 3-4 angstroms binned pixel across this wavelength range will keep the formal uncertainties to  $\sim 200\text{K}$  and  $\sim 0.02\text{dex}$  in effective temperature and surface gravity respectively (the limited existing SDSS spectroscopy of some objects is not of sufficient quality). Subsequently we will estimate the masses and the cooling times of the components by referring to the WD evolutionary tracks of Fontaine et al. (2001). The tight limits on effective temperature and surface gravity will allow the mass and cooling time of each WD to be determined to  $\sim 0.02 M_{\odot}$  and  $\sim 8\%$  respectively.

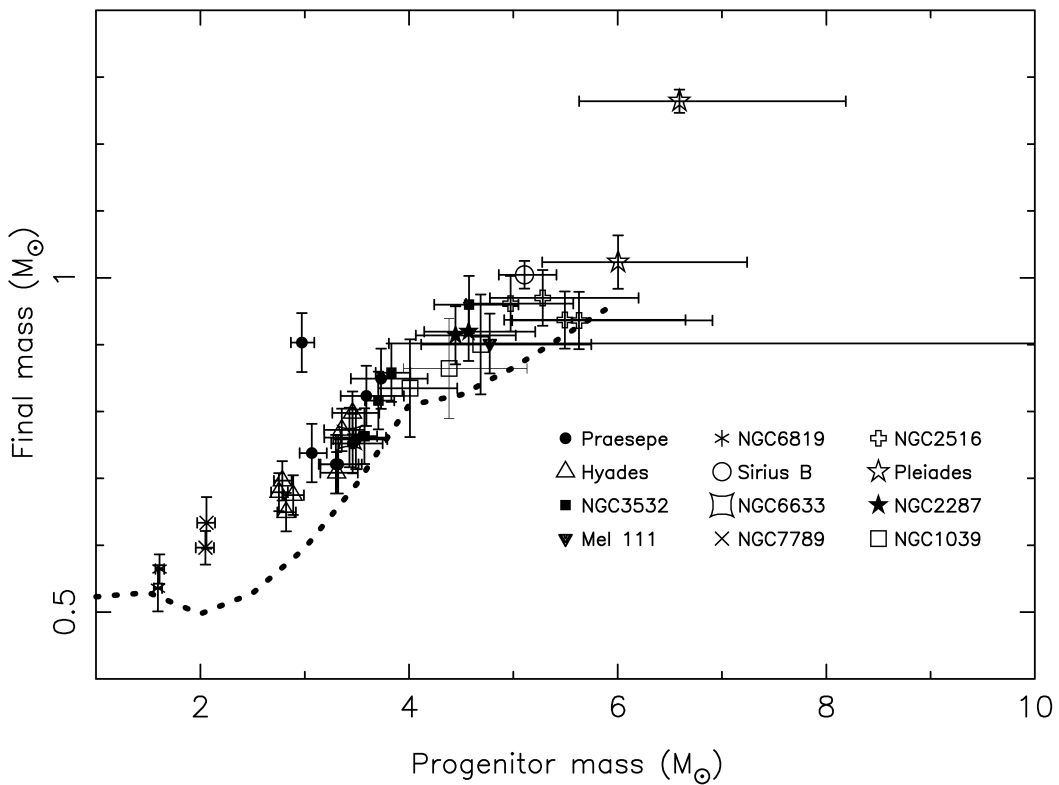


Figure 1: The IFMR for a compilation of WD members of open clusters (excepting the heavily studied Sirius B). The bulk of stars delineate a relatively tight trend which reflects the form of the core mass at the time of the first thermal pulse via initial mass relation (dotted line; Girardi et al. 2000), particularly at  $M_{\text{init}} > \sim 3 M_{\odot}$ .



**Technical Justification** (380 words)

As discussed in the Scientific Justification we require  $S/N > \sim 50$  per 3-4 angstrom binned pixel across the range 3800-5200 angstroms. We intend to observe our targets using the following settings: B600\_G5307 grating, 4x4 detector binning and a 1" or 1.5" slit, depending on the separation of the binary system. We have used the GMOS-N exposure time calculator (V4.0) to derive the following exposure times for the components of our wide double-degenerate binary systems, required to obtain  $S/N \sim 50$  at H-8 to H-9: 60mins for DD-03A (airmass  $< 1.5$ , 1" slit, IQ=70%, CC=70%, WV=Any and SB=Any), 60mins for DD-03B (airmass  $< 1.5$ , 1" slit, IQ=70%, CC=70%, WV=Any and SB=80%), 60mins for DD-04A (airmass  $< 1.5$ , 1" slit, IQ=70%, CC=90%, WV=Any and SB=80%), 60mins for DD-04B (airmass  $< 1.5$ , 1" slit, IQ=70%, CC=70%, WV=Any and SB=80%), 120mins for DD-05A (airmass  $< 1.5$ , 1" slit, IQ=70%, CC=70%, WV=Any and SB=80%), 120mins for DD-05B (airmass  $< 1.5$ , 1" slit, IQ=70%, CC=70%, WV=Any and SB=80%), 125mins for DD-06A (airmass  $< 1.5$ , 1.5" slit, IQ=85%, CC=70%, WV=Any and SB=50%), 125mins for DD-06B (airmass  $< 1.5$ , 1.5" slit, IQ=85%, CC=70%, WV=Any and SB=50%), 38mins for DD-08A (airmass  $< 1.5$ , 1" slit, IQ=70%, CC=90%, WV=Any and SB=80%) and 60mins for DD-08B (airmass  $< 1.5$ , 1" slit, IQ=70%, CC=90%, WV=Any and SB=80%). These  $S/N$  estimates allow for a factor 2 binning in the dispersion direction at the reduction stage. To ensure successful cosmic ray rejection from our data the observation of each star will be split into three sub-integrations. While arc observations from the standard calibration plan are adequate for wavelength calibration, we request the additional observation of a DC (spectrally featureless) white dwarf (WD1918+38; 3x10mins) so that we can reliably remove instrumental signature from our data (this is essential for detailed line profile modeling). Allowing for overheads ( $\sim 18$  mins of telescope and instrument set-up per target and 24 seconds per CCD readout), we estimate that our total time request is 17.8 hours.

## References

Dobbie, P.D., et al. 2009, MNRAS, accepted Ferrario, L., et al., 2005, MNRAS, 361, 1131 Fontaine, G., et al. 2001, PASP, 113, 409 Girardi, L., et al. 2000, A&AS, 141, 371 Kalirai, J., et al., 2007, ApJ, 671, 748 Marigo, P., & Girardi, L., 2007, A&A, 469, 239 Oswalt, T., et al., 1996, Nature, 382, 692 Weidemann, V., 2000, A&A, 363, 647 Williams et al. 2009, ApJ, 693, 355

## Band 3 Information

**Requested time in case of band 3 allocation:** 17.8 hours

**Minimum required time for a usable band 3 allocation:** 8.4 hours

**Use the following conditions for band 3 only:**

Name	Image Quality	Sky Background	Water Vapor	Cloud Cover
Band 3 Observing Conditions	70 %	80 %	Any	70 %

### Band 3 Consideration Comments (95 words)

All our northern targets can be observed in mediocre sky conditions and thus our program can be considered for Band 3. The components of some of our target systems are separated by only ~4-5 arcseconds so it will be necessary to observe these in IQ=70% conditions to minimise the contamination of the spectrum of an object with the light of its companion. In CC=70% our faintest targets, DD-06A and 06B, require a dark sky but are sufficiently well separated that we can open up the slit to 1.5" and observe them in poorer seeing (IQ=85%).

## Observation Details

Observation	RA	Dec	Brightness	Total Time (including overheads)
DD-03A	08:49:52.87	47:12:49.47	V=17.2	79.0 minutes
47636499(oiwfs)	8:49:29.964	47:13:43.77	12.94 UCmag,12.104 Jmag,11.763 Kmag	separation 3.99
Observing conditions: DD-03A		resources: GMOS North		
DD-03B	08:49:52.48	47:12:47.77	V=18.2	79.0 minutes
47636499(oiwfs)	8:49:29.964	47:13:43.77	12.94 UCmag,12.104 Jmag,11.763 Kmag	separation 3.94
Observing conditions: DD-03B		resources: GMOS North		
DD-04A	09:25:13.48	16:01:44.15	V=16.5	79.0 minutes
37361750(oiwfs)	9:25:03.002	15:58:19.7	14.02 UCmag,13.064 Jmag,12.710 Kmag	separation 4.24
Observing conditions: DD-04A		resources: GMOS North		
DD-04B	09:25:13.18	16:01:45.41	V=17.6	79.0 minutes
37361750(oiwfs)	9:25:03.002	15:58:19.7	14.02 UCmag,13.064 Jmag,12.710 Kmag	separation 4.21
Observing conditions: DD-04B		resources: GMOS North		
DD-05A	09:26:46.88	13:21:34.52	V=18.8	139.0 minutes
36470185(oiwfs)	9:26:45.256	13:22:18.9	9.63 UCmag,8.548 Jmag,8.243 Kmag	separation 0.84
Observing conditions: DD-05A		resources: GMOS North		
DD-05B	09:26:47.0	13:21:38.49	V=18.9	139.0 minutes
36470185(oiwfs)	9:26:45.256	13:22:18.9	9.63 UCmag,8.548 Jmag,8.243 Kmag	separation 0.8
Observing conditions: DD-05B		resources: GMOS North		
DD-06A	10:02:44.88	36:06:29.68	V=19.3	144.0 minutes
44485534(oiwfs)	10:02:24.839	36:04:25.8	10.33 UCmag,9.403 Jmag,9.014 Kmag	separation 4.54

Observing conditions: DD-06A		resources: GMOS North		
DD-06B	10:02:45.86	36:06:53.39	V=19.5	144.0 minutes
44485535(oiwfs)	10:02:25.621	36:05:29.61	12.83 UCmag,11.594 Jmag,11.117 Kmag	separation 4.32
Observing conditions: DD-06B		resources: GMOS North		
DD-08A	22:23:1.62	22:01:31.36	V=16.0	57.0 minutes
39594658(oiwfs)	22:23:16.834	21:59:00.96	9.04 UCmag,6.765 Jmag,5.821 Kmag	separation 4.33
Observing conditions: DD-08A		resources: GMOS North		
DD-08B	22:23:1.72	22:01:24.95	V=16.5	79.0 minutes
39594658(oiwfs)	22:23:16.834	21:59:00.96	9.04 UCmag,6.765 Jmag,5.821 Kmag	separation 4.25
Observing conditions: DD-08B		resources: GMOS North		
WD1918+38	19:18:58.0	38:43:35.0	B=15.1	49.0 minutes
50101419(oiwfs)	7:30:57.192	48:08:36.83		separation 7,732.59
Observing conditions: DC STANDARD		resources: GMOS North		

## Observing Conditions

Name	Image Quality	Sky Background	Water Vapor	Cloud Cover
Band 3 Observing Conditions	70 %	80 %	Any	70 %
DD-03A	70 %	Any	Any	70 %
DC STANDARD	Any	Any	Any	70 %
DD-03B	70 %	80 %	Any	70 %
DD-04A	70 %	80 %	Any	90 %
DD-04B	70 %	80 %	Any	70 %
DD-05A	70 %	80 %	Any	70 %
DD-05B	70 %	80 %	Any	70 %
DD-06A	85 %	50 %	Any	70 %
DD-06B	85 %	50 %	Any	70 %
DD-08A	70 %	80 %	Any	90 %
DD-08B	70 %	80 %	Any	90 %
Global Default	70 %	50 %	Any	50 %

## Resources

- Gemini North
  - GMOS North
    - Focal Plane Unit
      - Longslit 1.00 arcsec
    - Disperser
      - B600\_G5307
  - GMOS North
    - Focal Plane Unit
      - Longslit 1.00 arcsec
    - Disperser
      - B600\_G5307
  - GMOS North
    - Focal Plane Unit
      - Longslit 1.50 arcsec
    - Disperser



## Scheduling Information

### Scheduling constraints and non-usable dates

- (impossible):
- (optimal):
- (synchronous):

## Additional Information

**Keyword Category:** galactic  
**Keywords:** Binaries  
Evolution  
White dwarfs

### Allocations:

Reference	Time	% Useful	Status of previous data
GN-2007B-Q-88	2.0 hours	100%	Published: MNRAS, 2009 accepted, "Two distant brown dwarfs in the UKIRT Infrared Deep Sky Survey Deep Extragalactic Survey Data Release 2"
GN-2008B-Q-90	1.6 hours	100%	Published: MNRAS, 2009 accepted, "Two distant brown dwarfs in the UKIRT Infrared Deep Sky Survey Deep Extragalactic Survey Data Release 2"

### Publications:

- Casewell, S., Dobbie, P., et al. 2009 MNRAS, accepted, "High resolution optical spectroscopy of Praesepe white dwarfs"
- Dobbie P., et al., 2009 MNRAS, accepted, "A new detailed examination of white dwarfs in NGC3532 and NGC2287"
- Dobbie, P., et al. 2009 MNRAS, accepted, "A massive white dwarf in the Coma Berenices open cluster"

## Gemini South 2010B Proposal

# GEMINI OBSERVATORY

## *observing time request summary*

**Semester:** 2010A

**Observing Mode:** queue

**Instruments:**  
GMOS South

**Gemini Reference:**

**Time Awarded:**

**Thesis:**  
no

---

**Title:** Probing the stellar initial mass-final mass relation with wide double-degenerate binaries - the southern A semester systems  
**Principal Investigator:** Paul Dobbie  
**PI institution:** Anglo-Australian Observatory, P.O. Box 296 (167 Vimiera Road), Epping, NSW 2121, Australia  
**PI status:** PhD/Doctorate  
**PI phone/fax/e-mail:** +61 293724846 / +61 293724880 / pdd@aao.gov.au  
**Co-Investigators:** Quentin Parker: Anglo-Australian Observatory, qap@aao.gov.au  
Richard Baxter: Macquarie University, richardbrucebaxter@gmail.com

---

### **Partner Submission Details** (*multiple entries for joint proposals*)

Partner	Partner Lead Scientist	Time Requested	Minimum Time Requested	Reference Number	NTAC		
					Reco-mmended Time	Minimum Time Reco-mmended	Rank
Australia	Dobbie	6.5 hours	3.2 hours		0.0	0.0	
	<i>Total Time</i>	<i>6.5 hours</i>					

### **Abstract** (*118 words*)

We propose to obtain high S/N low-resolution GMOS spectroscopy of two wide double-degenerate binary systems which will allow us to test and extend our understanding of the fundamentally important stellar initial mass-final mass relation (IFMR). Several parts of this relation remain poorly delineated e.g. at initial masses  $M_{\text{init}} < 2.5\text{-}3.0 M_{\text{solar}}$  and  $M_{\text{init}} > 5\text{-}6 M_{\text{solar}}$ . Our new data will be used 1) to place tight limits on the effective temperatures and surface gravities of the binary components 2) in conjunction with WD evolutionary models to determine their masses and cooling times. Subsequently, we will exploit existing knowledge of the IFMR to estimate the progenitor masses, leading to the provision of extremely valuable additional data points on the IFMR in these initial mass regimes.

**Science Justification** (923 words)

We propose GMOS spectroscopy of several wide double-degenerate binaries that will allow us to test and extend understanding of the fundamentally important stellar initial mass-final mass relation (IFMR). This is a theoretically predicted positive correlation between the masses of single low/intermediate mass stars ( $M < 10 M_{\text{solar}}$ ) and the remnants left after they have expired. A comprehensive knowledge of its form is important to several areas of astrophysics: it is a key ingredient of galaxy chemical evolution models as it provides an estimate of the amount of gas, enriched with C, N and other metals, these stars return to the ISM; it is crucial to deciphering information locked up in the white dwarf (WD) luminosity functions of stellar populations (Oswalt et al. 1996); the relations upper end can be used to probe directly the maximum mass of a star that will evolve through the planetary nebula phase and thus indirectly the minimum mass of a star that will expire via a Type II SNe (Williams et al. 2009).

The finer details of the IFMR cannot be determined from first principles as the late stages in the lifecycle of a star, while brief, remain extremely challenging to model (e.g. Marigo & Girardi 2007). Observations play a key role in advancing our understanding of the relations form. Most existing empirical data has been obtained via study of open cluster WDs (Weidemann 2000). Here progenitor lifetimes can be determined from the difference between the age of the cluster and the cooling times of WD members. Subsequently, initial masses ( $M_{\text{init}}$ ) can be estimated by referring to stellar evolutionary models. Greater access to mosaic imagers and 8/10m telescopes with blue sensitive spectrographs has led to substantial recent progress in mapping the IFMR (Kalirai et al. 2007). Our latest work (Dobbie et al. 2009), where we compiled data for  $\sim 50$  open cluster WDs, indicates that the bulk of stars follow closely a monotonic relation. It has also shown that the IFMR is somewhat steeper in the range  $3 M_{\text{solar}} < M_{\text{init}} < 4 M_{\text{solar}}$  than elsewhere (Figure 1). This is consistent with theoretical expectations and the sharp drop seen in the number density of objects on the high mass side of the main peak in the field WD mass distribution (Ferrario et al. 2005).

Despite this headway, the IFMR remains sparsely sampled in several important initial mass regimes. For example, there are only two data points at  $M_{\text{init}} \sim 5\text{--}6 M_{\text{solar}}$ . Thus, the form of the upper IFMR remains substantially uncertain (Figure 1). Furthermore, there are very few objects at  $M_{\text{init}} < 2.5\text{--}3 M_{\text{solar}}$  yet it is crucial to have a good understanding of the fate of the numerous stars with masses more closely resembling that of our Sun. In the open cluster approach, mapping the higher initial mass regime of the IFMR requires targeting young ( $\sim 100\text{--}300 \text{ Myrs}$ ) populations sufficiently rich to have harboured a substantial number of stars with  $M_{\text{init}} \sim 5\text{--}6 M_{\text{solar}}$  and where the progeny of these stars are still relatively young, hot and luminous. Investigation of the lower initial mass regime requires targeting old ( $> 1\text{--}2 \text{ Gyrs}$ ) open clusters, populations sufficiently mature that stars with  $M_{\text{init}} < 2.5\text{--}3 M_{\text{solar}}$  have evolved beyond the main sequence. Such clusters are comparatively rare so it is necessary to probe large volumes to identify good examples. Consequently, while high S/N optical spectroscopy is critical to determining WD masses and cooling times, the great distances involved make it extremely challenging to obtain the necessary data even with today's large telescopes.

We focus here on a novel independent approach to probing the IFMR, involving the exploitation of wide (spatially resolved) double-degenerate field binaries in which the WDs have substantially different masses ( $\Delta M \sim 0.1 M_{\text{solar}}$ ). The components of these co-eval systems have essentially evolved as single stars since they have remained sufficiently well separated that neither object has ever overflowed its Roche Lobe and initiated mass transfer onto the other. If one of the WDs in such a system has a mass ( $M_{\text{final}}$ ) which places it on the part of the IFMR which is reasonably well delineated by existing data ( $M_{\text{final}} \sim 0.65\text{--}1.0 M_{\text{solar}}$ ; Figure 1) then it is possible to estimate the initial mass (and lifetime) of this component and thus the total age of the binary. The progenitor mass of the other component then follows as for a WD cluster member and can be used to probe a different initial mass regime.

We have used SDSS DR7 photometry and SuperCOSMOS proper motions to identify  $\sim 70$  likely wide double-degenerate binaries containing components with effective temperatures,  $T_{\text{eff}} > \sim 10000 \text{ K}$



(where atmospheres can be reliably modelled). The magnitudes and colours of all systems have been scrutinised to identify those where there appears to be a significant difference in the masses of the components (ie.  $\Delta M > \sim 0.1 M_{\odot}$ ). For example, the components of one system both have  $u-g = -0.08$ , indicating similar effective temperature. However, one WD is 1.0 magnitudes fainter than the other suggesting a smaller radius ( $\sim 65\%$ ) which translates to a larger mass ( $\sim 0.3 M_{\odot}$ ). As the finite age of the Galaxy dictates that single star evolution cannot yet have produced WDs with  $M_{\text{fin}} < 0.5-0.55 M_{\odot}$ , it is highly probable that the mass of at least one component of each system in this subset lies in the range  $M_{\text{fin}} = 0.65-1.0 M_{\odot}$ . Here we propose to obtain high S/N, low resolution spectroscopy spanning 3800-5200 angstroms for the components of the 2 systems visible this semester from Gemini-South.

Note that the two proposed targets are currently in the Gemini South queue but given their band 3 status there is considerable uncertainty as to whether they will be observed in the current semester. If they were to be observed in 09B we would notify the Australian Gemini scientist so that this 10A programme could be modified accordingly.

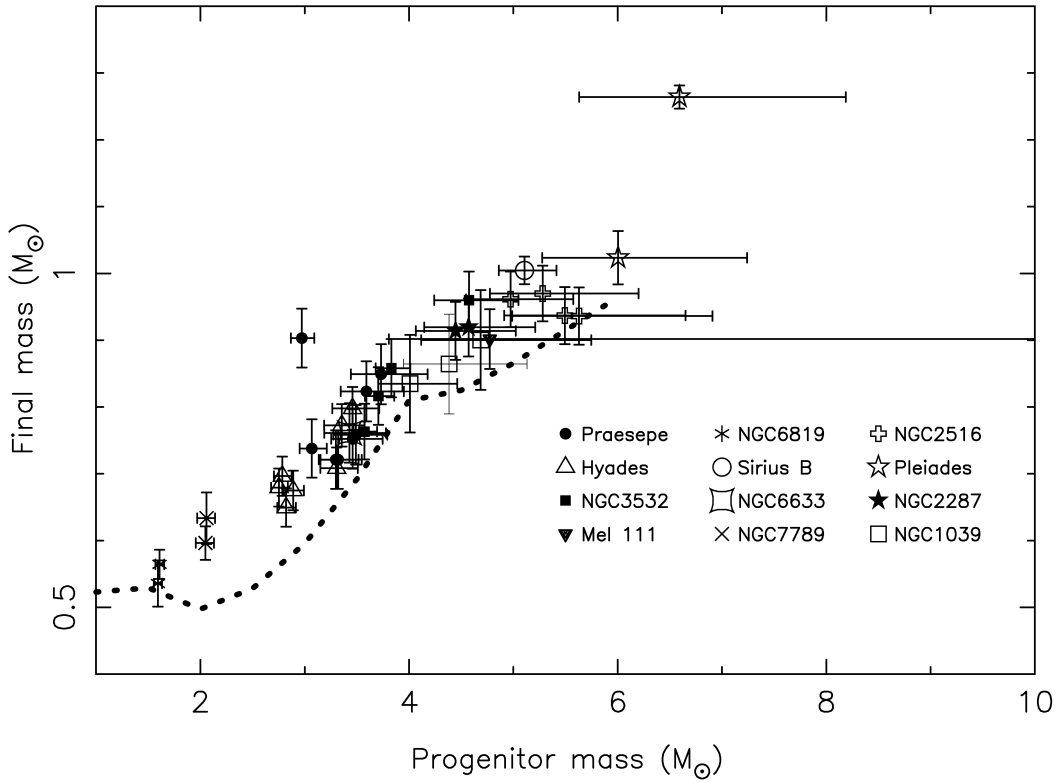


Figure 1: The IFMR for a compilation of WD members of open clusters (excepting the heavily studied Sirius B). The bulk of stars delineate a relatively tight trend which reflects the form of the core mass at the time of the first thermal pulse via initial mass relation (dotted line; Girardi et al. 2000), particularly at  $M_{\text{init}} > \sim 3 M_{\odot}$ .

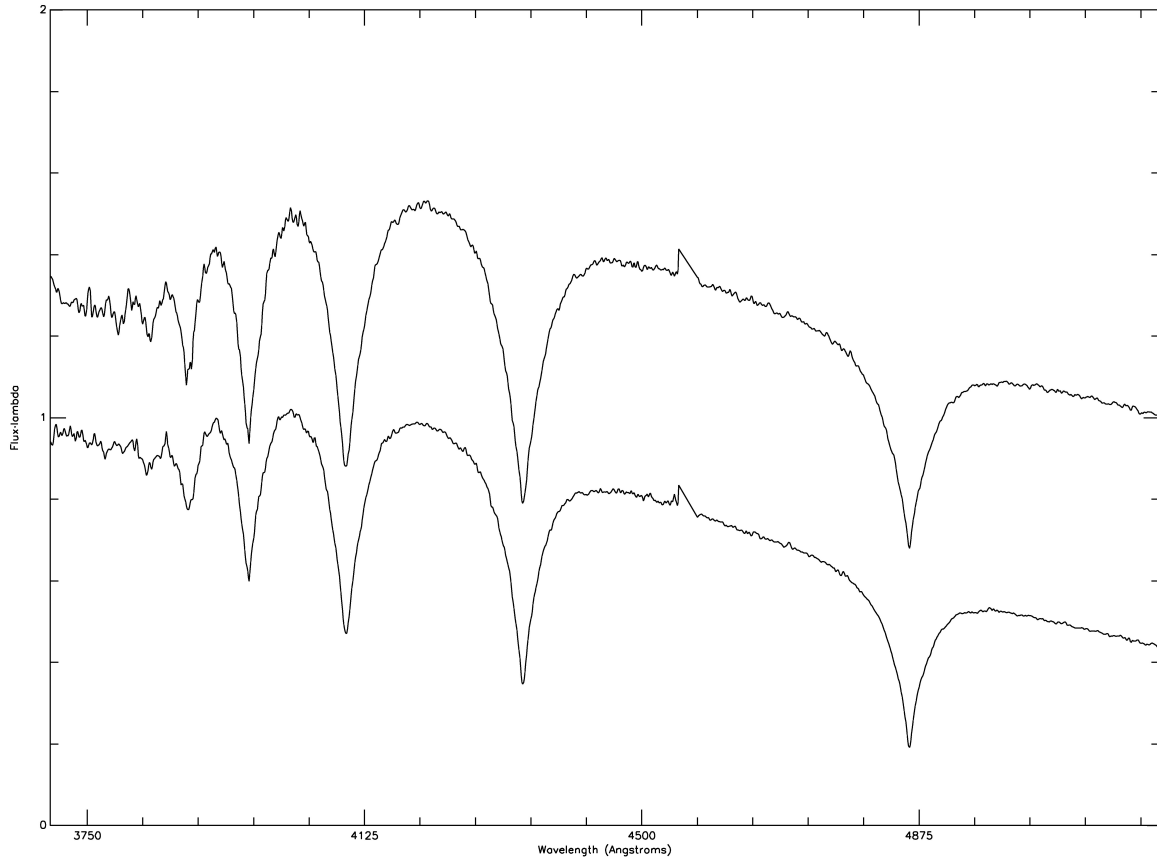


Figure 2: Gemini-N GMOS spectroscopy of DD-20A+B observed in the current semester. Preliminary analysis indicates  $T_{\text{eff}}=19000\text{K}$ ,  $25500\text{K}$  and  $\log g=8.1$  and  $8.0$  for A and B respectively. The system lies at a distance of  $\sim 200\text{pc}$ . As expected, the cooler component is the more massive.

## Technical Justification *(487 words)*

We will measure the effective temperature and the surface gravity for each WD by comparing the observed profiles of H-beta to H-8/9 lines to the predictions of state-of-the-art model atmospheres. Our extensive experience of the line fitting process indicates that  $S/N > \sim 50$  per 3-4 angstroms binned pixel across the wavelength range 3800-5200 angstroms will keep the formal uncertainties to  $\sim 200\text{K}$  and  $\sim 0.02\text{dex}$  in effective temperature and surface gravity respectively (the limited existing SDSS spectroscopy of some objects is not of sufficient quality, particularly at  $\lambda < \sim 4000\text{angstroms}$ ). Subsequently we will estimate the masses and the cooling times of the components by referring to the WD evolutionary tracks of Fontaine et al. (2001). The tight limits on effective temperature and surface gravity will allow the mass and cooling time of each WD to be determined to  $\sim 0.02\text{Msolar}$  and  $\sim 8\%$  respectively. When coupled with existing knowledge about the form of the IFMR this will permit the system age to be measured to  $\sim 25\%$ . As the lifetime of the progenitor star of each WD will be determined to a similar level of accuracy, the progenitor masses can be constrained to  $\sim 10\text{-}15\%$  (since  $M_{\text{progenitor}} \propto \text{lifetime}_{\text{progenitor}}^{-0.4}$ ).

To obtain the necessary data ( $S/N > \sim 50$  per 3-4 angstrom binned pixel ALL THE WAY from 3800-5200 angstroms ie. including  $\sim 3800\text{-}3850\text{angstroms}$ ) we intend to observe our targets using the following settings: B600\_G5323 grating, 4x4 detector binning and a 2.0" slit, aligned along the PA of the system (differential refraction should not be a problem with our wide slit and all systems have separation  $< 30''$ ). Using the GMOS-S exposure time calculator (V4.0) we derive an exposure time of 180mins to reach a  $S/N \sim 50$  at H-8 to H-9 for DD-01A+B:  $V=19,20$  (airmass  $< 1.5$ , 2" slit, IQ=70%, CC=70%, WV=Any and SB=50%). For DD-07A+B ( $V=16.8, 17.5$ ) we derive an exposure time of 120mins (airmass  $< 1.5$ , 1" slit, IQ=85%, CC=90%, WV=Any and SB=80%). These  $S/N$  estimates allow for a factor 2 binning in the dispersion direction at the reduction stage. To ensure successful cosmic ray rejection from our data the observation of each star will be split into three sub-integrations. While arc observations from the standard calibration plan are adequate for wavelength calibration, we request the additional observation of a DC (spectrally featureless) white dwarf (WD0000-345; 3x10mins) so that we can reliably remove instrumental signature from our data (this is essential for detailed line profile modeling). Allowing for overheads ( $\sim 18$  mins of telescope and instrument set-up per target and 24 seconds per CCD readout), we estimate that our total time request is 9.9 hours.

## References

Dobbie, P.D., et al. 2009, MNRAS, accepted Ferrario, L., et al., 2005, MNRAS, 361, 1131 Fontaine, G., et al. 2001, PASP, 113, 409 Girardi, L., et al. 2000, A&AS, 141, 371 Kalirai, J., et al., 2007, ApJ, 671, 748 Marigo, P., & Girardi, L., 2007, A&A, 469, 239 Oswalt, T., et al., 1996, Nature, 382, 692 Weidemann, V., 2000, A&A, 363, 647 Williams et al. 2009, ApJ, 693, 355

## Band 3 Information

**Requested time in case of band 3 allocation:** 3.5 hours

**Minimum required time for a usable band 3 allocation:** 3.5 hours

**Use the following conditions for band 3 only:**

Name	Image Quality	Sky Background	Water Vapor	Cloud Cover
Band 3 Observing Conditions	85 %	80 %	Any	90 %

### Band 3 Consideration Comments (42 words)

One of our targets can be observed in mediocre sky conditions and thus our program could be considered for Band 3. Our faintest target, DD-01A+B could not be observed in poorer conditions. It requires better sky conditions to obtain the necessary S/N.

## Observation Details

Observation	RA	Dec	Brightness	Total Time (including overheads)
DD-01A+B	00:29:25.29	00:15:59.8	V=20.0	200.0 minutes
31795371(oiwfs)	0:29:16.112	0:18:10.82	14.85 UCmag,13.397 Jmag,12.774 Kmag	separation 3.17
Observing conditions: DD-01A+B		resources: GMOS South		
DD-07A+B	22:22:36.57	-8:28:6.05	V=17.5	140.0 minutes
29023488(oiwfs)	22:22:19.397	-8:29:20.67	12.25 UCmag,11.239 Jmag,10.869 Kmag	separation 4.42
Observing conditions: DD-07A+B		resources: GMOS South		
WD0000-345	00:02:40.08	-34:13:39.6	B=15.4	49.0 minutes
17177811(oiwfs)	0:02:17.536	-34:14:14.76	10.53 UCmag,9.013 Jmag,8.345 Kmag	separation 4.7
Observing conditions: DC standard		resources: GMOS South		

## Observing Conditions

Name	Image Quality	Sky Background	Water Vapor	Cloud Cover
Band 3 Observing Conditions	85 %	80 %	Any	90 %
Global Default	70 %	50 %	Any	50 %
DD-01A+B	70 %	50 %	Any	70 %
DD-07A+B	70 %	80 %	Any	90 %
DC standard	85 %	Any	Any	90 %

## Resources

- Gemini South
  - GMOS South
    - Focal Plane Unit
      - Longslit 1.50 arcsec
    - Disperser
      - B600\_G5323

semester systems

GMOS South  
Focal Plane Unit  
Longslit 1.00 arcsec  
Disperser  
B600\_G5323  
GMOS South  
Focal Plane Unit  
Longslit 2.00 arcsec  
Disperser  
B600\_G5323  
GMOS South  
Focal Plane Unit  
Longslit 2.00 arcsec  
Disperser  
B600\_G5323  
GMOS South  
Focal Plane Unit  
Longslit 2.00 arcsec  
Disperser  
B600\_G5323

## Scheduling Information

### Scheduling constraints and non-usable dates

- (impossible):
- (optimal):
- (synchronous):

## Additional Information

**Keyword Category:** galactic  
**Keywords:** Binaries  
Evolution  
White dwarfs

### Allocations:

Reference	Time	% Useful	Status of previous data
GN-2007B-Q-88	2.0 hours	100%	Published: MNRAS, 2009 accepted, "Two distant brown dwarfs in the UKIRT Infrared Deep Sky Survey Deep Extragalactic Survey Data Release 2"
GN-2008B-Q-90	1.6 hours	100%	Published: MNRAS, 2009 accepted, "Two distant brown dwarfs in the UKIRT Infrared Deep Sky Survey Deep Extragalactic Survey Data Release 2"
GN-2009B-Q-80	4.8 hours	100%	Observations completed. Data reduced and a preliminary analysis performed (e.g. Figure 2)
GS-2009B-Q-63	9.4 hours	0%	No data obtained as yet.

### Publications:

- Casewell, S., Dobbie, P., et al. 2009 MNRAS, accepted, "High resolution optical spectroscopy of Praesepe white dwarfs"
- Dobbie P., et al., 2009 MNRAS, 395, 2248, "A new detailed examination of white dwarfs in NGC3532 and NGC2287"
- Dobbie, P., et al. 2009 MNRAS, 395, 1591, "A massive white dwarf in the Coma Berenices open cluster"

### **A.7.7 VLT Observing Proposals**

#### **VLT 2010A Proposal**



# EUROPEAN SOUTHERN OBSERVATORY

Organisation Européenne pour des Recherches Astronomiques dans l'Hémisphère Austral  
Europäische Organisation für astronomische Forschung in der südlichen Hemisphäre

OBSERVING PROGRAMMES OFFICE • Karl-Schwarzschild-Straße 2 • D-85748 Garching bei München • e-mail: opo@eso.org • Tel. : +49-89-32 00 64 73

## APPLICATION FOR OBSERVING TIME

PERIOD: **84A**

### Important Notice:

By submitting this proposal, the PI takes full responsibility for the content of the proposal, in particular with regard to the names of CoIs and the agreement to act according to the ESO policy and regulations, should observing time be granted

1. Title				Category: <b>D-7</b>				
Probing the pivotal initial mass between the PNe and Type II SNe evolutionary channels								
2. Abstract / Total Time Requested								
Total Amount of Time:								
We aim to greatly improve understanding of the form of the upper end of the fundamentally important stellar initial mass-final mass relation (IFMR). Despite recent progress the relation remains sparsely sampled by observations at $M_{\text{init}} \geq 5-6M_{\odot}$ . We propose to use the VLT+FORS to obtain high S/N low-resolution spectra of 10 WD candidate members of the open clusters NGC2287 and NGC3532 which have been identified as the likely progeny of stars in this initial mass regime. These new data will be used 1) to place <b>tight</b> limits on the $T_{\text{eff}}$ s and log g's of WDs so that their membership status can be thoroughly examined and 2) alongside WD evolutionary models, to accurately determine their masses and cooling times so we can apply prior knowledge of the cluster ages to estimate lifetimes and masses of progenitors. Our improved mapping of the IFMR at $M_{\text{init}} \geq 5-6M_{\odot}$ will lead to the augmentation of limits on the maximum mass of WD progenitors.								
3. Run	Period	Instrument	Time	Month	Moon	Seeing	Sky Trans.	Obs.Mode
A	84	FORS2	2n	feb	g	$\leq 1.4''$	THN	v
4. Number of nights/hours				Telescope(s)		Amount of time		
a) already awarded to this project:				VLT		24hr total in 079.D-0490/080.D-0654		
b) still required to complete this project:				0		0		
5. Special remarks:								
6. Principal Investigator: PDOBBIE								
Col(s): Q. Parker (1018), M. Burleigh (1244)								
7. Is this proposal linked to a PhD thesis preparation? State role of PhD student in this project								



## 8. Description of the proposed programme

### A) Scientific Rationale:

We propose VLT and FORS spectroscopy of 10 faint WD candidate members of the open clusters NGC2287 and NGC3535 that will provide crucial new data points at the high mass end of the fundamentally important stellar initial mass-final mass relation (IFMR). This is a theoretically predicted positive correlation between the masses of single, non-magnetic, low and intermediate mass stars ( $M \lesssim 10M_{\odot}$ ) and the remnants left behind after they have expired. A comprehensive knowledge of its form is important to several areas of astrophysics: it is a key ingredient of galaxy chemical evolution models as it provides an estimate of the amount of gas, enriched with C, N and other metals, these stars return to the ISM; it is crucial to deciphering information locked up in the white dwarf (WD) luminosity functions of stellar populations (Oswalt et al. 1996); the relations upper end can be used to directly probe the maximum mass of a star that will evolve through the planetary nebula phase and thus indirectly the minimum mass of a star that will expire via a Type II SNe (Williams et al. 2009).

The finer details of the IFMR cannot be determined from first principles since the late stages in the lifecycle of a star, while brief, are extremely challenging to model (e.g. Marigo & Girardi 2007). Therefore, observations play a key role in advancing our knowledge about the relations form. Arguably the best observational based constraints are obtained via the study of open cluster WDs (Weidemann 2000). Here progenitor lifetimes can be determined from the difference between the age of the cluster and the cooling times of WD members. Subsequently, initial masses can be estimated by referring to stellar evolutionary models. Greater access to mosaic imagers and 8/10m telescopes with blue sensitive spectrographs has led to major recent progress in mapping the IFMR (e.g. Kalirai et al. 2007). In our latest work (Dobbie et al. 2009), where we compiled data for  $\sim 50$  WDs from open clusters with near solar metallicity, we found that the bulk of these stars follow a monotonic relation relatively closely. We also showed that the IFMR is somewhat steeper in the range  $3M_{\odot} \lesssim M_{\text{init}} \lesssim 4M_{\odot}$  than elsewhere (Figure 1). This is consistent with theoretical expectations and the sharp drop seen in the number density of objects on the high mass side of the main peak in the field WD mass distribution (Ferrario et al. 2005).

Despite recent headway, the IFMR remains very poorly sampled by observations at  $M_{\text{init}} \gtrsim 5\text{--}6M_{\odot}$ . Indeed, there are only two data points (LB1497, GD50) and a limit (NGC2099-WD24) here, and the association of GD50 with the Pleiades is questionable as it lies  $\sim 90\text{pc}$  beyond the cluster's tidal bounds. Thus, the form of the upper IFMR remains substantially uncertain (Figure 1). To move towards obtaining crucial additional data points in this initial mass regime, we have used CCD photometry obtained as part of the ESO Imaging Survey to search the near solar metallicity open clusters NGC2287 and NGC3532 for their oldest WD members. These populations have several key properties which make them especially suitable for probing the uppermost reaches of the IFMR. NGC2287 and NGC3532 are relatively nearby,  $m\text{--}M=9.26^{+0.37}_{-0.32}$  (Sharma et al. 2006) and  $m\text{--}M=8.04^{+0.37}_{-0.32}$  (Robichon et al. 1999) respectively and despite both residing at low Galactic latitude, extinction along these lines of sight is low,  $E(B\text{--}V)\approx 0.01$  (Sharma et al. 2006) and  $E(B\text{--}V)\approx 0.04$  (Fernandez & Salgado 1980) respectively. Consequently, intrinsically faint high mass WD members appear comparatively bright and can be studied in detail with spectrographs on 8m class telescopes in reasonable integration times. Moreover, the ages of both clusters are relatively well constrained (NGC2287,  $\tau\approx 240\pm 40\text{Myrs}$ ; NGC3532,  $\tau\approx 300\pm 25\text{Myrs}$ ; from Dobbie et al. 2009), curtailing uncertainty in the progenitor mass determinations. Finally, NGC2287 and NGC3532 are sufficiently mature to have formed WD populations, but still young enough that the oldest and probably most massive of degenerates remain at  $T_{\text{eff}}\gtrsim 12500\text{K}$  where there is excellent agreement between spectroscopic and gravitational redshift mass determinations (e.g. Bergeron et al. 1995; Casewell et al. 2009).

Photographic plate surveys and spectroscopic follow-up investigations have, to date, led to the identification of two and four WD members of NGC2287 and NGC3532 respectively (e.g. Reimers & Koester 1993, Dobbie et al. 2009). However, none of these degenerates appears to have formed from a progenitor with a mass  $M_{\text{init}}\geq 5M_{\odot}$ . As both NGC2287 and NGC3532 are comparatively well populated it is probable that there are older fainter WD members that have merely remained undetected until now because they lie beyond the limits of the early surveys. For example, NGC3532 has an estimated total mass of  $M_{\text{cluster}}\gtrsim 2000M_{\odot}$  (Fernandez & Salgado 1980). This is about twice the mass of the 150Myr old cluster NGC2516 (Jeffries et al. 2001), the central regions of which harbour four massive WDs from progenitor stars with  $M_{\text{init}}\approx 5\text{--}5.5M_{\odot}$  (Figure 1). On the reasonable assumption that the initial mass functions of these two populations were comparable in form, it could be expected that  $4\pm 2$  degenerates from  $M_{\text{init}}\geq 5.5\text{--}6M_{\odot}$  reside within NGC3532. Based on the number of known WDs in our two target clusters, approximately half this number could be expected to reside in NGC2287.

V,V-I colour-magnitude diagrams for NGC2287 and NGC3532, based on the newer CCD data, are shown in Figure 2. The expected location of the WD cooling sequence in each cluster is highlighted (Holberg & Bergeron 2006, Fontaine et al. 2001). We identify a total of 15 objects, five in NGC2287 and ten in NGC3532 lying in the vicinity of the theoretical tracks, with magnitudes fainter (and which are thus probably older) than the known WD cluster members. Follow-up low-resolution multiobject spectroscopy obtained with the AAT and AAOmega confirms that 10 objects, 4 in NGC2287 and 6 in NGC3532, show the broad hydrogen Balmer lines characteristic of DA WDs. Our extensive experience of modelling these lines indicates that to obtain the accurate measurements on both the effective temperature and the surface gravity needed to reliably assess cluster membership status and estimate initial and final masses, we require a  $S/N\geq 50$  per  $\sim 5\text{\AA}$  binned pixel

## 8. Description of the proposed programme (continued)

from H- $\beta$  to H-8/-9. AAOmega spectroscopy cannot be of sufficient quality to achieve this goal due to the poor response of this system shortward of  $\sim 4000\text{\AA}$  where the key gravity diagnostic H- $\epsilon$ , H-8 and H-9 lines are located (see Figure 3).

### B) Immediate Objective:

With the proposed FORS spectra of the WD candidate members of NGC2287 and NGC3532 we will:

(1) accurately constrain their effective temperatures and surface gravities by comparing the observed profiles of the H-8 to H- $\beta$  lines to the predictions of state-of-the-art model atmospheres. Our extensive previous experience of the line fitting process indicates that  $S/N \geq 50$  per pixel at a resolution  $\approx 10\text{\AA}$  allows formal uncertainties to be kept to  $\pm \text{few } 100\text{K}$  and  $\pm \text{few } 0.01$  dex in effective temperature and surface gravity respectively. We will determine the absolute visual magnitude of each star by referring to the model WD photometry of Holberg & Bergeron (2006) and use this in conjunction with the CCD photometry to estimate distance. This will allow us to confirm (or otherwise) the cluster membership status of each WD (see Dobbie et al. 2009).

(2) estimate the masses and cooling times of the objects by referring to the WD evolutionary tracks of Fontaine et al. (2001). Our recent high resolution spectroscopic study of the Praesepe WDs has confirmed that the combination of TLUSTY model atmospheres and these evolutionary models lead to robust estimates of WD masses (see Casewell et al. 2009). The anticipated tight limits on the effective temperatures and surface gravities will allow us to constrain the mass and cooling time of each WD to  $\Delta M < 0.05 M_{\odot}$  and  $\sim 10\%$  respectively.

(3) determine the masses of the progenitor stars using solar composition stellar evolutionary models, having first estimated their lifetimes by subtracting the WD cooling times from the host cluster age. The stringent limits on the WD cooling times will ensure that the internal errors on the progenitor mass estimates are  $\leq 0.25 M_{\odot}$ . We will mitigate systematic uncertainty in our progenitor mass estimates by adopting for the age of each cluster the mean of several recently published determinations obtained using a number of independent stellar evolutionary model grids that all assume a moderate level of convective core overshooting (see Dobbie et al. 2009). Additionally, to translate progenitor lifetimes to masses we will use the stellar models of Girardi et al. (2000), which also assume moderate levels of core overshooting. We note that the core contraction gap observed in the sequences of the rich LMC open clusters NGC2173, SL556 and NGC2155 is best reproduced by evolutionary calculations which include moderate core overshooting (Woo et al. 2003). Moreover, data from eclipsing binary systems spanning the broad mass range  $M_{\text{init}} \sim 2\text{--}30 M_{\odot}$  are found to be generally consistent with stellar models which adopt moderate levels of overshooting (Claret 2007).

We anticipate that our new data points will lead to substantial progress in mapping the form of the IFMR at  $M_{\text{init}} > 5\text{--}6 M_{\odot}$  and augment the definition of the pivotal initial mass between the PNe and Type II SNe evolutionary channels.

**C) Telescope Justification:** For our primary science goals we require effective temperature and surface gravity estimates to a few 100K and a few 0.01 dex respectively. This can only be accomplished by obtaining good  $S/N$  optical spectroscopy with a resolution  $\leq 10\text{\AA}$  spanning the wavelength range 3750-5200 $\text{\AA}$ . Given the magnitudes of our targets data of this quality could only be obtained in reasonable integrations times on a 8/10m class telescope with a blue sensitive spectrograph. The combination of the VLT and FORS (with the E2V CCD) offers unparalleled sensitivity at  $\lambda < 4000\text{\AA}$ . Additionally, all our targets have southern declinations so are most efficiently viewed from the southern hemisphere.

**D) Observing Mode Justification (visitor or service):** We need to use the E2V CCD with FORS to attain sufficient  $S/N$  at  $\lambda < 4000\text{\AA}$ . This set-up is only now available in Visitor mode.

**E) Strategy for Data Reduction and Analysis:** All investigators have extensive experience of reducing optical spectroscopic data. Dobbie will reduce the data. Spectral analysis of each dataset to determine effective temperature and surface gravity will be performed by Dobbie/Burleigh. Parker will contribute through his extensive knowledge of the late stages of stellar evolution.

## 8. Attachments (Figures)

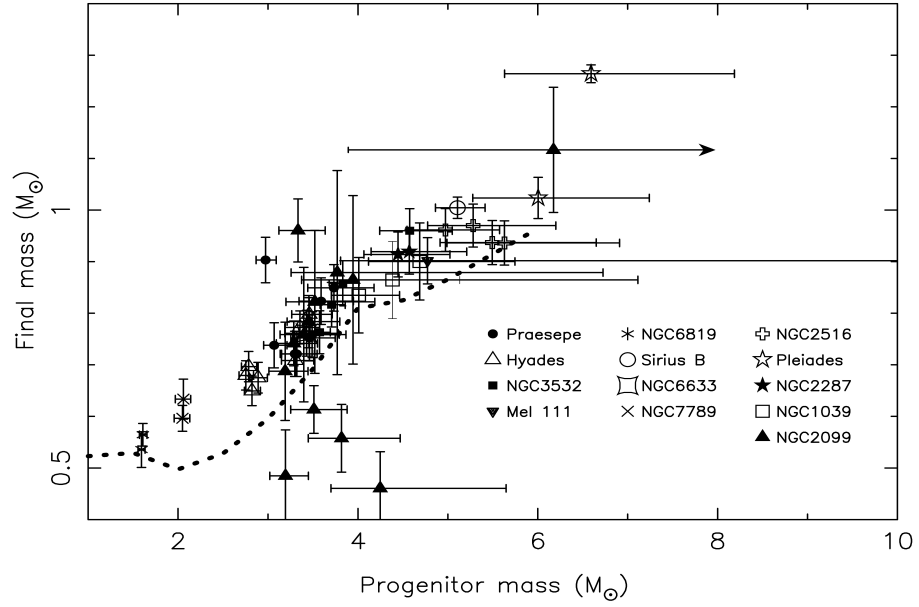


Fig. 1: The IFMR from  $\sim 50$  WD members of near-solar metallicity open star clusters (and Sirius B). The bulk of stars delineate a relatively tight trend which appears to be somewhat steeper between  $3M_{\odot} \lesssim M_{\text{init}} \lesssim 4M_{\odot}$  than elsewhere. The core mass as 1st TP v  $M_{\text{init}}$  relation from Girardi et al. (2000) is overplotted (dotted line).

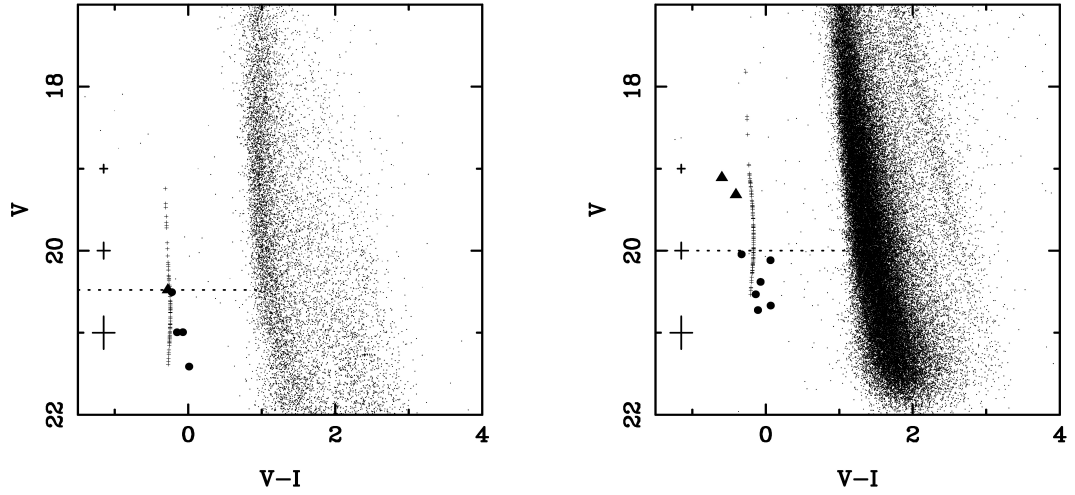


Fig. 2: V, V-I CMDs for NGC2287 (left) and NGC3532 (right) with the predicted location of the WD cooling sequence, overplotted. The faint magnitude limits of the currently known WD population in each cluster are shown (dotted horizontal lines). WD candidate members which we now wish to observe with VLT+FORS and known WD members of the two clusters are also marked (filled circles and triangles respectively).

## 8. Attachments (Figures)

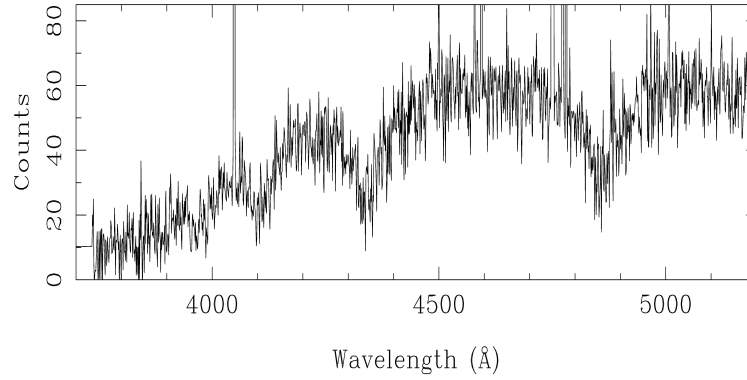


Fig. 3: An AAT and AAOmega spectrum of WD candidate WDC1107a in NGC3532. Despite 4hrs exposure the S/N is an order of magnitude below the level required to obtain accurately  $T_{\text{eff}}$  and  $\log g$ , particularly at  $\lambda \lesssim 4000\text{\AA}$ .

### References

- Bergeron, P., Wesemael, F., & Beauchamp, A. 1995, *PASP*, 107, 1047;  
Casewell, S., et al. 2009, *MNRAS*, accepted;  
Claret, A. 2007, *A&A*, 475, 1019;  
Dobbie, P.D., et al. 2009, *MNRAS*, accepted;  
Fernandez, J.A. & Salgado, C.W. 1980, *A&AS*, 39, 11;  
Ferrario, L., et al. 2005, *MNRAS*, 361, 1131;  
Fontaine, G., Brassard, P., Bergeron, P. 2001, *PASP*, 113, 409;  
Girardi, L., et al. 2000, *A&AS* 141, 371;  
Holberg, J.B., Bergeron, P. 2006, *AJ*, 132, 1221;  
Kalirai, J., et al. 2007, *ApJ*, 671, 748;  
Marigo, P. & Girardi, L. 2007, *A&A*, 469, 239;  
Oswalt, T., et al. 1996, *Nature*, 382, 692;  
Reimers, D., & Koester, D. 1993, *A&A*, 275, 479;  
Robichon, N, et al. 1999, *A&A*, 345, 471;  
Sharma, S., et al. 2006, *AJ*, 132, 1669;  
Weidemann, V., 2000, *A&A*, 188, 74;  
Williams, K.A., Bolte, M., & Koester, D. 2009, *ApJ*, 693, 355

## 9. Justification of requested observing time and lunar phase

**Lunar Phase Justification:** We need good S/N from  $\lambda=3750\text{-}5200\text{\AA}$  on our faint targets. This can be achieved in modest integration times (0.5-3hrs) during grey sky conditions (7 day old moon). Indeed, all ten of our targets can be observed in only two grey nights. Data of the required quality can in principle be obtained during bright sky conditions (14 day moon), but with integration times that are  $\sim 3\times$  as long. We would be happy to accept a larger allocation of bright nights if these conditions are substantially less oversubscribed than grey time.

**Time Justification: (including seeing overhead)** The following numbers are based on the FORS exposure time calculator (Ver. 3.2.7). We will observe our targets using standard settings, namely with the GRIS-600B+22 grism and a 1.0" slit. With this set-up we derive exposure times of 1500s, 2700s, 5400s and 11200s to reach a  $S/N \approx 50$  at H-8 to H-9 for  $V=20.0, 20.5, 21.0$  and  $21.5$  AO stars respectively (airmass 1.4, seeing 0.8", 7 day old moon). Our S/N estimate allows for a factor 3 binning in the dispersion direction at the reduction stage, since for our purposes we require data with a resolution of only  $\sim 10\text{\AA}$ . To ensure successful cosmic ray rejection from our data the observation of each star will consist of a number of sub-integrations, namely,  $3 \times 500$ ,  $3 \times 900$ ,  $3 \times 1800$ s and  $4 \times 2800$ s. Since our 10 targets are split approximately 2, 4, 3 and 1 per magnitude category listed above, we request a total time of 15.2 hours (which equates to the 2 nights in February). This estimate allows 16 minutes of overheads per OB (e.g. telescope preset, acquisition, centering on slit, CCD readout) and one observation each night of our calibration star (see below).

**Calibration Request:** Special Calibration - We plan to observe a DC white dwarf calibrator each night (900 secs on WD1055-072) so that we can remove to a high degree the signature of the FORS spectral response from the data.

## 10. Report on the use of ESO facilities during the last 2 years

Programme 79.D-0490 (PI: Dobbie), VLT/FORS1, 10 hours: published: "A new detailed examination of the white dwarf members of NGC3532 and NGC2287", Dobbie, P.D., Napiwotzki, R., Barstow, M.A., Burleigh, M.R., Jameson, R.F., MNRAS, in press, arXiv: 0902.4259

Programme 80.D-0654 (PI: Dobbie), VLT/FORS1, 14 hours: partly published: "A new detailed examination of the white dwarf members of NGC3532 and NGC2287", Dobbie, P.D., Napiwotzki, R., Barstow, M.A., Burleigh, M.R., Jameson, R.F., MNRAS, in press, arXiv: 0902.4259. Paper on remaining data about to be submitted. All results presented at 16th European Workshop on White Dwarfs (2008) and at MASH PNe workshop (02/09).

## 11. Applicant's publications related to the subject of this application during the last 2 years

Casewell S., Dobbie P., et al., 2009 MNRAS, accepted: *High resolution optical spectroscopy of Praesepe white dwarfs*

Dobbie P., et al., 2009 MNRAS, accepted: *A new detailed examination of white dwarfs in NGC3532 and NGC2287*

Dobbie P., et al., 2009 MNRAS, accepted: *A massive white dwarf member of the Coma Berenices Open Cluster*

## 12. List of targets proposed in this programme

Run	Target/Field	$\alpha$ (J2000)	$\delta$ (J2000)	ToT	Mag.	Diam.	Additional info	Reference star
A	WDC0644	06 44 40.28	-20 51 45.21	4.3	20.51		White dwarf	
A	WDC0645a	06 45 08.65	-20 51 30.16	4.3	21.41		White dwarf	
A	WDC0645b	06 45 22.06	-20 25 09.75	4.3	20.98		White dwarf	
A	WDC0646	06 46 01.08	-20 32 03.56	4.3	20.99		White dwarf	
A	WDC1103	11 03 27.82	-58 35 06.80	4.3	20.76		White dwarf	
A	WDC1105	11 05 23.87	-58 57 22.97	4.3	20.53		White dwarf	
A	WDC1106a	11 06 18.34	-59 05 17.27	4.3	20.04		White dwarf	
A	WDC1106b	11 06 51.64	-58 43 48.96	4.3	20.12		White dwarf	
A	WDC1107a	11 07 21.97	-58 42 12.60	4.3	20.38		White dwarf	
A	WDC1107b	11 07 29.49	-58 36 40.98	4.3	20.67		White dwarf	

12b. ESO Archive - Are the data requested by this proposal in the ESO Archive (<http://archive.eso.org>)? If yes, explain why the need for new data.

No

### 13. Scheduling requirements

### 14. Instrument configuration

Period	Instrument	Run ID	Parameter	Value or list
84	FORS2	A	LSS	GRIS-600B+22
84	FORS2	A	Detector	E2V

## A.8 original analytical method for determining the properties of the components of the wide double-degenerate systems

Although, the properties of the components of the wide DD systems are now calculated using a numerical method as described in Chapter 2, the original method for determining the properties of the components of the wide DD systems utilised a purely analytical approach. This method has been added here for reference.

The masses, the cooling times and the absolute magnitudes for the white dwarfs presented here were in general obtained by comparing my spectroscopic effective temperature ( $T_{eff}$ ) and surface gravity ( $\log g$ ) estimates to grids of synthetic photometry (Holberg and Bergeron 2005) and evolutionary models (Fontaine et al. 2001). Points in these grids were interpolated using a fortran software routine, `rbb_wd_dd_param.f` (see Appendix Section A.5.2), to apply bi-cubic spline fits. As these binaries consisted of white dwarfs with quite different characteristics, I had to apply a number of different methods to determine their component properties.

### A.8.1 Uncertainty Calculations

Uncertainties were calculated by the software by propagating the errors on the inputs ( $T_{eff}$  and  $\log g$ , distances and masses in some cases) using the standard error formula, given in equation (A.1).

$$\sigma_{output}^2 = \sigma_{input1}^2 \left( \frac{d_{output}}{d_{input1}} \right)^2 + \sigma_{input2}^2 \left( \frac{d_{output}}{d_{input2}} \right)^2 \quad (A.1)$$

The same software used in the derivation of the output parameters was used in the derivation of the errors in the output parameters (i.e. the derivatives were calculated numerically).

For the case of a Hot DA, for example within a Hot + Hot DA scenario, this involved propagating the error on the spectroscopic surface gravity and temperature through for the calculation of the absolute magnitude, mass, and cooling age errors. In this case the first input parameter was  $T_{eff}$  and the second input parameter was  $\log g$ . The distance error was calculated using both the apparent magnitude (g band) error and absolute magnitude error.

For the case of an isolated Cool DA, for example within a Cool DA + Cool DA (or Cool DA without Hot DA partner) scenario or a magnetic DA + cool DA scenario, this involved propagating the errors on the spectroscopic surface gravities and temperatures through for the calculation of the mass error (where the first input parameter was  $T_{eff}$  and the second input parameter was  $\log g$ ), and it then involved propagating the error on the temperature and corrected mass and through for the calculation of the absolute magnitude, surface gravities, and cooling age errors (where the first input parameter was  $T_{eff}$  and the second input parameter was  $M$ ). The distance error was calculated using both the apparent magnitude (g band) error and absolute magnitude error.



The error of a particular output parameter was calculated as follows;

First it involved calculation of the maximum error in the output parameter when the first input parameter ( $IP_{First}$ ) was set to its two respective extremes, divided by the maximum error in the first input parameter;

$$\frac{dOP}{dIP_{First}} = \frac{OP_{WhenFirstIPsetatMinErrRange} - OP_{WhenFirstIPSetAtMaxErrRange}}{IP_{FirstsetatMaxErrRange} - IP_{FirstsetatMinErrRange}} \quad (A.2)$$

Next it involved the calculation of the maximum error in the output parameter when the second input parameter ( $IP_{Second}$ ) was set to its two respective extremes, divided by the maximum error in the second input parameter;

$$\frac{dOP}{dIP_{Second}} = \frac{OP_{WhenSecondIPsetatMinErrRange} - OP_{WhenSecondIPSetAtMaxErrRange}}{IP_{SecondsetatMaxErrRange} - IP_{SecondsetatMinErrRange}} \quad (A.3)$$

And finally, the final error in the output parameter ( $OP$ ) was calculated as follows;

$$dOP = \sqrt{\left(\left(\frac{dOP}{dIP_{Second}}\right)^2 IP_{SecondErr}^2\right) + \left(\left(\frac{dOP}{dIP_{First}}\right)^2 IP_{FirstErr}^2\right)} \quad (A.4)$$

The distance error was calculated as follows, where  $OP_{AbsMag}$  is the absolute magnitude output parameter, and  $IP_{AppMag}$  is the apparent magnitude input parameter;

$$dd_{OP} = \sqrt{dOP_{AbsMag}^2 + dIP_{AppMag}^2} \quad (A.5)$$

For the case of a non-isolated Cool DA (i.e. with a Hot DA partner) or magnetic DA (with a non-magnetic partner), for example within a Cool DA + Hot DA, Magnetic DA and Hot DA, or Magnetic DA + Cool DA scenario, where one of the input parameters was a distance value and an absolute magnitude was inferred based upon this distance value and the apparent magnitudes of the system, then the errors of the apparent magnitudes of the system were also propagated through to the errors in the output parameters. This therefore involved propagating the errors in the distance, apparent magnitudes and temperature through for the calculation of the mass, absolute magnitude, surface gravities, and cooling age errors. In this case the first input parameter was  $T_{eff}$ , the second input parameter was distance, and the third input parameter was the apparent magnitude (in g band).

This method therefore additionally involved the calculation of the maximum error in the output parameter when the third input parameter was set to its two respective extremes, divided by the maximum error in the third input parameter;

$$\frac{dOP}{dIP_{Third}} = \frac{OP_{WhenThirdIPsetatMinErrRange} - OP_{WhenThirdIPSetAtMaxErrRange}}{IP_{ThirdsetatMaxErrRange} - IP_{ThirdsetatMinErrRange}} \quad (A.6)$$

Where the final error in the output parameter was calculated as follows;

$$dOP = \sqrt{\left(\left(\frac{dOP}{dIP_{First}}\right)^2 IP_{FirstErr}^2\right) + \dots + \left(\left(\frac{dOP}{dIP_{Third}}\right)^2 IP_{ThirdErr}^2\right)} \quad (A.7)$$

## Main Sequence Progenitor Calculations

For each WD component, an estimate of the DD system age may be derived by first calculating the initial (main sequence progenitor) mass of the WD component using a known IFMR form, for example Dobbie et al. (2006), calculating the age of the progenitor using the main sequence evolutionary grids of Girardi et al. (2000), and then adding the cooling age of the WD to its main sequence progenitor age. This method has been used extensively throughout this project for various purposes.

All system age comparisons using this method were derived using the Dobbie et al. (2006) linear IFMR form in this commentary. These system age calculations have been performed using code described in Appendix Section A.6.1, and my DD Data spreadsheet referenced in Appendix Section A.7.1.

## A.9 example IDL routine

```

*
; Title: Count Close Pairs
; File: CCPtestDetailed.pro
; Author: Richard Baxter
; Organisation: Macquarie University / AAO
; Version: 25 March 09a
; Summary:
;
; Postconditions;
;
; This program generates a list of blue object pairs within a given angular separation. In the
; output list each close pair is listed twice, A with B and B with A. The list has been ordered
; in terms of pair distance, DISTANCE.BETWEEN_PAIR. The output files are of the following format;
;
; SDSSblueObjectsDR7detailedClosePairsSortedOutputPart1.txt [RIGHT_ASCENSION A, DECLINATION A,
; GALATIC.LATITUDE A, GALATIC.LONGITUDE A, U A, G A, R A, POK A, DISTANCE.BETWEEN_PAIR,
; RIGHT_ASCENSION B, DECLINATION B, GALATIC.LATITUDE B, GALATIC.LONGITUDE B, U B, G B, R B, POK B
; ]
; SDSSblueObjectsDR7detailedClosePairsSortedOutputPart2.txt [ID A, ID B]
;
; Preconditions
;
; The input files are of the following format;
;
; repchr.pro [NASA]
; gettok.pro [NASA]
; readcol64bitvars.pro [RBB - modified NASA pro for 64bit unsigned longs {ID}]
; remchar.pro [NASA]
; skip_lun.pro [required for GDL]
; strsplit.pro [GDL library]
; strnumber64bitvars.pro [RBB - modified NASA pro for 64bit unsigned longs {ID}]
; SDSSblueObjectsDR7detailed.txt [ID, RIGHT_ASCENSION, DECLINATION, GALATIC.LATITUDE,
; GALATIC.LONGITUDE, ID, U, G, R, POK] for 56587 blue objects, tab delimited

; distances are given in arc seconds here

firstPairMaxDistance = 60
lastPairMaxDistance = 60
diffPairMaxDistance = 1

; ORIGINAL;
fieldSquareDegrees = 1000L ; or 1000 ; or 11663
fieldNumberOfStars = 4852L ; or 4852 ; or 56587
numberOfSamples = 100L

; TEST HARNESS - load from file;
fieldSquareDegrees = 11663L ; or 1000 ; or 11663
fieldNumberOfStars = 56587L ; or 4852 ; or 56587
numberOfSamples = 1L

fieldxDegrees = SQRT(fieldSquareDegrees) ; or 100
fieldyDegrees = SQRT(fieldSquareDegrees) ; or 100

IDLrandomNumberMin = 0L
IDLrandomNumberMax = 1L
IDLrandomNumberVariation = (IDLrandomNumberMax - IDLrandomNumberMin)

for maxDistanceIndex=firstPairMaxDistance, lastPairMaxDistance, diffPairMaxDistance do begin

```

```

maxDistanceForConsideredPairInArcSeconds = double(maxDistanceIndex)
maxDistanceForConsideredPairInArcDegrees = maxDistanceForConsideredPairInArcSeconds/60D/60D
totalNumberOfPairsFoundAcrossAllSamples = 0L

for sampleIndex=1L, numberOfSamples, 1L do begin

    numberOfLines = 56587
    numberOfColumns = 5
    NameOfFile = 'SDSSblueObjectsDR7detailed.txt'

    ;long precision is required for ID
    readcol64bitvars, NameOfFile, ID, RIGHT_ASCENSION, DECLINATION, GALATIC_LATITUDE,
        GALATIC_LONGITUDE, U, G, R, POK, FORMAT='G,D,D,D,D,D,D,D,D,D', SKIPLINE=1

    starID = transpose(ID)
    starYCoordinates = transpose(DECLINATION) ;GALATIC_LATITUDE
    starXCoordinates = transpose(RIGHT_ASCENSION) ;GALATIC_LONGITUDE

    starXCoordinatesSortIndicies = sort(starXCoordinates)
    starXCoordinatesSorted = starXCoordinates[starXCoordinatesSortIndicies]
    starYCoordinatesSortIndicies = sort(starYCoordinates)
    starYCoordinatesSorted = starYCoordinates[starYCoordinatesSortIndicies]

    maxNumberOfPairsExpected = 10000 ;300
    starIDArrayForClosePairs1 = lon64arr(maxNumberOfPairsExpected)
    starIDArrayForClosePairs2 = lon64arr(maxNumberOfPairsExpected)
    starDistanceArrayForClosePairs = dblarr(maxNumberOfPairsExpected)
    starDataArrayForClosePairs1 = dblarr(8, maxNumberOfPairsExpected)
    starDataArrayForClosePairs2 = dblarr(8, maxNumberOfPairsExpected)
    data = [transpose(RIGHT_ASCENSION), transpose(DECLINATION), transpose(GALATIC_LATITUDE),
        transpose(GALATIC_LONGITUDE), transpose(U), transpose(G), transpose(R), transpose(POK)]

    ;PRINT, "data = "
    ;PRINT, data

    ;stringmessage = "starXCoordinatesSorted ="
    ;PRINT, starXCoordinatesSorted

    totalNumberOfPairsFound = 0L

    for starIndex=1L, fieldNumberOfStars, 1L do begin

        numberOfPairsFound = 0L

        starIndexArray = starIndex-1

        centralPositionInStarXCoordinatesSorted = where(starXCoordinatesSortIndicies eq
            starIndexArray)
        centralValueInStarXCoordinatesSorted = starXCoordinatesSorted[
            centralPositionInStarXCoordinatesSorted]
        ;centralPositionInStarXCoordinates = starIndexArray
        ;or centralValueInStarXCoordinates = starXCoordinates[
            centralPositionInStarXCoordinates]
        centralPositionInStarYCoordinatesSorted = where(starYCoordinatesSortIndicies eq
            starIndexArray)
        centralValueInStarYCoordinatesSorted = starYCoordinatesSorted[
            centralPositionInStarYCoordinatesSorted]
        ;centralPositionInStarYCoordinates = starIndexArray
        ;or centralValueInStarYCoordinates = starYCoordinates[
            centralPositionInStarYCoordinates]

        ;hunt in positive x direction
        consideredPairIndex = 1L
        currentMaxDistanceBetweenPairX = 0D

        while (currentMaxDistanceBetweenPairX lt maxDistanceForConsideredPairInArcDegrees) do
            begin

                if (centralPositionInStarXCoordinatesSorted+consideredPairIndex) gt (
                    fieldNumberOfStars-1) then begin
                    currentMaxDistanceBetweenPairX = maxDistanceForConsideredPairInArcDegrees+9999
                endif else begin

                    currentPositionInStarXCoordinatesSorted =
                        centralPositionInStarXCoordinatesSorted + consideredPairIndex
                    currentValueInStarXCoordinatesSorted = starXCoordinatesSorted[
                        currentPositionInStarXCoordinatesSorted]
                    currentPositionInStarXCoordinates = starXCoordinatesSortIndicies[
                        currentPositionInStarXCoordinatesSorted]
                    currentPositionInStarYCoordinates = currentPositionInStarXCoordinates
                    currentValueInStarYCoordinates = starYCoordinates[
                        currentPositionInStarYCoordinates]
                    currentValueInStarYCoordinatesSorted = currentValueInStarYCoordinates

                    currentMaxDistanceBetweenPairX = ABS(currentValueInStarXCoordinatesSorted -
                        centralValueInStarXCoordinatesSorted)
                    currentMaxDistanceBetweenPairY = ABS(currentValueInStarYCoordinatesSorted -
                        centralValueInStarYCoordinatesSorted)
                    ;averageYDeclination = currentValueInStarYCoordinatesSorted +
                        centralValueInStarYCoordinatesSorted) / 2
                    averageYDeclination = centralValueInStarYCoordinatesSorted
                end
            end
        end
    end
end

```

```

currentMaxDistanceBetweenPairXCorrected = COS(averageYDeclination / 180.0 * PI) *
    currentMaxDistanceBetweenPairX
currentMaxDistanceBetweenPairYCorrected = currentMaxDistanceBetweenPairY

currentMaxDistanceBetweenPair = SQRT(currentMaxDistanceBetweenPairXCorrected^2 +
    currentMaxDistanceBetweenPairYCorrected^2)

if (currentMaxDistanceBetweenPair lt maxDistanceForConsideredPairInArcDegrees)
    then begin

        starIDArrayForClosePairs1 [totalNumberOfPairsFound+numberOfPairsFound] =
            starID [starIndexArray]
        starIDArrayForClosePairs2 [totalNumberOfPairsFound+numberOfPairsFound] =
            starID [currentPositionInStarXCoordinates]
        starDistanceArrayForClosePairs [totalNumberOfPairsFound+numberOfPairsFound] =
            currentMaxDistanceBetweenPair
        starDataArrayForClosePairs1 [*, totalNumberOfPairsFound+numberOfPairsFound] =
            data [*, starIndexArray]
        starDataArrayForClosePairs2 [*, totalNumberOfPairsFound+numberOfPairsFound] =
            data [*, currentPositionInStarXCoordinates]

        numberOfPairsFound = numberOfPairsFound + 1

    endif

    consideredPairIndex = consideredPairIndex + 1

endif

endwhile

; hunt in negative x direction
consideredPairIndex = -1
currentMaxDistanceBetweenPairX = 0
while (currentMaxDistanceBetweenPairX lt maxDistanceForConsideredPairInArcDegrees) do
    begin

        if (centralPositionInStarXCoordinatesSorted+consideredPairIndex) lt 0 then begin
            currentMaxDistanceBetweenPairX = maxDistanceForConsideredPairInArcDegrees+9999
        endif else begin

            currentPositionInStarXCoordinatesSorted =
                centralPositionInStarXCoordinatesSorted + consideredPairIndex
            currentValueInStarXCoordinatesSorted = starXCoordinatesSorted [
                currentPositionInStarXCoordinatesSorted]
            currentPositionInStarXCoordinates = starXCoordinatesSortIndicies [
                currentPositionInStarXCoordinatesSorted]
            currentPositionInStarYCoordinates = currentPositionInStarXCoordinates
            currentValueInStarYCoordinates = starYCoordinates [
                currentPositionInStarYCoordinates]
            currentValueInStarYCoordinatesSorted = currentValueInStarYCoordinates

            currentMaxDistanceBetweenPairX = ABS(currentValueInStarXCoordinatesSorted -
                centralValueInStarXCoordinatesSorted)
            currentMaxDistanceBetweenPairY = ABS(currentValueInStarYCoordinatesSorted -
                centralValueInStarYCoordinatesSorted)
            ; averageYDeclination = (currentValueInStarYCoordinatesSorted +
                centralValueInStarYCoordinatesSorted) / 2
            averageYDeclination = centralValueInStarYCoordinatesSorted
            currentMaxDistanceBetweenPairXCorrected = COS(averageYDeclination / 180.0 * PI) *
                currentMaxDistanceBetweenPairX
            currentMaxDistanceBetweenPairYCorrected = currentMaxDistanceBetweenPairY

            currentMaxDistanceBetweenPair = SQRT(currentMaxDistanceBetweenPairXCorrected^2 +
                currentMaxDistanceBetweenPairYCorrected^2)

            if (currentMaxDistanceBetweenPair lt maxDistanceForConsideredPairInArcDegrees)
                then begin

                    starIDArrayForClosePairs1 [totalNumberOfPairsFound+numberOfPairsFound] =
                        starID [starIndexArray]
                    starIDArrayForClosePairs2 [totalNumberOfPairsFound+numberOfPairsFound] =
                        starID [currentPositionInStarXCoordinates]
                    starDistanceArrayForClosePairs [totalNumberOfPairsFound+numberOfPairsFound] =
                        currentMaxDistanceBetweenPair
                    starDataArrayForClosePairs1 [*, totalNumberOfPairsFound+numberOfPairsFound] =
                        data [*, starIndexArray]
                    starDataArrayForClosePairs2 [*, totalNumberOfPairsFound+numberOfPairsFound] =
                        data [*, currentPositionInStarXCoordinates]

                    numberOfPairsFound = numberOfPairsFound + 1
                    ; currentMaxDistanceBetweenPairX = maxDistanceForConsideredPairInArcDegrees
                    ; +9999

                endif

                consideredPairIndex = consideredPairIndex - 1

            endif

        endwhile
    endwhile

```

[illegible]



## List of Symbols

The following list is neither exhaustive nor exclusive, but may be helpful.

"	.....	arcsecond
mas	.....	milliarcsecond
$M_{\odot}$	.....	solar mass
$\tau_c$	.....	cooling time
$T_{eff}$	.....	effective temperature
$\log g$	.....	log of surface gravity





## References

- K. N. Abazajian, J. K. Adelman-McCarthy, M. A. Ageros, S. S. Allam, C. Allende Prieto, D. An, K. S. J. Anderson, S. F. Anderson, J. Annis, N. A. Bahcall, C. A. L. Bailer-Jones, J. C. Barentine, B. A. Bassett, A. C. Becker, T. C. Beers, E. F. Bell, V. Belokurov, A. A. Berlind, E. F. Berman, M. Bernardi, S. J. Bickerton, D. Bizyaev, J. P. Blakeslee, M. R. Blanton, J. J. Bochanski, W. N. Boroski, H. J. Brewington, J. Brinchmann, J. Brinkmann, R. J. Brunner, T. Budavri, L. N. Carey, S. Carliles, M. A. Carr, F. J. Castander, D. Cinabro, A. J. Connolly, I. Csabai, C. E. Cunha, P. C. Czarapata, J. R. A. Davenport, E. de Haas, B. Dilday, M. Doi, D. J. Eisenstein, M. L. Evans, N. W. Evans, X. Fan, S. D. Friedman, J. A. Frieman, M. Fukugita, B. T. Gnsicke, E. Gates, B. Gillespie, G. Gilmore, B. Gonzalez, C. F. Gonzalez, E. K. Grebel, J. E. Gunn, Z. Gyry, P. B. Hall, P. Harding, F. H. Harris, M. Harvanek, S. L. Hawley, J. J. E. Hayes, T. M. Heckman, J. S. Hendry, G. S. Hennessy, R. B. Hindsley, J. Hoblitt, C. J. Hogan, D. W. Hogg, J. A. Holtzman, J. B. Hyde, S.-i. Ichikawa, T. Ichikawa, M. Im, . Ivezi, S. Jester, L. Jiang, J. A. Johnson, A. M. Jorgensen, M. Juri, S. M. Kent, R. Kessler, S. J. Kleinman, G. R. Knapp, K. Konishi, R. G. Kron, J. Krzesinski, N. Kuropatkin, H. Lampeitl, S. Lebedeva, M. G. Lee, Y. S. Lee, R. French Leger, S. Lpine, N. Li, M. Lima, H. Lin, D. C. Long, C. P. Loomis, J. Loveday, R. H. Lupton, E. Magnier, O. Malanushenko, V. Malanushenko, R. Mandelbaum, B. Margon, J. P. Marriner, D. Martinez-Delgado, T. Matsubara, P. M. McGehee, T. A. McKay, A. Meiksin, H. L. Morrison, F. Mullally, J. A. Munn, T. Murphy, T. Nash, A. Nebot, E. H. Neilsen, H. J. Newberg, P. R. Newman, R. C. Nichol, T. Nicinski, M. Nieto-Santisteban, A. Nitta, S. Okamura, D. J. Oravetz, J. P. Ostriker, R. Owen, N. Padmanabhan, K. Pan, C. Park, G. Pauls, J. Peoples, W. J. Percival, J. R. Pier, A. C. Pope, D. Pourbaix, P. A. Price, N. Purger, T. Quinn, M. J. Raddick, P. Re Fiorentin, G. T. Richards, M. W. Richmond, A. G. Riess, H. Rix, C. M. Rockosi, M. Sako, D. J. Schlegel, D. P. Schneider, R. Scholz, M. R. Schreiber, A. D. Schwope, U. Seljak, B. Sesar, E. Sheldon, K. Shimasaku, V. C. Sibley, A. E. Simmons, T. Sivarani, J. Allyn Smith, M. C. Smith, V. Smoli, S. A. Snedden, A. Stebbins, M. Steinmetz, C. Stoughton, M. A. Strauss, M. SubbaRao, Y. Suto, A. S. Szalay, I. Szapudi, P. Szkody, M. Tanaka, M. Tegmark, L. F. A. Teodoro, A. R. Thakar,

- C. A. Tremonti, D. L. Tucker, A. Uomoto, D. E. Vanden Berk, J. Vandenberg, S. Vidrih, M. S. Vogeley, W. Voges, N. P. Vogt, Y. Wadadekar, S. Watters, D. H. Weinberg, A. A. West, S. D. M. White, B. C. Wilhite, A. C. Wonders, B. Yanny, D. R. Yocum, D. G. York, I. Zehavi, S. Zibetti, and D. B. Zucker. The seventh data release of the sloan digital sky survey. *The Astrophysical Journal Supplement Series*, 182:543–558, June 2009. [23](#), [77](#)
- H. A. Abt and S. G. Levy. Multiplicity among solar-type stars. *The Astrophysical Journal Supplement Series*, 30:273–306, Mar. 1976. [79](#)
- N. F. Allard, G. Hbrard, J. Dupuis, P. Chayer, J. W. Kruk, J. Kielkopf, and I. Hubeny. Far ultraviolet spectroscopic explorer observations of g226-29: First detection of the h2 quasi-molecular satellite at 1150 . *The Astrophysical Journal*, 601:L183–L186, Feb. 2004. [59](#)
- L. H. Auer and D. Mihalas. Non-Lte model atmospheres. III. a Complete-Linearization method. *The Astrophysical Journal*, 158:641, Nov. 1969. [57](#)
- M. R. Bate, I. A. Bonnell, and N. M. Price. Modelling accretion in protobinary systems. *Monthly Notices of the Royal Astronomical Society*, 277:362–376, Nov. 1995. [14](#)
- P. Bergeron, R. A. Saffer, and J. Liebert. A spectroscopic determination of the mass distribution of DA white dwarfs. *Astrophysical Journal*, 394:228–247, July 1992. [13](#), [60](#), [80](#)
- P. Bergeron, D. Saumon, and F. Wesemael. New model atmospheres for very cool white dwarfs with mixed H/He and pure he compositions. *Astrophysical Journal*, 443:764–779, Apr. 1995a. [76](#)
- P. Bergeron, F. Wesemael, and A. Beauchamp. Photometric calibration of hydrogen- and Helium-Rich white dwarf models. *Publications of the Astronomical Society of the Pacific*, 107:1047, Nov. 1995b. [xiv](#), [26](#), [61](#)
- P. Bergeron, M. T. Ruiz, and S. K. Leggett. The chemical evolution of cool white dwarfs and the age of the local galactic disk. *The Astrophysical Journal Supplement Series*, 108:339, Jan. 1997. [49](#)
- P. Bergeron, S. K. Leggett, and M. T. Ruiz. Photometric and spectroscopic analysis of cool white dwarfs with trigonometric parallax measurements. *Astrophysical Journal Supplement Series*, 133:413–449, Apr. 2001. [49](#), [61](#)
- T. Bloeker. Evolutionary tracks and observational constraints. *Acta Astronomica*, 43: 305–313, Oct. 1993. [7](#)
- G. H. Bowen. Dynamical modeling of long-period variable star atmospheres. *The Astrophysical Journal*, 329:299–317, June 1988. [7](#)
- B. J. Boyle. The space distribution of DA white dwarfs. *Monthly Notices of the Royal Astronomical Society*, 240:533–549, Oct. 1989. [9](#)

- S. L. Casewell, P. D. Dobbie, S. T. Hodgkin, E. Moraux, R. F. Jameson, N. C. Hambly, J. Irwin, and N. Lodieu. Proper motion l and t dwarf candidate members of the pleiades. *Monthly Notices of the Royal Astronomical Society*, 378:1131–1140, July 2007. [67](#)
- S. L. Casewell, P. D. Dobbie, R. Napiwotzki, M. R. Burleigh, M. A. Barstow, and R. F. Jameson. High-resolution optical spectroscopy of praesepe white dwarfs. *Monthly Notices of the Royal Astronomical Society*, 395:1795–1804, June 2009. [xiii](#), [12](#), [14](#), [82](#), [114](#)
- S. Catalan, J. Isern, E. Garcia-Berro, and I. Ribas. The initial-final mass relationship of white dwarfs revisited: effect on the luminosity function and mass distribution. *0804.3034*, Apr. 2008. [89](#)
- S. Chandrasekhar. *An introduction to the study of stellar structure*. 1939. [2](#)
- S. Chandrasekhar. The maximum mass of ideal white dwarfs. *The Astrophysical Journal*, 74:81, July 1931. [2](#)
- C. F. Claver, J. Liebert, P. Bergeron, and D. Koester. The masses of white dwarfs in the praesepe open cluster. *Astrophysical Journal*, 563:987–998, Dec. 2001. [14](#), [21](#), [80](#)
- P. D. Dobbie, D. J. Pinfield, R. Napiwotzki, N. C. Hambly, M. R. Burleigh, M. A. Barstow, R. F. Jameson, and I. Hubeny. Praesepe and the seven white dwarfs. *Monthly Notices of the Royal Astronomical Society*, 355:L39–L43, Dec. 2004. [14](#)
- P. D. Dobbie, R. Napiwotzki, M. R. Burleigh, M. A. Barstow, D. D. Boyce, S. L. Casewell, R. F. Jameson, I. Hubeny, and G. Fontaine. New praesepe white dwarfs and the initial mass-final mass relation. *Monthly Notices of the Royal Astronomical Society*, 369:383–389, June 2006. [xvi](#), [xvii](#), [xviii](#), [14](#), [15](#), [78](#), [79](#), [80](#), [82](#), [83](#), [84](#), [87](#), [94](#), [95](#), [96](#), [98](#), [99](#), [100](#), [102](#), [103](#), [104](#), [119](#), [120](#), [202](#)
- P. D. Dobbie, R. Napiwotzki, M. R. Burleigh, K. A. Williams, R. Sharp, M. A. Barstow, S. L. Casewell, and I. Hubeny. A new detailed examination of white dwarfs in NGC 3532 and NGC 2287. *Monthly Notices of the Royal Astronomical Society*, 395:2248–2256, June 2009. [xiv](#), [14](#), [15](#), [16](#), [89](#)
- S. Dreizler and K. Werner. Spectral analysis of hot helium-rich white dwarfs. *Astronomy and Astrophysics*, 314:217–232, Oct. 1996. [8](#)
- A. K. Dupree. Mass loss from cool stars. *Annual Review of Astronomy and Astrophysics*, 24:377–420, 1986. [5](#)
- D. J. Eisenstein, J. Liebert, H. C. Harris, S. J. Kleinman, A. Nitta, N. Silvestri, S. A. Anderson, J. C. Barentine, H. J. Brewington, J. Brinkmann, M. Harvanek, J. Krzesinski, E. H. Neilsen, D. Long, D. P. Schneider, and S. A. Snedden. A catalog of spectroscopically confirmed white dwarfs from the sloan digital sky survey data release 4. *The Astrophysical Journal Supplement Series*, 167:40–58, Nov. 2006. [xix](#), [5](#), [32](#)

- L. Ferrario, D. Wickramasinghe, J. Liebert, and K. A. Williams. The open-cluster initial-final mass relationship and the high-mass tail of the white dwarf distribution. *Monthly Notices of the Royal Astronomical Society*, 361:1131–1135, Aug. 2005. [xiv](#), [15](#), [17](#)
- D. S. Finley and D. Koester. PG 0922+162: Discovery of the youngest visual double degenerate. *Astrophysical Journal*, 489:L79, Nov. 1997. [xiv](#), [18](#), [19](#), [20](#), [105](#)
- T. A. Fleming, J. Liebert, and R. F. Green. The luminosity function of DA white dwarfs. *The Astrophysical Journal*, 308:176–189, Sept. 1986. [9](#), [115](#)
- G. Fontaine, P. Brassard, and P. Bergeron. The potential of white dwarf cosmochronology. *Publications of the Astronomical Society of the Pacific*, 113:409–435, Apr. 2001. [61](#), [75](#), [200](#)
- R. H. Fowler. On dense matter. *Monthly Notices of the Royal Astronomical Society*, 87:114–122, Dec. 1926. [2](#)
- D. J. Frew. Planetary nebulae in the solar neighbourhood: Statistics, distance scale and luminosity function. <http://adsabs.harvard.edu/abs/2008PhDT.....109F>, July 2008. [9](#)
- B. Fuchs, C. Dettbarn, H. Rix, T. C. Beers, D. Bizyaev, H. Brewington, H. Jahrei, R. Klement, E. Malanushenko, V. Malanushenko, D. Oravetz, K. Pan, A. Simmons, and S. Snedden. The kinematics of Late-Type stars in the solar cylinder studied with SDSS data. *The Astronomical Journal*, 137:4149–4159, May 2009. [69](#)
- S. D. Gennaro, T. von Hippel, D. E. Winget, S. O. Kepler, A. Nitta, D. Koester, and L. Althaus. White dwarf luminosity and mass functions from sloan digital sky survey spectra. *The Astronomical Journal*, 135:1–9, 2008. [3](#)
- A. Gianninas, P. Bergeron, and M. T. Ruiz. Spectroscopic analysis of DA white dwarfs from the McCook & sion catalog. *Journal of Physics Conference Series*, 172:2021, June 2009. [xviii](#), [116](#), [117](#)
- A. Gianninas, P. Bergeron, and M. T. Ruiz. A spectroscopic survey & analysis of bright, Hydrogen-Rich white dwarfs, Sept. 2011. [110](#), [114](#)
- L. Girardi, A. Bressan, G. Bertelli, and C. Chiosi. Evolutionary tracks and isochrones for low- and intermediate-mass stars: From 0.15 to 7 msun, and from  $z=0.0004$  to 0.03. *Astronomy and Astrophysics Supplement Series*, 141:371–383, Feb. 2000. [5](#), [78](#), [79](#), [80](#), [82](#), [83](#), [202](#)
- J. Girven, B. T. Gnsicke, B. Klebi, D. Steeghs, S. Jordan, T. R. Marsh, and D. Koester. PG1258+593 and its common proper motion magnetic white dwarf counterpart. *Monthly Notices of the Royal Astronomical Society*, page 271, Feb. 2010. [18](#)

- J. L. Greenstein, N. Dolez, and G. Vauclair. Physical properties and evolution of the two white dwarfs in the Sanduleak-Pesch binary. *Astronomy and Astrophysics*, 127: 25–28, Oct. 1983. [18](#)
- J. Halbwachs. Statistical studies on wide pairs. *Astrophysics and Space Science*, 142: 237–244, Mar. 1988. [28](#)
- T. Hamada and E. E. Salpeter. Models for Zero-Temperature stars. *The Astrophysical Journal*, 134:683, Nov. 1961. [2](#), [3](#)
- R. S. Harrington. Stability criteria for triple stars. *Celestial Mechanics*, 6:322–327, Nov. 1972. [79](#)
- H. C. Harris, J. Liebert, S. J. Kleinman, A. Nitta, S. F. Anderson, G. R. Knapp, J. Krzesiski, G. Schmidt, M. A. Strauss, D. V. Berk, D. Eisenstein, S. Hawley, B. Margon, J. A. Munn, N. M. Silvestri, J. A. Smith, P. Szkody, M. J. Collinge, C. C. Dahn, X. Fan, P. B. Hall, D. P. Schneider, J. Brinkmann, S. Burles, J. E. Gunn, G. S. Hennessy, R. Hindsley, Z. Ivezi, S. Kent, D. Q. Lamb, R. H. Lupton, R. C. Nichol, J. R. Pier, D. J. Schlegel, M. SubbaRao, A. Uomoto, B. Yanny, and D. G. York. An initial survey of white dwarfs in the sloan digital sky survey. *Astronomical Journal*, 126:1023–1040, Aug. 2003. [xiv](#), [25](#), [26](#)
- H. C. Harris, J. A. Munn, M. Kilic, J. Liebert, K. A. Williams, T. von Hippel, S. E. Levine, D. G. Monet, D. J. Eisenstein, S. J. Kleinman, T. S. Metcalfe, A. Nitta, D. E. Winget, J. Brinkmann, M. Fukugita, G. R. Knapp, R. H. Lupton, J. A. Smith, and D. P. Schneider. The white dwarf luminosity function from sloan digital sky survey imaging data. *The Astronomical Journal*, 131:571–581, Jan. 2006. [9](#)
- F. Herwig. Evolution of asymptotic giant branch stars. *Annual Review of Astronomy and Astrophysics*, 43:435–479, Sept. 2005. [xiii](#), [6](#), [11](#)
- J. B. Holberg and P. Bergeron. Calibration of synthetic photometry using DA white dwarfs. volume 207, page 1158, Dec. 2005. [200](#)
- J. B. Holberg and P. Bergeron. Calibration of synthetic photometry using DA white dwarfs. *Astronomical Journal*, 132:1221–1233, Sept. 2006. [61](#), [75](#)
- J. B. Holberg, R. A. Saffer, R. W. Tweedy, and M. A. Barstow. The binary double-degenerate nature of the bright DAO white dwarf feige 55. *Astrophysical Journal*, 452:L133, Oct. 1995. [18](#)
- J. B. Holberg, T. D. Oswalt, and E. M. Sion. A determination of the local density of white dwarf stars. *The Astrophysical Journal*, 571:512–518, May 2002. [9](#)
- J. B. Holberg, E. M. Sion, T. Oswalt, G. P. McCook, S. Foran, and J. P. Subasavage. A new look at the local white dwarf population. *Astronomical Journal*, 135:1225–1238, Apr. 2008. [9](#)

- D. Homeier, D. Koester, H. Hagen, S. Jordan, U. Heber, D. Engels, D. Reimers, and S. Dreizler. An analysis of DA white dwarfs from the hamburg quasar survey. *Astronomy and Astrophysics*, 338:563–575, Oct. 1998. [xiv](#), [19](#), [20](#)
- D. A. Howell, M. Sullivan, P. E. Nugent, R. S. Ellis, A. J. Conley, D. L. Borgne, R. G. Carlberg, J. Guy, D. Balam, S. Basa, D. Fouchez, I. M. Hook, E. Y. Hsiao, J. D. Neill, R. Pain, K. M. Perrett, and C. J. Pritchett. The type ia supernova SNLS-03D3bb from a super-Chandrasekhar-mass white dwarf star. *Nature*, 443:308–311, Sept. 2006. [11](#)
- I. Hubeny. A computer program for calculating non-LTE model stellar atmospheres. *Computer Physics Communications*, 52:103–132, Dec. 1988. [57](#), [58](#), [59](#)
- I. Hubeny and T. Lanz. Non-LTE line-blanketed model atmospheres of hot stars. 1: Hybrid complete linearization/accelerated lambda iteration method. *The Astrophysical Journal*, 439:875–904, Feb. 1995. [57](#), [59](#)
- I. Hubeny and T. Lanz. Synspec version forty eight. 2001. URL <http://nova.astro.umd.edu/>. [57](#), [59](#)
- D. G. Hummer and D. Mihalas. The equation of state for stellar envelopes. i - an occupation probability formalism for the truncation of internal partition functions. *The Astrophysical Journal*, 331:794–814, Aug. 1988. [59](#)
- I. Iben. Mass Transfer/Loss from AGB stars in close binaries. volume 199, page 107, 2000. [114](#)
- I. Iben. Stellar evolution. II. the evolution of a 3 m<sub>sun</sub> star from the main sequence through core helium burning. *The Astrophysical Journal*, 142:1447, Nov. 1965. [5](#)
- I. Iben and M. Livio. Common envelopes in binary star evolution. *Publications of the Astronomical Society of the Pacific*, 105:1373–1406, Dec. 1993. [5](#), [80](#), [83](#)
- I. Iben and A. Renzini. Asymptotic giant branch evolution and beyond. *Annual Review of Astronomy and Astrophysics*, 21:271–342, 1983. [11](#)
- I. Iben and A. V. Tutukov. On the evolution of close binaries with components of initial mass between 3 solar masses and 12 solar masses. *The Astrophysical Journal Supplement Series*, 58:661–710, Aug. 1985. [79](#), [84](#)
- J. Isern, R. Mochkovitch, E. Garcia-Berro, and M. Hernanz. The physics of crystallizing white dwarfs. *The Astrophysical Journal*, 485:308, Aug. 1997. [3](#)
- S. Jordan. Analysis of three magnetic DA white dwarfs. page 333, 1993. [61](#)
- S. Jordan. Models of white dwarfs with high magnetic fields. *Astronomy and Astrophysics*, 265:570–576, Nov. 1992. [61](#)

- S. Jordan, D. Koester, G. Vauclair, N. Dolez, U. Heber, H. Hagen, D. Reimers, M. Chevreton, and S. Dreizler. HS0507+0434: a double DA degenerate with a ZZCeti component. *Astronomy and Astrophysics*, 330:277–284, Feb. 1998a. [105](#)
- S. Jordan, D. Koester, G. Vauclair, N. Dolez, U. Heber, H. Hagen, D. Reimers, M. Chevreton, and S. Dreizler. HS0507+0434: a double DA degenerate with a ZZCeti component. *Astronomy and Astrophysics*, 330:277–284, Feb. 1998b. [18](#)
- J. S. Kalirai, H. B. Richer, D. Reitzel, B. M. S. Hansen, R. M. Rich, G. G. Fahlman, B. K. Gibson, and T. von Hippel. The Initial-Final mass relationship: Spectroscopy of white dwarfs in NGC 2099 (M37). *Astrophysical Journal*, 618:L123–L127, 2005a. [14](#)
- J. S. Kalirai, H. B. Richer, D. Reitzel, B. M. S. Hansen, R. M. Rich, G. G. Fahlman, B. K. Gibson, and T. von Hippel. Spectroscopy of faint white dwarfs - the DA/DB ratio and the Initial-Final mass relation. volume 334, page 9, July 2005b. [116](#)
- J. S. Kalirai, P. Bergeron, B. M. S. Hansen, D. D. Kelson, D. B. Reitzel, R. M. Rich, and H. B. Richer. Stellar evolution in NGC 6791: Mass loss on the red giant branch and the formation of Low-Mass white dwarfs. *Astrophysical Journal*, 671:748–760, Dec. 2007. [15](#)
- J. S. Kalirai, B. M. S. Hansen, D. D. Kelson, D. B. Reitzel, R. M. Rich, and H. B. Richer. The Initial-Final mass relation: Direct constraints at the Low-Mass end. *Astrophysical Journal*, 676:594–609, Mar. 2008. [xvi](#), [xvii](#), [15](#), [78](#), [79](#), [80](#), [81](#), [82](#), [83](#), [84](#), [87](#), [89](#), [94](#), [95](#), [96](#), [97](#), [98](#), [99](#), [100](#), [101](#)
- A. I. Karakas, J. C. Lattanzio, and O. R. Pols. Parameterising the third dredge-up in asymptotic giant branch stars. *Publications of the Astronomical Society of Australia*, 19:515–526, 2002. [xiv](#), [16](#)
- S. O. Kepler, S. J. Kleinman, A. Nitta, D. Koester, B. G. Castanheira, O. Giovannini, A. F. M. Costa, and L. Althaus. White dwarf mass distribution in the SDSS. *Monthly Notices of the Royal Astronomical Society*, 375:1315–1324, Mar. 2007. [xiii](#), [xvii](#), [9](#), [10](#), [13](#), [25](#), [41](#), [105](#), [106](#), [108](#)
- R. Kippenhahn and A. Weigert. *Stellar Structure and Evolution*. 1990. [2](#)
- S. J. Kleinman, H. C. Harris, D. J. Eisenstein, J. Liebert, A. Nitta, J. Krzesiski, J. A. Munn, C. C. Dahn, S. L. Hawley, J. R. Pier, G. Schmidt, N. M. Silvestri, J. A. Smith, P. Szkody, M. A. Strauss, G. R. Knapp, M. J. Collinge, A. S. Mukadam, D. Koester, A. Uomoto, D. J. Schlegel, S. F. Anderson, J. Brinkmann, D. Q. Lamb, D. P. Schneider, and D. G. York. A catalog of spectroscopically identified white dwarf stars in the first data release of the sloan digital sky survey. *Astrophysical Journal*, 607:426–444, May 2004. [110](#)
- G. R. Knapp. Mass loss from evolved stars. VI - mass-loss mechanisms and luminosity evolution. *The Astrophysical Journal*, 311:731–741, Dec. 1986. [7](#)



- R. A. Knox, M. R. S. Hawkins, and N. C. Hambly. A survey for cool white dwarfs and the age of the galactic disc. *Monthly Notices of the Royal Astronomical Society*, 306: 736–752, July 1999. [9](#)
- D. Koester. White dwarf spectra and atmosphere models . *Memorie della Societa Astronomica Italiana*, 81:921, 2010. [76](#)
- D. Koester and D. Reimers. Spectroscopic identification of white dwarfs in galactic clusters. i NGC 2287 and NGC 2422. *Astronomy and Astrophysics*, 99:L8–L11, June 1981. [11](#)
- D. Koester, R. Napiwotzki, N. Christlieb, H. Drechsel, H. Hagen, U. Heber, D. Homeier, C. Karl, B. Leibundgut, S. Moehler, G. Nelemans, E. Pauli, D. Reimers, A. Renzini, and L. Yungelson. High-resolution UVES/VLT spectra of white dwarfs observed for the ESO SN ia progenitor survey (SPY). i. *Astronomy and Astrophysics*, 378: 556–568, Nov. 2001. [xiv](#), [19](#), [20](#)
- M. B. N. Kouwenhoven, A. G. A. Brown, H. Zinnecker, L. Kaper, and S. F. Portegies Zwart. The primordial binary population. i. a near-infrared adaptive optics search for close visual companions to a star members of scorpius OB2. *Astronomy and Astrophysics*, 430:137–154, Jan. 2005. [114](#)
- J. Kubat. The sphericity effects in the NLTE model atmospheres of hot white dwarfs. *Astronomy and Astrophysics*, 299:803, July 1995. [57](#)
- B. Klebi, S. Jordan, F. Euchner, B. T. Gnsicke, and H. Hirsch. Analysis of hydrogen-rich magnetic white dwarfs detected in the sloan digital sky survey. *Astronomy and Astrophysics*, 506:1341–1350, Nov. 2009. [61](#)
- D. Q. Lamb and H. M. van Horn. Evolution of crystallizing pure c-12 white dwarfs. *The Astrophysical Journal*, 200:306–323, Sept. 1975. [3](#)
- S. K. Leggett, M. T. Ruiz, and P. Bergeron. The cool white dwarf luminosity function and the age of the galactic disk. *The Astrophysical Journal*, 497:294, Apr. 1998. [9](#)
- M. Lemke. Extended VCS stark broadening tables for hydrogen – lyman to brackett series. *Astronomy and Astrophysics Supplement Series*, 122:285–292, Apr. 1997. [59](#)
- J. Liebert, C. C. Dahn, and D. G. Monet. The luminosity function of white dwarfs. *The Astrophysical Journal*, 332:891–909, Sept. 1988. [9](#)
- J. Liebert, P. Bergeron, and J. B. Holberg. The formation rate and mass and luminosity functions of DA white dwarfs from the palomar green survey. *The Astrophysical Journal Supplement Series*, 156:47–68, Jan. 2005a. [xiii](#), [xiv](#), [xvii](#), [9](#), [10](#), [17](#), [19](#), [20](#), [105](#), [107](#), [115](#)
- J. Liebert, D. T. Wickramasinghe, G. D. Schmidt, N. M. Silvestri, S. L. Hawley, P. Szkody, L. Ferrario, R. F. Webbink, T. D. Oswalt, J. A. Smith, and M. P. Lemagie. Where are the magnetic white dwarfs with detached, nondegenerate companions? *The Astronomical Journal*, 129:2376–2381, May 2005b. [84](#)



- C. W. H. D. Loore and C. Doom. Structure and evolution of single and binary stars. volume 179, 1992. [5](#), [6](#)
- J. Madej, M. Nalety, and L. G. Althaus. Mass distribution of DA white dwarfs in the first data release of the sloan digital sky survey. *Astronomy and Astrophysics*, 419: L5–L8, May 2004. [xiii](#), [10](#)
- P. Marigo and L. Girardi. Evolution of asymptotic giant branch stars. i. updated synthetic TP-AGB models and their basic calibration. *Astronomy and Astrophysics*, 469:239–263, July 2007. [xiv](#), [11](#), [16](#)
- M. C. Marsh, M. A. Barstow, D. A. Buckley, M. R. Burleigh, J. B. Holberg, D. Koester, D. O’Donoghue, A. J. Penny, and A. E. Sansom. An EUV-selected sample of DA white dwarfs from the ROSAT All-Sky survey - i. optically derived stellar parameters. *Monthly Notices of the Royal Astronomical Society*, 286:369–383, Apr. 1997. [xiv](#), [19](#), [20](#), [115](#)
- G. P. McCook and E. M. Sion. A catalog of spectroscopically identified white dwarfs. *The Astrophysical Journal Supplement Series*, 121:1–130, Mar. 1999. [4](#), [117](#)
- D. Mihalas. *Stellar atmospheres /2nd edition/*. 1978. [57](#), [58](#)
- E. Moraux, J. Bouvier, and J. R. Stauffer. Proper motion of very low mass stars and brown dwarfs in the pleiades cluster. *Astronomy and Astrophysics*, 367:211–217, Feb. 2001. [67](#)
- R. Napiwotzki, P. J. Green, and R. A. Saffer. A comparative study of the mass distribution of Extreme-Ultraviolet-selected white dwarfs. *The Astrophysical Journal*, 517:399–415, May 1999. [60](#), [77](#)
- M. S. O’Brien and S. D. Kawaler. Measurement of neutrino emission rates in cool Pre-White dwarfs. volume 189, page 1378, Dec. 1996. [3](#)
- M. A. C. Perryman, A. G. A. Brown, Y. Lebreton, A. Gomez, C. Turon, G. Cayrel de Strobel, J. C. Mermilliod, N. Robichon, J. Kovalevsky, and F. Crifo. The hyades: distance, structure, dynamics, and age. *Astronomy and Astrophysics*, 331:81–120, Mar. 1998. [80](#)
- S. R. Pottasch. Local space density and formation rate of planetary nebulae. *Astronomy and Astrophysics*, 307:561–578, Mar. 1996. [9](#)
- J. L. Provencal, H. L. Shipman, E. Hog, and P. Thejll. Testing the white dwarf Mass-Radius relation with HIPPARCOS. *The Astrophysical Journal*, 494:759, Feb. 1998. [4](#)
- D. Raghavan, H. A. McAlister, T. J. Henry, D. W. Latham, G. W. Marcy, B. D. Mason, D. R. Gies, R. J. White, and T. A. ten Brummelaar. A survey of stellar families: Multiplicity of solar-type stars. *The Astrophysical Journal Supplement Series*, 190: 1–42, Sept. 2010. [79](#)

- D. Reimers and D. Koester. Spectroscopic identification of white dwarfs in galactic clusters. II - NGC 2516. *Astronomy and Astrophysics*, 116:341–347, Dec. 1982. [11](#)
- A. Renzini and M. Voli. Advanced evolutionary stages of intermediate-mass stars. i - evolution of surface compositions. *Astronomy and Astrophysics*, 94:175–193, Jan. 1981. [7](#)
- K. H. R. Rubin, K. A. Williams, M. Bolte, and D. Koester. The white dwarf population in NGC 1039 (M34) and the white dwarf Initial-Final mass relation. *Astronomical Journal*, 135:2163–2176, June 2008. [14](#)
- M. Salaris, A. Serenelli, A. Weiss, and M. M. Bertolami. Semi-empirical white dwarf Initial-Final mass relationships: A thorough analysis of systematic uncertainties due to stellar evolution models. *Astrophysical Journal*, 692:1013–1032, Feb. 2009. [15](#), [19](#)
- E. E. Salpeter. Energy and pressure of a Zero-Temperature plasma. *The Astrophysical Journal*, 134:669, Nov. 1961. [2](#)
- E. L. Schatzman. *White dwarfs*, volume 5S. 1958. [7](#)
- G. D. Schmidt, H. C. Harris, J. Liebert, D. J. Eisenstein, S. F. Anderson, J. Brinkmann, P. B. Hall, M. Harvanek, S. Hawley, S. J. Kleinman, G. R. Knapp, J. Krzesinski, D. Q. Lamb, D. Long, J. A. Munn, E. H. Neilsen, P. R. Newman, A. Nitta, D. J. Schlegel, D. P. Schneider, N. M. Silvestri, J. A. Smith, S. A. Snedden, P. Szkody, and D. V. Berk. Magnetic white dwarfs from the sloan digital sky survey: The first data release. *Astrophysical Journal*, 595:1101–1113, Oct. 2003. [76](#)
- D. P. Schneider, G. T. Richards, P. B. Hall, M. A. Strauss, S. F. Anderson, T. A. Boroson, N. P. Ross, Y. Shen, W. N. Brandt, X. Fan, N. Inada, S. Jester, G. R. Knapp, C. M. Krawczyk, A. R. Thakar, D. E. V. Berk, W. Voges, B. Yanny, D. G. York, N. A. Bahcall, D. Bizyaev, M. R. Blanton, H. Brewington, J. Brinkmann, D. Eisenstein, J. A. Frieman, M. Fukugita, J. Gray, J. E. Gunn, P. Hibon, eljko Ivezi, S. M. Kent, R. G. Kron, M. G. Lee, R. H. Lupton, E. Malanushenko, V. Malanushenko, D. Oravetz, K. Pan, J. R. Pier, T. N. Price, D. H. Saxe, D. J. Schlegel, A. Simmons, S. A. Snedden, M. U. SubbaRao, A. S. Szalay, and D. H. Weinberg. The sloan digital sky survey quasar catalog. v. seventh data release. *The Astronomical Journal*, 139:2360–2373, June 2010. [28](#)
- D. Schoenberner. Late stages of stellar evolution. II - mass loss and the transition of asymptotic giant branch stars into hot remnants. *The Astrophysical Journal*, 272:708–714, Sept. 1983. [7](#), [8](#)
- L. Segretain, G. Chabrier, and R. Mochkovitch. The fate of merging white dwarfs. *The Astrophysical Journal*, 481:355, May 1997. [115](#)
- H. L. Shipman. Sirius b - a thermal soft x-ray source. *The Astrophysical Journal*, 206:L67–L69, May 1976. [58](#)

- E. M. Sion, J. L. Greenstein, J. D. Landstreet, J. Liebert, H. L. Shipman, and G. A. Wegner. A proposed new white dwarf spectral classification system. *The Astrophysical Journal*, 269:253–257, June 1983. 4
- J. R. Stauffer, G. Schultz, and J. D. Kirkpatrick. Keck spectra of pleiades brown dwarf candidates and a precise determination of the lithium depletion edge in the pleiades. *The Astrophysical Journal*, 499:L199, June 1998. 21, 80
- M. F. Sterzik and R. H. Durisen. Are binary separations related to their system mass? <http://adsabs.harvard.edu/abs/2004RMxAC..21...58S>, Aug. 2004. 114
- R. B. Stothers and C. Chin. Tests of two convection theories for red giant and red supergiant envelopes. *The Astrophysical Journal*, 440:297, 1995. ISSN 0004-637X. doi: 10.1086/175270. URL <http://adsabs.harvard.edu/abs/1995ApJ...440..297S>. 5
- I. Traulsen, A. I. D. Hoffmann, T. Rauch, K. Werner, S. Dreizler, and J. W. Kruk. HST and FUSE spectroscopy of hot Hydrogen-Rich central stars of planetary nebulae. volume 334, page 325, July 2005. xiii, 8
- P. Tremblay, P. Bergeron, and A. Gianninas. An improved spectroscopic analysis of DA white dwarfs from the sloan digital sky survey data release 4. *The Astrophysical Journal*, 730:128, Apr. 2011. xvi, 76, 85, 86
- P. G. van Dokkum. Cosmic-Ray rejection by laplacian edge detection. *Publications of the Astronomical Society of the Pacific*, 113:1420–1427, Nov. 2001. 49, 143
- S. Vennes, P. A. Thejll, R. G. Galvan, and J. Dupuis. Hot white dwarfs in the extreme ultraviolet explorer survey. II. mass distribution, space density, and population age. *The Astrophysical Journal*, 480:714, May 1997. xiv, 19, 20, 115
- S. Vennes, R. J. Smith, B. J. Boyle, S. M. Croom, A. Kawka, T. Shanks, L. Miller, and N. Loaring. White dwarfs in the 2dF QSO redshift survey - i. hydrogen-rich (DA) stars. *Monthly Notices of the Royal Astronomical Society*, 335:673–686, Sept. 2002. 9
- A. Wachter, K. Schröder, J. M. Winters, T. U. Arndt, and E. Sedlmayr. An improved mass-loss description for dust-driven superwinds and tip-AGB evolution models. *Astronomy and Astrophysics*, 384:452–459, Mar. 2002. 7
- G. Wegner, I. N. Reid, and R. K. McMahan. Gravitational redshift for the pleiad white dwarf LB 1497. *The Astrophysical Journal*, 376:186–189, July 1991. 80
- V. Weidemann. The initial-final mass relation - galactic disk and magellanic clouds. *Astronomy and Astrophysics*, 188:74–84, Dec. 1987. 13
- V. Weidemann. The initial/final mass relation for stellar evolution with mass loss. volume 89, pages 339–343, 1981. 11, 14

- V. Weidemann. Mass loss towards the white dwarf stage. *Astronomy and Astrophysics*, 59:411–418, Aug. 1977. [11](#)
- V. Weidemann. Revision of the initial-to-final mass relation. *Astronomy and Astrophysics*, 363:647–656, Nov. 2000. [xiv](#), [11](#), [13](#), [14](#), [16](#), [89](#)
- K. Werner. Construction of non-LTE model atmospheres using approximate lambda operators. *Astronomy and Astrophysics*, 161:177–182, June 1986. [57](#)
- F. Wesemael, J. L. Greenstein, J. Liebert, R. Lamontagne, G. Fontaine, P. Bergeron, and J. W. Glaspey. An atlas of optical spectra of white-dwarf stars. *Publications of the Astronomical Society of the Pacific*, 105:761–778, July 1993. [4](#)
- D. T. Wickramasinghe and L. Ferrario. The origin of the magnetic fields in white dwarfs. *Monthly Notices of the Royal Astronomical Society*, 356:1576–1582, Feb. 2005. [21](#)
- K. A. Williams. A new look at the empirical Initial–Final mass relation. volume 372, page 85, Sept. 2007. [21](#)
- K. A. Williams and M. Bolte. A photometric and spectroscopic search for white dwarfs in the open clusters NGC 6633 and NGC 7063. *Astronomical Journal*, 133:1490–1504, Apr. 2007. [14](#)
- K. A. Williams, M. Bolte, and J. W. Liebert. Spectroscopic identification of faint white dwarf candidates in the praesepe open star cluster. *Astronomical Journal*, 128:1784–1789, Oct. 2004. [14](#)
- K. A. Williams, M. Bolte, and D. Koester. Probing the lower mass limit for supernova progenitors and the High-Mass end of the Initial-Final mass relation from white dwarfs in the open cluster m35 (NGC 2168). *Astrophysical Journal*, 693:355–369, Mar. 2009. [xvi](#), [xvii](#), [11](#), [14](#), [78](#), [79](#), [80](#), [81](#), [82](#), [83](#), [84](#), [87](#), [88](#), [94](#), [95](#), [96](#), [97](#), [98](#), [99](#), [100](#), [101](#)
- D. E. Winget, C. J. Hansen, J. Liebert, H. M. van Horn, G. Fontaine, R. E. Nather, S. O. Kepler, and D. Q. Lamb. An independent method for determining the age of the universe. *The Astrophysical Journal*, 315:L77–L81, Apr. 1987. [8](#)
- M. A. Wood. Astero-archaeology: Reading the galactic history recorded in the white dwarf stars. <http://adsabs.harvard.edu/abs/1990PhDT.....5W>, 1990. [3](#), [8](#)
- M. A. Wood. Constraints on the age and evolution of the galaxy from the white dwarf luminosity function. *The Astrophysical Journal*, 386:539–561, Feb. 1992. [2](#), [14](#)